Molecular and Nanoscale Engineering for Enhanced Order in Organic Electro-Optic Materials

Scott R. Hammond

A dissertation submitted in partial fulfillment of the
requirements for the degree of:

Doctor of Philosophy

University of Washington

2007

Program Authorized to Offer Degree:
Department of Chemistry

INFORMATION TO USERS

The quality of this reproduction is dependent upon the quality of the copy submitted. Broken or indistinct print, colored or poor quality illustrations and photographs, print bleed-through, substandard margins, and improper alignment can adversely affect reproduction.

In the unlikely event that the author did not send a complete manuscript and there are missing pages, these will be noted. Also, if unauthorized copyright material had to be removed, a note will indicate the deletion.

ProQuest Information and Learning Company
300 North Zeeb Road
P.O. Box 1346
Ann Arbor, MI 48106-1346

University of Washington
Graduate School

This is to certify that I have examined this copy of a doctoral dissertation by

Scott R. Hammond

and have found that it is complete and satisfactory in all respects,
and that any and all revisions required by the final
examining committee have been made.

Chair of the Supervisory Committee:

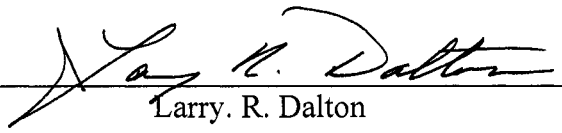

Larry. R. Dalton

Reading Committee:

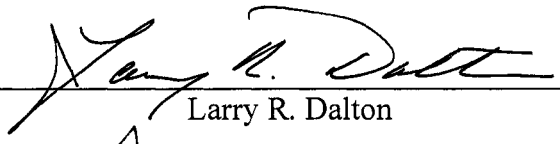

Larry R. Dalton

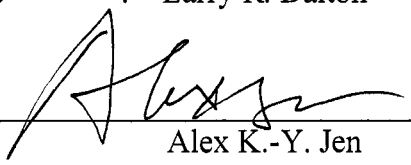

Alex K.-Y. Jen

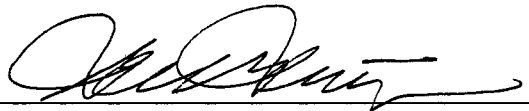

Glenn P. Bartholomew

Date: 5/2/07

In presenting this dissertation in partial fulfillment of the requirements for the doctoral degree at the University of Washington, I agree that the Library shall make its copies freely available for inspection. I further agree that extensive copying of the dissertation is allowable only for scholarly purposes, consistent with "fair use" as prescribed in the U.S. Copyright Law. Requests for copying or reproduction of this dissertation may be referred to Proquest Information and Learning, 300 North Zeeb Road, Ann Arbor, MI 48106-1346, 1-800-521-0600, to whom the author has granted "the right to reproduce and sell (a) copies of the manuscript in microform and/or (b) printed copies of the manuscript made from microform."

Signature 

Date 5/2/07

University of Washington

Abstract

Molecular and Nanoscale Engineering for Enhanced Order in Organic Electro-Optic Materials

Scott R. Hammond

Chairperson of the Supervisory Committee:
Professor Larry R. Dalton
Department of Chemistry

Intermolecular interactions play a critical role in organic electro-optic materials. Through careful molecular design and optimization, we explore the effect of these interactions on molecular properties, nanoscale acentric order, and ultimately macroscopic electro-optic activity. Discotic chromophores, designed to reduce centrosymmetric dipole-dipole interactions, incorporating a variety of functionalities exhibit a range of morphologies, including amorphous, crystalline, and liquid-crystalline phases. We present the characterization of these systems and the effect of the nanoscale order on their macroscopic properties, including electro-optic activity. Covalent attachment of zwitterionic and neutral ground state electro-optic chromophores provides a method to explore the effect of intermolecular interactions and dielectric environment on molecular properties such as dipole moment and hyperpolarizability. We also present our initial results on the characterization of the dielectric constants of organic electro-optic materials, and their effect on microscopic and macroscopic properties of the material

TABLE OF CONTENTS

page

LIST OF FIGURES

Figure Number Page

LIST OF SCHEMES

Scheme Number Page

LIST OF TABLES

Table Number Page

ACKNOWLEDGEMENTS

I would like to express my sincere appreciation to all the individuals who contributed in some way (large or small) to this work specifically, and my graduate education in general.

First, I wish to thank all of the past and present members of the Dalton Research Group at the University of Washington. Without the scientific, educational, and moral support, and friendship, of this diverse group I could not have completed my graduate education. In particular, I would like to thank Dr. Jessica Sinness for her fundamental role in the Discotic Chromophore project, which forms the bulk of this dissertation. I am also indebted to Dr. Kimberly A. Firestone and Dr. Philip A. Sullivan, who provided tremendous scientific and practical advice, along with true friendship.

Numerous individuals provided significant tangible scientific contributions to this work, some of which are listed here. Dr. Jessica Sinness and Dr. Olivier Clot played critical roles in the Discotic Chromophore project. Considerable synthetic contributions were provided by Sara Dubbury, particularly for the Bichromophore project. Dr. Kimberly Firestone performed important hyper-Rayleigh scattering studies. The Density Functional Theory calculations of Dr. Bruce Eichinger and the Monte Carlo statistical mechanics simulations of Prof. Bruce Robinson provided a critical theoretical framework for the design and analysis of these molecules and macromolecular systems. The crystallography performed by Jason Benedict and Dr. Zdzislaw Wawrzak provided critically important information for the analysis of the Discotic Chromophores.

I would also like to extend my profound thanks to my friends and family who supported me through this trying time. In particular, I would like to thank my parents, Stan and Sharon Hammond, for their love and continued support (financial and otherwise) throughout my educational career. My deepest thanks also to my wife, Ysa Hammond, without whom I could never have survived graduate school. Thanks are due to Jean Hammond and Michael Krasner for generous financial support. My grandfather Dr. Philip Hammond, a chemical engineer, provided important early encouragement for my chosen career in chemistry. Additionally, Dr. Seth Miller acted as my first chemistry mentor and taught me the skills of organic chemistry, for which I am immensely thankful.

Finally, I would like to thank my advisor, Prof. Larry Dalton, for the tremendous opportunity to participate in this stimulating research environment. The scientific, educational, and financial support provided by Prof. Dalton has been instrumental in my professional development. Financial support for this work was provided by the National Science Foundation (DMR-0120967) and DARPA (N00014-04-1-0094).

DEDICATION

I would like to dedicate this dissertation to Dr. Seth Miller, my first chemistry mentor, and Sara Dubbury, my first chemistry mentee. Together we form links in the human chain that is a critical part of the scientific endeavor.

Chapter 1: Introduction to Organic Electro-Optics

1.1 Introduction

In modern society, the transmission, storage, and processing of information is becoming an increasingly important endeavor. In every avenue of society: military, industrial, commercial, and residential the quantity of information input from remote sources has increased enormously. Since the discovery of the transistor in 1947 gave birth to the modern field of electronics,[1] the storage, processing, and transmission of data using electrons, advances have mostly kept pace with the increasing demands for information by society. In the current phase of the information age, however, electronics are nearing their fundamental operational limits in terms of the quantity and speed that information can be handled (~ 50 gigabits/s). As a result, further advances in electronics will be increasingly expensive with decreasing returns, while the demand for information is continually increasing.

Fortunately the field of photonics, the storage, processing, and transmission of data using photons, is rapidly developing.[2,3] Already, most of the long-distance telecommunications lines have been converted to fiber optic cables, which have a fundamental frequency range (bandwidth) of ~ 10 THz.[4] Through the use of wavelength division multiplexing (WDM),[4] a wider frequency range can be utilized to transmit more information per unit time than is possible with just time division multiplexing (TDM) alone. Thus, fiber optic cables can transmit enormous amounts of data in excess of several terabits/s.[4] The exploitation of this bandwidth potential is

limited, however, by the rate at which information can be converted from the optical domain of the fiber to and from the electrical domain of the computers used to process the information. This conversion can be accomplished using an electro-optic (EO) device, the Mach-Zehnder modulator (Section 1.4.1). Currently, most of these devices are made commercially using inorganic EO materials such as lithium niobate ($LiNbO_3$) and gallium arsenide (GaAs).[5] However, Lumera Corporation produces state-of-the-art organic EO material-based modulators that are competitive with their inorganic based counterparts.[6]

In inorganic EO materials, the anisotropic atomic lattice undergoes a distortion with application of an electric field,[7] which results in the change in refractive index of the material that is necessary for the Mach-Zehnder device. Atomic rearrangements are relatively slow, however, and thus these devices are limited to an operating bandwidth of around 40 GHz.[8] The inorganic materials also have a fixed response to the applied electric field, as measured by the EO coefficient (r_{33}, Section 1.3), of 31 pm/V for $LiNbO_3$ (at a wavelength of 1.31 μm).[9] Additionally, the large dielectric constant of these materials, $\varepsilon \sim 28$ for $LiNbO_3$,[9] results in poor speed match between the traveling electrical and optical signals in the device, limiting the effective device length. Taken together, these restrict inorganic devices to operating voltages (V_π) of around 2 V.[6] The processing of these materials also presents a challenge, as it requires the growth and careful polishing of large single-crystals, which are not easily integrated into very large scale integration (VLSI) electronics, increasing device cost. Despite these numerous disadvantages, inorganic modulators are the industry standard, in part because of the excellent optical transparency (0.5 dB/cm for $LiNbO_3$ at 1.53 μm) and thermal- and

photo-stability of the devices;[10,11] critical parameters for devices placed on satellites and along the ocean floor where replacement is not a feasible option.

Organic EO materials present an attractive alternative to inorganic materials for a variety of reasons. Of primary importance, organic EO materials respond to an applied electric field and change their index of refraction primarily by shifting their electron density, which is orders of magnitude faster than atomic rearrangement, allowing for fast response times. This allows organic EO modulators to reach high operating bandwidths; bandwidths up to 110 GHz have been demonstrated with organic EO modulators,[12] and up to several THz has been predicted as theoretically possible. Organic materials also have low dielectric constants ($\varepsilon \sim 3$) allowing for better speed matching of the optical and electric signals. Recently, organic EO materials have demonstrated extremely large EO coefficients up to 300 pm/V,[13] which combined with the low dielectric constant can allow very low drive voltages (V_π) of below 1 V,[14] allowing for direct integration with electronics. Additionally, organic polymeric and dendritic materials are easy to process into optical quality films and compatible with VLSI electronics, significantly increasing design flexibility and reducing fabrication cost. Finally, organic molecules are almost infinitely variable via synthetic modification, allowing tuning of their properties such as EO coefficient, processability, and thermal- and photo-stability. While organic EO materials appear very attractive, they do have problems restricting their adoption in commercial applications, particularly long-term thermal- and photo-stability.

1.2 Nonlinear Optical Phenomena

Electro-optics (EO) is a subset of nonlinear optics (NLO), which is concerned with the deviation from linear behavior that is evident in the interaction between the electromagnetic fields of a light wave and those of matter or other light waves. In the most generalized sense, any electric field (such as from an applied DC electric field, or from a light wave) can cause an induced polarization response in any material, **P**. If the field is weak, then the response is linear and given by:

$$\mathbf{P} = \chi^{(1)}\mathbf{E} \qquad (1.1)$$

where $\chi^{(1)}$ is the linear susceptibility of the material, and E is the electric field. If, however, the electric field is sufficiently intense, then the polarization of the material can be seen as nonlinear (Figure 1.1).

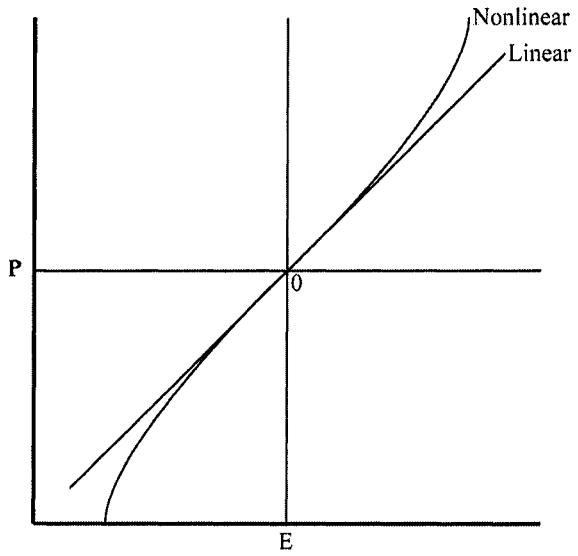

Figure 1.1. Representation of the nonlinear dependence of induced polarization (**P**) on electric field (E)

The field of NLO was first discovered by Kerr in 1875, when he discovered a quadratic dependence in the index of refraction of carbon disulfide on an applied

electric field.[15] The second example of NLO was Pockels' discovery of the linear EO effect (Section 1.3), a linear dependence in the index of refraction of quartz on an applied electric field in 1906.[16] Further advances in NLO were limited until the development of lasers in 1960,[17] because of the weak nature of the nonlinear interactions between matter and light. The advent of laser allowed for very intense light, which magnified the nonlinear interactions with matter.

1.2.1 Microscopic Polarization. In the case of organic EO materials, the macroscopic NLO behavior of the material arises from the properties of the individual component molecules. If one considers an arbitrary molecule in a non-magnetic and non-conducting medium, the application of an electric field (as from a light wave, or an AC/DC power source) results in a polarization of the molecule. This net alteration in the ground-state electron probability cloud can be treated as an induced dipole (μ_{ind}).[18] The magnitude of this response depends on both how strongly the electrons are bound (steepness of the potential well), and the strength of the applied electric field. As with most natural phenomena, linear response is only approximate, and with a sufficiently large applied field, a non-linear response is evident. As long as the polarization is not too large, it can be approximated by a power series expansion in the applied electric field ($\mathbf{E}$):[18]

$$\mu_{ind} = \mu_0 + \alpha\mathbf{E} + \beta\mathbf{EE} + \gamma\mathbf{EEE}... \qquad (1.2)$$

where μ_{ind} is the net induced dipole vector (or, equivalently, the net polarization vector), $\boldsymbol{\mu}_0$ is the dipole moment vector (if any) in the absence of an electric field, α is the linear polarizability, β is the first molecular hyperpolarizability, and γ is the second molecular hyperpolarizability. For all materials known, fourth and higher order effects are

negligible, so we will limit our discussion to third and lower order effects. α, β, and γ, are second, third, and fourth rank tensors, respectively, that relate the electric field vector to the polarization vector. The magnitude and dimensionality of the β tensor describes the degree and orientation of the 2nd order effects that the molecule exhibits, including second-harmonic generation (SHG, Section 2.4.2)[19,20] and hyper-Rayleigh scattering (HRS, Section 2.4.3).[21,22] The γ tensor describes the same features for 3rd order effects, such as two-photon absorption (TPA).[23,24] Symmetry properties dictate that for even-ordered terms in the expansion to be non-zero, the molecule must be asymmetric.[18] This can be understood conceptually as a conservation of charge. In the case of a symmetric molecule with no dipole moment, such as benzene:

$$\mu_{+}(1) = \alpha + \beta + \gamma \tag{1.3}$$

and,

$$\mu_{-}(-1) = -\alpha + \beta - \gamma \tag{1.4}$$

such that,

$$\mu_{+} + \mu_{-} = 2\beta \tag{1.5}$$

In a symmetric molecule, the polarization in opposite directions must be equal, or else charge has been generated to enhance the polarization in one direction. Thus, β must be zero in symmetric systems, and asymmetry is required for a non-zero β.

While asymmetry is required for β, which is responsible for the linear EO effect exploited in Mach-Zehnder devices, to be non-zero, the molecule must also possess easily polarized (shallow potential well) electrons for this term to be of significant magnitude. Such molecules are usually conjugated organic systems called chromophores. The most common type is the so-called push-pull, or donor-π-acceptor

chromophores, which include at least one electron-donating and one electron-accepting element, connected by a fully π-conjugated pathway (see Figure 1.2).[18] For such chromophores the dimensionality of the β tensor is such that the component along the charge-transfer axis, β_{zzz}, is the most important component. Other chromophore architectures include: through-space charge-transfer chromophores,[25] in which the π-conjugation pathway is partially disrupted, and octupolar chromophores,[26,27] in which an octupolar charge distribution is obtained through multiple donor and acceptor elements.

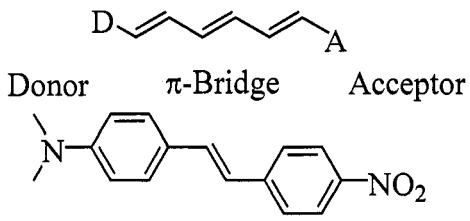

Figure 1.2. Donor-π-acceptor chromophore

1.2.2 Macroscopic Polarization. To be used in a device, organic EO materials must function on a macroscopic level, thus the second-order NLO activity must be extended from individual molecules to a collective ensemble. Organic EO materials traditionally consisted of either second-order NLO-active polar organic crystals,[28] or second-order NLO-active chromophores dispersed as guests into an NLO-inactive polymeric host.[29] If an applied electric field is small, then the material will respond in a linear manner, as described by Equation 1.1, above. If the chromophores are small with respect to the wavelength of light, and the composite material is non-conducting and non-magnetic, then the linear susceptibility (at a given frequency, ω) can also be related to the refractive index (n) and the dielectric constant (ε) by Equation 1.6.[18]

$$n_0^2(\omega) = \varepsilon(\omega) = 1 + 4\pi\chi^{(1)}(\omega) \quad (1.6)$$

If the applied electric field (**E**) is large, however, then the response is nonlinear, and if the magnitude of the polarization (**P**) is relatively small, then the nonlinear behavior can be described in a manner analogous to the microscopic case:

$$\mathbf{P} = \chi^{(1)}\mathbf{E} + \chi^{(2)}\mathbf{EE} + \chi^{(3)}\mathbf{EEE}... \quad (1.7)$$

where $\chi^{(2)}$ is the 2nd order, or the first nonlinear, susceptibility and $\chi^{(3)}$ is the 3rd order, or second nonlinear, susceptibility. Again, higher order terms are generally negligible, and will not be discussed. The magnitude and dimensionality of the $\chi^{(2)}$ and $\chi^{(3)}$ tensors describe the degree and orientation of the nonlinear response of the material. The $\chi^{(2)}$ tensor gives rise to 2nd order effects including the EO effect (Section 1.3)[16] and SHG (Section 3.5.1).[20] While the $\chi^{(3)}$ tensor dictates the response to 3rd order effects such as third-harmonic generation.[30] Taken together, they can describe a new equation:

$$\mathbf{P} = \chi_{eff}\mathbf{E} \quad (1.8)$$

where χ_{eff} describes the nonlinear polarization response, and is dependent upon the strength of the applied electric field.

The first nonlinear susceptibility, $\chi^{(2)}$, is a third-rank tensor and is also subject to the same symmetry requirements as for the microscopic case. This means that asymmetric organic chromophores must also be aligned noncentrosymmetrically in the matrix. This nanometer scale organization poses quite a challenge (Chapter 3), as most organic crystals possess a center of inversion, and most polymeric systems are isotropic. Additionally, the asymmetric chromophores usually have large ground-state dipole moments, which lead to strong centrosymmetric dipole-dipole interactions that oppose

attempts to introduce acentric order.[31] In the case of organic crystals, much effort has been extended towards engineering polar crystals (Section 3.2.1), but only moderate progress has been made due to the complex interactions involved. In the case of polymeric systems, anisotropy has traditionally been introduced via electric poling field (Section 3.2.4) of an isotropic melt of a chromophore-polymer solution. Additional methods explored include self-assembly (Section 3.2.2) and optical poling (Section 3.2.3).

1.3 The Electro-Optic Effect

The electro-optic (EO) or Pockels effect is a linear dependence in refractive index on an applied DC or low frequency (as compared to the frequencies present in optical light; radio-frequency to THz frequency) AC electric field. It arises from the nonlinear interaction between an EO active material, such as a noncentrosymmetric matrix of asymmetric chromophores, and the net electric field (**E**):

$$\mathbf{E} = \mathbf{E}(0) + \mathbf{E}(\omega) \tag{1.9}$$

where **E**(0) is the low-frequency field, and **E**(ω) is the optical field. The optical term can be re-written such that:

$$\mathbf{E} = \mathbf{E}(0) + E_0 \cos(\omega t - kz) \tag{1.10}$$

where E_0 is the amplitude of the optical field, and the cos(ωt-kz) term describes the frequency and phase of the optical field. This is where the low dielectric constant of organic materials is advantageous, as it ensures a good speed match between the low

frequency field and the optical field, so that they remain in phase throughout the material. Substituting this form of the E field into Equation 1.7 yields:

$$\mathbf{P} = \chi^{(1)}\left[\mathbf{E}(0) + E_0\cos(\omega t - kz)\right] + \chi^{(2)}\left[\mathbf{E}(0) + E_0\cos(\omega t - kz)\right]^2$$

$$+\chi^{(3)}\left[\mathbf{E}(0) + E_0\cos(\omega t - kz)\right]^3 \qquad (1.11)$$

This can be expanded and rewritten in terms of ω to give:

$$\mathbf{P}(\omega) = \left[\chi^{(1)} + 2\chi^{(2)}\mathbf{E}(0)E_0 + 3\chi^{(3)}\mathbf{E}^2(0)E_0 + \frac{3}{4}\chi^{(3)}E_0^3\right]E_0\cos(\omega t - kz) \quad (1.12)$$

where the term in brackets can be defined as the new χ_{eff}, so that:

$$\mathbf{P}(\omega) = \chi_{eff}E_0\cos(\omega t - kz) \qquad (1.13)$$

Substituting this into Equation 1.6 and replacing n (the field-dependent refractive index) for n_0 (the field-independent refractive index) yields:

$$n^2(\omega) = 1 + 4\pi\left[\chi^{(1)} + 2\chi^{(2)}\mathbf{E}(0)E_0 + 3\chi^{(3)}\mathbf{E}^2(0)E_0 + \frac{3}{4}\chi^{(3)}E_0^3\right]$$

$$= n_0^2(\omega) + 8\pi\chi^{(2)}\mathbf{E}(0) + 12\pi\chi^{(3)}\mathbf{E}^2(0) + 3\pi\chi^{(3)}E_0^2 \qquad (1.14)$$

Here the first term is the-field independent refractive index, while the other terms describe the deviation from this value due to the nonlinear effects. The second term depends linearly on the applied low-frequency field, and on the $\chi^{(2)}$ tensor of the material, and it describes the linear EO or Pockels effect. The third term describes the DC Kerr optical effect, a quadratic dependence in refractive index on the low-frequency applied electric field, which depends on the $\chi^{(3)}$ tensor. The fourth term also depends on the $\chi^{(3)}$ tensor, and it describes the AC Kerr effect, a quadratic dependence in refractive index on the optical frequency field, and thus on the intensity of light in the material.

If the $\chi^{(3)}$ tensor is assumed to be small, as is usually the case when the $\chi^{(2)}$ tensor is large, then the Kerr effects can be neglected, and the equation becomes

$$n^2(\omega) = n_0^2(\omega) + 8\pi\chi^{(2)}\mathbf{E}(0) \tag{1.15}$$

The linear EO effect is classically defined as[18]

$$\Delta\left(\frac{1}{n^2}\right) = \mathbf{r}\mathbf{E}(0) \tag{1.16}$$

where **r** is the electro-optic tensor. This can be converted to a more useful form by expanding the left side of the equation as follows, assuming the change in refractive index is small,

$$\Delta\left(\frac{1}{n^2}\right) = \frac{1}{n^2} - \frac{1}{n_0^2} = \frac{n_0^2 - n^2}{n^2 n_0^2} \approx \frac{n_0^2 - n^2}{n_0^4} = \frac{(n_0 + n)(n_0 - n)}{n_0^4}$$

$$\approx \frac{2n_0(n_0 - n)}{n_0^4} = -\frac{2\Delta n}{n_0^3} \tag{1.17}$$

The linear EO effect can thus be re-written as:

$$|\Delta n| = \frac{1}{2} n_0^3 \mathbf{r}\mathbf{E}(0) \tag{1.18}$$

which shows the change in refractive index depends linearly on the applied electric field, with the proportionality constant being the EO tensor times one-half the cube of the refractive index of the material. The EO tensor is a multidimensional property that can relate arbitrary vectors from the applied electric field and the optical electric field to a multidimensional change in refractive index. For the purposes of poled-polymer and related organic EO systems, however, the tensor collapses to two independent elements (Section 3.2.1), r_{333} and r_{133}, where the 333 axis is parallel to the poling axis, and the 133 axis is perpendicular to the poling axis. These terms are often abbreviated r_{33} and

r_{13} for simplicity. Based on symmetry arguments (Section 3.2),[18] the relationship between these elements is assumed to be:

$$r_{33} = 3r_{13} \tag{1.19}$$

Finally, by combining Equations 1.15, 1.16, and 1.17, the EO tensor can be related to the $\chi^{(2)}$ tensor as follows:

$$\mathbf{r} = -\frac{8\pi\chi^{(2)}}{n_0^4} \tag{1.20}$$

Thus the EO tensor is also linearly related to the first nonlinear susceptibility of the material, as previously suggested. To maximize the EO coefficient, and thus minimize the electric field necessary to obtain a desired index shift, therefore requires a high degree of noncentrosymmetric alignment (Chapter 3) of highly asymmetric second-order nonlinear chromophores (Chapter 2).

1.4 Device Applications of Electro-Optic Materials

While the Mach-Zehnder modulator is currently the most important and studied EO device, because of it's important role in the transition from electrical to optical signals, it is far from the only device application for EO materials. The ease in processing organic EO materials has enabled research into a number of new device architectures, both through more flexible design parameters and through more rapid prototyping. EO materials are poised to become key elements in three major areas of photonics: electrical-to-optical conversion,[12,14] optical signal processing,[32,33] and optical-to-electrical conversion.[34] We can begin to envision dense wavelength division

multiplexing (DWDM) chips based on organic EO materials,[35] as well as other photonic signal processing devices, replacing large rack-mounted electronic equipment that perform similar functions. Some examples of specific device applications include: THz emitters and sensors,[36] spatial light modulators,[37] reconfigurable optical add-drop multiplexers (ROADMs), and a variety of electric field, chemical, and biological sensors.[38] While a complete description of all the device applications currently being explored for organic EO materials is beyond the scope of this work, a brief description of the most important devices from the three major areas of photonics mentioned above will be provided.

1.4.1 Mach-Zehnder Modulator. The Mach-Zehnder modulator (MZM) is currently an important industrial product, with thousands of inorganic-based devices currently operating existing fiber-optic networks throughout the world.[4] The device, shown in Figure 1.3, consists of an input waveguide segment that splits via a y-branch into two straight-channel arms, which recombine to form a single output waveguide segment. The waveguide elements are made entirely out of an EO material, surrounded by passive cladding layers. The straight-channel segments are also outfitted with electrodes above and below. As light passes through the device, generally of 1.31 or 1.55 μm wavelength (the optical telecommunication wavelengths), if an electric field is applied to one arm of the device, the EO material in that arm exhibits a linear change in its refractive index due to the linear EO effect. This results in the phase angle of the light being retarded, with respect the phase of light in the other arm, and when the light in the two arms recombines there is partial destructive interference. The magnitude of the phase shift ($\Delta\phi$) can be described by[18]

$$\Delta\phi = n^3 r_{33} EL\pi / \lambda \qquad (1.21)$$

where n is the refractive index, r_{33} is the electro-optic coefficient, L is the coupling length, or the length of the index-shifted area, and λ is the wavelength of light. For most applications is it desirable to achieve a phase shift of π, such that there is complete destructive interference and no light is output from the device. In this way, electrical binary signals (on/off) can be converted into optical binary signals. The voltage (V_π) necessary to obtain such a condition can be given by:

$$V_\pi = \lambda h / n^3 r_{33} L \qquad (1.22)$$

where V_π is called the drive voltage, an important figure of merit, and h is the vertical height over which the electric field is applied. It is desirable to minimize the drive voltage to reduce power consumption, and if a voltage of around 0.1 V can be achieved, then MZMs could be directly interfaced with standard electronics, without the need for voltage amplifiers. A standard practice is to apply opposite voltages to the two arms, creating a push-pull MZM,[14] and thus doubling the effective phase shift for a given voltage.

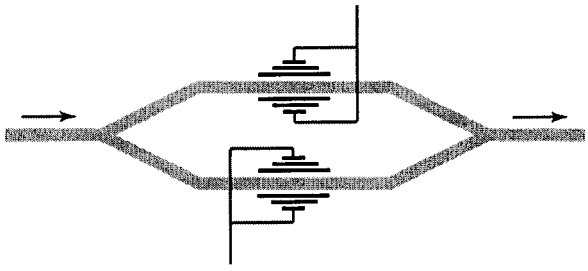

Figure 1.3. Schematic of a Mach-Zehnder modulator

For commercial inorganic push-pull MZMs, the drive voltage is around 2-6 V and there is little room for further improvement.[8] The wavelengths are fixed for a given application, generally at 1.31or 1.55 μm. The height of the EO material cannot go

below about 2 μm, to minimize optical loss due to waveguiding restrictions, and the total height must be larger than that because of cladding layers. The refractive index and r_{33} of inorganic materials are also fixed. The modulation length is also restricted in inorganic materials because of the large dielectric constant. The difference in speed between the traveling electrical and optical signals limits the interaction length to around 1 cm. Additionally, as previously mentioned, the speed of the EO response determines the effective bandwidth that the device can handle. For inorganic MZMs this is around 40 GHz,[8] with no room for improvement. Thus, inorganic MZMs have nearly reached their maximum potential, which falls well below the desired levels. Organic EO materials, however, can have tunable n, r_{33}, and L, because of synthetic versatility and the lower dielectric constant and thus better speed match. Organic EO based push-pull MZMs with sub-1 V drive voltages and bandwidths of 110 GHz have been demonstrated, [12,14] and there is still considerable room to improve these devices further based upon recent developments in organic EO materials.[13]

1.4.2 Micro-Ring Resonator. In the simplest sense, a micro-ring resonator (MRR) is a filter element. In the most basic configuration (see Figure 1.4), it consists of a straight-channel waveguide in very close proximity (within ~ 100 nm) to a circular waveguide with a radius on the order of 5-100 μm, depending on the material. Light passing through the straight-waveguide can be coupled into the micro-ring if its wavelength matches the resonance conditions, which depend on the radius and on the refractive index of the waveguide and cladding materials.[32,39] Light that is coupled into the ring is dissipated as it traverses the ring, and thus is filtered from the output. Two important device parameters are the quality factor (Q), which is the ratio of resonance wavelength

(λ) to the full width half max (FWHM) of the resonance peak ($\Delta\lambda$), and the free spectrum range (FSR), which is the distance between the resonance peaks.[32] By using EO materials as either the core or the cladding, one can apply an electric field and alter the refractive index of the core or cladding, thus shifting the resonance conditions and the wavelengths filtered.[33,39] This is a basic optical signal-processing element. Organic EO materials are advantageous for these applications because they are readily processed via variety of techniques, including spin-casting, photolithography, plasma-etching, ink-jet printing, and soft lithography.[40]

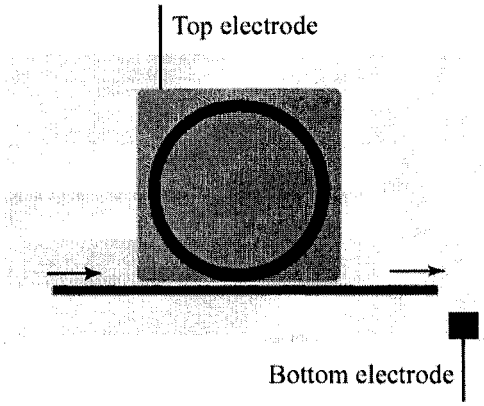

Figure 1.4. Schematic of a simple micro-ring resonator

Micro-ring resonators can be significantly more complex, allowing much more sophisticated optical logic elements to be created. For example, if a second straight-waveguide is placed on the opposite side of the ring, the filtered light can be coupled into this second waveguide. By using EO materials to shift the resonance wavelengths, variable-wavelength switches can be created.[32,39] Extending this concept by cascading multiple MRR,[41] one can design multidimensional variable-wavelength switches, such as ROADMs. Additionally, the small size of MRRs, as compared to MZMs, allows for efficient packaging of many elements on a single chip, allowing for low-cost fabrication

and facile integration of powerful photonic processing chips into existing systems. The ring resonator devices described here are only a small sampling of the complex optical logic elements that are being developed. As research progresses, more sophisticated systems are being created to perform extensive optical signal processing tasks.

Recently, a new slot-ring resonator device has attracted considerable attention.[34,42] These devices consist of silicon waveguides with a narrow slot (~ 60-100 nm) in their center (see Figure 1.5). This results in a high degree of mode confinement in the slot, yielding very high strength optical electric fields. EO material used as cladding can fill this slot, which results in larger-than usual wavelength shift because the optical mode is now confined primarily within the EO material, rather than interacting solely with the weak evanescent field in standard EO-cladded ring resonators. Additionally, the two halves of the silicon waveguide can be doped and act as the poling and modulating electrodes for the device, resulting in more effective application of the electric field than in most other device geometries. In principle, the slot-ring mode confinement technique can also be applied to other device architectures, including the MZM. Although considerable work is necessary to adapt the technique, this could allow for enhanced mode confinement, improved poling, and overall improved device performance in other device applications.

1.4.3 Optical Rectifier. Very recently, the slot-ring resonator device concept has been utilized to demonstrate a new effect in organic EO materials, low-power optical rectification.[34] This is the reverse process of that in MZMs, that is conversion of optical-to-electrical signals. The slot-ring mode confinement enhanced the optical

electric field such that it was able to act as a DC voltage source, and induce current flow in the poled EO material within the waveguide slot. While optical rectification has been demonstrated before with kW optical intensities,[43] this is the first demonstration of sub-mW optical rectification in EO materials. While the magnitude of the induced current was low, around 1 nA at best, it suggests the possibility of constructing efficient, low-power optical EO detectors. By combining organic EO material based MZMs and optical detectors, one could have complete electrical-optical-electrical signal conversion pathway that is compatible with VLSI. This could allow for easy integration of optical interconnects into future generations of microprocessors, allowing fast, low heat, interference free, communication between various components in computers.

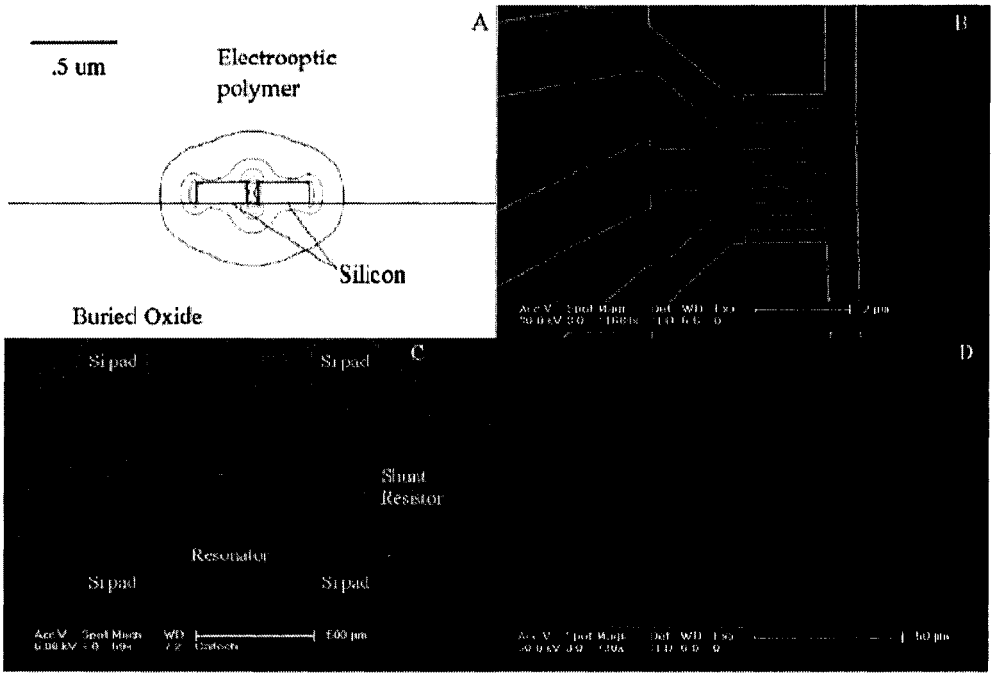

Figure 1.5. Slot-ring resonator: A) Theoretical treatment of mode confinement B) Electrical contacts to slot-ring resonator C) Full slot-ring resonator device D) Close-up of slot-ring resonator[34]

Notes to Chapter 1

(1) Shockley, W.; Pearson, G. L. Modulation of conductance of thin films of semiconductors by surface charges. *Phys. Rev.* **1948**, *74*, 232-233.

(2) Soref, R. The past, present, and future of silicon photonics. *IEEE J. Sel. Top. Quantum Electron.* **2006**, *12*, 1678-1687.

(3) Clare, A. G. Photonics: A light introduction. *Am. Ceram. Soc. Bull.* **2003**, *82*, 17-22.

(4) see, for example, www.fiber-optics.info

(5) Commercial sources include: United Technologies, Uniphase Telecommunication Technologies, and Lucent Technologies

(6) www.lumera.com

(7) Zook, J. D.; Chen, D.; Otto, G. N. Temperature dependence and model of the electrooptic effect in lithium niobate. *Appl. Phys. Lett.* **1967**, *11*, 159-161.

(8) Aoki, K.; Kondo, J.; Kondo, A.; Mori, T.; Mizuno, Y.; Shimodaira, S.; Imaeda, M.; Kozuka, Y.; Mitomi, O.; Minakata, M. High-performance optical modulator with a wide center electrode and thin x-cut linbo3 substrate. *IEEE Photonic Tech. Lett.* **2004**, *16*, 2610-2612.

(9) Turner, E. H. High-frequency electrooptic coefficients of lithium niobate. *Appl. Phys. Lett.* **1966**, *8*, 303-304.

(10) Fazludeen, R.; Barai, S.; Pattnaik, P. K.; Srinivas, T.; Selvarajan, A. A novel technique to measure the propagation loss of integrated optical waveguides. *IEEE Photonic Tech. Lett.* **2005**, *17*, 360-362.

(11) Ner, M. S.; Sharp, C.; Gibson, D. R. Environmental performance of lithium niobate (linbo3) based guided wave optical devices. *Proc. SPIE* **1990**, *1180*, 183-194.

(12) Chen, D.; Fetterman, H. R.; Chen, A.; Steier, W. H.; Dalton, L. R.; Wang, W.; Shi, Y. Demonstration of 110 ghz electro-optic polymer modulators. *Appl. Phys. Lett.* **1997**, *70*, 3335-3337.

(13) Kim, T.-D.; Kang, J.-W.; Luo, J.; Jang, S.-H.; Ka, J.-W.; Tucker, N.; Benedict, J. B.; Dalton, L. R.; Gray, T.; Overney, R. M.; Park, D. H.; Herman, W. N.; Jen, A. K. Y. Ultralarge and thermally stable electro-optic activities from

supramolecular self-assembled molecular glasses. *J. Am. Chem. Soc.* **2007**, *129*, 488-489.

(14) Shi, Y.; Zhang, C.; Zhang, H.; Bechtel, J. H.; Dalton, L. R.; Robinson, B. H.; Steier, W. H. Low (sub-1-volt) halfwave voltage polymeric electro-optic modulators achieved by controlling chromophore shape. *Science* **2000**, *288*, 119-122.

(15) Kerr, J. *Philos. Mag.* **1875**, *50*, 337.

(16) Pockels, F. *Lehrbuch der kristalloptic*; B. G. Teubner: Leipzig, 1906.

(17) Maiman, T. H. Stimulated optical radiation in ruby. *Nature* **1960**, *187*, 493-494.

(18) Prasad, P. N. W., D. J. *Introduction to nonlinear optical effects in molecules and polymers*; John Wiley and Sons: New York, 1991.

(19) Levine, B. F.; Bethea, C. G. Molecular hyperpolarizabilities determined from conjugated and nonconjugated organic liquids. *Appl. Phys. Lett.* **1974**, *24*, 445-447.

(20) Bergman, J. G.; McFee, J. H.; Crane, G. R. Pyroelectricity and optical second harmonic generation in poly(vinylidene fluoride) films. *Appl. Phys. Lett.* **1971**, *18*, 203-205.

(21) Clays, K.; Persoons, A. Hyper-rayleigh scattering in solution. *Phys. Rev. Lett.* **1991**, *66*, 2980.

(22) Clays, K.; Persoons, A. Hyper-rayleigh scattering in solution. *Rev. Sci. Instrum.* **1992**, *63*, 3285-3289.

(23) Albota, M.; Beljonne, D.; Bredas, J. L.; Ehrlich, J. E.; Fu, J. Y.; Heikal, A. A.; Hess, S. E.; Kogej, T.; Levin, M. D.; Marder, S. R.; McCord-Maughon, D.; Perry, J. W.; Rockel, H.; Rumi, M.; Subramaniam, G.; Webb, W. W.; Wu, X. L.; Xu, C. Design of organic molecules with large two-photon absorption cross sections. *Science* **1998**, *281*, 1653-1656.

(24) Drobizhev, M.; Karotki, A.; Dzenis, Y.; Rebane, A.; Suo, Z.; Spangler, C. W. Strong cooperative enhancement of two-photon absorption in dendrimers. *J. Phys. Chem. B* **2003**, *107*, 7540-7543.

(25) Bartholomew, G. P.; Ledoux, I.; Mukamel, S.; Bazan, G. C.; Zyss, J. Three-dimensional nonlinear optical chromophores based on through-space delocalization. *J. Am. Chem. Soc.* **2002**, *124*, 13480-13485.

(26) Blanchard-Desce, M.; Baudin, J.-B.; Jullien, L.; Lorne, R.; Ruel, O.; Brasselet, S.; Zyss, J. Towards highly efficient nonlinear optical chromophores: Molecular engineering of octupolar molecules. *Opt. Mater.* **1999**, *12*, 333-338.

(27) Coe Benjamin, J.; Harris James, A.; Brunschwig Bruce, S.; Asselberghs, I.; Clays, K.; Garin, J.; Orduna, J. Three-dimensional nonlinear optical chromophores based on metal-to-ligand charge-transfer from ruthenium(ii) or iron(ii) centers. *J. Am. Chem. Soc.* **2005**, *127*, 13399-13410.

(28) Bailey, R. T.; Cruickshank, F. R.; Pavlides, P.; Pugh, D.; Sherwood, J. N. Organic materials for nonlinear optics: Interrelationships between molecular properties, crystal structure, and optical properties. *J. Phys. D: Appl. Phys.* **1991**, *24*, 135-145.

(29) Zhang, C.; Wang, C.; Dalton, L. R.; Zhang, H.; Steier, W. H. Progress toward device-quality second-order nonlinear optical materials. 4. A trilink high mb nlo chromophore in thermoset polyurethane: A \"Guest-host\" Approach to larger electrooptic coefficients. *Macromolecules* **2001**, *34*, 253-261.

(30) Ramos-Ortiz, G.; Cha, M.; Kippelen, B.; Walker Gregory, A.; Barlow, S.; Marder Seth, R. Direct imaging through scattering media by use of efficient third-harmonic generation in organic materials. *Opt. Lett.* **2004**, *29*, 2515-2517.

(31) Dalton, L. R.; Harper, A. W.; Robinson, B. H. The role of london forces in defining noncentrosymmetric order of high dipole moment-high hyperpolarizability chromophores in electrically poled polymeric thin films. *Proc. Natl. Acad. Sci. U. S. A.* **1997**, *94*, 4842-4847.

(32) Chen, A.; Dalton, L.; Sherwood, T.; Jen, A. K.; Rabiei, P.; Steier, W.; Huang, Y.; Paloczi, G. T.; Poon, J. K. S.; Scherer, A.; Yariv, A. All-organic and organic-silicon photonic ring micro-resonators. *Proc. SPIE* **2005**, *5708*, 187-197.

(33) Bortnik, B.; Hung, Y.-C.; Tazawa, H.; Seo, B.-J.; Luo, J.; Jen, A. K. Y.; Steier, W. H.; Fetterman, H. R. Electrooptic polymer ring resonator modulation up to 165 ghz. *IEEE J. Sel. Top. Quantum Electron.* **2007**, *13*, 104-110.

(34) Baehr-Jones, T.; Hochberg, M.; Wang, G.; Lawson, R.; Liao, Y.; Sullivan, P. A.; Dalton, L.; Jen, A. K. Y.; Scherer, A. Optical modulation and detection in slotted silicon waveguides. *Opt. Express* **2005**, *13*, 5216-5226.

(35) Dalton, L.; Scherer, A.; Chen, A.; Jen, A.; Reid, P.; Robinson, B.; Eichinger, B.; Hochberg, M.; Baehr-Jones, T.; Pyajt, A.; Takayesu, J.; Sullivan, P.; Akelaitis, A.; Lawson, R.; Bale, D.; Haller, M.; Luo, J.; Liu, S.; Liao, Y.; Firestone, K.; Bhattacharjee, S.; Sinness, J.; Hammond, S.; Sgro, A.; Buker, N.; Snoeberger, R.; Lingwood, M.; Steier, W. Organic electro-optic glasses for wdm applications. *Proc. SPIE* **2005**, *6014*, 60140P/60141-60140P/60115.

(36) Zheng, X.; McLaughlin, C. V.; Leahy-Hoppa, M. R.; Sinyukov, A. M.; Hayden, L. M. Modeling a broadband terahertz system based on an electro-optic polymer emitter-sensor pair. *J. Opt. Soc. Am. B: Opt. Phys.* **2006**, *23*, 1338-1347.

(37) Gan, H.; Zhang, H.; DeRose, C. T.; Norwood, R. A.; Fallahi, M.; Luo, J.; Jen, A. K. Y.; Liu, B.; Ho, S.-T.; Peyghambarian, N. Hybrid fabry-perot etalon using an electro-optic polymer for optical modulation. *Appl. Phys. Lett.* **2006**, *89*, 141113/141111-141113/141113.

(38) Sun, H.; Pyajt, A.; Luo, J.; Shi, Z.; Hau, S.; Jen, A.; Dalton, L.; Chen, A. Broadband electric field sensor with electro-optic polymer micro-ring resonator on side-polished optical fiber. *Proc. SPIE* **2006**, *6117*, 611713/611711-611713/611712.

(39) Rabiei, P.; Steier, W. H.; Cheng, Z.; Dalton, L. R. Polymer micro-ring filters and modulators. *J. Lightwave Technol.* **2002**, *20*, 1968-1975.

(40) Huang, Y.; Paloczi, G. T.; Yariv, A.; Zhang, C.; Dalton, L. R. Fabrication and replication of polymer integrated optical devices using electron-beam lithography and soft lithography. *J. Phys. Chem. B* **2004**, *108*, 8606-8613.

(41) Grover, R.; Van, V.; Ibrahim, T. A.; Absil, P. P.; Calhoun, L. C.; Johnson, F. G.; Hryniewicz, J. V.; Ho, P. T. Parallel-cascaded semiconductor microring resonators for high-order and wide-fsr filters. *J. Lightwave Technol.* **2002**, *20*, 900-905.

(42) Hochberg, M.; Baehr-Jones, T.; Wang, G.; Shearn, M.; Harvard, K.; Luo, J.; Chen, B.; Shi, Z.; Lawson, R.; Sullivan, P.; Jen, A. K. Y.; Dalton, L.; Scherer, A. Terahertz all-optical modulation in a silicon-polymer hybrid system. *Nat. Mater.* **2006**, *5*, 703-709.

(43) Nahata, A.; Auston, D. H.; Wu, C.; Yardley, J. T. Generation of terahertz radiation from a poled polymer. *Appl. Phys. Lett.* **1995**, *67*, 1358-1360.

Chapter 2: Introduction to Optimizing Microscopic Nonlinearity

2.1 Introduction

Early organic electro-optic (EO) materials consisted of polar organic crystals such as hexamethylenetetramine,[1,2] urea,[3,4] and substituted benzenes such as *m*-dinitrobenzene,[4] due to their similarity to, and facile comparison with, inorganic EO crystals. These initial materials displayed low second-order susceptibilities, however, due to the relatively low first molecular hyperpolarizability (β) values. Polar crystals of m-nitroaniline were subsequently found to be significantly more nonlinear optically (NLO) active than those of *m*-dinitrobenzene,[4-6] which was attributed to an increased β due to the charge-transfer contribution from the donor-acceptor substitution.

Around this time, the extension of the DC-electric field induced second-harmonic generation (EFISH) technique from the vapor phase,[7] to the solution phase (Section 2.4.2), allowed the measurement of molecular hyperpolarizability (as a combination of the dipole moment, and the first and second molecular hyperpolarizabilities) of highly polar molecules that would decompose in the vapor-phase experiment.[8,9] As a result, the β values of *o*, *m*, and *p*-nitroaniline could be compared, and the *para* derivative was found to be significantly more NLO active than the *meta* derivative, which was in turn significantly more active than the *ortho* derivative.[10] This trend was explained by the increased charge-transfer character, and the increased spatial extension of the conjugated system, in the *para* and *meta* derivatives.

The EFISH data was critical in the derivation of Oudar and Chemla's two-level model (Section 2.2.4),[11] a practical model that has guided understanding of the structure-property relationships in donor-π-acceptor chromophores. This theory, in combination with the more rigorous sum-over-states theory (SOS, Section 2.2.3)[12] and the polyene-centric bond length alternation theory (BLA, Section 2.2.5),[13] have been pivotal in guiding the development of improved electron donors (Section 2.3.1), acceptors (2.3.2), and π-conjugated bridges (2.3.4).

Currently, the use of density function theory (DFT, Section 2.2.2)[14] allows for rapid and predictive quantitative evaluation of target EO chromophores.[15] Molecular engineering of state-of-the-art high β chromophores is now practical through coupling DFT predictions with accurate experimental β values that are independent of dipole moment (μ), from hyper-Rayleigh scattering (HRS, Section 2.4.3) measurements.[16] As a result, EO chromophores have been transformed from the simple nitroaniline derivatives to complex and powerful chromophore architectures, such as the ring-locked tetraene (CLD)[17] and thienylene-vinylene (FTC)[18] systems (Section 2.3.3) in use today.

2.2 Theoretical Guidance

Developing theoretical models, as well as analytical methods, to explain experimental results and predict new trends, especially due to the extremely complex and often non-intuitive structure-property relationships, is of utmost importance in the field of organic EO. A large number of theoretical modeling methods have been developed to help explain and predict the dependence of the molecular

hyperpolarizabilities on chromophore structure. Early models were relatively simple phenomenological treatments of the simple chromophores being explored. For example, the equivalent internal field (EIF) model treats the polarization ($\Delta\mu$) of the symmetric π-electron cloud of benzenes arising from an internal electric field (E_0) created by substitution with electronegative (or electropostitive) elements.[19] The difference in induced dipole moment (μ_{ind}, related to β by the power series expansion), between the symmetric and substituted benzenes in an applied electric field depends on the internal electric field, and thus the β value can be related to $\Delta\mu$. The β value derived from EIF modeling depends on the field applied, however, and the model only works for simple mono-substituted benzenes and stilbenes. Another example is the various additivity models for hyperpolarizability,[20,21] which attempt to treat the β tensor of a molecule as an additive property of the component bonds. These models are particularly inappropriate for modern chromophores, as the complex π-electron systems cannot adequately be treated as additive, rather they must be treated as a whole.

The most successful analytical methods for computational analysis of organic EO materials have all been quantum chemical methods. These models rely on the laws of quantum mechanics to define the properties of the molecules and their interactions with light. While a detailed description of quantum chemical methods is beyond the scope of this work, a brief overview of the most successful methods, and their salient features, is educational. All of these methods share the use of a Hamiltonian expression to define the electronic and nuclear positions, and thus the properties of the molecule; however, the form of the Hamiltonian and the method used to derive the hyperpolarizabilities can vary widely. Additionally, the results of the calculations

depend heavily on the atomic orbital basis set used to build up the molecules. There are a large number of basis sets, which vary considerably in terms of the orbitals included for each atom, their computational complexity, and to which types of calculations they are applicable.

2.2.1 Derivative Method. In the derivative method, all the hyperpolarizabilities are calculated as derivatives of the energy or the dipole moment,[22] which are obtained from the Hamiltonian solutions for the molecule in an applied electric field. This Hamiltonian is generally solved under the self-consistent field (SCF) Hartree-Fock formalism,[23] often limited to a time-independent model, eliminating the dispersion (wavelength dependence) of the hyperpolarizabilities. The solution provides expressions with optimized coefficients (to minimize the energy) for the molecular orbitals in terms of linear combinations of the atomic orbital basis sets. The molecular orbital description is then used to solve for the field-dependent descriptions of the energy or dipole moment, and the hyperpolarizabilities are finally obtained by numerical or analytical differentiation of these expressions. Such calculations are computationally intensive, limiting the size and number of molecules that can be investigated, thus semi-empirical parameterizations are often used to reduce computational complexity.[22] While these semi-empirical methods decrease computation time, the results are only as accurate as the parameterization used, which often restricts the applicability to relatively well-studied systems, reducing their usefulness.

2.2.2 Density Functional Theory. Density functional theory (DFT) is a unique quantum chemical model in that it utilizes a Hamiltonian that describes the electron density,[14]

rather than the positions of the electrons. Hohenberg and Kohn proved that the ground-state electron density and the ground state electron position wavefunction have a one-to-one mapping,[24] and thus they can be used equivalently. As a result, a complex multiple-electron wavefunction problem can be reduced to a simpler problem of describing the motion of individual electrons in a potential field. The nature of this potential field arises from the nuclear positions and the electron interactions: the exchange and correlation interactions. While treating these interactions analytically is extremely difficult, just as in Hartree-Fock formalism for the multiple-electron wavefunction approach,[23] approximations can be made, and a significant savings in computational time is achieved by separating out the electronic interactions. The simplest approximation is the local density approximation (LDA),[14] obtained from the free electron gas model, where the electron interactions depend solely on the density at the coordinate evaluated. The generalized gradient approximation (GGA) also takes into account the gradient of the density at the coordinate evaluated,[14] and as such is a more accurate approximation. However, the GGA approximation is "trained" on a set of molecules, and thus it is effectively a semi-empirical method. By minimizing the energy of the system, one obtains the most accurate description of the electron density, and then the dipole moment can be calculated directly from the electron density and nuclear positions. By varying the direction and magnitude of the applied electric field, expressions can be obtained for the various hyperpolarizability tensor elements, and by combining terms, the complete hyperpolarizability tensor can be determined. DFT can also be extended to the time-dependent domain (TDDFT),[25] which allows computation of excited states, and thus the dispersion properties of the hyperpolarizabilities.

2.2.3 Sum Over States Theory. Perhaps the most widely acknowledged rigorous analytical model is the sum-over-states (SOS) theory of Ward.[12] It is another quantum chemical method, where the hyperpolarizabilities are calculated from the corresponding order-of-dependence on the field strength terms obtained, via solution of the many-electron wavefunction Hamiltonian, for perturbation of the energy in an applied electric field (Stark energy). Although the SOS theory is rarely used anymore to compute hyperpolarizabilities, this model has unique significance. It provides the theoretical basis for a relatively simple description for the hyperpolarizability (the Two-Level Model, Section 2.2.4),[11] which allows intuitive interpretation of the structure-property relationships. This is a key contribution, as most quantum chemical methods provide complicated computational descriptions for the hyperpolarizabilities that provide little conceptual understanding, even if they are useful for accurately calculating values.

By considering the applied electric field (with frequency ω, as from an intense electro-magnetic wave) as a perturbation

$$H' = -e(E^{\omega} \cdot r)\sin(\omega t) \tag{2.1}$$

which induces electron currents that polarize the molecule, the resulting dipolar components can be calculated from the position of all the electrons (r_i) in the system

$$r = \sum_i r_i \tag{2.2}$$

The result is expressions for the polarizability tensors in terms of an infinite sum over all excited states. Under second-harmonic generation (SHG) conditions, the expression for β takes the form of:

$$\beta(-2\omega;\omega,\omega) = p\sum_{n_1 n_2}\left(\frac{e^3}{2\hbar^2}\right)\frac{r_{gn_2}r_{n_2n_1}r_{n_1g}}{\left(\omega-\omega_{n_1g}\right)\left(2\omega-\omega_{n_2g}\right)} \tag{2.3}$$

where p indicates that summation must be performed over all permutations of the Cartesian indices (molecular i, j, and k framework). The summation of the electronic position operators, $r_{n_2 n_1}$, and the electronic transitions, $\omega_{n_2 n_1}$, is performed over all electronic states, n, including the ground state, g. Since

$$-er = \mu, \tag{2.4}$$

when $n_1 = n_2$, the r term is a dipole moment, and when $n_1 \neq n_2$, the term is a transition dipole moment, and thus the sum involves products of dipole moments and transition dipole moments over a variety of states. It can be seen from the denominator in Equation 2.3 that as the fundamental frequency of the optical beam (ω) *or* its second-harmonic (2ω) approaches the frequency of an electronic transition in the molecule ($\omega_{n_x g}$), then β becomes significantly enhanced; a condition known as resonance enhancement. It does not become infinite, however, as at resonance the frequency is modulated by a complex damping term such that:

$$\omega = \omega_{n_x g} + i\Gamma_{n_x g} \tag{2.5}$$

These resonant enhancements have significant consequences for the development of EO materials. Although the resonant enhancement from the fundamental frequency does, in principle, translate to materials in an EO device, the operation of a device near an electronic transition would lead to unacceptable absorptive losses. The second-harmonic resonance condition, however, does not translate into an EO device, as the device does not operate under SHG conditions (-2ω;ω,ω), but rather under EO conditions (−ω;ω,0). Under the EO conditions the SOS equation for β would have a different form, without the second-harmonic term. Both quantitative techniques

used to measure β (EFISH, Section 2.4.2 and HRS, Section 2.4.3),[8,16] however, *do* operate under SHG conditions and thus are subject to second-harmonic resonance enhancement. Therefore, the accurate measurement of a β value that is applicable to EO devices is a difficult endeavor; one must take care to avoid measurement frequencies whose fundamental *and* second harmonic are near electronic transitions in the molecule of interest.

2.2.4 Two-Level Model. While the SOS model provides a rigorous analytical description of β and serves to illustrate the issue of resonance enhancement, due to the complexity of the resulting equation it does not provide significant insight into structure-property relationships for chromophores. To gain such understanding, one must look to the simplifying approximations of the two-level model (TLM) developed by Oudar and Chemla.[11] Originally, they proposed that the total β can be considered the sum of two components, an additive term (β_{add}) and a charge-transfer term (β_{ct}). They calculated the additive term from the EIF model,[19] assuming an additive effect from the two substituents on the internal field, and the charge-transfer term was calculated from the SOS description for β, applying the approximation that only the ground and first-excited states (the two charge-transfer states) contribute. Furthermore, they assume that the higher order states are accounted for in the β_{add} term, the non-charge-transfer component. The resulting equation for β_{ct}, again under SHG conditions, in terms of the frequency (ω) of the optical electric field is:

$$\beta(-2\omega;\omega,\omega) \approx \frac{3e^2}{2\hbar m}\frac{\omega_{eg} f \Delta\mu}{\left(\omega_{eg}^{\ 2}-\omega^2\right)\left(\omega_{eg}^{\ 2}-4\omega^2\right)} \propto \frac{\Delta\mu\mu_{eg}^2}{E_g^2} \qquad (2.6)$$

where ω_{eg} is the optical frequency of the transition between the two states, f is the oscillator strength (or, equivalently the extinction coefficient, ε), and is related to the transition moment between the two states (μ_{eg}) , and $\Delta\mu$ is the difference in dipole moments between the two states.

Equation 2.6 is advantageous in that it allows for the calculation of β from parameters that are primarily readily available from spectroscopic measurements, and all of which have a direct and relatively straightforward correlation with molecular structure. Utilizing ultraviolet-visible (UV-vis) absorption spectroscopy, the ω_{eg}, ε (f), and μ_{eg} terms of the charge-transfer band may be measured. The frequency (ω_{eg}) is directly proportional to the band gap (E_g), which depends on the energy of the highest occupied molecular orbital (HOMO, the ground state) and lowest unoccupied molecular orbital (LUMO, the first-excited state). The energy of these orbitals depends on the molecular structure, in particular on the nature of the π-electron bridge (Section 2.3.3), as well as the strength of the electron donor (Section 2.3.1) and electron acceptor (Section 2.3.2) elements. Increasing donor and acceptor strength, for a given bridge, generally increases and decreases the HOMO and LUMO energies, respectively, resulting in a smaller E_g and an increased β. However, this also results in a red-shift in the wavelength of maximum absorption (λ_{max}), which can lead to absorptive optical loss at the telecommunications frequencies of interest at 1.31 and 1.55 μm. As previously mentioned, ε/f is related to μ_{eg}, which can be obtained by integrating under the absorption peak. The transition moment is a function of the overlap between the two electronic states; thus making the two states more similar increases the transition moment, the oscillator strength, and β.

The difference in dipole moment between the two states is more difficult to measure. While the ground-state dipole moment can be measured from the capacitance and dissipation of dilute solutions,[26] it is generally calculated using computational means, but with questionable accuracy. The excited-state dipole moment is difficult to measure exactly, but it can be estimated from solvatochromism data (Section 2.4.1),[27] or calculated from the optimized structure of the chromophore using time-dependent quantum chemical methods. The correlation between the dipole moment difference and molecular structure is relatively straightforward, however, as the relative polarity of the ground and excited states can easily be understood. Increasing this difference in polarity should result in an increase in β, but also a *decrease* in the transition moment by decreasing the similarity of the two states. Therefore, $\Delta\mu$ and μ_{eg} present a trade-off, and the molecular structure must be carefully optimized to balance the degree of similarity (μ_{eg}) and difference ($\Delta\mu$) between the HOMO and LUMO orbitals.

Table 2.1. Comparison of calculated and experimental values of β for the three nitroaniline isomers[11]

	β_{add} (10^{-30} esu)	β_{ct} (10^{-30} esu)	β_T (10^{-30} esu)	β_{exp} (10^{-30} esu)
o-NA	2	10.9	12.7	10.2
m-NA	3.1	4	7	6
p-NA	3.5	19.6	23	34.5

Oudar and Chemla calculated the β_{add} and β_{ct} values for the nitroanilines (NA), and compared their vector sum (β_T) to experimental values (β_{exp}) obtained from EFISH and four wave mixing (FWM) experiments.[11] The results, shown in Table 2.1, demonstrate a high degree of accuracy for such simple calculations, and indicate the relatively small contribution from the β_{add} term with respect to the β_{ct} for *p*-nitroaniline (PNA), the strongest isomer. As chromophores were developed further, following the

guidance of the TLM structure-property relationships, the β_{add} term became increasingly negligible, as compared to the β_{ct} term, and it become increasingly less valid for the more complex chromophore structures. The theory eventually came to be considered as consisting solely of the charge-transfer or TLM form expressed in Equation 2.6. Ironically, as chromophores were developed using understanding of the structure-property relationship gleaned from the TLM, the model became less and less applicable. Only in the simplest of systems, such as the NA, is the TLM accurate. In the complicated chromophore systems currently being studied, while the ground and first excited states still contribute the most, and provide valuable information, higher states clearly contribute a significant amount and the TLM fails in providing accurate β values.

2.2.5 Bond Length Alternation Theory. While not a quantum chemical method, the bond length alternation (BLA) theory has provided a practical and predictive method for understanding the structure-property relationships in the polyene chromophores.[13,28,29] The polyenes (Section 2.3.3), composed of π-conjugated bridges consisting of alternating carbon-carbon single and double bonds, have been a key figure in the development of organic EO materials. This unique class of chromophores has been useful in furthering our understanding of chromophore structure-property relationships, and it contains one of the most successful chromophores to date (CLD, Section 2.3.3).[17] The development of such polyene chromophores was aided by BLA theory, originally developed by Marder and coworkers for optimizing second molecular hyperpolarizability (γ).[13]

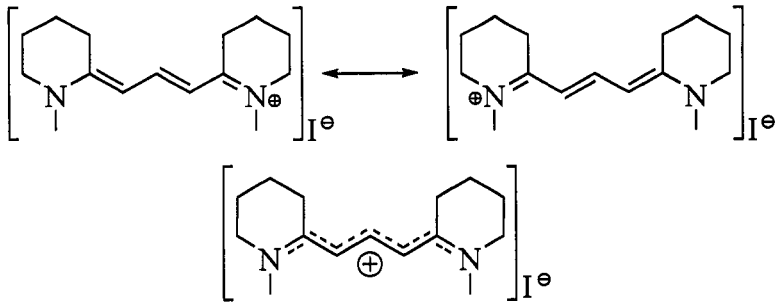

Figure 2.1. Two degenerate resonance structures and the charge-delocalized ground state of a cyanine dye

While it would appear that increasing the donor and acceptor strength, for a given bridge structure, should always increase β by reducing E_g, this is not always the case. As the donor and acceptor strengths increase, the chromophore approaches what is called the cyanine limit. The cyanines are a class of chromophores in which two nitrogen heterocycles are connected via a polymethine (polyene) chain.[30] Their unique feature is that the two resonance forms are degenerate (or nearly so) in structure and energy, and thus the ground state can be considered a hybrid of the two (Figure 2.1). Thus, the cyanine limit refers to the condition in any chromophore where both the HOMO and LUMO (both resonance forms) are roughly equivalent in energy. While this leads to a very small E_g and large μ_{eg}, the $\Delta\mu$ term would be practically zero and thus from the TLM β should be minimal as well.

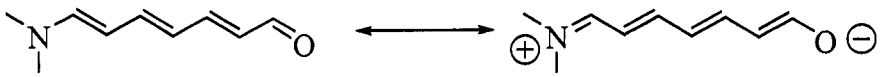

Figure 2.2. Resonance structures of chromophore for BLA study

Marder and coworkers chose to explore this phenomenon by correlating the donor and acceptor strengths with the BLA parameter, $\langle\Delta r\rangle$, which is defined as the difference between the average bond lengths for carbon-carbon single and double bonds in the polymethine backbone.[28] The geometry of a simple dimethylamino donor and

aldehyde acceptor polyene (Figure 2.2) was optimized in the presence of a static electric field, which served to vary the effective donor/acceptor strength, providing $<\Delta r>$, and the β was calculated via the derivative method (Section 2.2.1) using a finite field Hartree-Fock technique.[28,29] Starting from the left in Figure 2.3, small values of the static field represent weak donor/ acceptor (D/A) strength, which should produce little mixing of resonance states, and resulted in large values of $<\Delta r>$, around 0.1 Å, and low β values. As the D/A strength (static field) was increased, $<\Delta r>$ decreased due to increased mixing of the two states, and β values increased. A positive maximum in β occurred at $<\Delta r> \sim 0.03$-0.05 Å. Further increase in D/A strength lead to a decrease in β, with the expected vanishing of β at $<\Delta r> = 0$ Å, corresponding to the cyanine limit. As D/A strength was further increased, $<\Delta r>$ started to increase again, but β decreased into negative values. This corresponds to chromophores with a zwitterionic (ZI) ground state, or right-hand-side (RHS) chromophores, in contrast to chromophores with a positive beta, which possess a neutral ground state (NGS), and are called left-hand-side (LHS) chromophores. From the TLM (Section 2.2.4) it is clear that ZI chromophores should have a negative β; since their ground state is more polar than the excited state, and hence the $\Delta\mu$ term should be negative. As D/A strength was increased more, β achieved a maximum (negative) value, and then decreased as $<\Delta r>$ continued to increase.

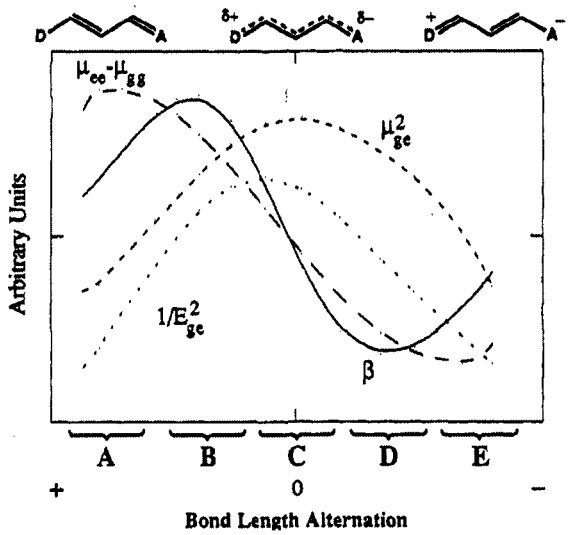

Figure 2.3. Calculated dependence of β, $\Delta\mu$, μ_{eg}, and E_g parameters on $<\Delta r>$[28]

While BLA theory is only strictly applicable to polyene chromophores, the concepts can also be applied to other types of chromophores. Although the BLA parameter is not easily defined for chromophores not based on polyene bridges, we can simply replace the parameter with D/A strength with which it is correlated. For every bridge structure there exists an ideal combination of D/A strength, which will produce a maximum in β; any increase or decrease in D/A strength will only reduce β. While in theory two maxima in β exist for every bridge, only certain structures can achieve ZI ground states at physically relevant D/A strengths. Highly aromatic bridges, for example, cannot achieve ZI ground states due to the high energy of the anti-aromatic state present in the ZI form. Conversely, bridges optimized for ZI chromophores, although capable of existing in NGS form, cannot achieve a positive maximum in β. The shape of the curve relating β and D/A strength will be different for every bridge, and in general will not have the sinusoidal shape of the polyenes. To summarize, one must choose a bridge structure optimized for either NGS/RHS or ZI/LHS

chromophores, and tailor the D/A strengths for the specific bridge structure in order to maximize β of the chosen sign.

2.3 Chromophore Structure

All organic EO chromophores consist of three basic elements: one or more electron donating moieties, one or more electron accepting moieties, and a bridge that connects them. The major focus of this work, as well as the bulk of the research literature, is on the donor-π-acceptor chromophore architecture, consisting of a single electron donor, a single electron acceptor, and a fully π-conjugated bridge between them. There are other chromophore architectures, however, such as the through-space charge transfer chromophores,[31] where the π-electron bridge is disrupted, and the octupolar chromophores, which have an octupolar charge distribution due to multiple donor and acceptor elements.[31-33] In all organic EO chromophores, the basic elements remain the same and are subject to the same optimization. By increasing the strength of both the electron donors and acceptors, as well as tuning the bridge to match the properties of the donor and acceptor, chromophores with higher β values can be obtained in all architectures.

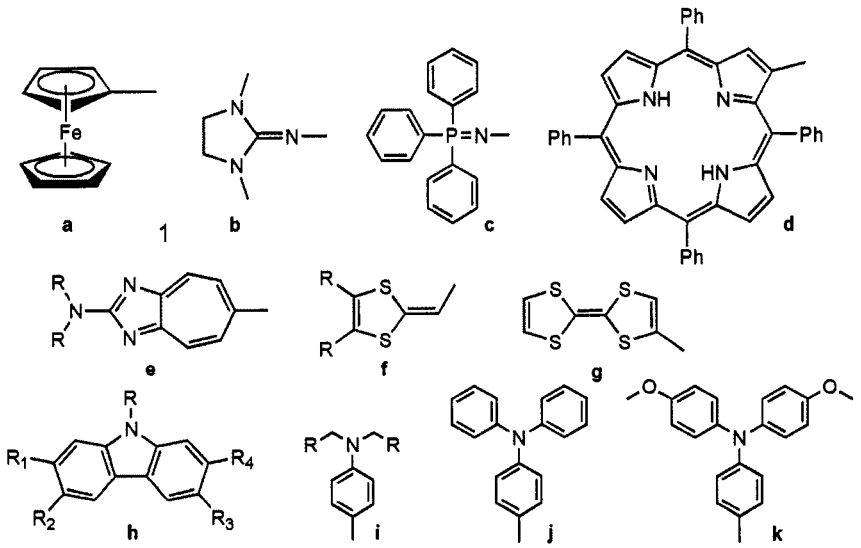

Figure 2.4. Recently used electron-rich donor moieties

2.3.1 Donors. A large number of electron donating groups have been explored over the past several decades. Recent studies have investigated ferrocenyl (Figure 2.4a),[15,34,35] guanidyl (Figure 2.4b),[36] azaphosphane (Figure 2.4c),[37] porphyrin (Figure 2.4d),[38] cycloheptimidazole (Figure 2.4e),[39] 1,3-dithiol-ring (Figure 2.4f),[35,40] tetrathiafulvalene (TTF, Figure 2.4g),[41] carbazole (Figure 2.4h),[42] and aryl-amine (Figure 2.4i,j,k)[43,44] based electron donor moieties. Aryl-amine based electron-rich moieties have remained the donors of choice for decades, since they exhibit large β values and good thermal stabilities in chromophores incorporating them, and also for their low-cost commercial availability. This class of materials attributes its large electron donating ability to the low ionization energy of nitrogen compared to those of phosphorous, sulfur, and oxygen.

Dialkyl-anilines have been among the most common derivatives, and functionalizable analogues are readily accessible, providing convenient points of attachment for macromolecular structures. Although triphenyl-amine based systems have been shown to exhibit enhanced thermal and photochemical stability as compared

to dialkyl-aniline based systems,[45] these chromophores tend to possess lower β values.[46] Recently, the introduction of *p*-alkoxy substituents on the phenyl groups has resulted in a dramatic increase in EO activity, while retaining the desirable thermal and photochemical stability of the triphenyl-amines.[44,47,48] The main disadvantage of these systems is the difficulty in functionalizing them, which makes them harder to incorporate into macromolecular systems.

2.3.2 Acceptors. Electron accepting moieties present a unique challenge in the synthesis of dipolar second-order nonlinear optical chromophores with high β values. While weak electron acceptors, such as nitro, nitrile, and *p*-nitrophenyl groups are highly stable and trivial to incorporate into chromophores, such systems exhibit low β values.[49] Powerful electron acceptors, however, are generally relatively unstable due to their extreme electron deficiency. Enhancing electron-accepting power while maintaining sufficient stability to synthesize, store, and incorporate such groups into chromophores has proved to be a significant challenge. Additionally the chemical and thermal stability of the completed chromophore, which can depend significantly on acceptor structure, must also be considered.

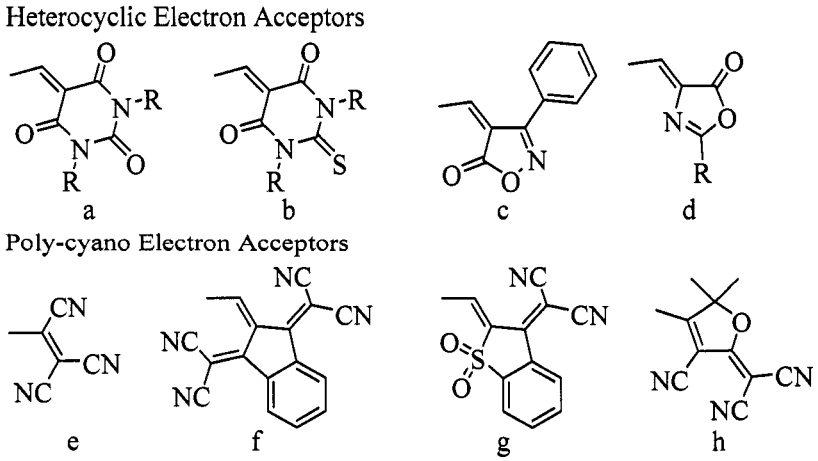

Figure 2.5. Electron accepting groups

Aside from the development of charged acceptors such as pyridinium and diazonium salts, which are useful for self-assembling chromophore systems,[50,51] much of the research has focused on developing highly electron-deficient heterocyclic rings. A wide variety of such structures have been explored, including barbituric and thiobarbituric acid derivatives (Figure 2.5a,b),[52,53] isoxazolones (Figure 2.5c),[53] and oxazolones (Figure 2.5d).[54] Nitrile groups have proven to be one of the most advantageous substituents for increasing electron deficiency in such rings while still maintaining acceptable thermal and chemical stability. Indeed, the easy to incorporate tricyanovinyl moiety (Figure 2.5e) is a stronger acceptor than many novel heterocyclic compounds.[49] Several polycyano-substituted rings have been synthesized by taking advantage of the facile condensation between malononitrile and carboxyl groups (Figure 2.5f-h).[55,56]

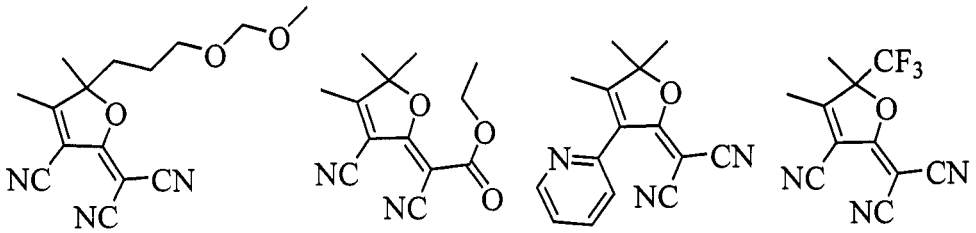

Figure 2.6. TCF-based acceptors

Arguably the most successful structure in acceptor design currently is the 2-cyanomethylene-3-cyano-4,5,5-trimethyl-2,5-dihydrofuran (TCF, Figure 2.5h) system and its derivatives (Figure 2.6).[57-60] This tri-cyano substituted dihydrofuran ring is highly electron-withdrawing and the nitrile groups are roughly aligned with the charge-transfer axis, further increasing its effectiveness. Chromophores incorporating the TCF acceptor exhibit significantly higher β values than similar structures with the previously

mentioned acceptors, yet possess relatively good chemical and thermal stabilities. TCF itself is easily synthesized by thermally activated condensation between two equivalents of malononitrile and the commercially available 3-hydroxy-3-methyl-2-butanone.[57] Attachment of TCF to the donor-bridge-aldehyde is achieved in high yields via standard Knoevenagel conditions, and the methyl position is sufficiently activated that often no base catalyst is required.

The TCF structure is also highly versatile, allowing for a wide range of derivatives to be developed by varying the α-hydroxyketone and the activated methylene (e.g. malononitrile) with which it is condensed. A number of derivatives have been prepared or explored, including a protected-hydroxyl (MOM-TCF, Figure 2.6a),[60] an ester (Figure 2.6b), a pyridinyl (Figure 2.6c), and a CF_3 (CF_3-TCF, Figure 2.6d) functionalized acceptor.[59] Synthesis of most of the derivatives relied on the development of an alternative synthetic methodology using a focused microwave reactor to provide rapid local heating.[58] This method afforded the cyclized imine intermediate produced from condensation of the α-hydroxyketone with only one equivalent of malononitrile (Scheme 2.1), which is reactive and rapidly condenses with a second equivalent of malononitrile under thermally activated conditions. Using the microwave conditions, structurally diverse activated methylenes can be condensed with the α-hydroxyketone or with the imine.

In theory, this synthetic method could provide access to nearly limitless TCF derivatives, as suggested by the generic synthesis outlined in Scheme 2.1. In practice, however, the range of structures accessible is significantly smaller. Obviously, the steric constraints of the ring limit the size of the substituents, particularly R_3 and R_4.

More importantly, the electronics of both the ring and the activated methylene are difficult to balance; if groups more electron withdrawing than nitrile are placed on the methylene it becomes less nucleophilic, and eventually will not condense with either the α-hydroxyketone or the imine. Additionally, if the substituents are too electron withdrawing, the imine becomes destabilized and it can decompose or react with trace water to form an inert lactone before it can be further condensed with an activated methylene.[58]

Scheme 2.1. Generic synthesis of TCF derivatives

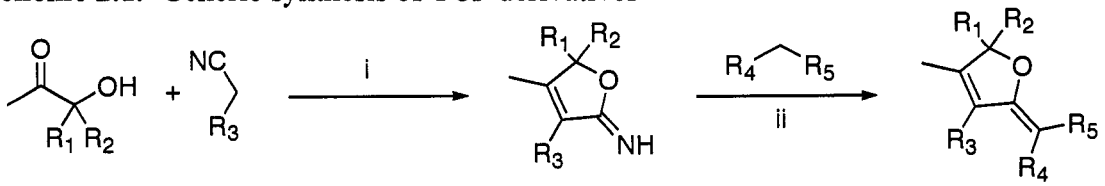

Conditions: i) NaOEt, EtOH, Focused Microwave Reactor ii) NaOEt, EtOH, Focused Microwave Reactor

Interestingly, one of the most powerful electron acceptors to date, CF_3-TCF, is derived from substitution at the unconjugated R_1/R_2 position, rather than at sites along the conjugated pathway (Figure 2.6).[59] While the CF_3 group is electron-deficient, the inductive effect alone cannot account for the significant enhancement in β values of chromophores incorporating CF_3-TCF compared to those containing TCF. It has been suggested that hyperconjugation between the C-F bonds and the lone pair electrons on the O atom and the p-orbital on the C_4 atom.[59] If accurate, the hyperconjugation enhances the effective area over which the electrons are delocalized, thus increasing the electron accepting ability of the acceptor and the β of chromophores containing it. Advantageously, this is achieved without significantly destabilizing the intermediates, the acceptor, or chromophores that incorporate it. As such, it is one of the most

successful TCF derivatives to date. This suggests that the use of additional electron-deficient hyperconjugating substituents in the R_1/R_2 positions could further enhance acceptor strength without decreasing reactivity and stability. Several derivatives based on CF_3-TCF have recently been developed that aim to increase the 3D structure of the acceptor to reduce intermolecular dipole-dipole interactions (Chapter 3),[48,61] in addition to enhancing acceptor strength.

2.3.3 Bridges. Although a number of different π-conjugated bridge structures have been investigated, a significant percentage of the most successful EO chromophores have been based on either a conformationally-restricted polyene-type bridge, such as CLD (Figure 2.7),[17] or a low HOMO – LUMO gap heteroaromatic bridge, such as the thiophene-based FTC (Figure 2.7).[18] Although elongation of these bridges via straightforward extension of the bridging units provides a tempting approach to increasing β values, the substantial red-shift in optical absorption accompanying bridge extension rapidly leads to unacceptable optical loss at the telecommunication frequencies.

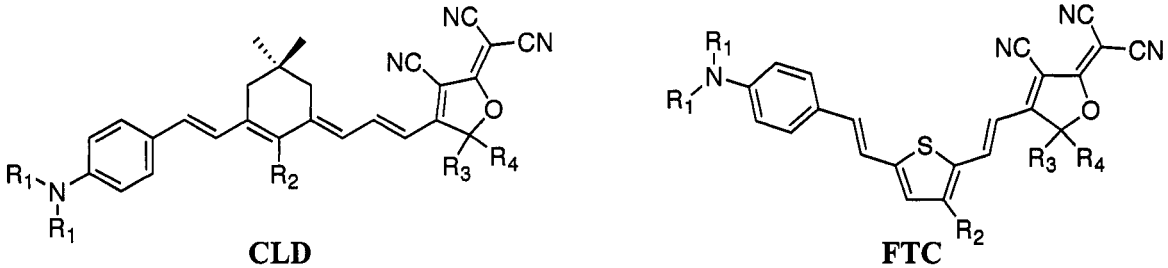

Figure 2.7. Highly successful EO chromophore bridges

Arguably, the most successful bridge class used in the synthesis of high β EO chromophores is that of the ring-locked tetraenes (CLD). Chromophores based upon the CLD bridge generally yield the highest β values, and are incorporated into the most

active EO materials to date.[17,48,62-65] This high nonlinearity comes at a price, as CLD chromophores are less stable and more difficult to functionalize than other bridges. The CLD bridge is typically synthesized starting with the Schmidt condensation of isophorone with various *p*-amino benzaldehydes to yield a ketone (Scheme 2.2). Use of a functionalized isophorone can afford side-functionalized CLD chromophores, but results in a significant reduction in yields.[65] Horner-Emmons olefination of the ketone using di-*iso*-propylcyanomethyl phosphonate produces a conjugated nitrile derivative, which can be reduced with DIBAL-H to produce an aldehyde. The conformation of the exocyclic double bond is a mixture of *cis* and *trans* in unfunctionalized isophorones, which is expected to affect the properties of the molecule. A potential benefit of side-functionalized CLDs is the restriction to the all-*trans* isomer in these systems.[65] A final Knoevenagel condensation with the activated methyl or methylene of the electron acceptors produces the targeted chromophore.

Scheme 2.2. General synthesis of CLD-type chromophores

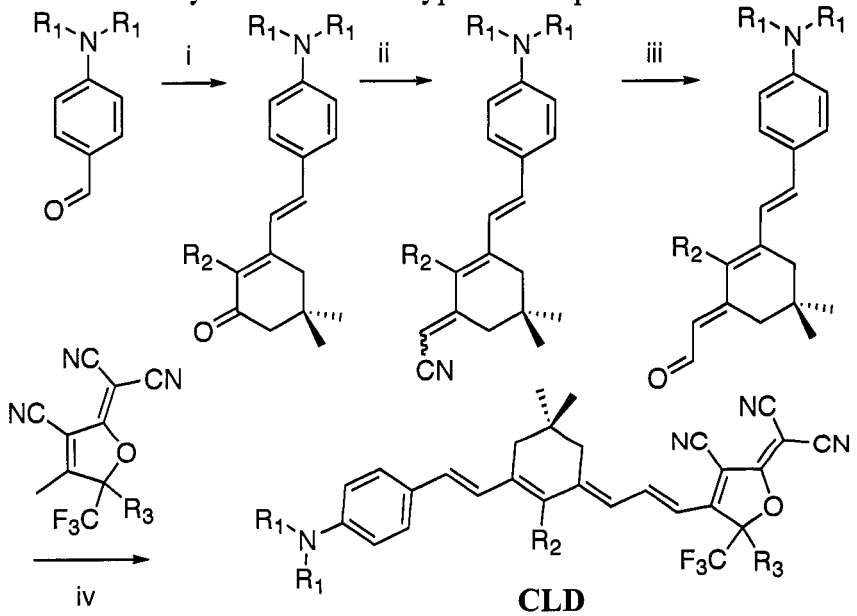

Conditions: i) isophorone, NaOEt, EtOH ii) *n*-BuLi, di-*iso*-propylcyanomethyl phosphonate iii) DIBAL-H, CH_2Cl_2 iv) EtOH

A second class of chromophore bridges that has seen widespread application is the thienyl-vinylene unit (FTC). The thiophene-based bridge offers only slightly lower β values than similar CLD-based chromophores combined with versatility in secondary functionalization, high thermal, chemical, and photostability, and ease of synthesis.[15,18,61,63,64,66-68] A diethyl thienylmethyl phosphonate is usually chosen for olefination of *p*-amino-benzaldehydes to yield the donor bridge structure in high yield (Scheme 2.3). The synthesis of side-functionalized FTCs typically requires additional functionalization of the thiophene 4-position at this step, commonly effected by kinetic formylation and subsequent reduction.[68] Further formylation then yields the donor-bridge-aldehyde. Knoevenagel condensation conditions can again be used to obtain the targeted chromophores in high yields.

Scheme 2.3. General synthesis of FTC-type chromophores

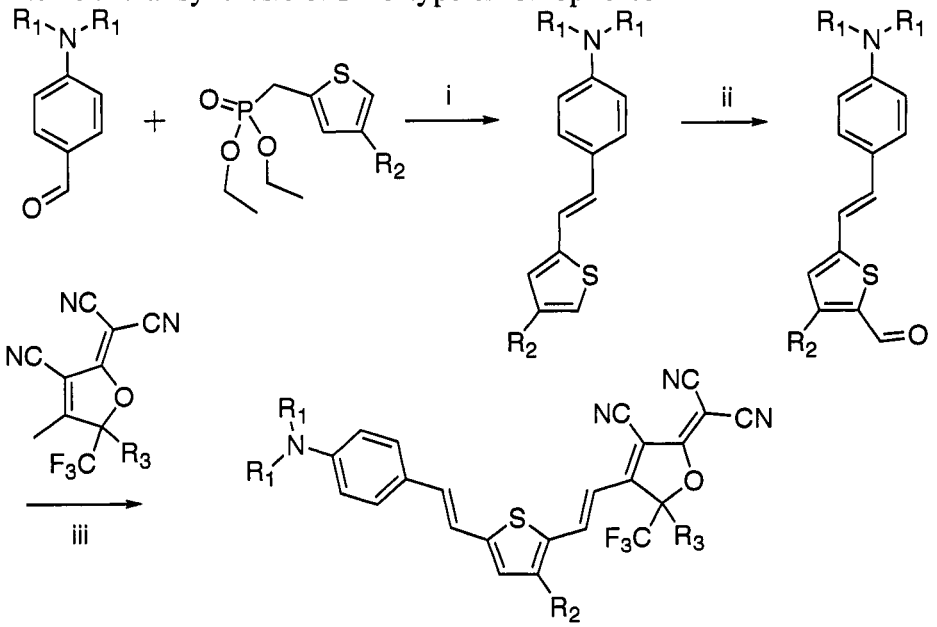

FTC

Conditions: i) *t*-BuOK, THF ii) *n*-BuLi, DMF, THF, –78 °C iii) EtOH

2.4. Microscopic Characterization

The experimental determination of molecular hyperpolarizability (β) is a key component in characterization of new EO chromophores. Unfortunately, measuring β is experimentally challenging and the results can be difficult to interpret. As previously discussed (Section 2.2.3), the principle methods for measuring β (EFISH, Section 2.4.2 and HRS, Section 2.4.3) are subject to resonance enhancement when either the fundamental frequency (ω) *or* the second-harmonic (2ω) of the optical measurement beam approach the frequency of an electronic transition in the molecule. However, neither of these enhancements translates into practical device utility, so it is easy to overestimate the effective β of a chromophore.

In the literature, this dispersive behavior is often accounted for within the TLM (Section 2.2.4),[11,69] by separating the frequency dependent term [D(ω)] from the frequency independent (β_0) term:

$$\beta(-2\omega;\omega,\omega) = \beta_0 D(\omega) \approx \frac{\Delta\mu\mu_{eg}^2}{E_g^2} \frac{\omega_{eg}^{\ 4}}{\left(\omega_{eg}^{\ 2} - \omega^2\right)\left(\omega_{eg}^{\ 2} - 4\omega^2\right)} \qquad (2.7)$$

Experimental results are converted to frequency-independent β_0 values by dividing out the D(ω) term. It has been shown, however, that the TLM does not adequately describe high β EO chromophores, and the D(ω) term in particular doesn't adequately incorporate the damping term (Equation 2.5).[70] Attempts have been made to incorporate the damping term and more accurately describe the dispersive nature of β,[70,71] but more work is necessary before β_0 values can be considered reliable. Until

such models are perfected, care must be taken to evaluate EO chromophores at off-resonance wavelengths.

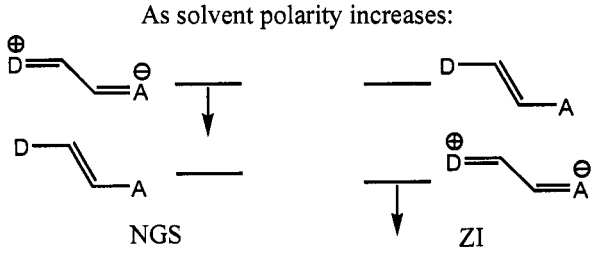

Figure 2.8. Solvatochromic behavior of ZI and NGS chromophores

2.4.1 Solvatochromism. The solvent-dependent shift in the position, shape, and intensity of optical transitions of a chromophore (solvatochromism) has long been used as a rapid benchmark of nonlinearity. If we restrict our discussion to the simplifications of the TLM (Section 2.2.4), the shift in position of the main charge-transfer band arises because the energy of the charge-separated state is highly dependant upon the polarity of the nanoscale environment surrounding the chromophore. The nature of this shift depends on whether the chromophore is NGS/LHS or ZI/RHS, as demonstrated in Figure 2.8. For NGS chromophores, the excited state is stabilized as the polarity of the environment is increased; thus the band gap is decreased, leading to a bathochromic (red) shift in the wavelength of maximum absorption (λ_{max}). For ZI chromophores, it is the ground state that is stabilized by increased polarity, resulting in a hypsochromic (blue) shift in λ_{max}. Thus, the direction of the shift indicates the type of chromophore, and the magnitude of the shift is a qualitative indicator of the polarizability and hyperpolarizability.

Solvatochromism can also be used to help provide a quantitative estimate of β without the use of expensive laser systems.[27] Changes in polarity can alter the dipole

moment of the ground and excited states ($\Delta\mu$) as well as the overlap between them (μ_{eg}), resulting in changes in the shape and intensity of the transitions. With sufficient approximations, the excited state dipole moment can be determined from solvatochromic shifts,[27] although this technique is fraught with complications and limitations that restrict it to relatively small and simple molecules.[72] Combining this data with μ_g (from capacitive measurements or calculations),[26] and with ω_{eg} and μ_{eg} determined from a spectrum, β can be calculated from the TLM, Equation 2.6. Again, the accuracy of this method is limited to relatively simple systems, due to the approximations in calculating μ_e, and within the TLM itself. It remains a relatively accessible technique, however, for low-cost estimation of β. Interestingly, it is also wavelength independent, allowing for calculation of dispersion properties, albeit within the limitations of the TLM.

As should be clear from the preceding discussion, the properties of an EO chromophore depend significantly upon its nanoscale environment. In particular, the polarity of the medium can be expected to affect the β value of the chromophore. Additionally, the macroscopic activity can also be modulated through field-factor terms (Section 3.2). The magnitude of these effects is not yet known; these phenomena and their implications in the development of organic EO materials have been relatively unexplored thus far. Recent developments in binary organic glasses (Section 3.4.3) have brought this issue to the forefront. The effects of the relative polarity of the medium (Chapter 6) and the close approach of dissimilar chromophores (Chapter 5) on the microscopic and macroscopic behavior of these materials is of utmost importance in optimizing these highly active yet poorly understood new EO materials.

2.4.2 Electric Field Induced Second-Harmonic Generation. As previously mentioned, EFISH began as a vapor-phase technique measuring the nonlinearity of relatively poor EO materials.[7] Extension of the technique to the solution phase allowed investigation of early dipolar EO chromophores, such as the nitroanilines, which would have decomposed in the vapor-phase experiment.[8,9] This data was critical in the development of the TLM and ultimately, the progress of organic EO materials as a whole. As such, EFISH played a very important role in the early development of the EO field, and it continues to be used to this day.

In EFISH, a dilute solution of dipolar chromophores, to ensure minimal intermolecular interactions and a high degree of acentric order, is oriented using a large DC-electric field. A laser beam is propagated through the sample cell, and radiation at the second-harmonic is collected. The intensity of the second-harmonic generated (SHG) radiation depends on μ and β_z, the purely dipolar component of the hyperpolarizability. Some of the major advantages of this technique include the relatively simple laser systems involved and the strong SHG signal obtained. A few drawbacks to this technique include the restriction to evaluation of non-ionic, dipolar chromophores, as the orienting electric field precludes the use of charged, or octupolar species, the requirement of very large DC electric fields, and the complexity of the data analysis due to the nature of the parameter measured.

Although EFISH is apparently a SHG experiment ($-2\omega;\omega,\omega$), it is actually a four-wave mixing process where the fourth wave is the static electric field ($-2\omega;\omega,\omega,0$).[72] As such, there is a contribution from third-order processes, which depend on the second hyperpolarizability (γ). The actual parameter measured in EFISH is:

$$\gamma + \frac{\mu\beta_z}{5kT} \tag{2.8}$$

To accurately determine β_z then, one must independently measure the γ, from degenerate four-wave mixing experiments,[72] and μ from calculations or capacitance measurements.[26] Further complications arise in calculating β due to field factors present in the solution that were not present when the experiment was developed in the vapor-phase.[7,8,72] Attempts have been made to account for these complications, but EFISH remains an inelegant technique to measure β.

2.4.3 Hyper-Rayleigh Scattering. Rayleigh scattering is an elastic process involving coupled electronic-vibrational interactions between incident photons and a molecule, resulting in photons of identical frequency being scattered ($-\omega;\omega$). Hyper-Rayleigh scattering (HRS) is the two-photon equivalent of this process, wherein two incoming photons are annihilated, and a photon of twice the frequency is scattered from the molecule ($-2\omega;\omega,\omega$). The cross-section for this process is directly proportional to the square of β, and thus HRS presents an attractive alternative to EFISH for the direct measurement of hyperpolarizability. Although the phenomenon was first observed in 1965,[73] it was not until the 1990's that the technique was developed for NLO characterization by Clays and Persoons.[16,74]

In HRS, a dilute solution of a chromophore is irradiated with a high-intensity laser beam at frequency ω [$I_0(\omega)$], under constant flow to minimize photodegradation, and the intensity of the second-harmonic signal [$I(2\omega)$] is collected at an angle θ with respect to the incident beam. Random fluctuations in the concentration and orientation

of the chromophores in solution produce the anisotropy necessary for the 2ω signal to propagate. The intensity of this signal can be given by[75]

$$I(2\omega) = G\left(N_{solv}\left\langle\beta_{solv}^2\right\rangle + N_{chrom}\left\langle\beta_{chrom}^2\right\rangle\right)\left[\sin^2(2\theta)I_0(\omega)\right]^2 \qquad (2.9)$$

where G is an instrumental factor, N is the concentration or number density, and $<\beta^2>$ is an orientational average of the square of all the tensorial components of β. By using solutions of know concentration, and a solvent with a known β value, the β of a chromophore can be determined directly from a single experiment.[75] Although the β is averaged over all the tensor elements and is thus often reported as β_{HRS}, this technique still represents a significant improvement over the complexities of EFISH. In the case of dipolar chromophores, β_{zzz} is expected to be the major component. Unlike the EFISH technique, the HRS technique can be performed on charged and non-dipolar (e.g. octupolar) species, in addition to dipolar chromophores.

The major disadvantage of HRS is that the intensity of the 2ω signal is very weak, since the majority of the signal is eliminated due to destructive interference. This technique thus requires high-power laser systems and sensitive detectors, increasing the cost of HRS systems. To minimize photodegradation from high laser power, short pulse width laser systems are required, ideally of femtosecond durations, further increasing the cost and complexity of the systems. An additional complication arises from contamination of the HRS signal with multi-photon fluorescence, although time- or spectral-resolved femtosecond spectroscopy can correct for this factor.[75] As with all SHG-based techniques, the β derived from HRS is subject to resonance enhancement.

HRS is a key technique in the characterization of EO chromophores because of the direct, accurate measurement of β. Conclusively comparing hyperpolarizabilities of two chromophores, after accounting for resonance enhancement, allows for the determination of structure-property relationships. Combining HRS measurements with DFT calculations, which can exhibit excellent agreement,[15] allows theorists and experimentalists to provide synthetic guidance for the rapid development of state-of-the-art high β chromophores with exceptional secondary parameters.

2.4.4 Secondary Parameters. Although a large β is an important property for EO chromophores, several other parameters are also important. Thus, a brief discussion of such parameters is warranted.

The photochemical stability of organic EO materials is often considered as the main factor preventing their large-scale adoption in commercial EO devices. Although there is a considerable body of research on the photostability of EO chromophores,[76-81] it is not a mature field. It is known that singlet-oxygen is the cause of most photodegradation,[76] but there are few clear structure-property relationships with regards to enhancing stability.[77] Some recent work has shown that there are multiple degradation pathways, and that physical singlet-oxygen quenchers can retard one or more of those pathways, significantly increasing lifetimes.[82] Photostability is measured on a custom-built apparatus that subjects EO films or crystals to constant irradiation at telecommunication relevant wavelengths, and estimate decomposition from reduction the in the main charge-transfer absorption peak.[82]

The decomposition temperature (T_D) of a chromophore must be sufficiently high to avoid undue degradation during materials and device processing steps. Generally,

the T_D must be in excess of 200 °C for a chromophore to be considered useable, and higher temperatures are always desirable. The structure of the donor has been implicated as being particularly important in determining the thermal stability,[45] although the bridge and acceptor structures can also be important. The thermal stability is often estimated from differential scanning calorimetry (DSC) measurements, although more accurate values are obtained from Thermal Gravimetric Analysis (TGA) experiments.

The optical loss of a chromophore-polymer system is also of significant importance for device applications. Absorption-induced loss can arise from red-shifts in the main charge-transfer band and absorption tails due to aggregates or excitonic effects,[83,84] or from C-H stretching overtones in the IR frequencies.[84,85] Chromophores must not be made too long, or with excessively strong donors and acceptors for a given bridge, in order to avoid reducing the band gap and shifting the absorption too far to the red. Chromophores must be sufficiently soluble to minimize the formation of aggregates, or be derivatized to prevent close approach of chromophores to avoid scattering from aggregates and absorption from long-wavelength excitons.[84] Minimizing the number of C-H bonds, often by fluorine substitution, is a common technique to control optical loss.[85] Optical loss is commonly measured by immersing slab waveguide films in a high-index fluid, and measuring the intensity of a signal as a function of the length propagated through the slab,[86] although other techniques exist.[87]

Notes to Chapter 2

(1) McQuaid, R. W. The pockels effect of hexamethylenetetramine, in letters to the editor. *Appl. Opt.* **1963**, *2*, 319-323.

(2) Lee, R. W. Linear electro-optic (pockels) effect in hexamethylenetetramine: Influence of crystal strain. *J. Opt. Soc. Am.* **1969**, *59*, 1574-1580.

(3) Morrell, J. A.; Albrecht, A. C.; Levin, K. H.; Tang, C. L. The electrooptic coefficients of urea. *J. Chem. Phys.* **1979**, *71*, 5063-5068.

(4) Kurtz, S. K.; Perry, T. T. Powder technique for the evaluation of nonlinear optical materials. *J. Appl. Phys.* **1968**, *39*, 3798-3813.

(5) Levine, B. F.; Bethea, C. G.; Thurmond, C. D.; Lynch, R. T.; Bernstein, J. L. An organic crystal with an exceptionally large optical second-harmonic coefficient: 2-methyl-4-nitroaniline. *J. Appl. Phys.* **1979**, *50*, 2523-2527.

(6) Lipscomb, G. F.; Garito, A. F.; Narang, R. S. A large linear electrooptic effect in a polar organic crystal 2-methyl-4-nitroaniline. *Appl. Phys. Lett.* **1981**, *38*, 663-665.

(7) Finn, R. S.; Ward, J. F. Measurements of hyperpolarizabilities for some halogenated methanes. *J. Chem. Phys.* **1974**, *60*, 454-458.

(8) Levine, B. F.; Bethea, C. G. Molecular hyperpolarizabilities determined from conjugated and nonconjugated organic liquids. *Appl. Phys. Lett.* **1974**, *24*, 445-447.

(9) Bethea, C. G. Experimental technique of d.C. Induced shg [second harmonic generation] in liquids. Measurement of the nonlinearity of diiodomethane. *Appl. Opt.* **1975**, *14*, 1447-1451.

(10) Levine, B. F. Donor--acceptor charge transfer contributions to the second order hyperpolarizability. *Chem. Phys. Lett.* **1976**, *37*, 516-520.

(11) Oudar, J. L.; Chemla, D. S. Hyperpolarizabilities of the nitroanilines and their relations to the excited state dipole moment. *J. Chem. Phys.* **1977**, *66*, 2664-2668.

(12) Ward, J. F. Calculation of nonlinear optical susceptibilities using diagrammatic perturbation theory. *Rev. Mod. Phys.* **1965**, *37*, 1.

(13) Marder, S. R.; Perry, J. W.; Bourhill, G.; Gorman, C. B.; Tiemann, B. G.; Mansour, K. Relation between bond-length alternation and second electronic

hyperpolarizability of conjugated organic molecules. *Science* **1993**, *261*, 186-189.

(14) Argaman, N.; Makov, G. Density functional theory: An introduction. *Am. J. Phys.* **2000**, *68*, 69-79.

(15) Liao, Y.; Eichinger, B. E.; Firestone, K. A.; Haller, M.; Luo, J.; Kaminsky, W.; Benedict, J. B.; Reid, P. J.; Jen, A. K. Y.; Dalton, L. R.; Robinson, B. H. Systematic study of the structure-property relationship of a series of ferrocenyl nonlinear optical chromophores. *J. Am. Chem. Soc.* **2005**, *127*, 2758-2766.

(16) Clays, K.; Persoons, A. Hyper-rayleigh scattering in solution. *Phys. Rev. Lett.* **1991**, *66*, 2980.

(17) Shi, Y.; Zhang, C.; Zhang, H.; Bechtel, J. H.; Dalton, L. R.; Robinson, B. H.; Steier, W. H. Low (sub-1-volt) halfwave voltage polymeric electro-optic modulators achieved by controlling chromophore shape. *Science* **2000**, *288*, 119-122.

(18) Robinson, B. H.; Dalton, L. R.; Harper, A. W.; Ren, A.; Wang, F.; Zhang, C.; Todorova, G.; Lee, M.; Aniszfeld, R.; Garner, S.; Chen, A.; Steier, W. H.; Houbrecht, S.; Persoons, A.; Ledoux, I.; Zyss, J.; Jen, A. K. Y. The molecular and supramolecular engineering of polymeric electro-optic materials. *Chem. Phys.* **1999**, *245*, 35-50.

(19) Oudar, J. L.; Chemla, D. S. Theory of second-order optical susceptibilities of benzene substitutes. *Opt. Commun.* **1975**, *13*, 164-168.

(20) Levine, B. F. Conjugated electron contributions to the second order hyperpolarizability of substituted benzene molecules. *J. Chem. Phys.* **1975**, *63*, 115-117.

(21) Sundberg, K. R. A group--dipole interaction model of the molecular polarizability and the molecular first and second hyperpolarizabilities. *J. Chem. Phys.* **1977**, *66*, 114-118.

(22) Prasad, P. N. W., D. J. *Introduction to nonlinear optical effects in molecules and polymers*; John Wiley and Sons: New York, 1991.

(23) Hehre, W. J.; Radom, L.; Schleyer, P. R.; Pople, J. A. *Ab initio molecular orbital theory*; Wiley Interscience: New York, 1986.

(24) Hohenberg, P.; Kohn, W. Inhomogeneous electron gas. *Phys. Rev.* **1964**, *136*, B864.

(25) Burke, K.; Werschnik, J.; Gross, E. K. U. Time-dependent density functional theory: Past, present, and future. *J. Chem. Phys.* **2005**, *123*, 062206-062209.

(26) Breitung, E. M.; Vaughan, W. E.; McMahon, R. J. Measurement of solute dipole moments in dilute solution: A simple three-terminal cell. *Rev. Sci. Instrum.* **2000**, *71*, 224-227.

(27) Paley, M. S.; Harris, J. M.; Looser, H.; Baumert, J. C.; Bjorklund, G. C.; Jundt, D.; Twieg, R. J. A solvatochromic method for determining second-order polarizabilities of organic molecules. *J. Org. Chem.* **1989**, *54*, 3774-3778.

(28) Bourhill, G.; Bredas, J.-L.; Cheng, L.-T.; Marder, S. R.; Meyers, F.; Perry, J. W.; Tiemann, B. G. Experimental demonstration of the dependence of the first hyperpolarizability of donor-acceptor-substituted polyenes on the ground-state polarization and bond length alternation. *J. Am. Chem. Soc.* **1994**, *116*, 2619-2620.

(29) Meyers, F.; Marder, S. R.; Pierce, B. M.; Bredas, J. L. Electric field modulated nonlinear optical properties of donor-acceptor polyenes: Sum-over-states investigation of the relationship between molecular polarizabilities (.Alpha., .Beta., and .Gamma.) and bond length alternation. *J. Am. Chem. Soc.* **1994**, *116*, 10703-10714.

(30) Brooker, L. G. S.; Sprague, R. H.; Smyth, C. P.; Lewis, G. L. Color and constitution. I. Halochromism of anhydronium bases related to the cyanine dyes. *J. Am. Chem. Soc.* **1940**, *62*, 1116-1125.

(31) Bartholomew, G. P.; Ledoux, I.; Mukamel, S.; Bazan, G. C.; Zyss, J. Three-dimensional nonlinear optical chromophores based on through-space delocalization. *J. Am. Chem. Soc.* **2002**, *124*, 13480-13485.

(32) Blanchard-Desce, M.; Baudin, J.-B.; Jullien, L.; Lorne, R.; Ruel, O.; Brasselet, S.; Zyss, J. Towards highly efficient nonlinear optical chromophores: Molecular engineering of octupolar molecules. *Opt. Mater.* **1999**, *12*, 333-338.

(33) Coe Benjamin, J.; Harris James, A.; Brunschwig Bruce, S.; Asselberghs, I.; Clays, K.; Garin, J.; Orduna, J. Three-dimensional nonlinear optical chromophores based on metal-to-ligand charge-transfer from ruthenium(ii) or iron(ii) centers. *J. Am. Chem. Soc.* **2005**, *127*, 13399-13410.

(34) Janowska, I.; Zakrzewski, J.; Nakatani, K.; Delaire, J. A.; Palusiak, M.; Walak, M.; Scholl, H. Ferrocenyl d-[pi]-a chromophores containing 3-dicyanomethylidene-1-indanone and 1,3-bis(dicyanomethylidene)indane acceptor groups. *J. Organomet. Chem.* **2003**, *675*, 35-41.

(35) Moore, A. J.; Chesney, A.; Bryce, M. R.; Batsanov, A. S.; Kelly, J. F.; Howard, J. A. K.; Perepichka, I. F.; Perepichka, D. F.; Meshulam, G.; Berkovic, G.; Kotler, Z.; Mazor, R.; Khodorkovsky, V. Synthesis, structures and nonlinear optical properties of novel d-p-a chromophores: Intramolecular charge transfer from 1,3-dithiole or ferrocene moieties to polynitrofluorene or

dicyanomethylene moieties through conjugated linkers. *Eur. J. Org. Chem.* **2001**, *2001*, 2671-2687.

(36) Boldt, P.; Eisenträger, T.; Glania, C.; Göldenitz, J.; Krämer, P.; Matschiner, R.; Rase, J.; Schwesinger, R.; Wichern, J.; Wortmann, R. Guanidyl and phosphoraniminyl substituents: New electron donors in second-order nonlinear optical chromophores. *Adv. Mater.* **1996**, *8*, 672-675.

(37) Katti, K. V.; Raghuraman, K.; Pillarsetty, N.; Karra, S. R.; Gulotty, R. J.; Chartier, M. A.; Langhoff, C. A. First examples of azaphosphanes as efficient electron donors in the chemical architecture of thermally stable new nonlinear optical materials. *Chem. Mater.* **2002**, *14*, 2436-2438.

(38) Annoni, E.; Pizzotti, M.; Ugo, R.; Quici, S.; Morotti, T.; Bruschi, M.; Mussini, P. Synthesis, electronic characterisation and significant second-order non-linear optical responses of meso-tetraphenylporphyrins and their zn(ii) complexes carrying a push or pull group in the beta pyrrolic position. *Eur. J. Inorg. Chem.* **2005**, *2005*, 3857-3874.

(39) Zhang, S.; Zhou, G.; Yang, Z.; Qin, A.; Wang, P.; Ye, C. Design and synthesis of low dipole moment chromophores: 2,6-disubstitute cycloheptimidazoles. *Synth. Met.* **2003**, *137*, 1545-1546.

(40) Nguyen, T. T.; Salle, M.; Delaunay, J.; Riou, A.; Richomme, P.; Raimundo, J. M.; Gorgues, A.; Ledoux, I.; Dhenaut, C.; Zyss, J.; Orduna, J.; Garin, J. Functionalized polyolefinic nonlinear optic chromophores incorporating the 1,3-dithiol-2-ylidene moiety as the electron-donating part. *J. Mater. Chem.* **1998**, *8*, 1185-1192.

(41) Gonzalez, M.; Segura, J. L.; Seoane, C.; Martin, N.; Garin, J.; Orduna, J.; Alcala, R.; Villacampa, B.; Hernandez, V.; LopezNavarrete, J. T. Tetrathiafulvalene derivatives as nlo-phores: Synthesis, electrochemistry, raman spectroscopy, theoretical calculations, and nlo properties of novel ttf-derived donor-pi-acceptor dyads. *J. Org. Chem.* **2001**, *66*, 8872-8882.

(42) Diaz, J. L.; Dobarro, A.; Villacampa, B.; Velasco, D. Structure and optical properties of 2,3,7,9-polysubstituted carbazole derivatives. Experimental and theoretical studies. *Chem. Mater.* **2001**, *13*, 2528-2536.

(43) Pan, Q.; Fang, C.; Zhang, Z.; Qin, Z.; Li, F.; Gu, Q.; Wu, X.; Yu, J. Synthesis and characterization of nonlinear optical chromophores containing [alpha]-cyan with thermal stability. *Opt. Mater.* **2003**, *22*, 45-49.

(44) Suresh, S.; Zengin, H.; Spraul, B. K.; Sassa, T.; Wada, T.; Smith, J. D. W. Synthesis and hyperpolarizabilities of high temperature triarylamine-polyene chromophores. *Tetrahedron Lett.* **2005**, *46*, 3913-3916.

(45) Staub, K.; Levina, G. A.; Barlow, S.; Kowalczyk, T. C.; Lackritz, H. S.; Barzoukas, M.; Fort, A.; Marder, S. R. Synthesis and stability studies of conformationally locked 4-(diarylamino)aryl- and 4-(dialkylamino)phenyl-substituted second-order nonlinear optical polyene chromophores. *J. Mater. Chem.* **2003**, *13*, 825-833.

(46) Pauley, M. A.; Wang, C. H. Hyper-rayleigh scattering measurements of nonlinear optical chromophores at 1907 nm. *Chem. Phys. Lett.* **1997**, *280*, 544-550.

(47) Spraul, B. K.; Suresh, S.; Sassa, T.; Angeles Herranz, M.; Echegoyen, L.; Wada, T.; Perahia, D.; Smith, D. W. Thermally stable triaryl amino chromophores with high molecular hyperpolarizabilities. *Tetrahedron Lett.* **2004**, *45*, 3253-3256.

(48) Cheng, Y. J.; Luo, J.; Hau, S.; Bale, D. H.; Kim, T. D.; Shi, Z.; Lao, D. B.; Tucker, N. M.; Tian, Y.; Dalton, L. R.; Reid, P. J.; Jen, A. K. Y. Large electro-optic activity and enhanced thermal stability from diarylaminophenyl-containing high-beta nonlinear optical chromophores. *Chem. Mater.* **2007**, *19*, 1154-1163.

(49) Dalton, L. R.; Harper, A. W.; Ghosn, R.; Steier, W. H.; Ziari, M.; Fetterman, H.; Shi, Y.; Mustacich, R. V.; Jen, A. K. Y.; Shea, K. J. Synthesis and processing of improved organic second-order nonlinear optical materials for applications in photonics. *Chem. Mater.* **1995**, *7*, 1060-1081.

(50) Facchetti, A.; Abbotto, A.; Beverina, L.; van der Boom, M. E.; Dutta, P.; Evmenenko, G.; Marks, T. J.; Pagani, G. A. Azinium-p-bridge-pyrrole nlo-phores: Influence of heterocycle acceptors on chromophoric and self-assembled thin-film properties. *Chem. Mater.* **2002**, *14*, 4996-5005.

(51) Ashwell, G. J. Langmuir-blodgett films: Molecular engineering of non-centrosymmetric structures for second-order nonlinear optical applications. *J. Mater. Chem.* **1999**, *9*, 1991-2003.

(52) Zheng, Q.; Yao, Z.; Cheng, J.; Shen, Y.; Lu, Z. Synthesis and nonlinear optical properties of p-(dimethylamino)benzylidene dyes containing different acceptors. *Chem. Lett.* **2000**, 1426-1427.

(53) Marder, S. R.; Cheng, L. T.; Tiemann, B. G.; Friedli, A. C.; Blanchard-Desce, M.; Perry, J. W.; Skindhoej, J. Large first hyperpolarizabilities in push-pull polyenes by tuning of the bond length alternation and aromaticity. *Science* **1994**, *263*, 511-514.

(54) Diaz, J. L.; Villacampa, B.; Lopez-Calahorra, F.; Velasco, D. Experimental and theoretical study of a new class of acceptor group in chromophores for nonlinear optics: 2-substituted 4-methylene-4-h-oxazol-5-ones. *Chem. Mater.* **2002**, *14*, 2240-2251.

(55) Alain, V.; Fort, A.; Barzoukas, M.; Chen, C.-T.; Blanchard-Desce, M.; Marder, S. R.; Perry, J. W. The linear and non-linear optical properties of some conjugated ferrocene compounds with potent heterocyclic acceptors. *Inorg. Chim. Acta* **1996**, *242*, 43-49.

(56) Sun, S.-S.; Zhang, C.; Dalton, L. R.; Garner, S. M.; Chen, A.; Steier, W. H. 1,3-bis(dicyanomethylidene)indane-based second-order nlo materials. *Chem. Mater.* **1996**, *8*, 2539-2541.

(57) Melikian, G.; Rouessac, F. P.; Alexandre, C. Synthesis of substituted dicyanomethylendihydrofurans. *Synth. Commun.* **1995**, *25*, 3045-3051.

(58) Villemin, D.; Liao, L. Rapid and efficient synthesis of 2-[3-cyano-4-(2-arylidene)-5,5-dimethyl-5h-furan-2-ylidene]-malononitrile under focused microwave irradiation. *Synth. Commun.* **2001**, *31*, 1771-1780.

(59) Liu, S.; Haller, M. A.; Ma, H.; Dalton, L. R.; Jang, S.-H.; Jen, A. K. Y. Focused microwave-assisted synthesis of 2,5-dihydrofuran derivatives as electron acceptors for highly efficient nonlinear optical chromophores. *Adv. Mater.* **2003**, *15*, 603-607.

(60) Huang, D.; Chen, B.; (USA). Application: US
US, 2004; pp 23 pp , Cont -in-part of U S Ser No 395,610.

(61) Liao, Y.; Anderson, C. A.; Sullivan, P. A.; Akelaitis, A. J. P.; Robinson, B. H.; Dalton, L. R. Electro-optical properties of polymers containing alternating nonlinear optical chromophores and bulky spacers. *Chem. Mater.* **2006**, *18*, 1062-1067.

(62) Zhang, C.; Dalton, L. R.; Oh, M.-C.; Zhang, H.; Steier, W. H. Low vp electrooptic modulators from cld-1: Chromophore design and synthesis, material processing, and characterization. *Chem. Mater.* **2001**, *13*, 3043-3050.

(63) Kim, T.-D.; Kang, J.-W.; Luo, J.; Jang, S.-H.; Ka, J.-W.; Tucker, N.; Benedict, J. B.; Dalton, L. R.; Gray, T.; Overney, R. M.; Park, D. H.; Herman, W. N.; Jen, A. K. Y. Ultralarge and thermally stable electro-optic activities from supramolecular self-assembled molecular glasses. *J. Am. Chem. Soc.* **2007**, *129*, 488-489.

(64) Kim, T.-D.; Luo, J.; Ka, J.-W.; Hau, S.; Tian, Y.; Shi, Z.; Tucker, N. M.; Jang, S.-H.; Kang, J.-W.; Jen, A. K. Y. Ultralarge and thermally stable electro-optic activities from diels-alder crosslinkable polymers containing binary chromophore systems. *Adv. Mater.* **2006**, *18*, 3038-3042.

(65) Luo, J.; Cheng, Y.-J.; Kim, T.-D.; Hau, S.; Jang, S.-H.; Shi, Z.; Zhou, X.-H.; Jen, A. K. Y. Facile synthesis of highly efficient phenyltetraene-based nonlinear optical chromophores for electrooptics. *Org. Lett.* **2006**, *8*, 1387-1390.

(66) Michalak, R. J.; Kuo, Y.-H.; Nash, F. D.; Szep, A.; Caffey, J. R.; Payson, P. M.; Haas, F.; McKeon, B. F.; Cook, P. R.; Brost, G. A.; Luo, J.; Jen, A. K. Y.; Dalton, L. R.; Steier, W. H. High-speed ajl8/apc polymer modulator. *IEEE Photonic Tech. Lett.* **2006**, *18*, 1207-1209.

(67) Bortnik, B.; Hung, Y.-C.; Tazawa, H.; Seo, B.-J.; Luo, J.; Jen, A. K. Y.; Steier, W. H.; Fetterman, H. R. Electrooptic polymer ring resonator modulation up to 165 ghz. *IEEE J. Sel. Top. Quantum Electron.* **2007**, *13*, 104-110.

(68) Sullivan, P. A.; Akelaitis, A. J. P.; Lee, S. K.; McGrew, G.; Lee, S. K.; Choi, D. H.; Dalton, L. R. Novel dendritic chromophores for electro-optics: Influence of binding mode and attachment flexibility on electro-optic behavior. *Chem. Mater.* **2006**, *18*, 344-351.

(69) Whittall, I. R.; Cifuentes, M. P.; Humphrey, M. G.; Luther-Davies, B.; Samoc, M.; Houbrechts, S.; Persoons, A.; Heath, G. A.; Bogsanyi, D. Organometallic complexes for nonlinear optics. 11. Molecular quadratic and cubic hyperpolarizabilities of systematically varied (cyclopentadienyl)(triphenylphosphine)nickel sigma-arylacetylides. *Organometallics* **1997**, *16*, 2631-2637.

(70) Wang, C. H. Effects of dephasing and vibronic structure on the first hyperpolarizability of strongly charge-transfer molecules. *J. Chem. Phys.* **2000**, *112*, 1917-1924.

(71) Hsu, C.-C.; Liu, S.; Wang, C. C.; Wang, C. H. Dispersion of the first hyperpolarizability of a strongly charge-transfer chromophore investigated by tunable wavelength hyper-rayleigh scattering. *J. Chem. Phys.* **2001**, *114*, 7103-7108.

(72) Bosshard, C.; Knopfle, G.; Pretre, P.; Gunter, P. Second-order polarizabilities of nitropyridine derivatives determined with electric-field-induced second-harmonic generation and a solvatochromic method: A comparative study. *J. Appl. Phys.* **1992**, *71*, 1594-1605.

(73) Terhune, R. W.; Maker, P. D.; Savage, C. M. Measurements of nonlinear light scattering. *Phys. Rev. Lett.* **1965**, *14*, 681.

(74) Clays, K.; Persoons, A. Hyper-rayleigh scattering in solution. *Rev. Sci. Instrum.* **1992**, *63*, 3285-3289.

(75) Firestone, K. A., University, 2005.

(76) Galvan-Gonzalez, A.; Canva, M.; Stegeman, G. I.; Twieg, R.; Kowalczyk, T. C.; Lackritz, H. S. Effect of temperature and atmospheric environment on the photodegradation of disperse red 1-type polymers. *Opt. Lett.* **1999**, *24*, 1741-1743.

(77) Galvan-Gonzalez, A.; Belfield, K. D.; Stegeman, G. I.; Canva, M.; Chan, K. P.; Park, K.; Sukhomlinova, L.; Twieg, R. J. Photostability enhancement of an azobenzene photonic polymer. *Appl. Phys. Lett.* **2000**, *77*, 2083-2085.

(78) Galvan-Gonzalez, A.; Belfield, K. D.; Stegeman, G. I.; Canva, M.; Marder, S. R.; Staub, K.; Levina, G.; Twieg, R. J. Photodegradation of selected p-conjugated electrooptic chromophores. *J. Appl. Phys.* **2003**, *94*, 756-763.

(79) Galvan-Gonzalez, A.; Stegeman, G. I.; Jen, A. K. Y.; Wu, X.; Canva, M.; Kowalczyk, A. C.; Zhang, X. Q.; Lackritz, H. S.; Marder, S.; Thayumanavan, S.; Levina, G. Photostability of electro-optic polymers possessing chromophores with efficient amino donors and cyano-containing acceptors. *J. Opt. Soc. Am. B: Opt. Phys.* **2001**, *18*, 1846-1853.

(80) DeRosa, M. E.; He, M.; Cites, J. S.; Garner, S. M.; Tang, Y. R. Photostability of high beta electro-optic chromophores at 1550 nm. *J. Phys. Chem. A* **2004**, *108*, 8725-8730.

(81) Dubois, A.; Canva, M.; Brun, A.; Chaput, F.; Boilot, J.-P. Photostability of dye molecules trapped in solid matrixes. *Appl. Opt.* **1996**, *35*, 3193-3199.

(82) Rezzonico, D.; Jazbinsek, M.; Bosshard, C.; Günter, P.; Bale, D.; Liao, Y.; Dalton, L. R.; Reid, P. J. Photostability of pi-conjugated chromophores by resonant and nonresonant light excitations for long-life polymeric telecommunication devices. *in preparation* **2007**.

(83) Otomo, A.; Jager, M.; Stegeman, G. I.; Flipse, M. C.; Diemeer, M. Key trade-offs for second harmonic generation in poled polymers. *Appl. Phys. Lett.* **1996**, *69*, 1991-1993.

(84) Kim, M.-s.; Ju, J. J.; Park, S. K.; Do, J. Y.; Lee, M.-H. Evaluation of nonlinear optical polymers for second-harmonic generation: Toward the balance of absorption and nonlinearity against intrinsic trade-off. *Chem. Phys. Lett.* **2006**, *417*, 277-281.

(85) Eldada, L.; Shacklette, L. W. Advances in polymer integrated optics. *IEEE J. Sel. Top. Quantum Electron.* **2000**, *6*, 54-68.

(86) Teng, C. C. Precision measurements of the optical attenuation profile along the propagation path in thin-film waveguides. *Appl. Opt.* **1993**, *32*, 1051-1054.

(87) Okamura, Y.; Yoshinaka, S.; Yamamoto, S. Measuring mode propagation losses of integrated optical waveguides: A simple method. *Appl. Opt.* **1983**, *22*, 3892-3894.

Chapter 3: Introduction to Optimizing Macroscopic Nonlinearity

3.1 Introduction

Early organic electro-optic (EO) materials consisted of highly ordered acentric organic crystals composed of low hyperpolarizability (β) molecules such as urea,[1,2] and substituted benzenes such as *m*-dinitrobenzene and m-nitroaniline.[3,4] Although these crystals exhibit a high degree of molecular order, along with high chromophore density, the macroscopic nonlinearity is relatively low in these materials due to the extremely low β of these molecules. The relationship between order, β, and r_{33} can be described by (see Section 3.2)[5]

$$r_{33} = \frac{8\pi N \beta_z f(0) f^2(\omega) \langle \cos^3 \theta \rangle}{n_3^4} \tag{3.1}$$

where N is the chromophore number density, $\beta_z = \beta_{zxx} + \beta_{zyy} + \beta_{zzz} \sim \beta_{zzz}$, the $f(0)$ and $f(\omega)$ terms are static and dynamic field factors, respectively, n_3 is the index of refraction in the direction of the macroscopic orientation axis (transverse magnetic, TM, for a poled-polymer film), and $\langle \cos^3\theta \rangle$ is an orientationally averaged order parameter. This order parameter describes the degree of noncentrosymmetric chromophore alignment, with respect to the angle (θ) between the chromophores and a macroscopic orientation axis, such as the polar axis in an EO crystal, or the poling axis in poled-polymer films.

As advances were made in optimizing microscopic nonlinearity (Chapter 2), the new molecules with higher β values did not generally crystallize in noncentrosymmetric point groups,[6] if they crystallized at all. As a result, considerable effort has been

directed at achieving a noncentrosymmetric alignment of high β chromophores via a variety of methods. These can be separated into four major areas: crystal engineering (Section 3.2.1), self-assembly (Section 3.2.2), optical poling (Section 3.2.3), and electric field poling (3.2.4). Although considerable advances have been made in enhancing microscopic nonlinearity of organic EO chromophores over the past decades, commensurate gains in the macroscopic nonlinearity of EO materials have, in general, lagged behind considerably until very recently.

Theoretical models have had considerable success in explaining the deficiencies in macroscopic nonlinearity in poled polymer systems, particularly through the aid of statistical mechanics Monte-Carlo simulations. These insights have been instrumental in the optimization of poled polymer systems in particular, although their predictions are also applicable to recently developed multi-chromophore dendrimers and other polymer-free organic glasses. Optimization of these systems is especially attractive, as binary organic glasses have exhibited some of the largest r_{33} values to date, some in excess of 300 pm/V.

3.2 Achieving Noncentrosymmetric Order

The introduction of acentric order into organic EO materials is a non-trivial endeavor. This requires a nanometer scale organization of the component molecules, which poses quite a challenge, as most organic systems are isotropic. Although many techniques have been developed to introduce such order to organic materials in general, they all pose additional constraints on the materials. Additionally, high β chromophores

usually possess large ground-state dipole moments (μ) , which lead to strong centrosymmetric dipole-dipole interactions that further oppose attempts to introduce acentric order.

3.2.1 Crystal Engineering. The engineering of noncentrosymmetric organic EO crystals is an extremely challenging field. Although the earliest organic EO materials crystallized in noncentrosymmetric point groups, most high β chromophores crystallize in centrosymmetric point groups.[7] This is due primarily to the strong dipole-dipole interactions. Crystal engineering of non-EO organic materials, such as pharmaceuticals, is a well-studied field that is still not well understood. Minor changes in the molecular structure or counter-ion can have dramatic consequences in the resulting crystal structure, and variations in crystallization conditions can result in different structures (polymorphs) and crystals of different quality.[8] The addition of the dipole-dipole interactions further complicates matters, as these strong forces can dominate over the other forces used to tune the crystal structure.[9]

The advantages of organic EO crystals include the potential for the maximum achievable chromophore number density and degree of acentic order. As such, organic EO crystals can possess extremely large r_{33} values. The potential of organic EO crystals is best demonstrated by *trans*-4-[4-(dimethylamino)styryl]-1-methyl pyridinium *p*-toluenesulfonate (DAST), which is shown in Figure 3.1. Although the constituent chromophores exhibits a β_{zzz} value of only 1540 x 10^{-40} m^4/V (as determined by HRS at 1542 nm) in solution, and even lower values in the solid state due to intermolecular interactions, crystals of DAST can exhibit r_{11} values of up to 445 pm/V and r_{21} values up 148 pm/V (both at 750 nm, which suggests potential resonance enhancement).[8]

However, despite considerable work,[7,9,10] DAST remains the best organic EO crystal to date, and the component chromophore has a relatively low β value. Attempts to engineer crystals of newer, higher β chromophores remain unsuccessful.

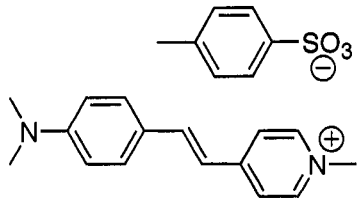

Figure 3.1. Structure of the DAST compound used in organic EO crystals

Furthermore, the use of organic EO crystals would negate a number of the potential advantages of organic materials over inorganic materials. Among the disadvantages of inorganic materials was the high cost and slow fabrication speed of devices based upon single crystals that must be laboriously grown, cleaved, and polished. Organic EO crystals must also undergo these procedures, however they are even further complicated by other factors. Even the acentric crystals often have a tendency to grow in needle-like structures, which cannot be used for device applications. When the crystals instead grow in the useful plate form, obtaining crystals of sufficient size is often difficult.[8] Finally, variations in crystal quality, demonstrated by the range of r_{33} values they can exhibit,[8] are another significant disadvantage of organic EO crystals. As a result, most of the research has focused on other methods of achieving acentric order.

3.2.2 Self-Assembly. One of the most challenging, yet conceptually most exciting, chromophore architectures for organic electro-optic materials is self-assembling systems. Broadly defined, self-assembly refers to any process in which the pieces involved possess the necessary elements for the development of any kind of systemic

order, which is often achieved through a stable or meta-stable balance of relatively weak forces. Theoretically, a self-assembling system could adopt a nearly entirely noncentrosymmetric lattice of chromophores, approaching the levels of order exhibited in crystals. In practice, defects and the strong dipole-dipole interactions tend to dominate over long distances, resulting in significantly reduced order parameters for device-relevant film thicknesses.[11-13] Despite these problems, self-assembling systems still show great promise to improve on the relatively low order parameters achieved by electric-field poling (Section 3.2.4), as evidenced by the large values obtained from very thin films.[11,14]

Despite considerable research, a number of self-assembling systems for electro-optics have yet to produce materials with adequate properties for device-relevance. While extensively studied, Langmuir-Blodgett films exhibit large variations in film quality and electro-optic properties with small changes in components and deposition procedures.[11] Combined with the extremely fragile nature of these films, which can be irreversibly degraded by even moderate temperature changes, this makes Langmuir-Blodgett films an extremely challenging avenue of research. As a result, these materials have seen little use in device applications.

Liquid crystalline (LC) EO materials have also been explored, with chromophores incorporated both as side-chains in liquid crystalline polymers,[15] and as the primary mesogenic material.[16,17] The tendency for strong electron acceptors to disrupt the phase-forming ability of common mesogenic cores has limited the development of such systems to low β chromophores.[15,17] Thus materials exhibit low

electro-optic activity, and combined with the unpredictable nature of liquid crystalline systems, these factors have limited the development of device-relevant materials.

Layer-by-layer electrostatic or ionic self-assembled electro-optic films have received less attention than Langmuir-Blodgett films or liquid crystalline systems, yet show more promise to produce device quality materials.[12,18] By altering the pH and ionic strength of the solutions used to deposit the polycation and polyanion layers from solutions the interlayer interactions can be tuned, providing some control over the film properties.[18] The chromophores can be either ionic, as the primary charged element of one of the layers,[12] or they can be neutral and incorporated as a passive side-chain.[18] The main advantage of these systems is the ionic interactions between the two layers drive the formation of robust thin films that also serve to orient the incorporated chromophore molecules in a noncentrosymmetric and thermodynamically stable manner. As a result, these films exhibit excellent stability at both room and elevated temperatures.[18] The main draw-backs of this technique are the difficulty in preserving a high degree order in thick films and the relatively low β chromophores currently used, which results in low EO activity materials.[12]

The technique of layer-by-layer covalent assembly of intrinsically acentric superlattices is arguably the most mature of the self-assembly techniques for electro-optics.[13,14,19,20] The most common variation of this technique,[19,20] shown schematically in Scheme 3.1, involves a hydroxyl-terminated surface that is functionalized with a reactive halide-terminated siloxane capping layer. Chromophore precursors are then deposited to yield a highly ordered monolayer of covalently attached charged

pyridinium chromphores. A recent improvement has incorporated protecting groups on the terminal end of the chromophore to ensure high-quality monolayers are formed.[20] These protecting groups are then removed, and another siloxane capping layer is deposited, which both crosslinks the chromophores, locking the order in place, and generates a new layer of reactive halides for deposition of the next chromophore layer. By repeating this process, high quality films with a high degree of order and large electro-optic responses have been produced.[19,20]

Scheme 3.1. Synthesis of siloxane-based self-assembled superlattices

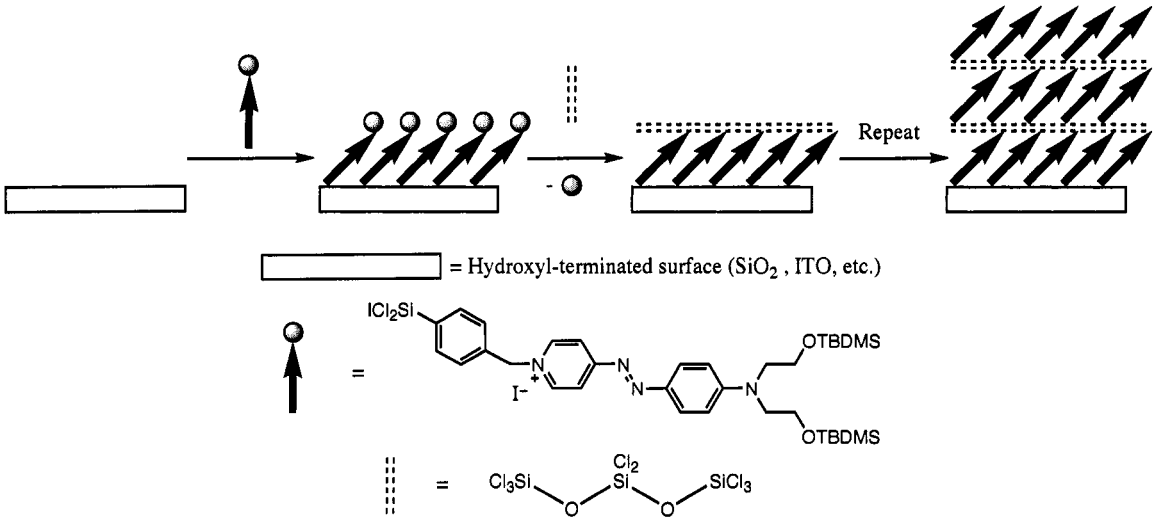

As with most self-assembled systems, however, as the number of layers becomes large the degree of order drops, likely due to increased defect propagation and dipole-dipole interactions. Through considerable effort, optimized materials have been prepared and incorporated into devices that utilize relatively thin acentric superlattice films with passive, partially wave-guiding polymer cladding layers.[20] While these devices exhibited relatively large V_π values as compared to those for state-of-the-art poled-polymer materials based devices, further improvement in both the relatively weak

chromophore units and device optimization could result in competitive materials and devices.

One of the newest self-assembly techniques for electro-optics is physical vapor deposition of hydrogen-bond oriented thin films.[21-24] This technique allows a high degree of control over the rapid, continuous deposition of highly ordered films up to micron-scale thickness, which is a significant advantage over other self-assembly systems which involve slow, sequential deposition of nanometer-scale films with decreasing order. Additionally, such films often exhibit excellent thermal and temporal stability.[21] A key requirement is low molecular weight, volatile chromophores with hydrogen bond donors and acceptors oriented to ensure acentric assembly (Figure 3.2).[21-24] Unfortunately, this requirement limits the scope of chromophores to relatively low $\mu\beta$ systems, resulting in relatively low r_{33} values.

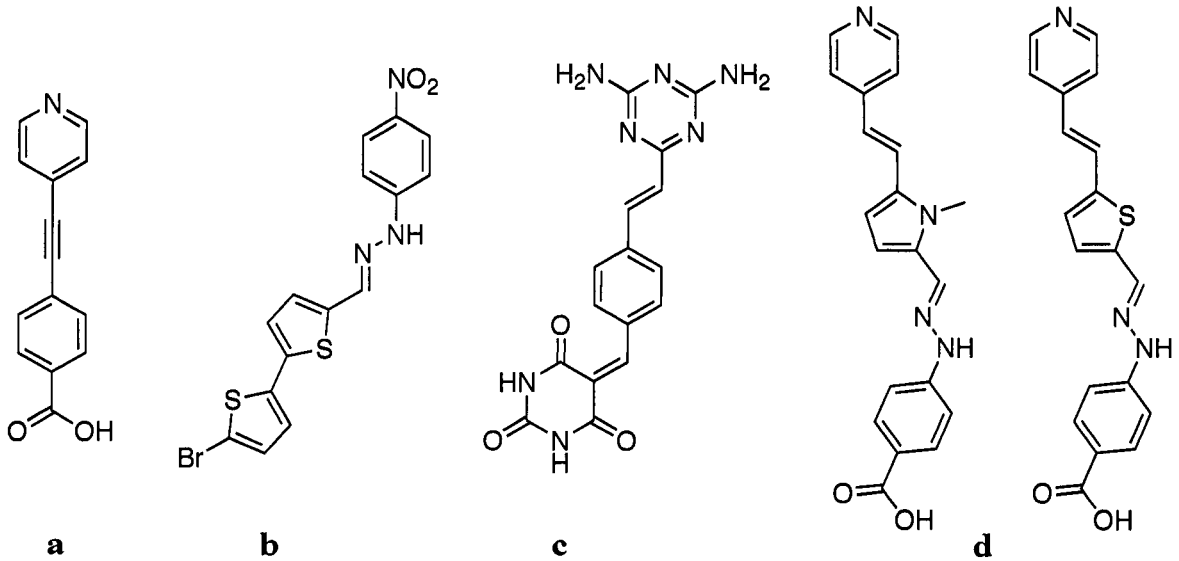

a **b** **c** **d**

Figure 3.2. Hydrogen-bonded chromophores for physical vapor deposition

Early work with simple double-ended hydrogen-bonding chromophores such as **a** (Figure 3.2) demonstrated the feasibility of this technique with high degrees of the

less-useful in-plane order, but low electro-optic activity.[21] Chromophore **b** (Figure 3.2) uses a side/end hydrogen-bond configuration that likely produces a slipped head to tail conformation, and hydroxyl-terminated surfaces to produce a high degree of out-of-place order, albeit still with low electro-optic activity.[22] Chromophore **c** (Figure 3.2) uses a unique triple hydrogen-bond donor/acceptor combination and a hydrogen-bond donor functionalized surface to produce excellent out-of-plane order, again with relatively low electro-optic activity.[23] Chromophores such as **d** with hydrogen bonding groups at both ends and on the side have been used to produce high degrees of out-of-plane order with moderate r_{33} values (on the order of lithium niobate) in pyridinium-chromophore monolayer templated, and hydroxyl-terminated surface, physical vapor deposited films.[24] The rapid improvement in materials from this technique demonstrates the enormous potential of such systems for electro-optic materials and devices.

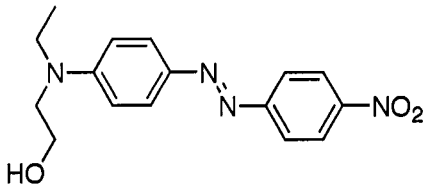

Figure 3.3. Structure of the disperse red 1 EO chromophore

3.2.3 Optical Poling. The process of optical poling is restricted to a very narrow range of materials. So far, it has primarily been applied to azobenzene-based chromophores, such as disperse red 1 (DR1, Figure 3.3).[25-27] This is because azobenzenes are readily isomerized from the more stable *trans* to the bent *cis*, or back, via application of specific wavelengths of light.[25] If you consider an azobenzene molecule in the *trans* conformation, a photon of a wavelength around 488 nm can trigger isomerization to the *cis* state. Rapid relaxation of the molecule back to the *trans* conformation reproduces

the original molecular state, but with a slight net rotation of the molecule. If linearly polarized light is used, then over many cycles of photo-excitation and relaxation, the molecule would tend to align its charge-transfer axis, and thus the transition dipole moment responsible for the absorption process, perpendicular to the electric field vector of the incoming light. In this configuration, the molecule is unable to absorb the incoming light, and thus the molecule would tend to remain in this orientation if the material is below its glass transition temperature (T_g), as is often the case in optical poling.[27]

Optical poling alone does not ensure acentric order, however, so it is often combined with electric-field poling.[26] In these cases, optically-assisted poling can enhance the degree of order in both guest-host and side-chain polymer azobenzene systems with respect to simple electric-field poling.[26] By themselves, such systems give relatively low r_{33} values due to the relatively low β of azobenzene chromophores. Recently, however, the practice of doping large β chromophores into EO active hosts has demonstrated unprecedented large r_{33} values in unrelated systems.[28,29] As such, DR1 side-chain functionalized polymethylmethacrylate (DR1-PMMA) presents an attractive host for inducing a potentially high degree of order on the host chromophores, which may be transmitted to the guest chromophores.

3.2.4 Electric-Field Poling. By far the most investigated technique for induced acentric order into organic EO materials is electric-field poling of polymeric or dendrimeric systems.[28,30-33] Traditionally, such systems consisted of EO chromophores doped as guests into NLO inactive polymeric hosts (3.4.1),[30,34,35] such as amorphous polycarbonates (APCs), polymethylmethacrylates (PMMAs), or a variety of specialty

polymers. Chromophores can also be covalently attached to the polymer host (Section 3.4.2),[16,25,32] or they can be present as polymer-free organic glasses (Section 3.4.3),[28,36] such as highly dendronized, high molecular weight chromophores, or multi-chromophore dendrimers. Each of these systems exhibits different features, which will be discussed in their own sections.

To apply an electric field, either the corona poling or contact poling method is used. In corona poling the bottom electrode consists of a transparent conducting oxide layer, such as indium tin oxide (ITO), on glass as the film substrate, and the top electrode is a needle suspended above the film.[37] The application of a large voltage (several hundred volts) ionizes the air, and creates charges on the surface of the film that serve to apply the effective poling field across the film. This method requires very large voltages, produces relatively weak, inhomogeneous fields, and can inject charges into the film.[33,37] In contact poling the bottom electrode remains the same, and the top electrode consists of a thin (~300 nm) sputter-coated gold layer, whose dimensions can be controlled via the use a physical mask. Contact poling requires lower voltages, produces larger, uniform fields, and has advantages for EO characterization (Section 3.5).[29,35,36] As such, the remainder of the discussion will focus on contact poling.

Electric-field contact poling is achieved by heating the ITO/glass-EO film-gold electrode sample while applying a potential difference across the two electrodes. As the material approaches its T_g, the chromophores become free to rotate in response to the electric field in the material. The net orientation is governed by the potential energy of the chromophore dipoles in the net field, which is a combination of the applied field and the effective field from the surrounding dipoles.[31,38] This is in turn modified by the

medium's dielectric properties and random motion due to thermal energy. After sufficient time to ensure equilibration, the sample is cooled below T_g to (theoretically) freeze the order in place.

Although conceptually simple, numerous factors complicate electric field poling. Intuitively, increasing the applied voltage should increase the effective field and result in improved poling-induced order. The usable voltage is limited by the dielectric breakdown voltage of the material, however. Fields of around 50-100 V/μm are typical, although it depends on their material used, and sample damage (usually evidenced by holes in the electrode) can occur at these fields. As the material approaches the T_g, the increased mobility usually results in increase current flow, which can reduce the effective voltage and field, and increase the chances of dielectric breakdown. Achieving the optimal balance of chromophore mobility and effective field is a difficult endeavor. Finally, the effect of intermolecular interactions, in particular the centrosymmetric dipole-dipole interactions,[31,38,39] on the effective field in the material and the efficiency of poling is of critical importance. Theoretical treatments have been instrumental in analyzing these effects and providing direction for improving the poling process.[31,38,39]

3.3 Theoretical Guidance

As in the optimization of microscopic nonlinearity, both theoretical models and computational methods have proven to be critical in the optimization of the poling-induced macroscopic order of organic EO materials. In the macroscopic case, however,

such analyses are significantly more difficult. This is due, at least in part, to the enormous complexity of the poling process. There are numerous different factors involved, including: van der Waal forces, dipole-dipole and dipole-poling field potential gradients, dielectric effects, hydrophobic/hydrophilic interactions, and thermal randomization due to kinetic energy.[30,31,38,39] To simplify the analysis, most models ignore many of these interactions. Additionally, the massive ensemble of molecules involved in such a process necessarily prevents the application of rigorous quantum mechanical calculations such as DFT. As a result, statistical mechanics calculations, including equilibrium and Monte Carlo variations, have been the method of choice for computing macroscopic order parameters under poling conditions.[31,38,39]

3.3.1 Electro-Optic Tensor Analysis. The poling process is assumed to introduce a polar axis into the EO material due to at least partial orientation of all chromophores in the macroscopic poling axis.[5] This assumption may be false, due to the strong intermolecular dipole-dipole interactions producing centrosymmetric dipole-pairs, but it serves as the basis for the following analysis. The induced axis can be treated as an infinite-fold rotation axis with an infinite number of mirror axes, with symmetry $C_{\infty v}$. Each chromophore is assumed to be aligned at some angle, θ, with respect to the polar axis. Under these conditions, the 18 elements of the arbitrary $\chi^{(2)}$ and **r** tensors reduce to 3 independent tensor elements.[5] In the case of the EO tensor, these are: $r_{333} = r_{33}$, $r_{133} = r_{13}$, and $r_{131} = r_{113} = r_{15}$. As long as all the frequencies involved in the NLO processes are far from the resonances (absorptions) of the chromophore, then all energy is elastically exchanged between fields and Kleinman symmetry states that only 2 independent elements remain: r_{33} and r_{13}.[5]

Williams and coworkers applied the oriented gas model to give a general expression for the $\chi^{(2)}$ tensor elements in poled-polymer systems.[40] Applying their results to the larger of the two independent tensor elements under EO conditions yields

$$\chi_{zzz}^{(2)}(-\omega;\omega,0) = Nf(0)f^2(\omega)\beta_z\langle\cos^3\theta\rangle \tag{3.2}$$

where N is the chromophore number density, $\beta_z = \beta_{zxx} + \beta_{zyy} + \beta_{zzz} \sim \beta_{zzz}$, the $f(0)$ and $f(\omega)$ terms are static and dynamic field factors, respectively, and $\langle\cos^3\theta\rangle$ is the orientationally averaged order parameter. Equation 3.1 for the r_{33} tensor element follows directly from Equation 3.2. In this model, r_{33} is three times r_{13} (Equation 1.19). The effect of the various terms on the overall value obtained is the subject of much research. Optimization of β was already treated in Chapter 2, and will not be discussed further.

The field factors in Equation 3.2 and 3.1 relate the applied modulation electric field vector (E_m) to the actual field felt by the molecules (E_{eff}). This effective field depends on the screening effects of nearby charges or dipoles, and any induced polarizations in nearby molecules. The former represent the static field factors, $f(0)$, also known as Onsager local field factors, which are generally given by[41]

$$f(0) = \frac{\varepsilon_0(\varepsilon_\omega + 2)}{2\varepsilon_0 + \varepsilon_\omega} \tag{3.3}$$

where ε_0 is the static dielectric constant, and ε_w is the dielectric constant at the optical frequency ω. This is subject to a variety of assumptions, including a spherical molecule and a uniform cavity. The dynamic field factors, $f(\omega)$, are generally treated by the Lorenz correction factor[40]

$$f(\omega) = \frac{\varepsilon_\omega + 2}{3} \qquad (3.4)$$

assuming a linear dielectric medium with a high degree of symmetry and a uniform polarization surrounding the molecule. Clearly, the assumptions present in estimating these field factors are not generally applicable to polymeric organic EO materials. In the limit of non-interacting spherical chromophores uniformly dispersed in a polymer host, the above equations could be relatively accurate, but for a non-uniform mixture of interacting ellipsoidal chromophores in polymer host, these corrections can only be approximate at best.

These dielectric effects are significant, however. In addition to the attenuation of E_m and the dipole-dipole interactions, they can also enhance the μ and β of the chromophores (2.4.1), and alter the effective magnitude and direction of the electric poling field (E_p), affecting the poling-induced order. These phenomena and their implications in the development of organic EO materials have been relatively unexplored so far; a careful, rigorous analysis of such effects on organic EO materials is lacking. Recent developments in binary organic glasses (Section 3.4.3) have brought this issue to the forefront. The effects of the relative polarity of the medium (Chapter 6) and the close approach of dissimilar chromophores (Chapter 5) on the microscopic and macroscopic behavior of these materials is of utmost importance in optimizing these highly active yet poorly understood new EO materials.

3.3.2 Orientational Order Analysis. Aside from the β value of the chromophores, the order parameter is the most important factor affecting the macroscopic activity of an organic EO material. As such, considerable work had been directed at modeling the

poling-induced order.[31,38,39] This problem can be investigated by finding the fraction of molecules with an orientation between θ and θ+dθ, which can be described by[31,38,39]

$$G(\theta)\sin\theta d\theta \tag{3.5}$$

where G(θ) is the dipole orientational function. Under the mean-field approximation, the orientation of a single chromophore is determined from its interaction with the effective potential, U(θ), created by the poling field and all of its surroundings, including the other chromophores. Under this approximation, the dipole orientational function is given by[31,38,39]

$$G(\theta) = \frac{e^{\frac{-U(\theta)}{kT}}}{\int_{-1}^{1} e^{\frac{-U(\theta)}{kT}} \sin(\theta) d\theta} \tag{3.6}$$

where k is the Boltzmann constant, T is the poling temperature, and U(θ) is the mean field potential. This expression can be used to calculate the average value of any function that depends on θ, such as the <cos^{3}θ> order parameter:

$$\left\langle \cos^3\theta \right\rangle = \int_{-1}^{1} G(\theta)\cos^3\theta \sin\theta d\theta \tag{3.7}$$

The nature of the mean-field potential is thus of utmost importance for calculating order parameters. It can be separated into terms based on the order of dependence on the applied field strength:

$$U(\theta) = U_0(\theta) + U_1(\theta) + U_2(\theta) + \ldots \tag{3.8}$$

The dipole-poling field interactions thus fall under $U_1(\theta)$, while the dipole-dipole interactions fall under $U_0(\theta)$. Using a variety of assumptions and neglecting various forces has resulted in a number of models with varying degrees of validity and accuracy, which are discussed below. It is important to note that the more rigorous

models indicate that N and $\langle\cos^3\theta\rangle$ are not independent variables, and thus their product, which is referred to as the loading parameter,[31,38,39] is often treated together.

3.3.3 Chromophore Gas Model. Under this model, all terms except for $U_1(\theta)$ are zero, and this term is given simply by $U_1(\theta) = -\mu f(0)E\cos\theta$.[5] Thus, this model ignores all forces except the dipole-poling field interaction, and the attenuation of it due to local field factors, and is also referred to as the isotropic model. The solution for the order parameter is the third-order Langevin function, $L_3[\mu f(0)E/kT]$, which can be expanded to give:

$$\left\langle \cos^3\theta \right\rangle_{isotropic} = L_3\left(\frac{\mu f(0)E}{kT}\right) = \frac{1}{5}\left(\frac{\mu f(0)E}{kT}\right) + \frac{1}{105}\left(\frac{\mu f(0)E}{kT}\right)^3 + \ldots \qquad (3.9)$$

In the weak field regime, where $\mu f(0)E/kT << 1$, the second and higher terms are negligible, and the expression for r_{33} becomes

$$r_{33} = \frac{8\pi N\beta_z f^2(0) f^2(\omega)\mu E}{5kTn_3^4} \qquad (3.10)$$

This model predicts a linear increase in r_{33} with chromophore number density and dipole moment, and with poling field.[5] Early examples of poled-polymer films, based upon low β chromophores, appeared to follow this model.[5] As chromophores were developed, they exhibited increased μ and β values, and deviation was seen from this simple model.[39] For modern systems, with chromophores dipole moments in excess of 13 Debye, poling voltages of around 100 V/μm, and poling temperatures of ~ 130 °C, the weak field approximation does not even hold, let alone the assumption of negligible intermolecular interactions.

3.3.4 The Ising Lattice. In this model the expression takes the same form as for the chromophore gas model, except the angles that the chromophore can take are restricted to $\theta = 0, \pi$, corresponding to the dipole either parallel or antiparallel with the applied field.[5] In this case, the solution for the order parameter is the first-order Langevin function, $L_1[\mu f(0)E/kT]$. Again assuming the weak field approximation, the resulting expression for the order parameter is:

$$\langle \cos^3 \theta \rangle_{Ising} = \frac{\mu f(0) E}{kT} = 5 \langle \cos^3 \theta \rangle_{Isotropic} \qquad (3.11)$$

Thus, the reduction in degrees of freedom of the chromophore results in a 5-fold improvement in the order obtained.[5] While the actual enhancement in any real system would be less than this, it would still be expected to be a significant improvement. This is the basis for studies involving liquid crystalline (LC) hosts and LC covalent EO-polymers (Section 3.2.2),[15-17] and optically assisted poling (3.2.3),[25-27] both of which are expected to reduce the degrees of freedom of chromophores in the ordered lattice.

3.3.5 Intermolecular Interactions – London Forces. Dalton, Robinson, and coworkers have explicitly accounted for the dipole-dipole intermolecular forces,[31,38,39] known as London forces,[39] within the framework of equilibrium statistical mechanics, following the methods of Piekara.[42] The London forces consist of dipole-dipole interactions, dipole-induced dipole interactions (induction forces) and induced-dipole-induced dipole interactions (dispersion forces).

Although numerical methods are needed to rigorously analyze the 3x3 rotation matrices such interactions demand, following the method of Piekara and assuming an effective interaction field on an individual chromophore and spherical chromophores

allows an analytical solution to be obtained.[42] After averaging over the relative chromophore-chromophore orientations, the result for the mean field potential is[31,39]

$$U_{tot} = \mu f(0) E \cos\theta - W \cos\phi \tag{3.12}$$

which depends on the angle, ϕ, between a chromophore and the effective intermolecular interaction field. Here W is the effective intermolecular interaction, and is given by

$$W = \frac{1}{R^6}\left(\frac{2\mu^4}{3kT} + 2\mu^2\alpha + \frac{3}{4} I\alpha^2\right) \tag{3.13}$$

where R is the averaged distance between chromophores, α is the polarizability, and I is the ionization potential.

From the mean field potential derived from London theory, the expression obtained for the order parameter under conditions relevant to modern EO chromophores, i.e. not weak field, is[31,39]

$$\left\langle \cos^3\theta \right\rangle_{london} = L_3\left(\frac{\mu f(0) E}{kT}\right)\left[1 - L_1^2\left(\frac{W}{kT}\right)\right] = \left[1 - L_1^2\left(\frac{W}{kT}\right)\right]\left\langle \cos^3\theta \right\rangle_{isotropic} \tag{3.14}$$

This expression is significantly more complex than those previously derived, but it is clear that the intermolecular interactions serve to attenuate the original Langevin order. By inserting Equation 3.14 in Equation 3.1, it is clear that this theory predicts that there will be a maximum in order parameter, and thus r_{33}, as a function of loading density, and that the location of this maximum depends on the dipole moment (Figure 3.4). This theory accurately reproduces the observed trends with regards to maxima in r_{33} vs. N as a function of μ.[31,39]

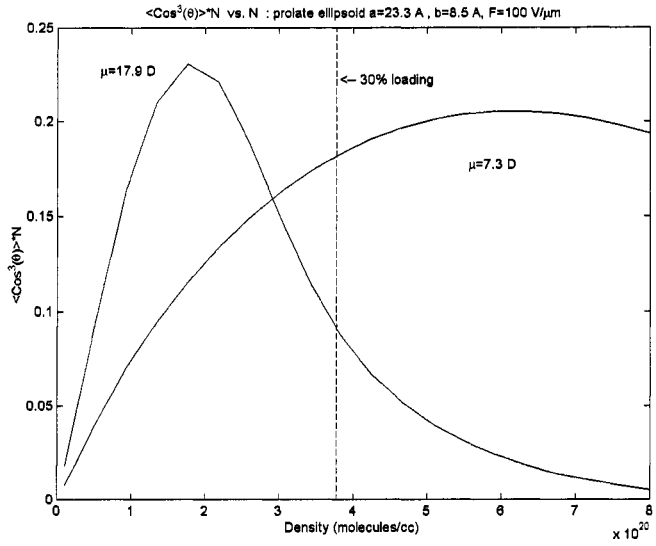

Figure 3.4. Dependence of order parameter on dipole moment[43]

3.3.6 Numerical Treatment of Spatial Anisotropy. Although analytical results for treatment of chromophore anisotropy (nonsphereical shape) analogous to those obtained for the dipole-dependence of the poling-induced order are not feasible, strictly numerical analysis methods and Monte Carlo simulations can treat the affect of spatial anisotropy from the 3x3 rotation matrices mentioned above. Dalton, Robinson, and coworkers have explored such anisotropic interactions, and they found that spherical chromophores in all cases yield maxima in the $\langle\cos^3\theta\rangle$ order parameter as a function of chromophore number density (N) at higher densities than prolate ellipsoidal chromophores with identical electrostatic properties.[31,39] They have also obtained excellent theoretical agreement with experimental results for derivatizing chromophores to obtain a more spherical shape (Figure 3.5). Thus, functionalization of chromophores to enhance spherical shape has been a major focus in the improvement of simple guest-host EO materials.

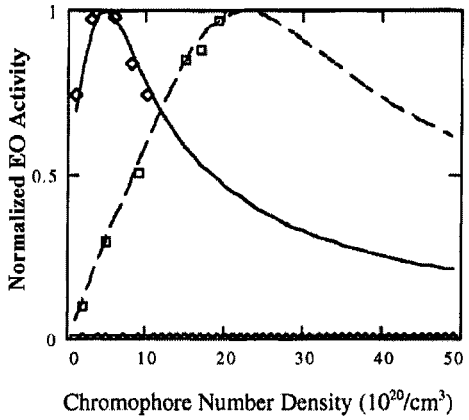

Figure 3.5. Dependence of order parameter on chromophore shape, prolate ellipsoid (diamonds) vs. spheres (squares)[39]

3.4 Optimizing Poled Electro-Optic Materials

Poled organic EO materials remain the most actively investigated area of organic EO materials, although alternatives methods of introducing noncentrosymmetric continue to receive attention (Section 3.2). Poled EO materials can take many forms; here we separate them into three main classes: traditional chromophore guest-polymer host blends (Section 3.4.1),[30,34,35] covalently functionalized chromophore-polymer systems (Section 3.4.2),[15,16,27,44] and the recently developed organic EO glasses (Section 3.4.3),[28,29,36,45,46] including highly dendronized chromophores and multichromophore dendrimers. Although each of the three classes have common attributes and behaviors, each also exhibit positive and negative features that are unique to their class. Thus, we will discuss each separately.

3.4.1 Guest-Host Systems. Guest-host systems represent the first class of organic EO materials developed after chromophores with improved hyperpolarizabilities no longer crystallized in noncentrosymmetric point groups (see Sections 2.1). It remains an

attractive method due to its simplicity, which allows for rapid sample prototyping. In an era of rapid improvement in molecular hyperpolarizability (β), this allowed fast evaluation of the improvements in a device-relevant format. As discussed in Sections 3.3.5 and 3.3.6, however, intermolecular dipole-dipole interactions play a critical role in determining the poling-induced noncentrosymmetric order, particularly at high loading densities.[31,39] Thus, although considerable improvements were made in microscopic activity over the last several decades, it is only in the last decade that comparable improvements in the macroscopic activities have been achieved. A considerable amount of that improvement can be attributed to the focus on derivatization of chromophore structure to obtain a more spherical structure,[30,35] and thus reduce dipole-dipole interactions. One common method to enhance spherical shape is to incorporate bulky dendron groups, which can also incorporate additional desired functionalities, such as crosslinking groups.[47]

One of the main disadvantages that must be considered with this method is phase separation of the chromophores from the polymer. Many of polymer hosts employed for organic EO chromophores, such as amorphous polycarbonates (APCs) and polymethylmethacrylates (PMMAs) are relatively non-polar. Obtaining good quality dispersions of the highly polar chromophores in these materials can be a challenge, and on heating there can be a tendency, particularly at high chromophore loading densities, for the chromophores to phase segregate.[48] At best, this results in extensive dipole-dipole pairing and low r_{33} values, and it often resulting in catastrophic sample failure. Although the use of more polar hosts has been explored,[49] these hosts suffer from disadvantages of their own.

These strong dipole-dipole interactions are also the source of the other major disadvantage to guest-host systems; the tendency for the material to relax over time, resulting in steadily decreasing r_{33} values.[48] The noncentrosymmetric order introduced by poling is not thermodynamically stable, as the lowest energy configuration involves extensive centrosymmetric dipole pairing. Although this is a significant problem in all poled organic EO materials, it is particularly problematic in guest-host systems, where the order generally exhibits poor long-term stability even at temperatures significantly below T_g.[48] Although one method to combat this is to use polymer hosts with even higher T_g values, to ensure temporal stability in the temperature range desired, this generally results in reduced initial order and r_{33} values.[48,49] This can be attributed to a combination of increased randomization of dipole orientation due to thermal energy at the higher poling temperatures thus required, and lower chromophore mobility in these conformationally restricted polymer systems, even at and above T_g. Therefore, a considerable amount of work has focused on finding alternative methods of enhancing thermal stability.

In order to achieve exceptional poling-induced order stability without sacrificing a high degree of poling efficiency, a post-poling lattice-hardening technique is desirable. This has been achieved through a variety of crosslinking mechanisms, including urethane condensations,[50,51] photocrosslinking,[52] thermal initiated,[47,52,53] and Diels-Alder [4+2] cycloadditions.[54] It should be emphasized that crosslinking is not unique to guest-host systems, indeed it has been utilized to enhance thermal stability in all three types of poled EO systems (guest-host, covalently functionalized polymers, and organic glasses). Although not all crosslinking mechanisms have been in explored

in each class of poled EO materials, the main features of the following discussion apply equally well to all three of the classes. Once heavily studied, urethane condensations are no longer used due to deteriorated film quality arising from of the water byproduct of the condensation reaction. Although photocrosslinking is an attractive method for lattice hardening because it allows decoupling of the poling and crosslinking processes, many modern chromophores appear sensitive to the radicals and other intermediates involved in these mechanisms.

Scheme 3.2. Trifluorovinyl ether thermally initiated crosslinking reaction

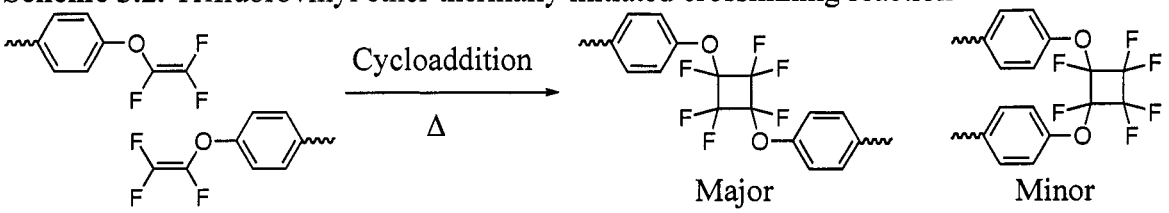

Thermal crosslinking has been used for many decades in all forms of polymers and has been efficiently incorporated into EO systems. One of the most commonly used thermally initiated crosslinking groups has been the aryl trifluorovinyl ether (TFVE) functionality, which affords high crosslinking efficiencies, and excellent processability, optical, and thermal properties.[55-57] The crosslinking mechanism is illustrated in Scheme 3.2, in which a [2 + 2] cycloaddition reaction occurs between two aryl trifluorovinyl ether monomers producing a perfluorocyclobutyl (PFCB) unit with incredible selectivity. The system is not without flaw, however, as poling of these materials is complicated by the conflict between the chromophore mobility required for efficient poling and the continual reduction in conformational mobility as the crosslinking reaction proceeds. The progression of crosslinking as the film is heated causes continual changing of the T_g and the high temperatures required to crosslink

(130 to above 250 °C) can promote thermal randomization of the chromophores as well as chromophore decomposition.

Diels-Alder crosslinking was introduced in an attempt to eliminate these poling difficulties by separating the poling and crosslinking temperature regions.[54,58] As the films are initially heated, the activation energy of the Diels-Alder reaction between the diene and dienophile is reached and some crosslinking occurs, but as the film is heated further to the high temperatures required to pole the chromophores, the reaction is disfavored for entropic reasons. On cooling after achieving a high degree of order, however, the [4 + 2] cycloaddition occurs throughout the film, resulting in effective crosslinking without significantly disrupting the poling process. By varying the diene and dienophile, the activation energies and crosslinking temperature ranges of the reaction can be tuned, and even the reversible or nonreversible nature of the reaction can be controlled. This allows development of materials with custom thermal properties that can be hardened and set once or multiple times.

A further improvement to the Diels-Alder crosslinking mechanism involves the use of a dienophile that is initially reversibly protected by a diene, which is deprotected upon heating to poling temperatures.[29] This can virtually entirely eliminate crosslinking of the film before the poling process is complete, allowing for nearly complete separation of the poling and crosslinking processes. A common protected dienophile used is the furan-protected malimide, which is deprotected at around 120 °C, and can then reaction with common dienes such as furan (reversible) and anthracene (irreversible) derivatives on cooling (Scheme 3.3). The Diels-Alder crosslinking mechanism is not without disadvantages, however. The system must have a relatively

high initial T_g (around 120 °C at minimum) to ensure optimal poling of the chromophores, without excessive thermal randomization, in the temperature range that disfavors the Diels-Alder reaction and promotes the retro-Diels-Alder (for the protected system). In the case of the reversible crosslinking, the thermal stability of the crosslinked material will always be limited by the activation temperature of the retro-Diels-Alder reaction. Although all of these parameters and temperature ranges are tunable by altering the diene and dienophile structures, this is not a straightforward endeavor and there are fundamental thermodynamic limits to the accessible temperature ranges.

Scheme 3.3. Diels-Alder crosslinking reaction

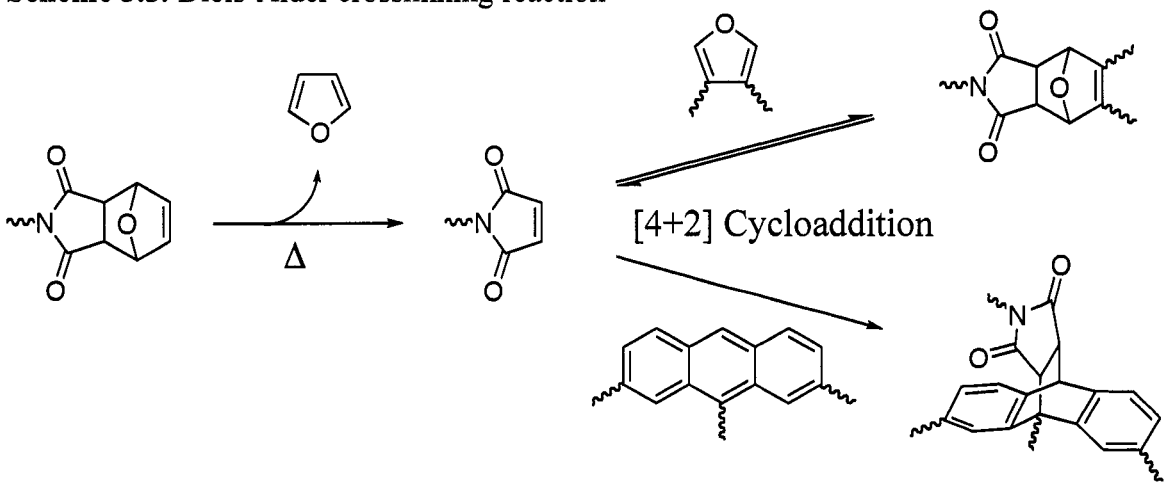

3.4.2 Covalently Functionalized Chromophore-Polymer Systems. Based upon the limitations of simple guest-host systems, researchers began covalently attaching the chromophores to the polymer host in an effort to improve the properties of the system. This helps prevent chromophore relaxation and allows for higher loading densities by eliminating the problem of phase separation. Chromophores can either be attached at both ends to the polymer, in so-called main-chain polymer systems,[16,59,60] or they can be attached at a single point to produce side-chain functionalized polymers.[15,27,32,52] Main

chain polymers tend to be very rigid, with high T_g values and low poling efficiencies,[59,60] and thus have received little attention recently. Side-chain polymer systems exhibit increased thermal stability with respect to simple guest-host systems while maintaining sufficient conformational flexibility to allow for excellent poling efficiencies.[27,32,52,61] Additionally, as discussed in the previous section, a variety of crosslinking mechanisms have been exploited to enhance the thermal stability of poled EO systems, and side-chain polymers have been a key area for this research. In particular, the TFVE and Diels-Alder based crosslinking schemes have seen considerable application in side-chain polymer systems,[55,58] with significant improvements demonstrated.

The concepts of chromophore derivatization to achieve a more spherical shape and reduce dipole-dipole interactions applied in guest-host systems can also be applied in side-chain polymer systems. Exemplifying this principal, research performed by Jen and coworkers examined the effect of functionalization on the system shown in Figure 3.6.[61] Chromophore **a** exhibited an r_{33} after poling of 45 pm/V when doped into polymethylmethacrylate (PMMA) at 20 wt. %. By functionalizing the chromophore with a small dendron (Fiigure 3.6**b**), a slight increase in the EO activity, to 49 pm/V, was achieved after poling at a similar loading density. Covalently attaching the undendronized chromophore to a polystyrene polymer backbone (Figure 3.6**c**), at similar active chromophore loading density, resulted in a small decrease in the r_{33} after poling to 33 pm/V. This was attributed to reduced chromophore mobility with respect to that of the free chromophore in PMMA, which has a relatively low T_g. Finally, attaching the chromophore to the dendronized polystyrene backbone (Figure 3.6**d**)

resulted in an increase in the r_{33} after poling to 81 pm/V. This was attributed to site isolation of the chromophore by the dendron, resulting in reduced dipole-dipole interactions, and thus an increased poling efficiency of the system.

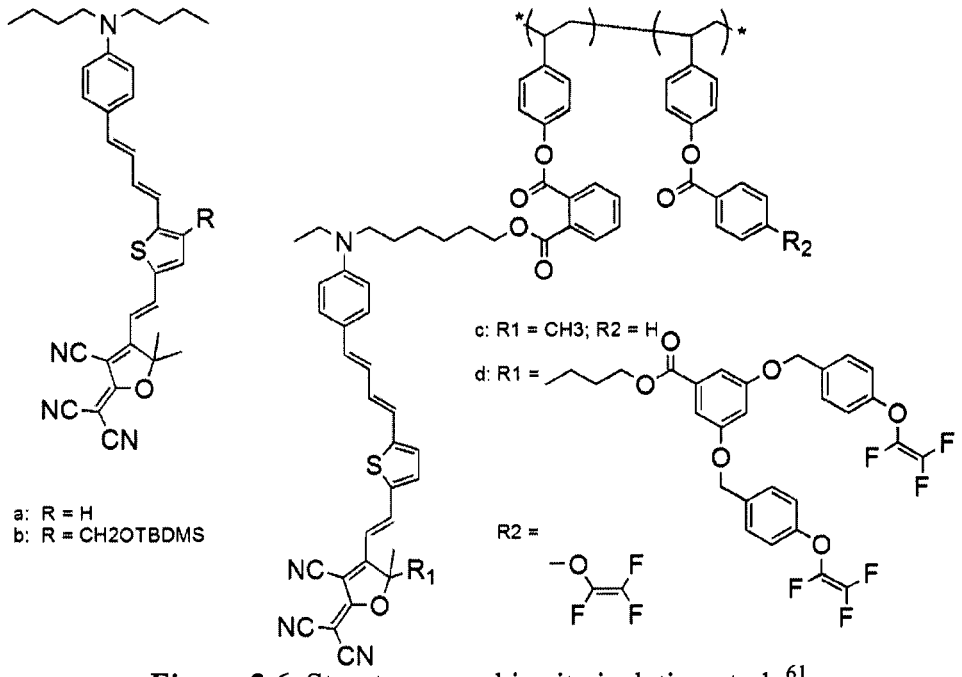

Figure 3.6. Structures used in site isolation study[61]

In addition to linear polymers, hyperbranched polymer systems have also received significant attention of late.[62-64] These systems are desirable because they combine the advantages of a polymer system, particularly ease of synthesis and control of physical properties, with the greater extent of site-isolated free volume found in multichromophore dendrimers, which permits greater chromophore movement and enhanced poling efficiencies. By incorporating crosslinking functionalities into hyperbranched polymer systems, such as the TFVE or Diels-Alder diene and dienophile moieties previously discussed, rapidly developed materials with large and thermally stable EO activities may be attainable.

3.4.3 Organic Electro-Optic Glasses. Recently, highly dendronized EO chromophores and multichromophore dendrimers with large molecular masses have been found to form high quality glassy films without the addition of polymer hosts.[46,56] These systems can achieve very large chromophore loading densities, and yet retain good poling efficiencies. Indeed, this class of EO materials generally exhibits improved poling-induced EO coefficients (r_{33} values) as compared to simple guest host materials containing analogous chromophores loaded at similar concentrations.[46,56] In the case of the dendronized chromophores, this is attributed to the extensive functionalization with dendrons approximating spherical shapes, and thus minimizing dipole-dipole interactions. In the case of dendrimers, it has been attributed to a high degree of effectively site-isolated free molecular volumes, which allow for excellent chromophore mobility. Dendritic organization of chromophores is also thought to impose local ordering effects,[65] which may contribute to the overall macroscopic $\langle\cos^3\theta\rangle$ order in such systems. Differences in chromophore tethering have been shown to play a significant role in influencing the dynamics of dipole response, and ultimate achievable order, of dendrimer systems under the influence of an externally applied poling field.[46]

Although these organic glasses generally exhibit relatively low T_g values, and thus low thermal stability of the EO activity,[46] the use of crosslinking to stabilize the high degree of electric field poling induced alignment has led to the realization of dendrimer based EO materials exhibiting highly enhanced, thermally stable r_{33} values.[66] The thermally initiated cycloaddition of TFVE to produce PFCB is one such method that has been explored. The Diels-Alder reaction has also been studied for these applications, as the effective separation of the poling and crosslinking processes ensures

the optimal EO activity is attained.[29,67] Additionally, the use of non-covalent crosslinking mechanisms provides another potential method to enhance the thermal stability of this class of materials.[28]

Very recently, these organic glasses have been used as hosts for the addition of structurally distinct EO chromophore guests. These binary organic glasses have demonstrated extremely large r_{33} values of 300 pm/V and larger.[28,67] Although the exact mechanism for achieving these results is not known, it is attributed in part to a synergistic effect of host order on guest order, and vice versa. There is some evidence that these systems do exhibit enhanced order,[28] although considerably more work is necessary to conclusively establish this is the case. Additionally, there is some evidence that dielectric effects may play a significant role (Chapter 6). Although these materials exhibit relatively low T_g values, as no covalent crosslinking has been incorporated as of yet, enhanced temporal stability at room temperature has been obtained through the use of noncovalent crosslinking mechanisms.[28] Clearly, developing a thorough understanding of the properties and behaviors of these systems presents a challenging but important task for the future. Understanding these systems could provide the direction needed to achieve ultra-large r_{33} values of up to 600 pm/V, and to allow transfer of these properties into device relevant materials. This could result in actual devices with ultra-low operating voltages of 0.1 V and less, which would allow direct integration with current electronics, paving the way for hybrid electronic-photonic systems in a broad range of applications.

3.5 Macroscopic Characterization

The experimental determination of macroscopic EO activity, particularly r_{33} and r_{13}, is a critical part of the evaluation of any new EO material. There are numerous methods of achieving this, each with their own advantages and disadvantages. Fortunately, most of the macroscopic characterization methods are not effected by second harmonic (2ω) resonance enhancement, unlike in the case of microscopic characterization (Section 2.4). This is because the electro-optic process is not a second-harmonic process, and so there is no dependence on 2ω in the frequency dispersion expression for the process, although there is a dependence on ω. Thus, there is a resonance enhancement when the measurement wavelength is near the main charge-transfer absorption of the chromophores in the EO material. Although technically this enhancement could be translated into device activity, operation of a device near the chromophore absorption would lead to unacceptable optical loss. EO activity is therefore typically measured far from the chromophore absorption, at the device relevant wavelengths of 1.3 and 1.55 μm.

3.5.1 Second-Harmonic Generation. As in the case of microscopic activity, second harmonic generation (SHG) can also be used to measure the EO activity of macroscopic materials.[68,69] This is the only commonly used technique to measure macroscopic EO activity that is subject to 2ω enhancement, and thus care must be taken in evaluating the experimental results. The experiment is performed by simply illuminating the sample film with a laser (of an appropriate wavelength) and collecting the emission at twice the frequency (half the wavelength), with appropriate accounting for the geometry. The

parameter measured is actually a tensor element of the d coefficient (d_{33} or d_{13} depending on the geometry of the experiment), a measure of the SHG activity. This parameter is not directly comparable to the EO coefficient tensor elements (r_{33} or r_{13}), although both depend on the noncentrosymmetric ($<\cos^3\theta>$) order and can be related to $\chi^{(2)}$. SHG is thus often used as a qualitative measure of the noncentrosymmetric alignment during a poling or deposition process, such as in the layer-by-layer fabrication of Langmuir-Blodgett (LB) films.[11] In these systems, the intensity of the SHG signal ($I_{2\omega}$) should be proportional to the square of the number of chromophore-containing layers or bilayers (N), depending on the LB film type. Sub-quadratic dependence indicates non-uniform order from layer to layer, which can be used to identify problems in the system under study. Through real-time monitoring of the poling process, SHG can provide information on the orientational dynamics, allowing optimization of the poling procedure.

3.5.2 Simple Reflection Ellipsometry. Independently introduced by Teng and Man and Schildkraut in 1990,[70,71] and further developed by numerous others,[36,72-74] simple reflection ellipsometry remains the simplest and fastest method for experimentally determining the EO coefficient. The technique is non-contact and non-destructive, which is an advantage over prism-coupling techniques such as attenuated total internal reflection (ATR, Section 3.5.3).[75] Additionally, it can be adapted to allow *in-situ* monitoring of EO activity in real-time during the poling process, which allows considerably more information to be obtained about the orinetational dynamics.[46,67,76] As with real-time SHG measurements (Section 3.5.1), this can allow optimization of the poling process and estimation of the orientational stability as a function of temperature,

both of which are important for comprehensive evaluation of EO materials. As this is the technique used for EO measurement in this work, the technique will be discussed in some detail. A complete description of the technique is beyond the scope of this work, however, for that the reader is directed elsewhere.[36,70,71,74]

A thin film sample consisting of a glass substrate coated with a transparent conductive bottom electrode (generally indium tin oxide [ITO]), an EO film on the order of 1 μm thick or greater, and a thin (around 300 nm) top gold electrode is interrogated with a laser. The beam impinges on the sample at an angle of $\theta = 45°$, transmits through the bottom substrate, through the EO film, bounces off the gold electrode, back through the film and substrate, and is collected by a photodetector at 90° with respect to the laser source. The laser is initially polarized such that there are equal contributions from the s and p polarizations (polarizer angle = 45°), and it is then passed through a Soleil-Babinet (SB) compensator that can be scanned to vary the phase angle (Ψ_{sp}) between the two wave polarizations. Before detection, the reflected beam is passed through slits to remove beams arising from reflections besides the desired one described above, and passed through a polarizer at 90° to the initial polarizer (analyzer). A scan of the SB compensator results in a periodic detector signal I_0 (in terms of voltage) given by

$$I_0 = 2I_c \sin^2(\psi_{sp}/2) \tag{3.15}$$

where I_c is the half-maximum intensity. By applying an AC voltage across the sample at a frequency ω given by

$$V(t) = V_m \sin(\omega t) \tag{3.16}$$

a modulated signal with half-maximum intensity of I_m that is directly proportional to V_m is observed through the use of a lock-in amplifier (at frequency ω), which arises from the linear EO (Pockels) effect in the film caused by the AC electric field. The EO effect results in a slight change in the refractive indices of the film, δn_o and δn_e, which can be related to the EO coefficients, r_{13} and r_{33}, respectively. By making a variety of assumptions,[36,74] including a relationship of $r_{33} = 3r_{13}$ based upon symmetry arguments (Section 3.3.1) and low birefringence ($n_o = n_e = n$), the r_{33} can be related to the ratio I_m/I_c by

$$r_{33} = \frac{3\lambda I_m}{4\pi V_m I_c n^2} \frac{(n^2 - \sin^2\theta)^{1/2}}{\sin^2\theta} \propto I_m / I_c \qquad (3.17)$$

where λ is the wavelength of measurement, generally 1.3 μm, as ITO is too absorptive at 1.55 μm.[36,74] In our case, the I_m and I_c values are obtained from curve-fits for the modulated (AC) and unmodulated signals as a function of Ψ_{sp}, respectively, which are obtained by scanning the SB compensator. The fitting function is

$$K_0 + K_1 \sin(K_2 x + K_3) \qquad (3.18)$$

where K_1 is the (half-maximum) amplitude of interest.

The numerous assumptions involved in deriving Equation 3.17 give rise to several sources of error, including poling induced birefringence, thin-film effects, and, if sample absorption at the measurement wavelength is an issue, absorption and electrochromic effects. The contribution of a number of these errors is reduced by utilizing the curve-fitting method described above, as opposed to the two-point analysis often used in the literature.[36,70,73] Despite the drawbacks, the technique is extremely useful for rapid EO sample analysis, particularly when configured for *in situ* use.

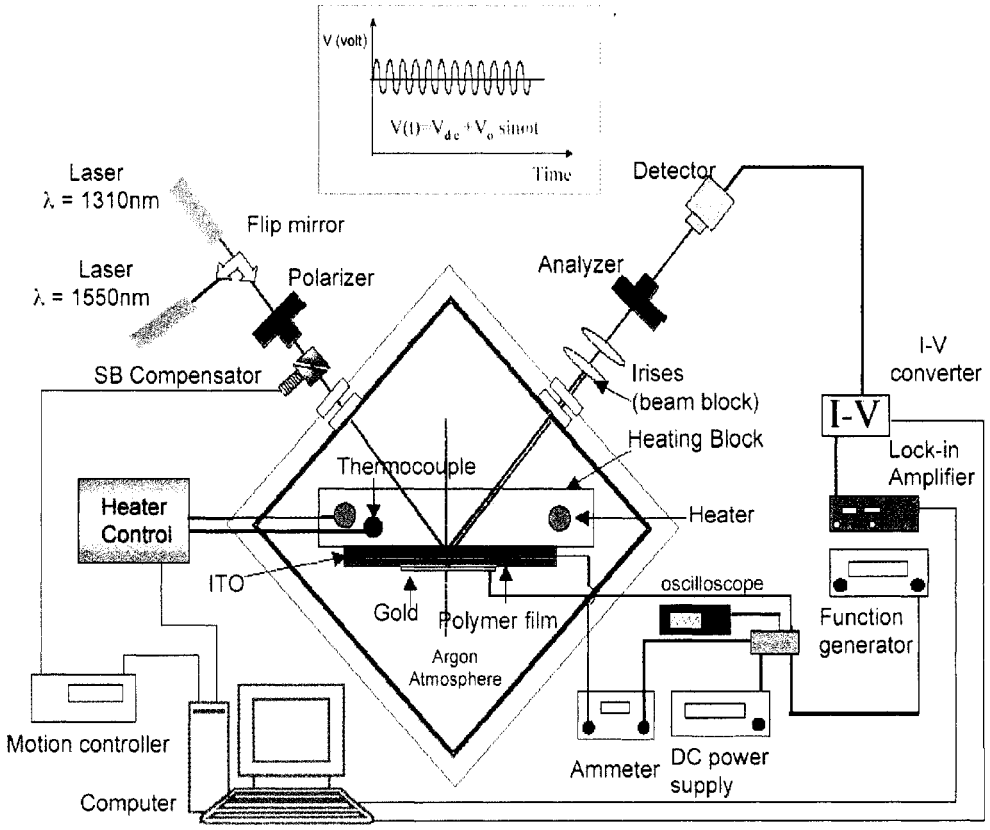

Figure 3.7. Schematic of *in situ* pole and probe simple reflection apparatus[46,67]

The instrument used in this work was developed by Dr. Phil Sullivan to allow *in situ* pole and probe simple reflection analysis of EO samples.[46,67] This affords considerable information on the orinetational dynamics, which was used to optimize of the poling process and estimate the orientational stability as a function of temperature for a series of pseudo-discotic EO chromophores (Chapter 4). The DC poling voltage (V_{DC}) is applied on top of the AC modulation voltage (V_m) as given by

$$V(t) = V_{DC} + V_m \sin \omega t \qquad (3.19)$$

To ensure an optimal I_m/I_c signal during the real-time poling procedure, the SB compensator position was set to a specific position determined for each sample. For analysis of samples with a sub-room temperature T_g (Section 4.5), the SB compensator

was scanned and the curves fit as before while the DC field was still applied, as in Equation 3.19. A schematic of the instrument is presented in Figure 3.7, for a full description, we refer you to other sources.[46,67]

3.5.3 Attenuated Total Internal Reflection. For a completely independent analysis of the EO coefficient tensor elements (r_{33} and r_{13}) of organic EO materials, the attenuated total internal reflection (ATR) between a prism and a thin-film waveguide must be used.[75] In this technique, a prism is pressed directly onto the top gold electrode of a thin-film EO sample and a laser beam is coupled through the prism and into the EO film. As long as the film is thick enough to support two modes, then the shift in position of the modes with an applied E field across the sample allows calculation of the EO coefficient. By choosing either TE or TM laser polarization (with respect to the sample geometry), both r_{33} and r_{13} can be calculated. This allows independent evaluation of the assumption used in simple reflection (Section 3.5.2) that $r_{33}=3r_{13}$. In general, this assumption appears to hold true.[75]

Although ATR is more thorough, and in theory more accurate, than simple reflection, it has many disadvantages. Unlike simple reflection, it is not amenable to real-time *in situ* monitoring of the poling process. It is also a contact method, which can result in sample damage. Additionally, obtaining good contact between the prism and the film, particularly through the gold electrode, can be problematic, and poor contact can result in lower measured values for the EO coefficients. EO materials generally have refractive index values of 1.6-1.7, which means that in order to support two modes at 1.3 or 1.55 μm, the films generally have to be on the order of 2 μm thick, which is thicker than easily obtainable for some systems. Taken altogether, these

factors result in ATR being a relative difficult and time-consuming technique. Thus simple reflection is generally used in preference to ATR for rapid EO sample characterization.

3.5.4 Device Performance. Ultimately, organic EO materials are being developed to function in active EO devices, with a wide variety of potential applications. Thus, an important benchmark of the EO activity of a material is determined by its performance in a device. Although many devices exist, the Mach-Zehnder modulator (MZM, Section 1.4.1) and the micro-ring resonator (MRR, Section 1.4.2) are two industrially important devices that can be used to characterize material performance. In particular, the MZM is often used to analyze material performance based upon the device figure of merit V_π, which is the voltage required to induce a phase shift of π and consequent destructive interference (off state).[77] This parameter obviously depends on the geometry of the device, which must be considered when analyzing the results. The EO material r_{33} can be calculated based on these parameters using Equation 1.22. Unfortunately, the r_{33} determined from MZM device behavior is always significantly lower than the value measured in a thin-film by techniques such as simple reflection (Section 3.5.2) or ATR (Section 3.5.3). This is due in part to the multilayer device structure, which results in very different poling voltages, leakage currents, and temperature gradients across the EO material in the device as compared to the thin-film sample format. Additionally, the multi-step fabrication process has numerous variables that can affect the device quality and thus the r_{33} measured. For this reason, although device performance is critical for actual applications of EO materials, it is not a useful method for rapid material characterization.

3.5.5 Secondary Parameters. Although the EO activity is the key property of interest for an EO material, numerous other factors are important for practical application of these materials. A brief discussion of the most important of these factors is warranted.

The glass transition temperature (T_g) is a key characteristic of EO materials that contributes to the temporal and thermal stability of the EO activity.[29,52,54] Long-term stability of the EO activity is critical to device applications such as on satellites and on the ocean floor, where replacement is not feasible. Additionally, many applications require stability at elevated temperatures due to the demands of the operating environment. Crosslinking (see Section 3.4.1) provides a method for enhancing the T_g and temporal stability of EO materials.[58,66] Glass transition temperatures are generally measured from bulk samples by differential scanning calorimetry (DSC), although dynamic measurements of EO activity in thin films (Sections 3.5.1 and 3.5.2) are more informative.[46] The temporal stability is simply determined by measuring the r_{33} of a sample, under identical experimental conditions, as a function of sample storage time in an appropriate environment.

The refractive index (n) describes the speed of light in the material, and is a key optical parameter of an EO material as this is the parameter actually changed by the EO effect. The exact value is of n is of significant importance, particularly in the fabrication of devices, where it must be accounted for to design the optimal performance. Generally, EO materials have n values around 1.6-1.7 at the telecommunication frequencies of 1.3 and 1.55 μm. Additionally, the poling induced birefringence ($\Delta n = n_o - n_e$) has important consequences for the EO characterization,[73] particularly via the simple reflection method (see Section 4.5.5). The exact values of n_o

and n_e for EO films can be determined directly from the attenuated total internal reflection measurement (ATR, Section 3.5.3),[75] or it can be measured via commercial prism coupling instruments.[78] A related parameter, the dielectric constant (ε), describes the material response to electric fields. It is also a rough measure of the polarity of the material. Recently, the effect of dielectric on the EO properties of materials has received some attention,[49] and there is reason to believe this is an important parameter of EO materials (see Chapter 6).

The photochemical stability of organic EO materials is often considered the main factor preventing their adoption. Although there is a considerable body of research on the photostability of organic EO materials,[57,79-83] it is not a mature field. It is known that singlet-oxygen is the cause of most photodegradation,[79] but there are few clear structure-property relationships with regards to enhancing stability.[57] Some recent work has shown that there are multiple degradation pathways, and that physical singlet-oxygen quenchers can retard one or more of those pathways, significantly increasing lifetimes.[84] Photostability is measured on custom-built apparatus that subject EO films or crystals to constant irradiation at telecommunication relevant wavelengths, and estimate decomposition from reduction in the main charge-transfer absorption peak.[84]

The optical loss of an EO material is also of significant importance for device applications. Absorption-induced loss can arise from red-shifts in the main charge-transfer band and absorption tails due to aggregates or excitonic effects,[69,85] or from C-H stretching overtones in the IR frequencies.[85,86] Chromophores must not be made too long, or with excessively strong donors and acceptors for a given bridge, to avoid reducing the band gap and shifting the absorption too far to the red. To avoid scattering

from aggregates and absorption from long-wavelength excitons, chromophores must be sufficiently soluble to break up aggregates, or be derivatized to prevent close approach of chromophores.[85] Minimizing the number of C-H bonds, often by fluorine substitution, is a common technique to control optical loss.[86] The optical loss is commonly measured by immersing slab waveguide films in a high-index fluid, and measuring the intensity of a signal as a function of the length propagated through the slab,[87] although other techniques exist.[88]

Notes to Chapter 3

(1) Kurtz, S. K.; Perry, T. T. Powder technique for the evaluation of nonlinear optical materials. *J. Appl. Phys.* **1968**, *39*, 3798-3813.

(2) Morrell, J. A.; Albrecht, A. C.; Levin, K. H.; Tang, C. L. The electrooptic coefficients of urea. *J. Chem. Phys.* **1979**, *71*, 5063-5068.

(3) Levine, B. F.; Bethea, C. G.; Thurmond, C. D.; Lynch, R. T.; Bernstein, J. L. An organic crystal with an exceptionally large optical second-harmonic coefficient: 2-methyl-4-nitroaniline. *J. Appl. Phys.* **1979**, *50*, 2523-2527.

(4) Lipscomb, G. F.; Garito, A. F.; Narang, R. S. A large linear electrooptic effect in a polar organic crystal 2-methyl-4-nitroaniline. *Appl. Phys. Lett.* **1981**, *38*, 663-665.

(5) Prasad, P. N. W., D. J. *Introduction to nonlinear optical effects in molecules and polymers*; John Wiley and Sons: New York, 1991.

(6) Levine, B. F. Donor--acceptor charge transfer contributions to the second order hyperpolarizability. *Chem. Phys. Lett.* **1976**, *37*, 516-520.

(7) Pan, F.; Wong, M. S.; Gramlich, V.; Bosshard, C.; Guenter, P. A novel and perfectly aligned highly electro-optic organic cocrystal of a merocyanine dye and 2,4-dihydroxybenzaldehyde. *J. Am. Chem. Soc.* **1996**, *118*, 6315-6316.

(8) Pan, F.; Wong, M. S.; Bosshard, C.; Guenter, P. Crystal growth and characterization of the organic salt 4-n,n-dimethylamino-4'-n'-methyl-stilbazolium tosylate (dast). *Adv. Mater.* **1996**, *8*, 592-595.

(9) Kwon, S.-J.; Kwon, O. P.; Jazbinsek, M.; Gramlich, V.; Gunter, P. Nonlinear optical co-crystal of analogous polyene chromophores with tailored physical properties. *Chem. Commun.* **2006**, 3729-3731.

(10) Kwon, O. P.; Ruiz, B.; Choubey, A.; Mutter, L.; Schneider, A.; Jazbinsek, M.; Gramlich, V.; Guenter, P. Organic nonlinear optical crystals based on configurationally locked polyene for melt growth. *Chem. Mater.* **2006**, *18*, 4049-4054.

(11) Ashwell, G. J. Langmuir-blodgett films: Molecular engineering of non-centrosymmetric structures for second-order nonlinear optical applications. *J. Mater. Chem.* **1999**, *9*, 1991-2003.

(12) Lindsay, G. A.; Roberts, M. J.; Chafin, A. P.; Hollins, R. A.; Merwin, L. H.; Stenger-Smith, J. D.; Yee, R. Y.; Zarras, P.; Wynne, K. J. Ordered films by

alternating polyelectrolyte deposition of cationic side chain and anionic main chain chromophoric polymers. *Chem. Mater.* **1999**, *11*, 924-929.

(13) Lin, W.; Lin, W.; Wong, G. K.; Marks, T. J. Supramolecular approaches to second-order nonlinear optical materials. Self-assembly and microstructural characterization of intrinsically acentric [(aminophenyl)azo]pyridinium superlattices. *J. Am. Chem. Soc.* **1996**, *118*, 8034-8042.

(14) Yitzchaik, S.; Marks, T. J. Chromophoric self-assembled superlattices. *Acc. Chem. Res.* **1996**, *29*, 197-202.

(15) Sandhya, K. Y.; Pillai, C. K. S.; Sato, M.; Tsutsumi, N. Nonlinear optical properties and liquid-crystalline behavior of new polyesters with dipole moments aligned transverse to the backbone. *Macromol. Chem. Phys.* **2002**, *203*, 1126-1134.

(16) Koch, A. T. H.; Fridrikh, S. V.; Warner, M.; Schwarzwalder, C. E.; Moratti, S. C.; Friend, R. H. Second order nonlinear optical response of nematic liquid crystalline main chain polymers. *Synth. Met.* **1999**, *101*, 244-245.

(17) Lemaitre, N.; Attias, A. J.; Ledoux, I.; Zyss, J. New second-order nlo chromophores based on 3,3'-bipyridine: Tuning of liquid crystal and nlo properties. *Chem. Mater.* **2001**, *13*, 1420-1427.

(18) Lee, S.-H.; Balasubramanian, S.; Kim, D. Y.; Viswanathan, N. K.; Bian, S.; Kumar, J.; Tripathy, S. K. Azo polymer multilayer films by electrostatic self-assembly and layer-by-layer post azo functionalization. *Macromolecules* **2000**, *33*, 6534-6540.

(19) van der Boom, M. E.; Richter, A. G.; Malinsky, J. E.; Lee, P. A.; Armstrong, N. R.; Dutta, P.; Marks, T. J. Single reactor route to polar superlattices. Layer-by-layer self-assembly of large-response molecular electrooptic materials by protection-deprotection. *Chem. Mater.* **2001**, *13*, 15-17.

(20) Zhu, P.; van der Boom, M. E.; Kang, H.; Evmenenko, G.; Dutta, P.; Marks, T. J. Realization of expeditious layer-by-layer siloxane-based self-assembly as an efficient route to structurally regular acentric superlattices with large electro-optic responses. *Chem. Mater.* **2002**, *14*, 4982-4989.

(21) Cai, C.; Bosch, M. M.; Tao, Y.; Muller, B.; Gan, Z.; Kundig, A.; Bosshard, C.; Liakatas, I.; Jager, M.; Gunter, P. Self-assembly in ultrahigh vacuum: Growth of organic thin films with a stable in-plane directional order. *J. Am. Chem. Soc.* **1998**, *120*, 8563-8564.

(22) Rashid, A. N.; Erny, C.; Gunter, P. Hydrogen-bond-directed orientation in nonlinear optical thin films. *Adv. Mater.* **2003**, *15*, 2024-2027.

(23) Zhu, P.; Kang, H.; Facchetti, A.; Evmenenko, G.; Dutta, P.; Marks, T. J. Vapor phase self-assembly of electrooptic thin films via triple hydrogen bonds. *J. Am. Chem. Soc.* **2003**, *125*, 11496-11497.

(24) Facchetti, A.; Annoni, E.; Beverina, L.; Morone, M.; Zhu, P.; Marks, T. J.; Pagani, G. A. Very large electro-optic responses in h-bonded heteroaromatic films grown by physical vapor deposition. *Nat. Mater.* **2004**, *3*, 910-917.

(25) Chalupczak, W.; Fiorini, C.; Charra, F.; Nunzi, J.-M.; Raimond, P. Efficient all-optical poling of an azo-dye copolymer using a low power laser. *Opt. Commun.* **1996**, *126*, 103-107.

(26) Donval, A.; Toussaere, E.; Brasselet, S.; Zyss, J. Comparative assessment of electrical, photoassisted and all optical in-plane poling of polymer based electrooptic modulators. *Opt. Mater.* **1999**, *12*, 215-219.

(27) Xu, G.; Si, J.; Liu, X.; Yang, Q. G.; Ye, P.; Li, Z.; Shen, Y. Comparison of the temperature dependence of optical poling between guest-host and side-chain polymer films. *J. Appl. Phys.* **1999**, *85*, 681-685.

(28) Kim, T.-D.; Kang, J.-W.; Luo, J.; Jang, S.-H.; Ka, J.-W.; Tucker, N.; Benedict, J. B.; Dalton, L. R.; Gray, T.; Overney, R. M.; Park, D. H.; Herman, W. N.; Jen, A. K. Y. Ultralarge and thermally stable electro-optic activities from supramolecular self-assembled molecular glasses. *J. Am. Chem. Soc.* **2007**, *129*, 488-489.

(29) Kim, T.-D.; Luo, J.; Ka, J.-W.; Hau, S.; Tian, Y.; Shi, Z.; Tucker, N. M.; Jang, S.-H.; Kang, J.-W.; Jen, A. K. Y. Ultralarge and thermally stable electro-optic activities from diels-alder crosslinkable polymers containing binary chromophore systems. *Adv. Mater.* **2006**, *18*, 3038-3042.

(30) Robinson, B. H.; Dalton, L. R.; Harper, A. W.; Ren, A.; Wang, F.; Zhang, C.; Todorova, G.; Lee, M.; Aniszfeld, R.; Garner, S.; Chen, A.; Steier, W. H.; Houbrecht, S.; Persoons, A.; Ledoux, I.; Zyss, J.; Jen, A. K. Y. The molecular and supramolecular engineering of polymeric electro-optic materials. *Chem. Phys.* **1999**, *245*, 35-50.

(31) Robinson, B. H.; Dalton, L. R. Monte carlo statistical mechanical simulations of the competition of intermolecular electrostatic and poling-field interactions in defining macroscopic electro-optic activity for organic chromophore/polymer materials. *J. Phys. Chem. A* **2000**, *104*, 4785-4795.

(32) Gray, T.; Overney, R. M.; Haller, M.; Luo, J.; Jen, A. K. Y. Low temperature relaxations and effects on poling efficiencies of dendronized nonlinear optical side-chain polymers. *Appl. Phys. Lett.* **2005**, *86*, 211908-211903.

(33) Yitzchaik, S.; Di Bella, S.; Lundquist, P. M.; Wong, G. K.; Marks, T. J. Anomalous second-order nonlinear optical response of in-plane poled glassy polymers. Spectroscopic and theoretical support for the importance of charged chromophore aggregates. *J. Am. Chem. Soc.* **1997**, *119*, 2995-3002.

(34) Sun, S.-S.; Zhang, C.; Dalton, L. R.; Garner, S. M.; Chen, A.; Steier, W. H. 1,3-bis(dicyanomethylidene)indane-based second-order nlo materials. *Chem. Mater.* **1996**, *8*, 2539-2541.

(35) Shi, Y.; Zhang, C.; Zhang, H.; Bechtel, J. H.; Dalton, L. R.; Robinson, B. H.; Steier, W. H. Low (sub-1-volt) halfwave voltage polymeric electro-optic modulators achieved by controlling chromophore shape. *Science* **2000**, *288*, 119-122.

(36) Park, D. H.; Kang, J. W.; Luo, J. D.; Kim, T. D.; Jen, A. K. Y.; Lee, C. H.; Herman, W. N. Nonlinear ellipsometric analysis of poled organic glasses having very large electro-optic coefficients. *Proc. SPIE* **2005**, *5935*, 59350O/59351-59350O/59312.

(37) Dao, P. T.; Williams, D. J. Constant current corona charging as a technique for poling organic nonlinear optical thin films and the effect of ambient gas. *J. Appl. Phys.* **1993**, *73*, 2043-2050.

(38) Nielsen, R. D.; Rommel, H. L.; Robinson, B. H. Simulation of the loading parameter in organic nonlinear optical materials. *J. Phys. Chem. B* **2004**, *108*, 8659-8667.

(39) Dalton, L. R.; Harper, A. W.; Robinson, B. H. The role of london forces in defining noncentrosymmetric order of high dipole moment-high hyperpolarizability chromophores in electrically poled polymeric thin films. *Proc. Natl. Acad. Sci. U. S. A.* **1997**, *94*, 4842-4847.

(40) Chemla, D. S.; Zyss, J. *Nonlinear optical properties of organic molecules and crystals*; Academic: New York, 1987; Vol. 1.

(41) Onsager, L. Electric moments of molecules in liquids. *J. Am. Chem. Soc.* **1936**, *58*, 1486-1493.

(42) Piekara, A. A theory of electric polarization, electro-optical kerr effect and electric saturation in liquids and solutions. *Proc. R. Soc. London A* **1939**, *172*, 360-383.

(43) Nielsen, R. University of Washington, Dept. of Chemistry, unpublished results

(44) Huang, D.; Chen, B.; (USA). Application: US
US, 2004; pp 23 pp , Cont -in-part of U S Ser No 395,610.

(45) Dalton, L.; Scherer, A.; Chen, A.; Jen, A.; Reid, P.; Robinson, B.; Eichinger, B.; Hochberg, M.; Baehr-Jones, T.; Pyajt, A.; Takayesu, J.; Sullivan, P.; Akelaitis, A.; Lawson, R.; Bale, D.; Haller, M.; Luo, J.; Liu, S.; Liao, Y.; Firestone, K.; Bhattacharjee, S.; Sinness, J.; Hammond, S.; Sgro, A.; Buker, N.; Snoeberger, R.; Lingwood, M.; Steier, W. Organic electro-optic glasses for wdm applications. *Proc. SPIE* **2005**, *6014*, 60140P/60141-60140P/60115.

(46) Sullivan, P. A.; Akelaitis, A. J. P.; Lee, S. K.; McGrew, G.; Lee, S. K.; Choi, D. H.; Dalton, L. R. Novel dendritic chromophores for electro-optics: Influence of binding mode and attachment flexibility on electro-optic behavior. *Chem. Mater.* **2006**, *18*, 344-351.

(47) Zhang, C.; Wang, C.; Dalton, L. R.; Zhang, H.; Steier, W. H. Progress toward device-quality second-order nonlinear optical materials. 4. A trilink high mb nlo chromophore in thermoset polyurethane: A \"Guest-host\" Approach to larger electrooptic coefficients. *Macromolecules* **2001**, *34*, 253-261.

(48) Ma, H.; Jen, A. K. Y.; Dalton, L. R. Polymer-based optical waveguides: Materials, processing, and devices. *Adv. Mater.* **2002**, *14*, 1339-1365.

(49) Ostinelli, O., ETH, 2000.

(50) Liang, Z.; Yang, Z.; Sun, S.-S.; Wu, B.; Dalton, L. R.; Garner, S. M.; Kalluri, S.; Chen, A.; Steier, W. H. Processible and thermally stable heterocyclic polymers for second-order nonlinear optical studies. *Chem. Mater.* **1996**, *8*, 2681-2685.

(51) Mao, S. S. H.; Ra, Y.; Guo, L.; Zhang, C.; Dalton, L. R.; Chen, A.; Garner, S. M.; Steier, W. H. Progress toward device-quality second-order nonlinear optical materials. 1. Influence of composition and processing conditions on nonlinearity, temporal stability, and optical loss. *Chem. Mater.* **1998**, *10*, 146-155.

(52) Lu, J.; Yin, J. Synthesis and characterization of photocrosslinkable, side-chain, second-order nonlinear optical poly(ester imide)s with great film-forming ability and long-term dipole orientation stability. *J. Polym. Sci., Part A: Polym. Chem.* **2002**, *41*, 303-312.

(53) Dalton, L. D. Nonlinear optical polymeric materials: From chromophore design to commercial applications. In *Polymers for photonics applications i*; Springer Berlin: Heidelberg, 2002; Vol. 158; pp 1-86.

(54) Haller, M.; Luo, J.; Li, H.; Kim, T.-D.; Liao, Y.; Robinson, B. H.; Dalton, L. R.; Jen, A. K.-Y. A novel lattice-hardening process to achieve highly efficient and thermally stable nonlinear optical polymers. *Macromolecules* **2004**, *37*, 688-690.

(55) Wong, S.; Ma, H.; Jen, A. K.-Y.; Barto, R.; Frank, C. W. Highly fluorinated trifluorovinyl aryl ether monomers and perfluorocyclobutane aromatic ether

polymers for optical waveguide applications. *Macromolecules* **2003**, *36*, 8001-8007.

(56) Ma, H.; Chen, B.; Sassa, T.; Dalton, L. R.; Jen, A. K.-Y. Highly efficient and thermally stable nonlinear optical dendrimer for electrooptics. *J. Am. Chem. Soc.* **2001**, *123*, 986-987.

(57) Galvan-Gonzalez, A.; Belfield, K. D.; Stegeman, G. I.; Canva, M.; Chan, K. P.; Park, K.; Sukhomlinova, L.; Twieg, R. J. Photostability enhancement of an azobenzene photonic polymer. *Appl. Phys. Lett.* **2000**, *77*, 2083-2085.

(58) Luo, J.; Haller, M.; Li, H.; Kim, T.-D.; Jen, A. K.-Y. Highly efficient and thermally stable electro-optic polymer from a smartly controlled crosslinking process. *Adv. Mater.* **2003**, *15*, 1635-1638.

(59) Stenger-Smith, J. D.; Zarras, P.; Hollins, R. A.; Chafin, A. P.; Merwin, L. H.; Yee, R.; Lindsay, G. A.; Herman, W. N.; Gratz, R. F.; Nickel, E. G. Main-chain syndioregic nonlinear optical polymers. Ii. Extended pi conjugated and improved thermal properties. *J. Polym. Sci., Part A: Polym. Chem.* **2000**, *38*.

(60) Huang, D.; Zhang, C.; Dalton, L. R.; Weber, W. P. Synthesis and characterization of main-chain nlo oligomers and polymer that contain 4-dialkylamino-4'(alkylsulfonyl)azobenzene chromophores. *J. Polym. Sci., Part A: Polym. Chem.* **2000**, *38*, 546-559.

(61) Luo, J.; Liu, S.; Haller, M.; Liu, L.; Ma, H.; Jen, A. K.-Y. Design, synthesis, and properties of highly efficient side-chain dendronized nonlinear optical polymers for electro-optics. *Adv. Mater.* **2002**, *14*, 1763-1768.

(62) Zhang, Y.; Wada, T.; Sasabe, H. A new hyperbranched polymer with polar chromophores for nonlinear optics. *Polymer* **1997**, *38*, 2893-2897.

(63) Kang, S. H.; Luo, J.; Ma, H.; Barto, R. R.; Frank, C. W.; Dalton, L. R.; Jen, A. K.-Y. A hyperbranched aromatic fluoropolyester for photonic applications. *Macromolecules* **2003**, *36*, 4355-4359.

(64) Bai, Y.; Song, N.; Gao, J. P.; Sun, X.; Wang, X.; Yu, G.; Wang, Z. Y. A new approach to highly electrooptically active materials using cross-linkable, hyperbranced chromophore-containing oligomers as a macromolecular dopant. *J. Am. Chem. Soc.* **2005**, *127*, 2060-2061.

(65) Pereverzev, Y. V.; Prezhdo, O. V.; Dalton, L. R. Structural origin of the enhanced electro-optic response of dendrimer systems. *Chem. Phys. Lett.* **2003**, *373*, 207-212.

(66) Ma, H.; Liu, S.; Luo, J.; Suresh, S.; Liu, L.; Kang, S. H.; Haller, M.; Sassa, T.; Dalton, L. R.; Jen, A. K.-Y. Highly efficient and thermally stable electro-optical dendrimers for photonics. *Adv. Funct. Mater.* **2002**, *12*, 565-574.

(67) Sullivan, P. A., University of Washington, 2006.

(68) Bergman, J. G.; McFee, J. H.; Crane, G. R. Pyroelectricity and optical second harmonic generation in poly(vinylidene fluoride) films. *Appl. Phys. Lett.* **1971**, *18*, 203-205.

(69) Otomo, A.; Jager, M.; Stegeman, G. I.; Flipse, M. C.; Diemeer, M. Key trade-offs for second harmonic generation in poled polymers. *Appl. Phys. Lett.* **1996**, *69*, 1991-1993.

(70) Teng, C. C.; Man, H. T. Simple reflection technique for measuring the electro-optic coefficient of poled polymers. *Appl. Phys. Lett.* **1990**, *56*, 1734-1736.

(71) Schildkraut, J. S. Determination of the electrooptic coefficient of a poled polymer film. *Appl. Opt.* **1990**, *29*, 2839-2841.

(72) Chollet, P. A.; Gadret, G.; Kajzar, F.; Raimond, P. Electro-optic coefficient determination in stratified organized molecular thin films: Application to poled polymers. *Thin Solid Films* **1994**, *242*, 132-138.

(73) Han, S. H.; Wu, J. W. Single-beam polarization interferometry measurement of the linear electro-optic effect in poled polymer films with a reflection configuration. *J. Opt. Soc. Am. B: Opt. Phys.* **1997**, *14*, 1131-1137.

(74) Park, D. H.; Lee, C. H.; Herman, W. N. Analysis of multiple relfection effects in reflective measurements of electro-optic coefficients of poled polymers in multilayer structures. *Opt. Express* **2006**, *14*, 8866-8884.

(75) Jiang, Y.; Cao, Z.; Shen, Q.; Dou, X.; Chen, Y.; Ozaki, Y. Improved attenuated-total-reflection technique for measuring the electro-optic coefficients of nonlinear optical polymers. *J. Opt. Soc. Am. B: Opt. Phys.* **2000**, *17*, 805-808.

(76) Michelotti, F.; Toussaere, E.; Levenson, R.; Liang, J.; Zyss, J. Real-time pole and probe assessment of orientational processes in electro-optic polymers. *Appl. Phys. Lett.* **1995**, *67*, 2765-2767.

(77) Zhang, C.; Dalton, L. R.; Oh, M.-C.; Zhang, H.; Steier, W. H. Low vp electrooptic modulators from cld-1: Chromophore design and synthesis, material processing, and characterization. *Chem. Mater.* **2001**, *13*, 3043-3050.

(78) e.g. Model 2010 Prism Coupler from Metricon Corporation

(79) Galvan-Gonzalez, A.; Canva, M.; Stegeman, G. I.; Twieg, R.; Kowalczyk, T. C.; Lackritz, H. S. Effect of temperature and atmospheric environment on the photodegradation of disperse red 1-type polymers. *Opt. Lett.* **1999**, *24*, 1741-1743.

(80) Galvan-Gonzalez, A.; Belfield, K. D.; Stegeman, G. I.; Canva, M.; Marder, S. R.; Staub, K.; Levina, G.; Twieg, R. J. Photodegradation of selected p-conjugated electrooptic chromophores. *J. Appl. Phys.* **2003**, *94*, 756-763.

(81) Galvan-Gonzalez, A.; Stegeman, G. I.; Jen, A. K. Y.; Wu, X.; Canva, M.; Kowalczyk, A. C.; Zhang, X. Q.; Lackritz, H. S.; Marder, S.; Thayumanavan, S.; Levina, G. Photostability of electro-optic polymers possessing chromophores with efficient amino donors and cyano-containing acceptors. *J. Opt. Soc. Am. B: Opt. Phys.* **2001**, *18*, 1846-1853.

(82) DeRosa, M. E.; He, M.; Cites, J. S.; Garner, S. M.; Tang, Y. R. Photostability of high beta electro-optic chromophores at 1550 nm. *J. Phys. Chem. A* **2004**, *108*, 8725-8730.

(83) Dubois, A.; Canva, M.; Brun, A.; Chaput, F.; Boilot, J.-P. Photostability of dye molecules trapped in solid matrixes. *Appl. Opt.* **1996**, *35*, 3193-3199.

(84) Rezzonico, D.; Jazbinsek, M.; Bosshard, C.; Günter, P.; Bale, D.; Liao, Y.; Dalton, L. R.; Reid, P. J. Photostability of pi-conjugated chromophores by resonant and nonresonant light excitations for long-life polymeric telecommunication devices. *in preparation* **2007**.

(85) Kim, M.-s.; Ju, J. J.; Park, S. K.; Do, J. Y.; Lee, M.-H. Evaluation of nonlinear optical polymers for second-harmonic generation: Toward the balance of absorption and nonlinearity against intrinsic trade-off. *Chem. Phys. Lett.* **2006**, *417*, 277-281.

(86) Eldada, L.; Shacklette, L. W. Advances in polymer integrated optics. *IEEE J. Sel. Top. Quantum Electron.* **2000**, *6*, 54-68.

(87) Teng, C. C. Precision measurements of the optical attenuation profile along the propagation path in thin-film waveguides. *Appl. Opt.* **1993**, *32*, 1051-1054.

(88) Okamura, Y.; Yoshinaka, S.; Yamamoto, S. Measuring mode propagation losses of integrated optical waveguides: A simple method. *Appl. Opt.* **1983**, *22*, 3892-3894.

Chapter 4: Nanoscale Engineering of Discotic Chromophores

4.1 Introduction

One of the biggest problems in achieving highly active organic electro-optic (EO) materials is the introduction of a high degree of stable acentric order of EO chromophores in a matrix (Chapter 3). In terms of guest-host poled polymers and related systems, Robinson, Dalton, and coworkers have demonstrated that the intermolecular centrosymmetric dipole-dipole interactions play a critical role in restricting the degree of noncentrosymmetric order achieved (Sections 3.3.5 and 3.3.6).[1,2] The result is a maximum in the r_{33} coefficient as a function of loading density (N), where the position of the maximum depends on both the dipole moment (μ), and the chromophore shape. The implications of the μ dependence of r_{33} for EO chromophores are explored in Chapter 5. The shape-dependence indicates that spherical chromophores should have reduced dipole-dipole interactions and thus larger r_{33} maxima at higher loading densities, as compared to the prolate ellipsoids of standard linear donor-π-acceptor chromophores. Based on these calculations, much work has been directed at functionalization to enhance the overall spherical shape of EO chromophores.[1,3,4]

Recent calculations from Dr. Robert Nielsen, Harrison Rommel, and Dr. Bruce Robinson used Monte Carlo and equilibrium statistical mechanics methods to explore the effect of lattice geometry on the poling-induced order of point-dipoles.[5] By varying the spacing between the point-dipoles in both the *z* direction (poling field direction) and

the *xy* plane they could explore the order of the system as a function of the effective *xy* : *z* distance aspect ratio (A). As they increased A from 1 to 2, they saw formation of distinct columns of acentric order, with the <cosθ> alignment within a given column in excess of 0.85 in the presence of a poling field. This can be attributed to strong head-to-tail dipole-dipole interactions within a column, and weak side-on-side dipole-dipole interactions between the columns. Overall, they saw a factor of 2 increase in the $N\langle\cos^3\theta\rangle$ loading parameter, which is directly proportional to r_{33}, as they increased A from 1 to 2. Additionally, they found that after an initial rise (past $N = 2.5 \times 10^{20}$ molecules/cc), the loading parameter was relatively constant as N increased further, unlike in the A = 1 case, where the loading parameter dropped off as N increased. In the absence of a poling field, they still saw formation of columnar order, although the net overall distribution was centrosymmetric due to opposite columnar orientations.

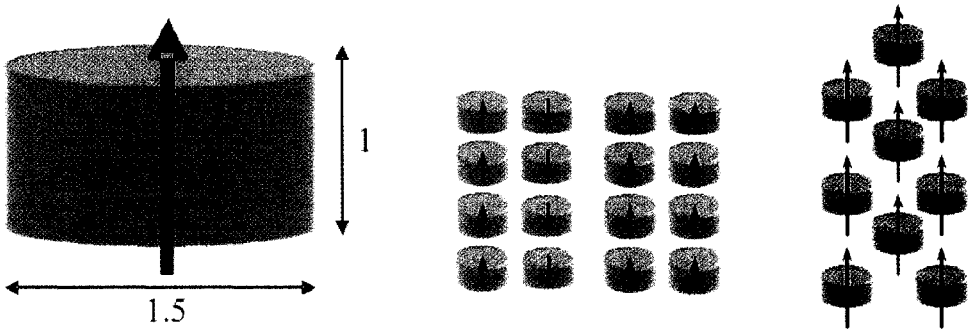

Figure 4.1. Potential discotic chromophore interactions (a) Chromophore aspect ratio (b) Columnar stacking of chromophores (c) Interdigitation of chromophores

Further discussions suggest that these effects are readily apparent even at intermediate values of A, as low as about 1.4.[6] This suggests that if EO chromophores could be functionalized into oblate ellipsoids, with width : charge-transfer axis length aspect ratios of around 1.5 (Figure 4.1a), they might tend to self-assemble in

noncentrosymmetric columns (Figure 4.1b) or interdigitated networks (Figure 4.1c). Although the overall net orientation of these columns or domains may be centrosmmetric, the weak side-on dipole-dipole interactions should allow efficient poling of the individual columns or domains to attain a high degree of uniformly aligned noncentrosymmetric order and thus large r_{33} values. The acentric order of these systems is also predicted to be considerably more temporally stable than in conventional guest-host systems, due to the presence of a local energy minimum created by the attractive head-to-tail dipole-dipole interactions within the columns.[6]

If a molecule truly has an aspect ratio of 2:1, then it would presumably resemble a disc. The self-assembly of disc-shaped molecules in an nanostructured or oriented fashion is already a well known phenomenon, discovered by Chandrasekhar *et al.* in 1977.[7] Molecules with this behavior are called discotic liquid crystals (DLCs), and they usually exhibit highly nanostructured 2-dimensional lattices of aperiodic, "liquid-like" columns with extensive long-range order (columnar phase), or occasionally they exhibit orientational but not positional order (nematic discotic phase, N_D).[8] While linear D-π-A chromophores are clearly very different from DLCs, which are generally composed of rigid aromatic cores with many flexible alkyl chains on the periphery (Figure 4.2), with sufficient modification they may mimic some of their important features. The head-to-tail dipole-dipole interaction can be expected to provide a driving force for assembly in a manner similar to the π-π stacking interactions that drive assembly of many DLCs. Indeed, examples exist of DLCs using dipole-dipole forces to drive assembly.[9]

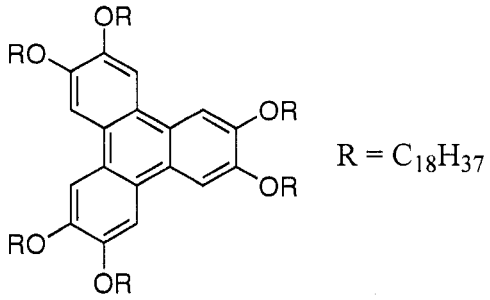

Figure 4.2. Representative discotic liquid crystal

The distinct rod shape of D-π-A chromophores makes it difficult to achieve a true disc shape. Synthetic modification can alter the shape by attaching large space-filling pendant groups to provide steric "bulk," but to achieve a true disc shape would require such a large amount as to reduce the effective loading density of the chromophore too far for practical application. A compromise must be established between sufficient space-filling to achieve the minimum 1.4:1 width:length ratio and an approximation of a disc-shape, while sustaining a reasonable loading density. Average loading densities of chromophores in polymers suggests anything below 10-15 % (weight/weight %) is impractical.[10,11] The space-filling steric bulk serves the added purpose of providing the alkyl chains that are critical to the formation of true LC phases; they appear to act as "entropy reservoirs," forming liquid-like regions between the columns.[12] In DLCs, the choice of linkage between the central core and the peripheral alkyl groups provides a variable for tuning the intra-column forces, and thus the LC phase behavior.[8] The steric bulk in discotic chromophores will provide an analogous function, allowing tuning of both intra- and inter-columnar forces, and thus the phase behavior.

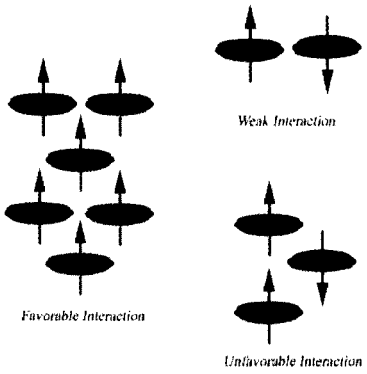

Figure 4.3. Revised pseudo-discotic chromophore concept

Based upon the limitations of synthetic derivitization of chromophores as discussed above, a modified concept of the "discotic" chromophores must be considered. True disc-shape is not required, as long as the system adopts pseudo-DLC behavior. As can been seen in Figure 4.3, a waist-functionalized, pseudo-disc chromophore shape could conceivably provide sufficient modification of the dipole-dipole interactions to enhance the system's order. The waist functionalization should prevent close approach of the dipoles in a centrosymmetric fashion, but allow close approach in a head-to-tail fashion. Additionally, if one considers a collective assembly, which is critical for accurately approximating the system's behavior, one can imagine that interdigitation will further drive noncentrosymmetric packing due to unfavorable head-to-head and tail-to-tail interactions required by interdigitation in the centrosymmetric lattice. The lattice pictured suggests the system may form a N_D DLC phase, or perhaps some non-hexagonal distorted or tilted columnar lattice. It should be noted that while the system is expected to exhibit a high degree of local order, particularly if any of the DLC phases are adopted, poling will still be required to align the regions of local order into a uniformly aligned macroscopic material.

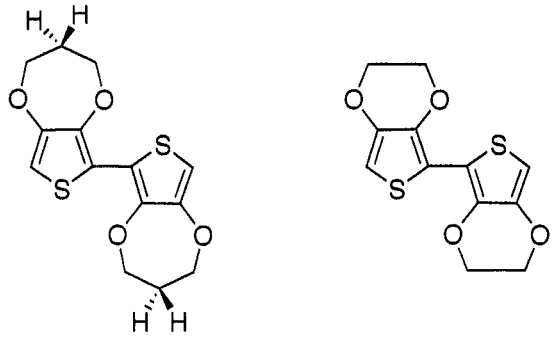

bis-ProDOT bis-EDOT

Figure 4.4. Structures of bis-ProDOT and bis-EDOT

Pervious work in the Dalton group by Dr. Olivier Clot and coworkers has explored the synthesis and characterization of waist-functionalized EO chromophores with enhanced 3D shapes.[13] This work focused on the use of chromophores based upon the bis-propylenedioxythiophene (bis-ProDOT) bridge (Figure 4.4). ProDOT, along with the related ethylenedioxythiophene (EDOT) (Figure 4.4), have seen considerable use in organic electrochromic,[14,15] light-emitting diode (LED),[16,17] field-effect transistor[17,18] (FET), and related applications.[19,20] In organic EO, Roncali and coworkers have synthesized chromophores using the bis-EDOT (BEDOT) bridge,[21-23] which exhibit a dramatic increase in $\mu\beta$ (as measured by EFISH) with respect to the bithiophoene-based reference chromophore. They attributed the improvement to the sulfur-oxygen interaction between adjacent EDOT rings, as indicated by the unusually short distance between these atoms in X-ray crystal structures.[21] This interaction results in a rigid, nearly planar configuration of the BEDOT structure, as opposed to the twisted bithiophene conformation.[24]

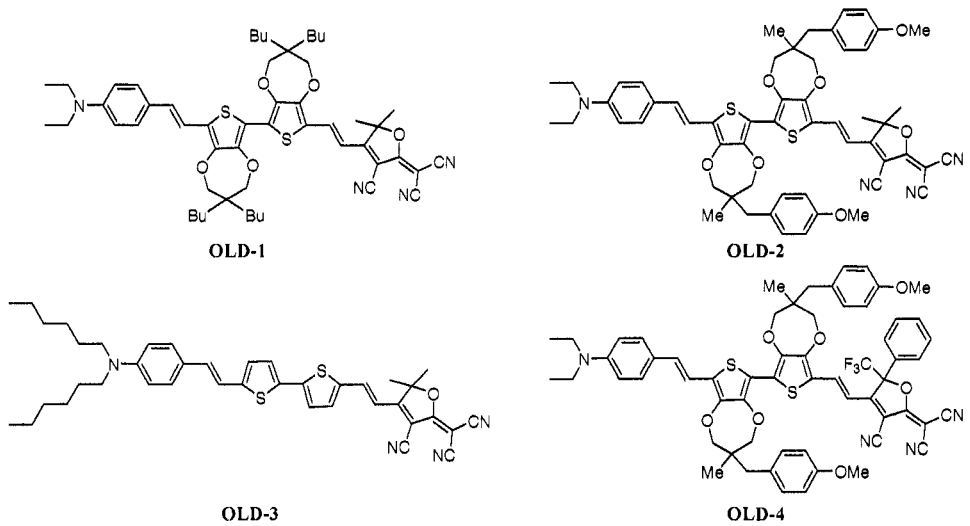

Figure 4.5. Structures of OLD chromophores

The bis-ProDOT bridge used in the work by Clot *et al.* retains the attractive features of the BEDOT chromophores,[25] but also allows for waist-functionalization of the chromophores. In particular, the tetrahedral geometry of the central carbon in the propylene chain allows for an enhanced three-dimensional shape of functionalized bis-ProDOT derivatives. As a result, the chromophores should be more spherical, and should exhibit enhanced poling-induced macroscopic EO activity. All of the bis-ProDOT chromophores studied (Figure 4.5) demonstrate significantly enhanced β_{HRS} values (Table 4.1)[13,26] with respect to EZ-FTC and CLD-5 benchmark chromophores.[26] The bithiophene reference chromophore **OLD-3**, on the other hand, is only slightly more active than CLD-5. The β_{HRS} value for **OLD-4** is significantly (2ω) resonance-enhanced as evidenced by its red-shifted wavelength of maximum absorption (λ_{max}; for a discussion of resonance enhancement, see Section 2.4), and thus must be considered as an overestimation of its activity. In terms of the macroscopic activity, the bis-ProDOT based chromophores exhibit considerably enhanced r_{33} values, at similar loading densities, with respect to those of **OLD-3** (Table 4.1). Thus, the bis-ProDOT

based chromophores demonstrate excellent microscopic activity and promising enhancements in the macroscopic activity as well.

Table 4.1. Comparison of OLD and benchmark chromophores.[13,26]

			r_{33} (pm/V)[d]	
Chromophore	**λ_{max} (nm)[a]**	**β_{rel}(1907 nm)[b]**	**20 wt %[e]**	**30 wt %[e]**
OLD-1	750	4584 +/- 181	47	NA
OLD-2	746	4859 +/- 523	35	58
OLD-3	674	3823 +/- 398	15	NA
OLD-4	825	14790 +/- 970[c]	69	NA
EZ-FTC	676	2780 +/- 1440	NA	NA
CLD-5	658	3519 +/- 319	NA	NA

[a]in $CHCl_3$ [b]HRS data is measured relative to chloroform [c]Resonance enhanced [d]measured by Simple Reflection[27] at 1.31 μm in Alex Jen's group (Department of Materials Science and Engineering, University of Washington) [e]wt % of chromophore in APC polymer host NA – Not available

4.2 Synthesis of Discotic Chromophores

Based upon the theoretical predictions and the results from the previous bis-ProDOT based OLD chromophores, we set out to synthesize a bis-ProDOT based chromophore that was readily waist functionalizable about the tetrahedral propylene carbon to afford chromophores with aspect ratios (A) approaching 1.5. Towards this end, we identified **OLD-5** (Figure 4.6) as an attractive target. This chromophore retains the desirable features of the previous bis-ProDOT based chromophores, yet allows for extensive functionalization through facile cleavage of the *t*-butyldimethylsilyl (TBDMS) protecting groups, followed by esterification of the hydroxyl groups with carboxylic acid containing dendrons. The dendrons allow us to incorporate the steric

bulk necessary to achieve aspect ratios of 1.5, and provide a means to tune the intermolecular interactions.

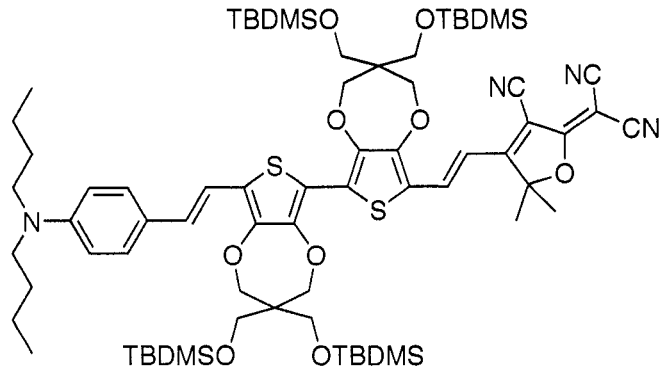

OLD-5

Figure 4.6. Structure of **OLD-5** target chromophore

The synthesis of **OLD-5** (Schemes 4.1 and 4.2) was developed by Dr. Jessica Sinness and Dr. Olivier Clot (Dalton Group Department of Chemistry, University of Washington), and accomplished by Dr. Sinness.[28,29] To synthesize the bridge (Scheme 4.1), 3,4-dimethoxythiophene (**4.1**) was coupled to 2,2-bis(bromomethyl)-1,3-propanediol (**4.2**) in a transetherification reaction to give the dibromo ProDOT moiety (**4.3**) in 72.0% yield.[30] This was then converted to the benzyl protected dihydroxy ProDOT (**4.4**) via a Williamson etherification in 83.7% yield. This route was required as the ProDOT ring formation reaction can be disrupted by the presence of extraneous alkoxy moieties in the molecules, and the use of pentaerythritol [$C(CH_2OH)_4$] leads to the undesirable formation of two connected ProDOT rings.[31] The benzyl group was then removed using a Birch reduction (**4.5**, 86.7%) and replaced with a TBDMS group (**4.6**, 92.2%), which allows for facile deprotection of the final chromophore. The TBDMS-protected ProDOT (**4.6**) was dimerized with ^{n}BuLi, tetraethylenediamine (TMEDA), and $Fe(acac)_3$ to give **4.7** in 47.7% yield. The dimer (**4.7**) was then

selectively mono-formylated using 1 equivalent of ^{n}BuLi with DMF to give **4.8** in 76.3% yield.

Scheme 4.1. Synthesis of ProDOT(CH_2OTBDMS)$_2$-based bridge

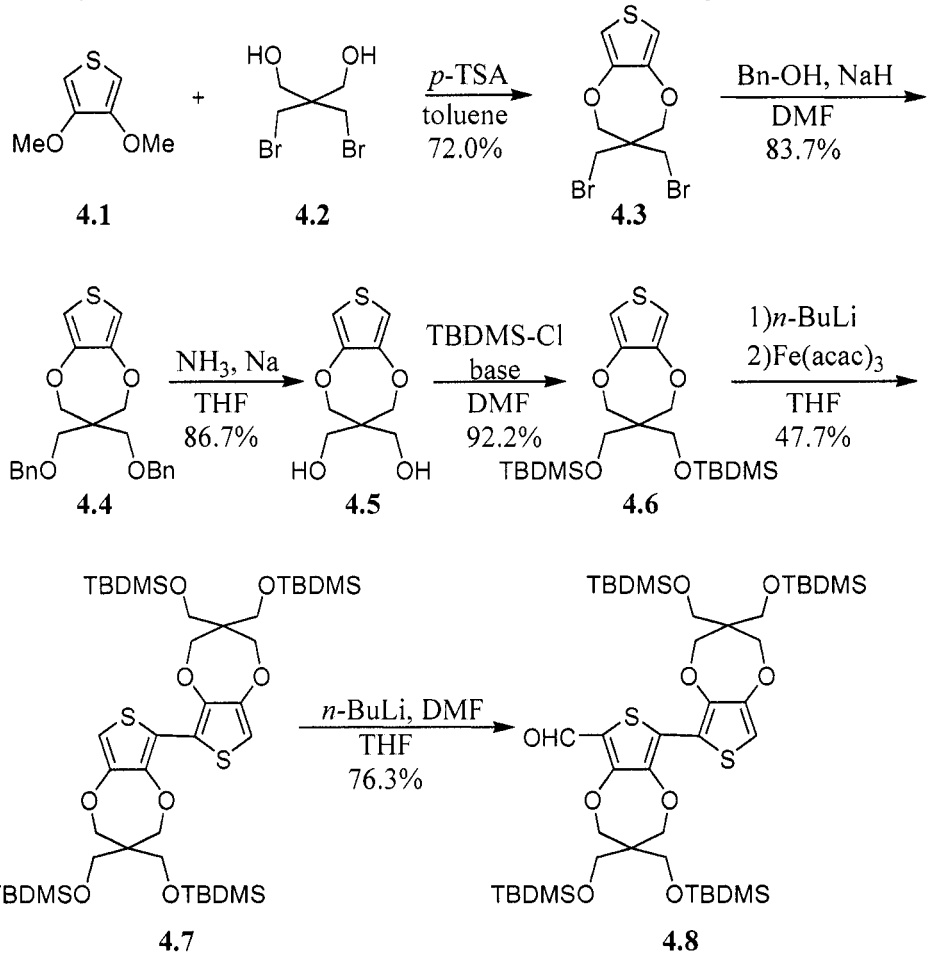

Once the bridge-aldehyde (**4.8**) had been synthesized, the donor (**4.9**) was attached (Scheme 4.2) using a Horner-Wadsworth-Emmons reaction to give the donor-bridge (**4.10**) in 84.0% yield. The donor-bridge (**4.10**) was then formylated using ^{n}BuLi and DMF to give **4.11** in 84.4% yield. Finally, the TCF acceptor (**4.12**) was attached using a Knoevenagel condensation in 88.7% yield to give the final chromophore (**OLD-5**). In theory, **OLD-5** itself could be explored as an EO chromophore in guest-host films. To our surprise, however, did not prove to be sufficiently soluble. Although

OLD-5 is moderately soluble in common organic solvents, it does not display the high degree of solubility necessary for spin casting high-quality EO films. It can, however, be further derivatized into high-molecular weight dendronized chromophores with aspect ratios approaching 1.5.

Scheme 4.2. Synthesis of **OLD-5** chromophore

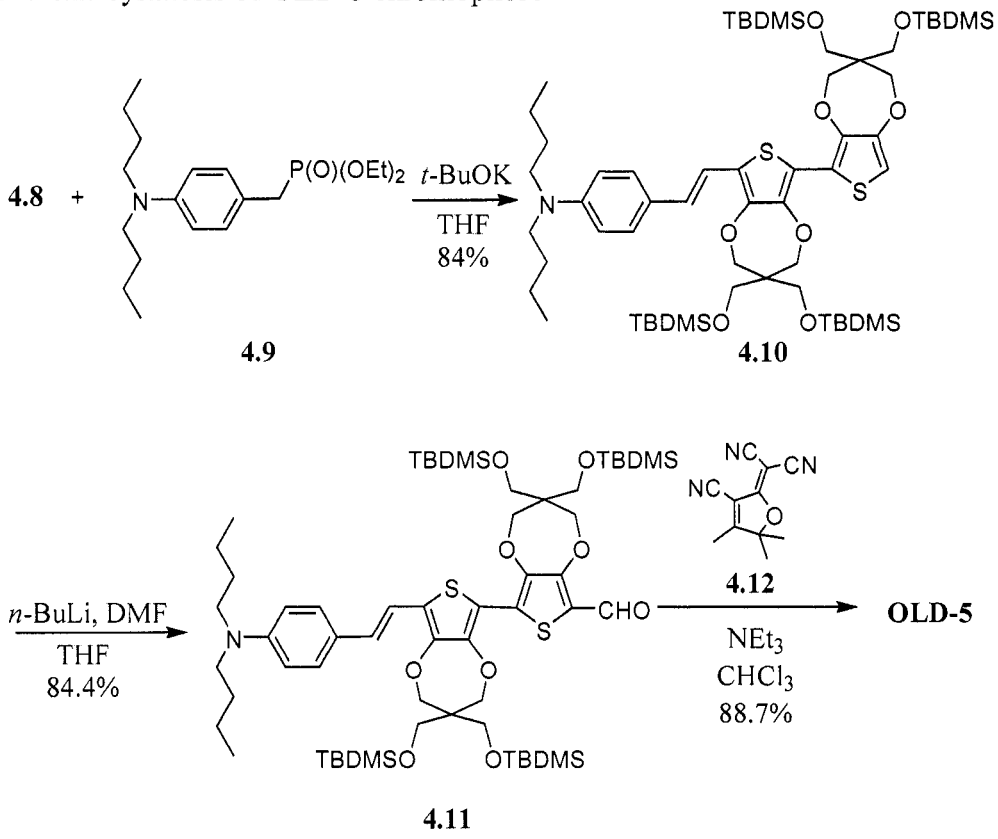

As the ProDOT ring is highly acid sensitive, **OLD-5** must be deprotected under mildly basic tetrabutylammounium fluoride (TBAF) conditions (Scheme 4.3), which affords the tetra-alcohol derivative (**4.13**) in 85.8 % yield. The tetra-ol product (**4.13**) can then be esterified under dicyclohexylcarbodimide (DCC) and dimethylaminopyridine (DMAP) conditions, with a small amount of N,N-dimethylformamide (DMF) to promote dissolution of the tetra-ol, with a variety of carboxylic acid containing dendrons to afford the (pseudo) discotic chromophores. The

yields for this reaction varied widely from 56.1 % to 90.0 %, depending on the dendron structure. In general, the partially dendronized material (with 2 or 3 dendrons attached) could be recovered and subsequently re-reacted to maximize use of the precious **OLD-5** material. We have incorporated a variety of functionalities in the dendrons to explore the effect of different intermolecular interactions on the properties of these discotic chromophores. The rationale behind these choices is presented in their individual sections; here we present only their synthesis.

Scheme 4.3. Generic synthesis of discotic chromophores

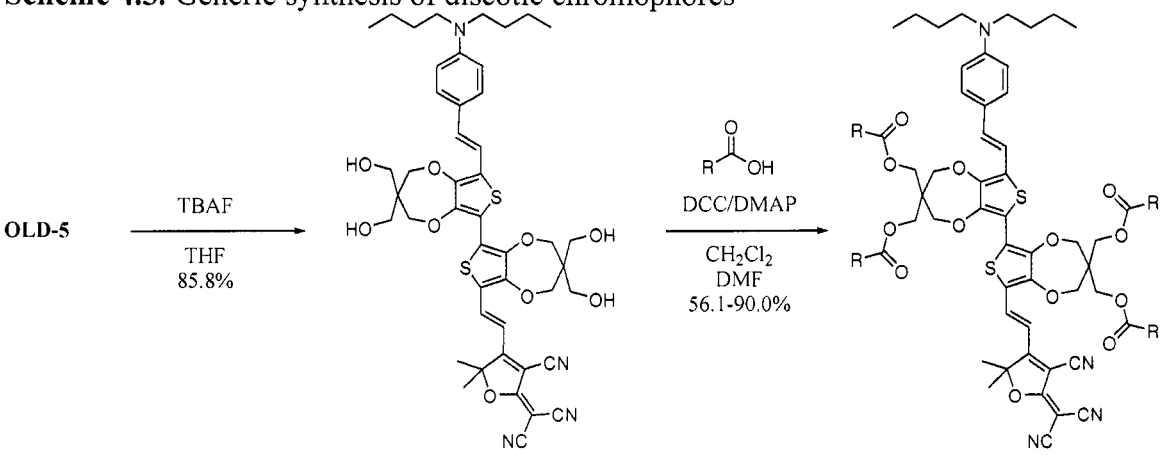

The first dendron was synthesized by Dr. Nishant Bhatambrekar (Dalton Group, Department of Chemistry, University of Washington) as outlined in Scheme 4.4. The commercially available methyl 3,4,5-trihydroxybenzoate (**4.14**) was alkylated with 1-bromo-2-ethylhexane to afford the tris-2-ethylhexyl derivative (**4.15**) in 42.9 % yield. This was then deprotected with potassium hydroxide (KOH) in methanol (MeOH), tetrahydrofuran (THF), and water to afford the carboxylic acid (**4.16**) in 83.7 % yield. This dendron was attached to **4.13** to afford **SJLD-1** (Figure 4.9) in 60.5 % yield. Although this yield appears rather low, it corresponds to an 88 % yield per dendron attached. Additionally, this procedure was not optimized, and the partially dendronized

material was recovered and subsequently re-reacted, providing additional product. The second dendron was synthesized (Scheme 4.4) by alkylating the commercially available methyl 3,5-dihydroxybenzoate (**4.17**) with 1-bromohexane to afford the dihexyl derivative (**4.18**) in 75.9 % yield. This was then deprotected using KOH in MeOH/THF/water to afford the acid (**4.19**) in 93.8 % yield. This dendron was attached to **4.13** to afford **SJLD-2** (Figure 4.19) in up to 85.4 % yield (optimized), corresponding to a 96 % yield per dendron. The third dendron was synthesized (Scheme 4.4) by esterification of the commercially available 2,2,2-trichloroethyl 3,5-dihydroxybenzoate (**4.20**) with monomethyl succinate to afford the bis-diester derivative (**4.21**) in 89.9 % yield. This was then selectively deprotected with zinc dust in acetic acid and THF to afford the carboxylic acid derivative (**4.22**) in 79.1 % yield. This dendron was attached to **4.13** to afford **SJLD-3** (Figure 4.31) in up to 56.1 % yield. For **SJLD-3** in particular yields were consistently low, even for the re-reaction of partially dendronized material. The fourth dendron used was the commercially available 3,5-dibenzyloxybenzoic acid (**4.23**), which was attached to **4.13** to afford **SJLD-4** (Figure 4.38) in 90.0 % yield (optimized), corresponding to a 97.4 % yield per dendron. The fifth and final dendron studied to date was synthesized (Scheme 4.4) by Dr. Andrew Akelaitis (Dalton Group, Department of Chemistry, University of Washington) via Mitsunobu coupling of **4.20** and 2,3,4,5,6-pentafluorobenzyl alcohol with triphenylphosphine (PPh_3) and diethylazodicarboxylate (DEAD) to afford the bis-pentafluorobenzyl derivative (**4.24**). This was then selectively deprotected with zinc dust in acetic acid and THF to afford the acid (**4.25**). This dendron was attached to **4.13** to afford **SJLD-5** (Figure 4.47) in 85.4 % yield (optimized), corresponding to a 96 % yield per dendron.

Scheme 4.4. Synthesis of dendrons for discotic chromophores

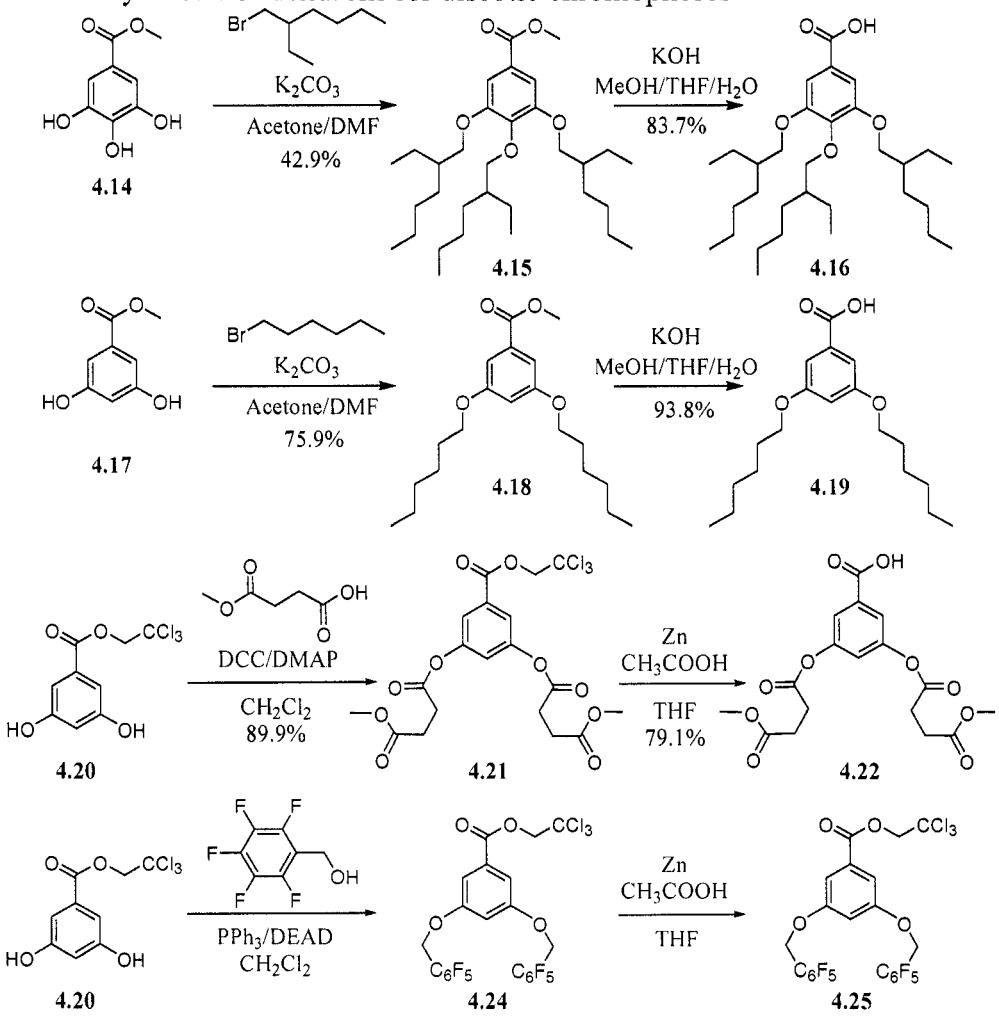

4.3 Overview of Discotic Chromophores

Although the detailed behavior of each of the discotic chromophores will be presented in their individual sections (Sections 4.4 – 4.8), here we present an overview of the general features of the discotic chromophores. We have attempted to explore a variety of intermolecular interactions by incorporating a range of functional groups into the dendrons. These include nonpolar alkyl chains (**SJLD-1** and **SJLD-2**), polar diester

chains (**SJLD-3**), phenyl rings (all systems), and fluorinated phenyl rings (**SJLD-5**), which can give rise to a variety of intermolecular interactions. In the case of nonpolar alkyl chains, weak van der Waals interactions are expected, with potential for extensive interdigitation of alkyl chains and phase separation of the nonpolar regions from polar regions. The diester chains are expected to exhibit stronger van der Waals interactions, with potential for interdigitation, and should be more rigid in nature than the alkyl chains. The phenyl and pentafluorophenyl rings could potentially both exhibit π-π stacking and edge-to-face van der Waals type interactions. Previous research suggests, however, that the pentafluorophenyl rings should exhibit stronger π-π interactions with electron-rich aromatic moieties than the non-fluorinated version. Additionally, the fluorinated rings may preferentially interact with each other, exhibiting phase segregation from the nonfluorinated material.

Table 4.2. Comparison of discotic chromophore properties

	Molecular Mass (g/mol)	Active Loading Density	Number Density ($x10^{20}$ molecules/cc)	Aspect ratio (A)
SJLD-1	2824.03	17.3%	2.13	1.49
SJLD-2	2086.75	23.3%	2.89	1.48
SJLD-3	2326.27	20.9%	2.56	1.48
SJLD-4	2134.46	22.8%	2.82	1.48
SJLD-5	2854.07	17.0%	2.11	1.46

The variety of functional groups incorporated into the discotic chromophores results in a range of molecular masses, active chomophore loading and number densities, and calculated aspect ratios (A), all of which are presented in Table 4.2. The active chromophore loading percent, which describes the ratio of EO active to EO inactive material in a system, is an important characteristic of an organic EO material. For our materials, it is defined by the ratio of masses of the active charge-transfer

backbone (highlighted in blue in the respective figures) to the whole system. Unlike in guest-host systems, where the chromophore content can be varied, this value is fixed for each discotic chromophore. Guest-host systems typically value around 25 total chromophore wt. %,[10] corresponding to roughly 20 active wt. %, although this varies considerably. Thus, the discotic systems exhibit similar or slightly lower loading than average guest-host systems. The chromophore number density (N), in terms of molecules/cc, is a related property often used in theoretical calculations. It is calculated for our systems from the molecular mass by assuming, as is generally done, a density of 1 g/cc. Comparing the results for our chromophores to the Monte Carlo simulations of loading parameter as a function of N for the A values studied (Figure 10 of Reference 5), we find our systems are at the low end of the densities that exhibit distinct acentric columnar behavior. Thus, the intra-column interactions may not be at their strongest and systems with higher N values might exhibit the predicted behavior more strongly. Molecular mechanics calculations (MM2 geometry optimization, Chem 3D, Cambridge Software) of the molecules were used to estimate the aspect ratio (A) in an extended molecular conformation. Although all of the systems exhibit values close to 1.5, which should be sufficient to exhibit the self-assembling columnar behavior predicted by the Monte Carlo asymmetric lattice calculations, it must be considered that the A values may be lower in the actual materials due to presence of different molecular conformations.

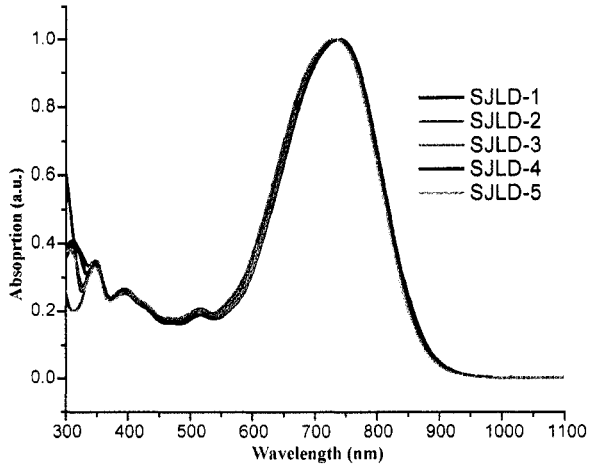

Figure 4.7. Normalized UV-vis spectra of the discotic chromophores in chloroform

UV-visible absorption spectroscopy of the discotic chromophores in dilute chloroform solutions (Figure 4.7), where intermolecular interactions should be minimal, all of the chromophores exhibit nearly identical λ_{max} (733-738 nm) and extinction coefficients (ε around 66000 L/mol*cm). This suggests that all the chromophores possess nearly identical molecular linear and nonlinear optical properties (e.g. β values). In cured, spin-cast thin films, however, where intermolecular interactions dominate, the materials exhibit very different properties (Figure 4.8). The **SJLD-1** and **SJLD-5** films exhibit a small blue shift in λ_{max}, with respect to the solution values, and a slight shoulder peak is evident. In contrast, the films of **SJLD-2-4** exhibit large red-shifts in λ_{max} and spectral broadening, with the existence of multiple peaks. Note that the anomalously high baseline for the **SJLD-3** spectrum is due to an excessive optical density of the film, and the discontinuity at around 850 nm is due to an instrumental error. All of the red-shifted films do exhibit a considerable absorption tail that extends out to around 1.3 μm, which has consequences for EO characterization. Finally, it should be noted that dissolution of the films in chloroform reproduces the solution

spectra, indicating that decomoposition or other irreversible reactions are not responsible for this behavior. The preliminary characterization of these materials has been previously presented,[32,33] and these materials are currently protected under a provisional US patent.

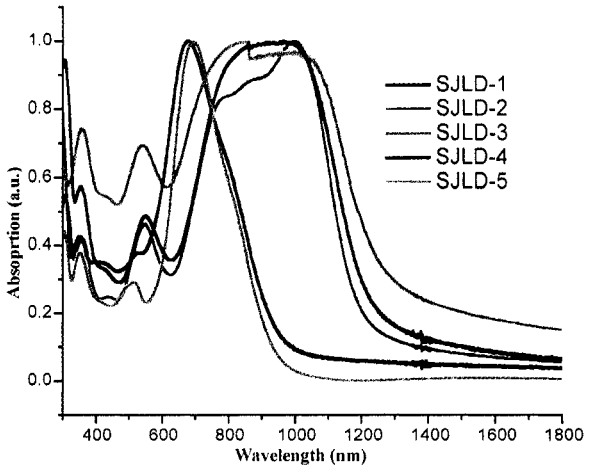

Figure 4.8. Normalized UV-vis-NIR spectra of cured discotic chromophore films

4.4 SJLD-1

The first discotic chromophore system studied was **SJLD-1** (Figure 4.9), which incorporates the tris-2ethylhexylphenyl-based dendron. This system was specifically designed with the structure-property relationships of DLCs in mind. The dendron consists of a phenyl core, which can potentially participate in π-π stacking interactions, and three bulky 2-ethylhexyl chains to simultaneously provide steric bulk, act as entropy reservoirs,[12] and reduce potential interdigitation of alkyl chains. Molecular mechanics calculations (MM2 geometry optimization, Chem 3D, Cambridge Software) of **SJLD-1** predict an aspect ratio (A) of 1.49, in an extended conformation.

Additionally, this system was calculated to possess active chromophore loading and number densities of 17.3 wt. % and 2.13 x 10^{20} molecules/cc, respectively.

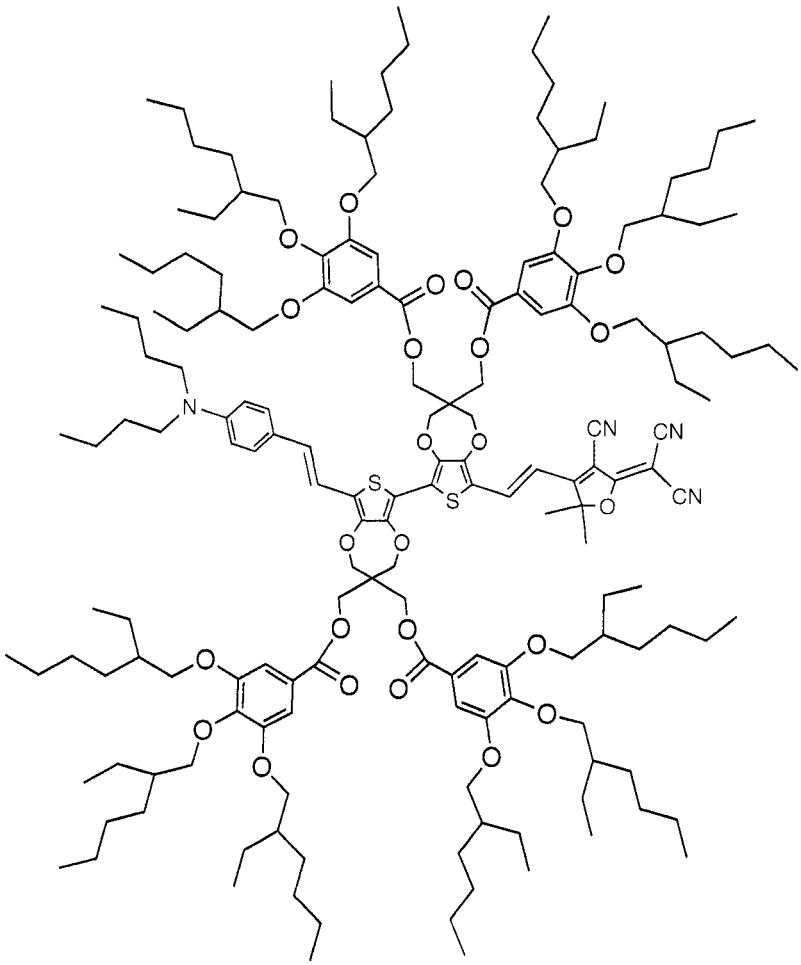

Figure 4.9. Structure of **SJLD-1** with active chromophore highlighted

4.4.1 Molecular Properties. **SJLD-1** dissolved readily in chloroform to give dilute solutions for UV-visible absorption spectroscopy with a λ_{max} of 734 nm and an extinction coefficient (ε) of 68700 L/mol*cm (Figure 4.10). This is very similar to the values obtained for OLD-1 and OLD-2 (Table 4.1),[13] suggesting the bulky dendrons do not significantly alter the planarity or β of the chromophore backbone. Additionally, **SJLD-1** is also soluble in hexanes, with a λ_{max} of 662 nm, and an ε of 44200 L/mol*cm (Figure 4.10). This relatively large positive solvatochromic shift (72 nm) suggests that

the chromophores are not entirely shielded from the solvent environment by the large dendrons.

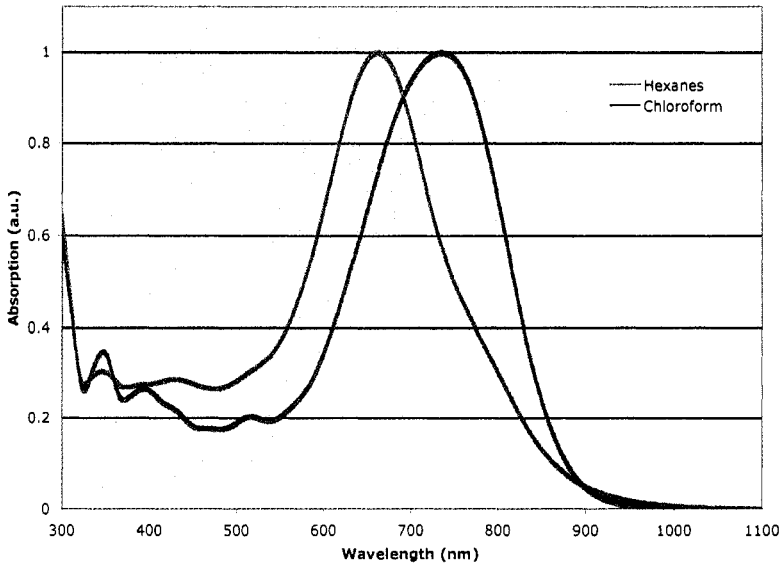

Figure 4.10. Normalized solution UV-Vis absorption spectra for **SJLD-1**

4.4.2 Thermal Properties. The thermal properties of **SJLD-1** were investigated with differential scanning calorimetry (DSC). An initial sample of bulk material showed no obvious peaks until the material decomposed around 330 °C, indicating excellent thermal stability. A second sample was initially heated to 300 °C with no obvious transitions, slowly cooled to room temperature, and heated again to show a distinct glass transition temperature (T_g) at 48 °C. This indicates the material's sensitivity to previous thermal treatment.

The thermal properties of **SJLD-1** were investigated more closely using variable temperature microscopy (VTM). A sample of as-prepared material was placed between microscope slide cover slips and heated initially to 100 °C, at which point it was a freely flowing liquid, to clear the sample of previous thermal treatment effects. The sample was then slowly cooled to room temperature, and then re-heated to 45 °C, at

which point the sample was rigid and resisted shearing. On heating to 50 °C the sample still would not flow, but was much less resistant to shearing. This suggests it was above the T_g, in accordance with the DSC data. The sample observed to fully melt around 80 °C, at which time the sample was free flowing and readily sheared. It is interesting to note that this transition was not apparent from the DSC data. On rapid cooling from 150 °C to room temperature and subsequent heating the sample displayed no differences in behavior. The sample was also examined under crossed polarizers (polarized optical microscopy, POM) during every stage of the heating/cooling cycles, and at no point did the material exhibit any birefringence, suggesting no liquid crystalline (LC) behavior.

4.4.3 Film Properties. Surprisingly, **SJLD-1** exhibited relatively poor solubility considering the highly functionalized structure. Although it is sufficiently soluble in common organic solvents such as hexanes, methylene chloride, chloroform, and acetone to permit routine manipulation, purification, and characterization, it does not exhibit the high degree of solubility required for EO characterization. Simple drop-cast tests of the chromophore were performed in common spin-casting solvents including 1,1,2-trichloroethane (TCE), 1,2-dichloroethane (DCE), toluene, cyclopentanone (CP), and dioxane, to examine the film forming properties. Tests indicated that DCE, CP, and dioxane all gave cloudy, poor-quality films, while TCE and toluene gave shiny, potentially good-quality films. However, even in these solvents, **SJLD-1** has limited solubility with 5-6 weight percent solutions exhibiting some particulates. Drop-cast tests were also performed from high boiling-point non-polar solvents such as *n*-octane, with similarly poor results. It appears that while the non-polar surface character from

the 2-ethyhexyl chains affords some solubility in non-polar solvents, it also partially retards the solubility in polar solvents. The resulting conflict between the polar core and non-polar surface results in limited overall solubility over a wide range of solvent polarities.

As the best results were obtained from TCE and toluene solutions, films were spin cast from these dilute (~5-6 wt. %) solutions, after filtering through a 0.2 μm filter. Due to the relatively low viscosity of these solutions, very low spin-speeds were required (300-700 RPM) to obtain films of reasonable thickness (> 500 nm), reducing the film quality. Early attempts with a soft-baking step performed at 45 °C resulted in widespread aggregation throughout the samples. Subsequent attempts demonstrated that a brief high-temperature (100 °C) soft-baking step immediately after spin casting resulted in an improved amorphous quality films, presumably due to rapid removal of the residual solvent that prevented the chromophore from aggregating. However, these films still exhibited small local aggregates, likely due to the saturated solutions from which they were cast. The aggregates caused inhomogenaities in film thickness, which, combined with the relatively thin films (~0.6 μm), resulted in electrical shorts between the top gold electrode and the ITO, preventing contact poling and EO characterization of the samples. Attempts to form optical-quality drop-cast and doctor-blade films were also unsuccessful.[34]

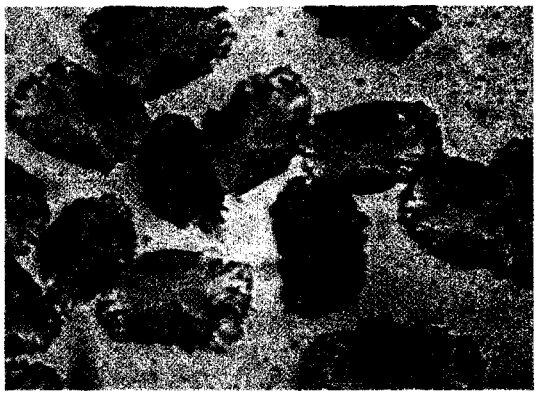

Figure 4.11. Crystallites of **SJLD-1** in cured films (100x)

Serendipitously, mostly-amorphous films (cast from toluene) that were cured in a vacuum oven at 70 °C overnight exhibited widespread crystallization in the form of platelets (Figure 4.11). It appears that temperatures above the T_g but below the T_m provided sufficient thermal energy for the molecules to rearrange in the amorphous film to form crystallites. These crystallites then grew out of the amorphous films, eventually resulting in purely polycrystalline films. These crystals were seen to melt into amorphous material above 80 °C, confirming the T_m identified by VTM.

4.4.4 Crystallography. The strong tendency for **SJLD-1** to aggregate, as evidenced by the poor solubility, aggregate-filled films, and crystallites, is indicative of strong intermolecular interactions. The nature of these interactions is clearly of the utmost importance in understanding the behavior of this system and designing new materials with improved properties. The ability for **SJLD-1** to crystallize, while surprising, suggests the possibility of growing single crystals and obtaining an X-ray diffraction (XRD) crystal structure. Such a structure could provide detailed information about the intermolecular interactions that lead to aggregation, allowing evaluation of the discotic chromophore design concepts and providing direction for the design of future systems.

Towards this end, a variety of crystallization techniques were explored to grow high-quality single-crystalline samples of **SJLD-1**. Single-solvent thermal gradient and evaporation methods produced only oily, amorphous materials. Binary solvent diffusion experiments proved more successful. A solution of a 5-10 mg of **SJLD-1** in about 0.5 mL of methylene chloride was gently layered with about 1 mL of methanol (in which the chromophore is totally insoluble) in an NMR tube and allowed to slowly diffuse over two weeks. This afforded dark blue-black single-crystalline needles, but of a size too small XRD. Subsequent experiments established an optimized procedure, involving layering of a solution of a 5-10 mg of **SJLD-1** in 0.5 mL of *n*-hexane on 5.5 mL of ethanol in a vial, and allowing to slowly diffuse for several days. This technique afforded dark blue-black prisms of sufficient size for XRD, but they are both touch sensitive and decompose on evaporation of the solvent, suggesting uptake of *n*-hexane into the crystal. As a result, the crystals are extremely difficult to work with. Additionally, this indicates the crystals are clearly different from those obtained both in the films, and from the methylene chloride/methanol experiment. This suggests the existence of multiple polymorphisms, with potentially different geometries, although the key intermolecular interactions likely remain the same.

Initial crystallography experiments were performed in collaboration with Jason Benedict (Prof. Bart Kahr, Department of Chemistry, University of Washington) and Dr. Werner Kaminsky (Department of Chemistry, University of Washington). Numerous attempts to use conventional XRD techniques, including sealed-capillary XRD, were unsuccessful in obtaining a full crystal structure. The crystals were indexed, however, to a triclinic unit cell the following parameters: a = 24.4580 Å, b =

28.8070 Å, c = 32.5960 Å; $\alpha = 66.9090^{\circ}$, $\beta = 68.2040^{\circ}$, $\gamma = 68.4820^{\circ}$. Comparing these values to the calculated (MM2 geometry optimization, Chem 3D, Cambridge Software) chromophore length of 27.4 Å and fully-extended width of 40.2 Å suggests inter-digitation or folding of the dendrons. Additional attempts were also made to use a protein crystallography XRD geometry, due to the large size of the unit cell, but these were also unsuccessful in obtaining a full crystal structure. In all cases, the failure was attributed to the weak intensity of reflections, rather than due to a lack of reflections, which suggests the potential of using a high-intensity synchrotron X-ray source.

Synchrotron XRD crystallography experiments were performed in collaboration with Dr. Zdzislaw Wawrzak (LS-CAT, Advanced Photon Source, Argonne National Laboratory). Freshly grown crystals, prepared via the *n*-hexane/ethanol method, were trapped in small nylon loops (cryogenic loops) in liquid nitrogen (with assistance from Jason Benedict). The cryo-loops were then shipped in liquid nitrogen vapors using a cryogenic shipper to the Advanced Photon Source at Argonne National Laboratory, where they were analyzed at LS-CAT at Sector 21 of the synchrotron, also under liquid nitrogen vapors. The use of cryogenic crystallography (cryo-crystallography) techniques ensured that solvent evaporation would not result in decomposition of the crystal. Two initial attempts, each consisting of 5-10 samples, were unsuccessful in obtaining data of sufficient quality to obtain a crystal structure. Very recently, however, a third attempt resulted in one sample that diffracted out to 0.95 Å, and the data allowed the solution of a partial crystal structure.

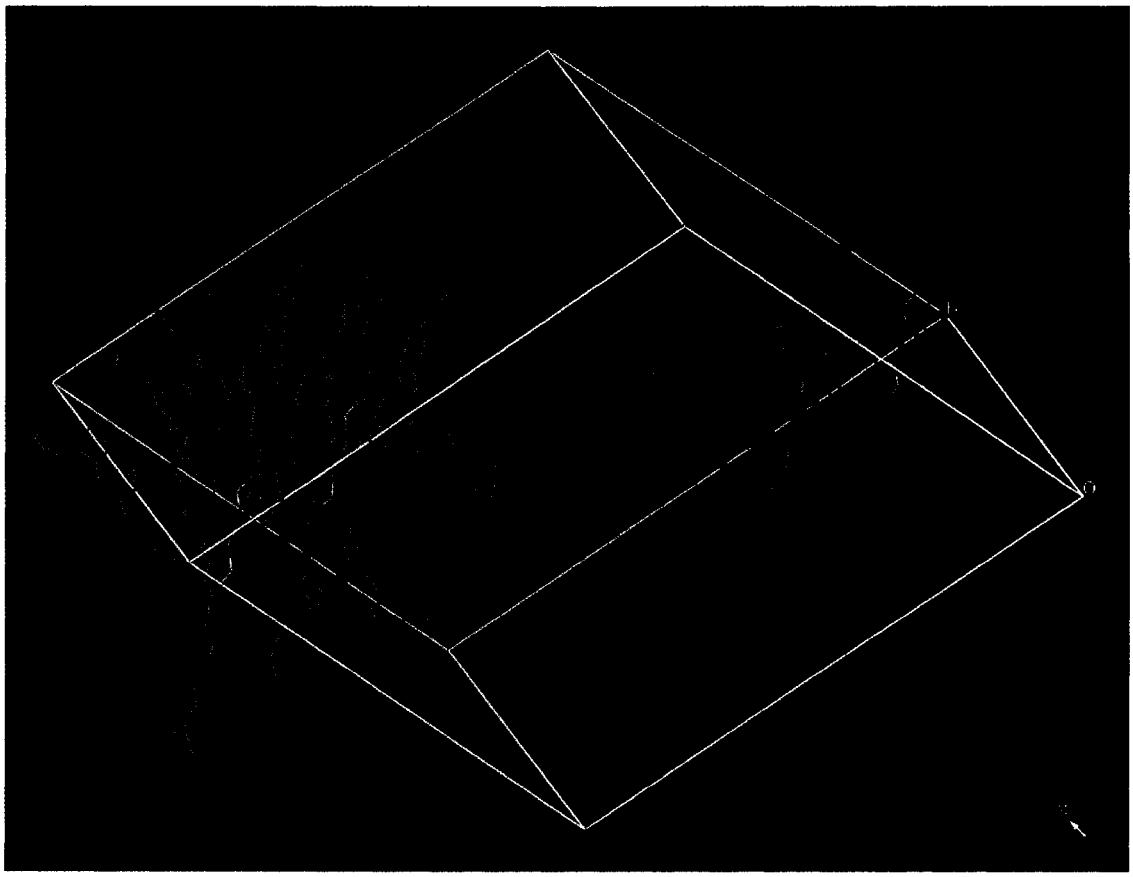

Figure 4.12. Unit cell of **SJLD-1** crystal structure

The crystal that provided the solution was indexed to a triclinic unit cell in a $P\bar{1}$ space group (centrosymmetric, low symmetry), with the following dimensions: a = 23.6 Å, b = 28.1 Å, c = 32.0Å; $\alpha = 67.8°$, $\beta = 70.1°$, $\gamma = 69.0°$. These dimensions are slightly different from those of the previously indexed crystals, with smaller lengths and larger angles. This likely has less to do with polymorphism than simply a better quality crystal yielding better quality index data. The unit cell is displayed in Figure 4.12, and it consists of two unique molecules and four total molecules. A striking feature of the structure is the presence of a distinctly noncentrosymmetric aggregate, with two of the **SJLD-1** molecules pointing in the same direction and in very close proximity. These molecules are about 3.5 Å apart at their closest approach (at the overlap between the

ProDOT rings in the two molecules), which is well within π-π stacking distance. For comparison, the inter-plane spacing in graphite is 3.347 Å. The molecules are canted slightly, however, and the molecules are further apart at every other point. The molecules are also slipped by about 5 Å with respect to each other, such that the second of the two ProDOT rings on one molecule interacts with the first ProDOT ring on the second molecule. Additionally, there are significant interactions between the dendrons on the two molecules, including Van der Waals interactions and possibly π-π stacking or edge-to-face interactions between the various phenyl rings. The noncentrosymmetric pair is related to the second pair by a center of inversion, resulting in an overall centrosymmetric crystal structure. The interactions between these two pairs are very weak, mainly Van der Waals interactions between the 2-ethylhexyl chains on the dendrons and incorporated *n*-hexane.

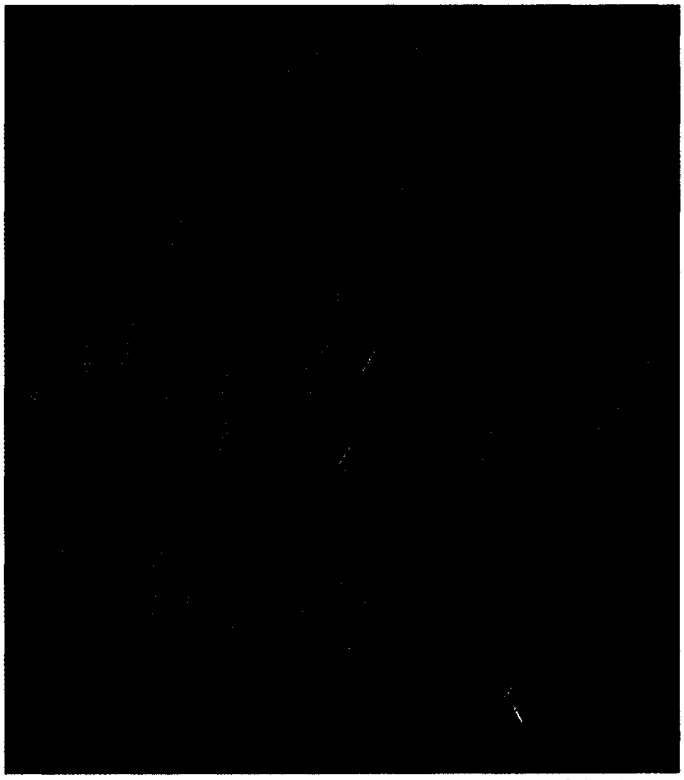

Figure 4.13. Synchrotron X-ray structure of **SJLD-1**

It should be noted that the structure is not entirely complete; the space between the pairs is likely filled with *n*-hexane and the 2-ethylhexyl chains from the dendrons, which are not entirely resolved. This is evidenced in part by the incorrect assignment of some carbon-carbon double and triple bonds, which simply indicates the appropriate hydrogen atoms were not resolved in the structure. These errors are more clearly observed in the individual molecular structure presented in Figure 4.13. Also evident is that the structure of the chromophore backbone is largely resolved and correct, and the overall structural details of the entire molecule are reasonably accurate. As such, we feel confident that the structure accurately represents the important details of the crystals, including the key intermolecular interactions.

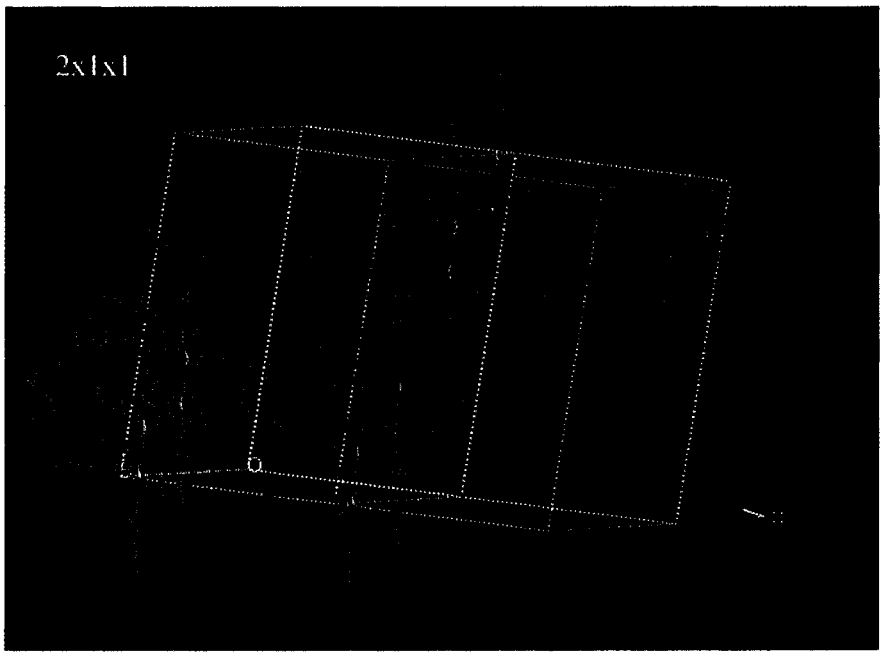

Figure 4.14. 2 by 1 by 1 cell crystal structure of **SJLD-1**

Further information on the nature of these interactions can be gained by examining the extended cells presented in Figures 4.14-4.16, obtained by tiling out the unit cell in the directions indicated. From Figure 4.14 it is clear there is a strong

centrosymmetric interaction between the two closest chromophore pairs along the crystallographic a axis. There is significant overlap between two molecules, with each donor nitrogen nearly parallel with the sulfur from the first ProDOT thiophene on the other molecule, and perhaps π-π interaction between the donor phenyl rings. There also appears to be significant Van der Waals interactions between the butyl chains on the donors and the 2-ethylhexyl chains on the dendrons between these two closest molecules. Additionally, there appears to be some interaction between the dendrons of the two noncentrosymmetric pairs that are related by translation along the a axis. Along the b crystallographic axis (Figure 4.15), the two closest chromophore pairs appear to be aligned noncentrosymmetrically, and the only interaction appears to be relatively weak Van der Waals interactions between dendron alkyl chains. The relatively weak interactions here likely contribute to the extremely touch sensitive nature of these crystals. Along the crystallographic c axis (Figure 4.16), the interactions appear even weaker, with a weak noncentrosymmetric interaction between the molecular pairs related by translation along the c axis, and Van der Waals interactions between the various alkyl chains and the incorporated *n*-hexane throughout.

The combination of weak interactions in both the crystallographic b and c directions explains the extremely touch sensitive nature of the crystals. Ready cleavage likely occurs along either of the corresponding crystallographic faces. This fact certainly contributed to the difficulty in working with the crystals and obtaining a high-quality crystal structure. These cleavage planes are more easily seen when looking along the crystallographic axes, as in Figure 4.17.

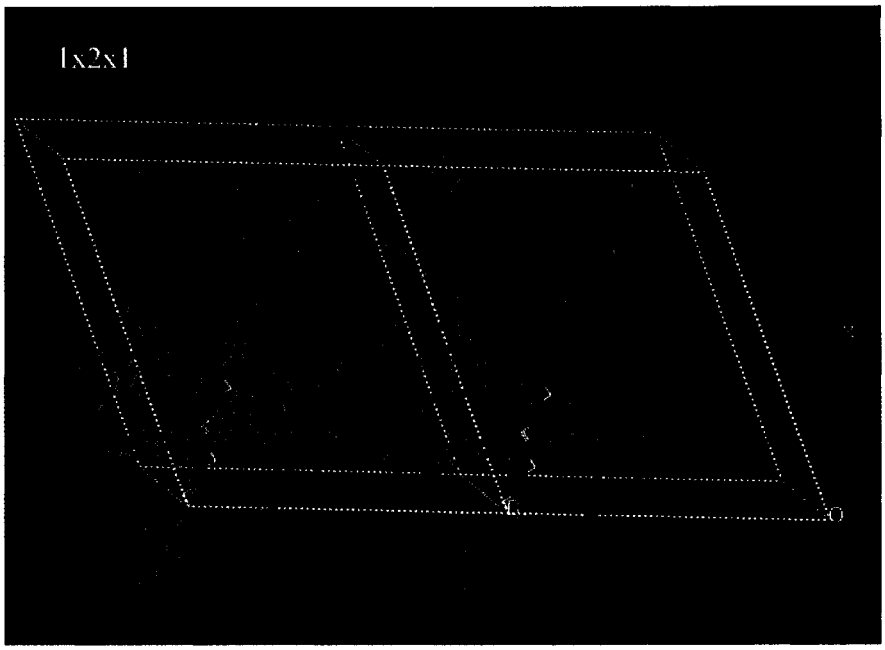

Figure 4.15. 1 by 2 by 1 cell crystal structure of **SJLD-1**

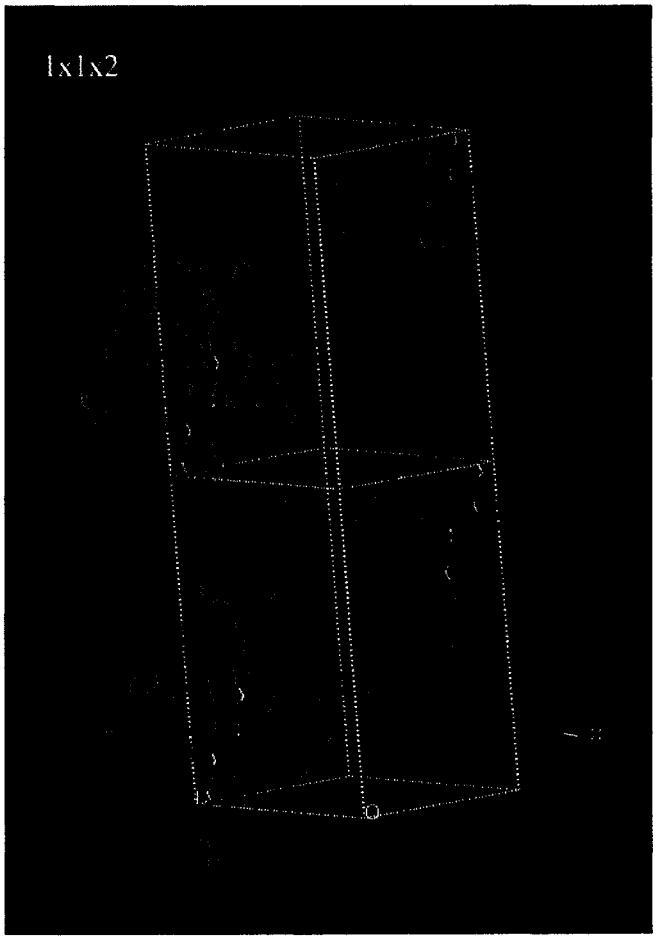

Figure 4.16. 1 by 1 by 2 cell crystal structure of **SJLD-1**

Although the crystal is overall centrosymmetric, we believe that the noncentrosymmetric pairs are the key interaction in **SJLD-1** in particular, and the discotic chromophores in general. The strong π-π stacking interaction between the two chromophores is likely to significantly alter the molecular properties, as is the close interaction of the two dipole moments (see Chapter 5). One readily apparent effect of these interactions should be a distinct solvatochromic red-shift of the charge-transfer band of the chromophores in these pairs (Section 2.4.1). We chose to focus on this property to obtain immediate feedback on the hypotheses outlined. Additionally, DFT calculations using the crystal structure geometry are under way to explore these effects in greater detail.

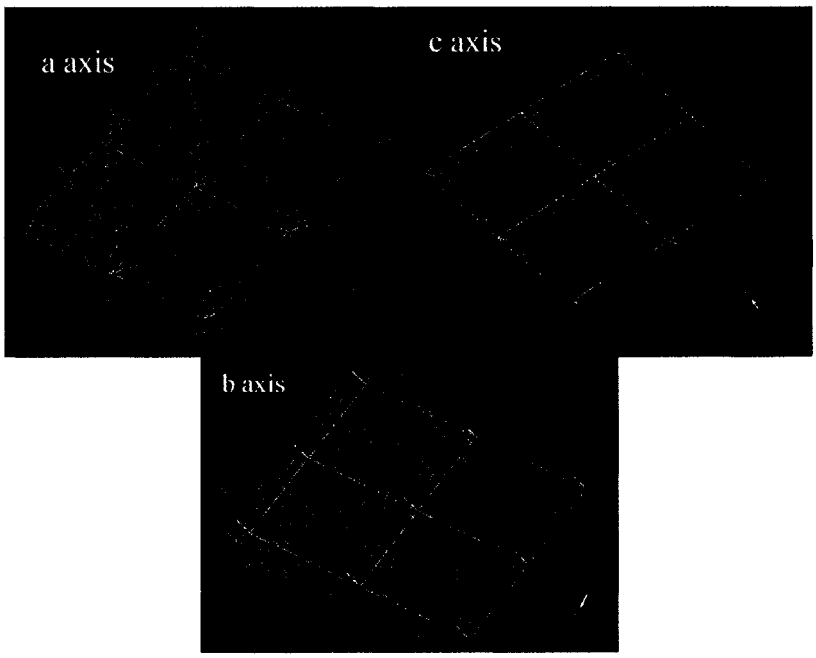

Figure 4.17. Crystallographic planes of **SJLD-1**

The enormous optical density of these crystals, their extremely fragile nature, and the tendency to decompose on evaporation of solvent all combine to make UV-vis absorption spectroscopy extremely difficult. Reflectance spectroscopy would likely be

the ideal method to obtain spectroscopic data from these crystals; however, we did not have reflectance spectroscopy readily available to us. We attempted to use a fiber-coupled broadband light source and spectrometer apparatus, normally used for photostability measurements (Sections 2.4.4 and 3.5.5),[35] but the intensity proved too low to transmit through the sample. We settled upon taking a powder absorption measurement in a standard UV-vis spectroscopy instrument. Crystals were suspended in ethanol and powdered between microscope cover slips, and the spectrum (Figure 4.18) was taken rapidly to avoid evaporation of all the solvent. Although the quality of the data is relatively poor, a large red shift in the charge transfer band is evident. This spectrum looks similar to those obtained from cured films of **SJLD-2-4**, suggesting a similar aggregation is occurring in those films.

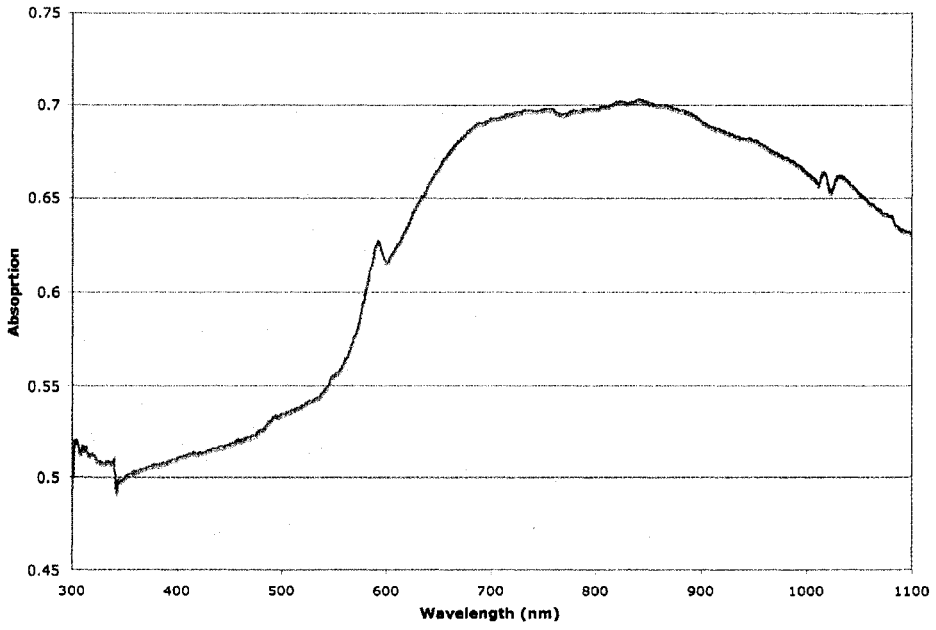

Figure 4.18. UV-vis absorption spectroscopy of **SJLD-1** crystal powder

4.4.5 Conclusions. **SJLD-1** proved to be an extremely poor EO material. The limited solubility of **SJLD-1**, likely due to the combination of nonpolar surface character and

polar core, remains the biggest problem of this system. It prevented the formation of optical quality films, one of the most important properties of such materials. As a result, no EO characterization was possible. The relatively low T_g of this material is also a serious impediment to practical device application. The excellent thermal stability of this material is promising however.

Although **SJLD-1** proved to have poor properties for EO applications, it has provided a wealth of information that can be used to understand and improve the discotic chromophores. Contrary to the design principles, **SJLD-1** did not exhibit a tendency to form acentric columns, nor did it exhibit LC behavior. In fact, despite the intention to reduce side-on-side aggregation, the system exhibits a strong tendency to form such aggregates, although in a noncentrosymmetric, rather than centrosymmetric, fashion. Preliminary DFT calculations from the crystal structure geometry suggest the main force behind the formation of this aggregate is the high degree of Van der Waals overlap, and other steric interactions, in such a conformation. In contrast, the energetic contributions from electrostatic interactions (in a bond-dipole rather than point dipole approximation) appear relatively minor.

In the future, we will continue to examine the crystal structure theoretically and experimentally to elucidate the consequences such a structure has on the molecular properties. We also plan to attempt to explore the structures of other crystal polymorphs via synchrotron XRD experiments, in the hopes of gaining further understanding into the intermolecular interactions and possibly finding a noncentrosymmetric crystal. Such a crystal might have extremely large EO coefficients, although it would have all the drawbacks inherent in EO crystals.

4.5 SJLD-2

The second discotic chromophore system studied was **SJLD-2** (Figure 4.19), which was designed in direct response to the initial failures of **SJLD-1** with respect to poor solubility and lack of LC behavior. The crystal structure data was not available when designing **SJLD-2**, or any of the other discotic chromophores. Although **SJLD-1** did not exhibit LC behavior, it did exhibit both amorphous and crystalline morphologies, suggesting it may be close to the delicate balance of forces required to form such phases. As a reduction in nonpolar surface character was also desirable, to improve the solubility and film-forming properties, **SJLD-2** was designed with two hexyl chains per dendron, as opposed to the three 2-ethylhexyl chains in **SJLD-1**. This also resulted in an advantageous increase in active chromophore loading and number density, 23.3 % and 2.89 x 10^{20} molecules/cc respectively, while retaining a similar A of about 1.48 (MM2 geometry optimization, Chem 3D, Cambridge Software; fully extended conformation).

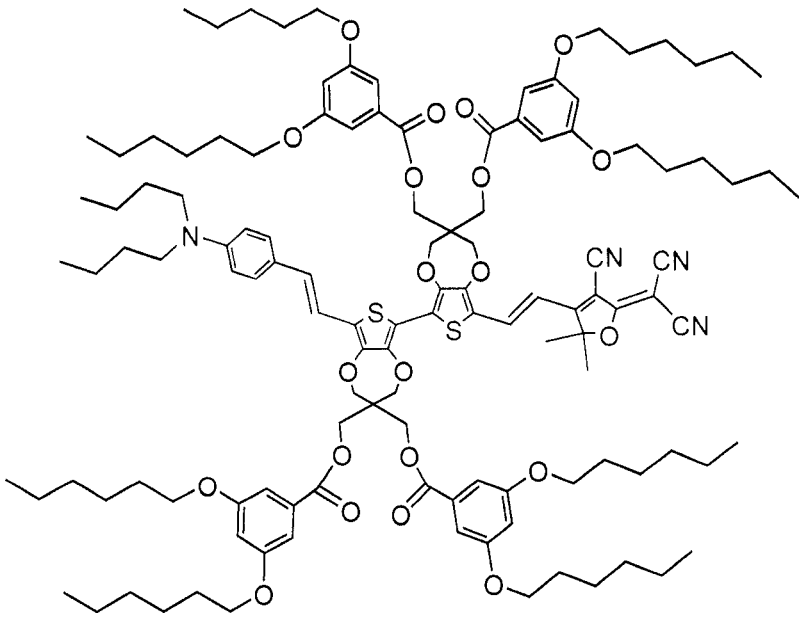

Figure 4.19. Structure of **SJLD-2** with active chromophore highlighted

4.5.1 Molecular Properties. **SJLD-2** exhibited enhanced solubility in polar organic solvents with respect to **SJLD-1**, as was desired, yet also retained solubility in such nonpolar solvents as hexanes. UV-vis spectroscopy in hexanes (Figure 4.20) identified a λ_{max} of 642 nm, with an anomalously low ε of 21,300 L/mol*cm. In cholorform, **SJLD-2** exhibited a λ_{max} of 739 nm (Figure 4.20), and again a relatively low ε of 43,000 L/mol*cm. Although the λ_{max} values are similar to the previous systems, the ε values are significantly lower than all of the other discotic chromophores and bis-ProDOT based OLD chromophores, and are suspected to be inaccurate due to experimental error. These experiments will be repeated as soon as feasible. The positive solvatochromic shift of 97 nm is even larger than that in **SJLD-1** (72 nm), as might be expected from the less shielded dendron environment in **SJLD-2**.

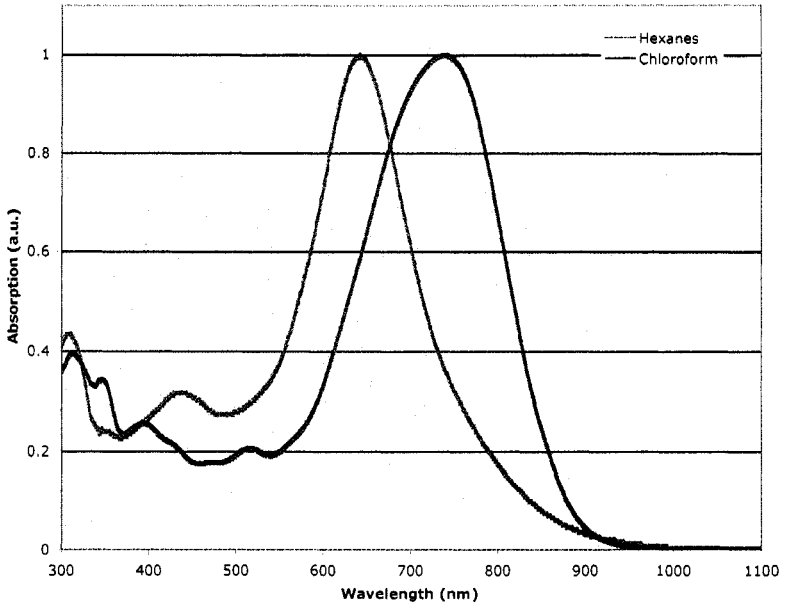

Figure 4.20. Normalized solution UV-vis spectra for **SJLD-2**

4.5.2 Film-Forming Properties. Due to the enhanced solubility of **SJLD-2**, with respect to **SJLD-1**, optical quality films were obtained. Initial drop-cast tests identified 1,2-dichloroethane (DCE) and toluene as potentially good spin-casting solvents. Although **SJLD-2** is more soluble than **SJLD-1**, it is still not highly soluble, and the solubility limit in these solutions is between 7 and 8 wt. %. Initially, films spin-cast at 700 RPM from filtered (0.2 μm) solutions of around 6 wt. % in both solvents suggested the DCE films were thicker (around 0.6 μm as measured by profilometry), but of worse quality, while the toluene films were thinner (around 0.5 μm), but highly amorphous. Immediately after spinning, the films appeared green, but on soft-baking at 100 °C on a hot-plate, the films rapidly turned purple in color. Eventually, an optimized procedure was developed involving filtered (0.2 μm) 7 wt. % toluene solutions of **SJLD-2** initially being spread for 5 seconds at 500 RPM with an acceleration parameter of 5, followed by 30 seconds at 850 RPM with an acceleration of 10. The soft-baking step was not required to obtain good film quality, and it was eliminated. While these films were

relatively thin, around 400 nm, they had the best optical quality. It was decided that the improved optical quality was worth the reduced thickness.

It was discovered that the properties of the films produced with the optimized procedure could be controlled by altering the curing step. Films cured in a vacuum oven at room temperature overnight remained green in appearance, while those cured at 85 °C in the vacuum oven overnight had the purple appearance initially seen during the soft-baking step. The absorption properties of these films were investigated using UV-vis-NIR absorption spectroscopy (Figure 4.21) of ultra-thin films (around 200 nm) spun at very high rates (around 5000 RPM). The films cured at room temperature (green films) have a λ_{max} (697 nm) that is slightly blue-shifted with respect to the chloroform solution value, and a slight shoulder at about 816 nm.

In contrast, the films cured at elevated temperature have an enormous red-shift and spectral broadening, with a λ_{max} of 996 nm, although additional peaks are evident (878 nm and 788 nm). This suggests the purple color arises primarily from the secondary (non-charge transfer) peak (λ_{max} around 550 nm), rather than from the charge-transfer band, which is mostly beyond the visible spectrum. The spectrum for these red-shifted films is reminiscent of the crystal powder spectrum obtained from **SJLD-1**, suggesting a similar interaction may be involved. It should be noted that the red-shift and broadening leads to a strong absorption tail that extends as far out as 1.3 μm, and possibly further. Significant absorption at the measurement wavelength can lead to artificial enhancement of the r_{33} value. Additionally, such absorption may cause unacceptable optical loss for device applications.

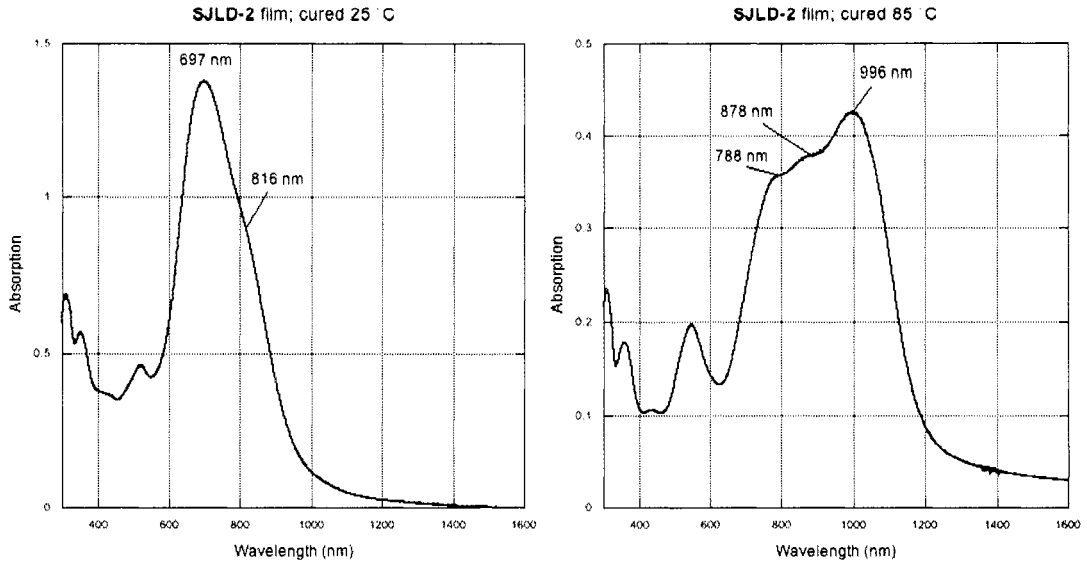

Figure 4.21. UV-vis-NIR spectra of cured **SJLD-2** films, 25 °C (right) and 85 °C (left)

4.5.3 Film Morphology. The morphologies of these films were examined using thin-film small-angle XRD performed in the laboratories of Prof. Kannan Krishnan (Department of Materials Science and Engineering, University of Washington), with assistance from Xiaosong Ji. For films cured at room temperature (green), an initial scan over the full angular range of the apparatus identified only a single, broad peak at around 24 ° (2θ), which is characteristic of an amorphous morphology. A spectrum of a more limited angular range is presented in Figure 4.22 (left). Films that were cured at elevated temperatures (purple), exhibited two peaks in the small-angle region (Figure 4.22, right), in addition to the broad amorphous peak. This suggests a self-assembled (SA) or LC morphology. Although two peaks are insufficient to conclusively assign the LC phase, the positions of the peaks (2.98° and 8.92° 2θ) are at a spacing of 1:3, which is consistent with a Semectic A (SmA) or Semectic C (SmC) phase.[36,37] Based upon the results for similarly red-shifted films of **SJLD-4** (Section 4.7.2), which can be

conclusively assigned to either a SmA or SmC phase, we tentatively assign the films of **SJLD-2** to these phases as well.

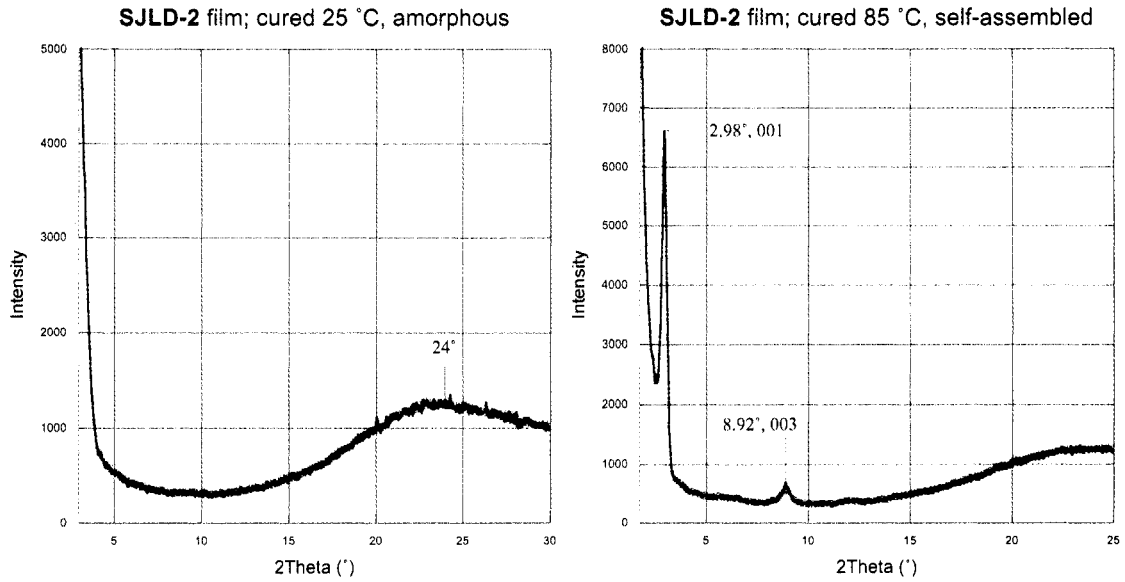

Figure 4.22. XRD spectra of amorphous (left) and LC (right) cured **SJLD-2** films, with tentative *hkl* assignment

The Semectic A and C phases both correspond to a series of weakly interacting lamellae, or planes, where the molecules have a defined orientation but no positional order within the lamellae.[37] In the SmA phase, the orientation of the molecules is directly normal to the plane surfaces, while in SmC the molecules are at some acute angle with respect to the surface normal. It should be emphasized that in both cases the molecules can take either orientation within the layers, resulting in net centrosymmetry. From the XRD alone it is impossible to distinguish between these two phases.

Based on a 1-D layered semectic phase assignment, however, we can tentatively assign *hkl* values of 001 and 003 to the 2.98° and 8.92° peaks, respectively. From the Bragg diffraction relationship and the wavelength of X-rays used (Cu Kα, 1.54 Å), we can then calculate an interlayer (d) spacing of 29.6 Å. This value is slightly larger than the calculated chromophore length (MM2 geometry optimization, Chem 3D, Cambridge

Software; fully extended conformation) of 27.4 Å, whereas in SmA the d spacing is generally slightly smaller than the calculated length due to the imperfect orientational order and the conformational disorder of the molecules.[37] This suggests that the phase may be SmC, where the d spacing corresponds roughly to

$$d \approx w \sin\theta \qquad (4.1)$$

where w is the chromophore width and θ is the chromophore angle with respect to the surface normal. From this, we calculate θ ~ 47.6°, although this value is only approximate as it is based upon a fully extended conformation that likely does not exist within the films. A smaller width would result in a larger angle. Overall, this matches well with the refractive index data from films of **SJLD-4** (Section 4.7.2), which shows a relatively weak birefringence in the SA films (similar to that of the amorphous films). In contrast, if the chromophores were all aligned normal to the surface, one would expect a large birefringence.

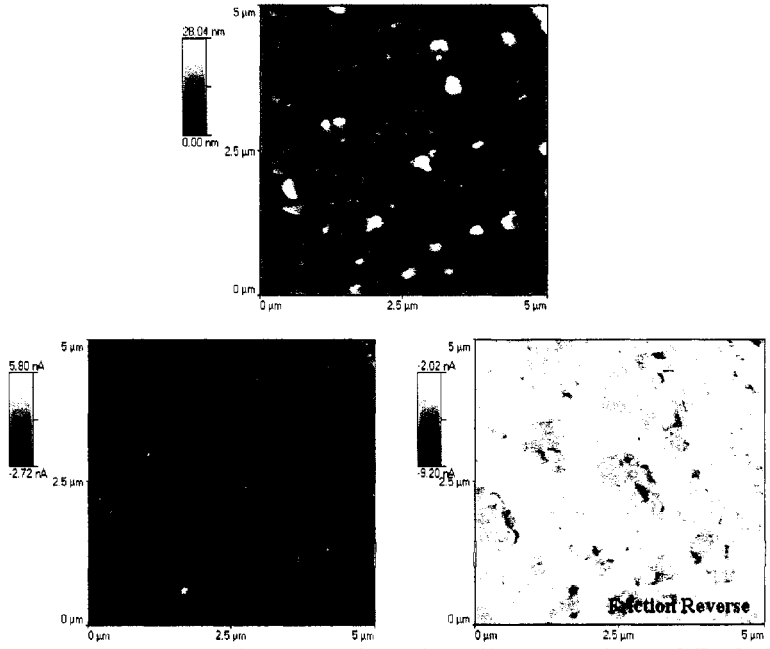

Figure 4.23. SM-SFM images of a primarily amorphous **SJLD-2** film

Some preliminary experiments were also performed to explore the morphology with both atomic force microscopy (AFM) in the Nanotechnology User Facility (NUF, Center for Nanotechnology, University of Washington) and shear-modulated scanning force microscopy (SM-SFM) in collaboration with Tomoko Gray (Prof. René Overney, Department of Chemical Engineering, University of Washington).[38] For the AFM experiments, both amorphous (cured at room temperature, green) and LC (cured at 85 °C, purple) films were examined in contact mode. The AFM of the amorphous films suggest a somewhat rough surface, with the appearance of multiple phases, which was confirmed from the SF-SFM data, which showed inverse images for the forward and reverse friction experiments (Figure 4.23). This is likely due to the spontaneous self-assembly of the molecules, as the material is above its T_g (see Sections 4.5.4 and 4.5.5). In contrast, the LC films showed relatively uniform, although rough (about 9.5 nm root-mean-squared [RMS] surface roughness), morphologies (Figure 4.24). It should be considered, however, as the material is above its T_g the tip may be physically deforming the sample. Tapping mode would be the preferred method of examining these materials in the future.

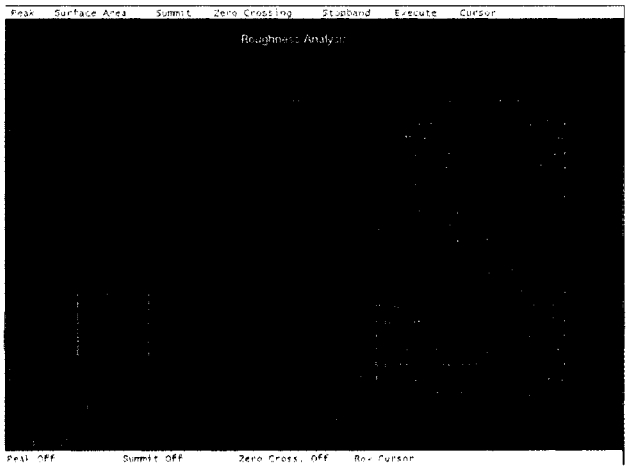

Figure 4.24. AFM of a LC **SJLD-2** film

4.5.4 Thermal Properties. The thermal properties of **SJLD-2** were initially investigated with DSC. DSC of the as-prepared bulk material (Figure 4.25) in all cases failed to identify a T_g, although a distinct melting transition was identified at 153 °C. Additionally, a transition of unknown identity was tentatively identified at around 72 °C. The T_d of the material was also estimated as approximately 265 °C. While this is significantly lower than **SJLD-1**, it still more than adequate for EO applications, and significantly higher than, for example, CLD-based chromophores.[39]

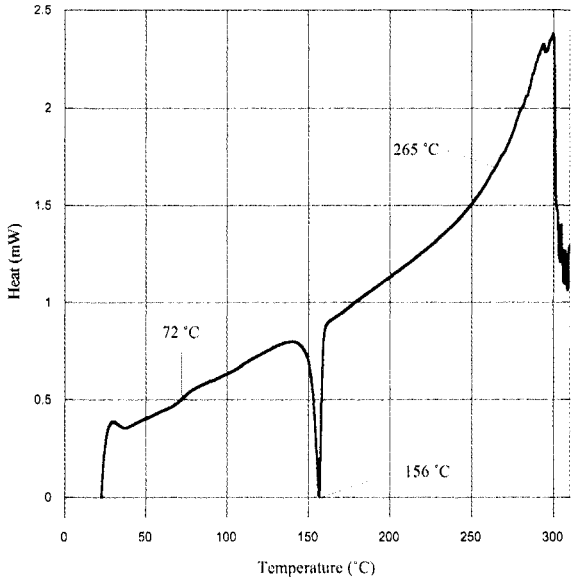

Figure 4.25. DSC of bulk **SJLD-2**

The thermal properties of **SJLD-2** were investigated in more detail with VTM of cured amorphous films. As the films were slowly heated from room temperature, the first change was apparent at around 65 °C, when the green color of the initial films started to bleach to a gray color. As the temperature was increased further, the gray color developed into the purple color characteristic of the close noncentrosymmetric interaction between the chromophores. This likely corresponds to the transition around 72 °C from the DSC data, and is almost certainly the isotropic glass to semectic C

transition ($T_{I\text{-}SmC}$). On further heating there were no observable changes until around 145 °C, at which time the purple color began to revert to the green color, suggesting clearing (melting), although this is slightly below the melting transition identified by DSC. This could simply be due to discrepancies in temperature calibrations or heating rates, or it is possible the system adopts a temporary nematic phase, wherein the orientational order is transiently preserved although the layered structure is disrupted. Regardless, it is clear from the color change that the close noncentrosymmetric interaction between chromophores is disrupted. On slowly cooling from the melt, the sample reverts to the purple LC phase at around 120 °C. No further transitions are evident on cooling to room temperature. In both heating and cooling cycles, the formation of crystallites (visible initially as bright spots under crossed polarizers) was seen at temperatures around 140 °C. Fast heating or cooling could prevent the formation of these crystallites, however.

It is extremely interesting to note that although the sample was examined under POM at all stages of the thermal gradient program, there was no sign of characteristic LC optical textures. These textures are associated with defects in the LC lattice that are of microscopic size, due to extended distortions of the LC structure resulting from the weak forces present.[40] For the SmA and SmC phases in particular, it is feasible to obtain large-area defect-free samples that do not exhibit a significant texture, which are referred to as homeotropic or pseudoisotropic textures.[37,40] If this is the case, then it suggests all of the lamellae are aligned parallel to the substrate, which is the lowest energy conformation. Another possible explanation for the lack of texture is the restriction of defects to submicroscopic regions, due to the presence of strong forces

(such as dipole-dipole interactions), rather than the relatively weak forces present in most LC systems.[40] This theory is supported by data from extremely old (>6 months) amorphous films of **SJLD-2**, which show distinct microscopic feathery or dendritic patterns (Figure 4.26). These textures likely arise from spontaneously self-assembled LC regions that have grown from the small regions seen in the SM-SFM experiments (Figure 4.23), to sufficient size to be visible under the optical microscopy (500x magnification). This supports the concept of defects in these LC phases being restricted to submicroscopic regions, particularly for the other discotic systems with significantly higher glass transition temperatures.

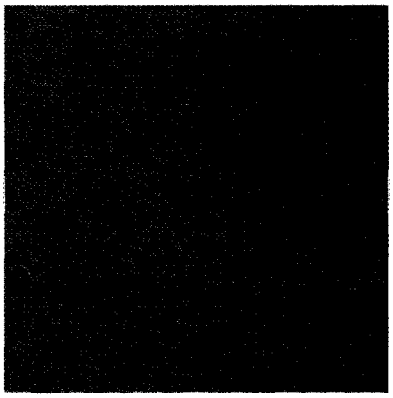

Figure 4.26. Dendritic patterns in aged amorphous **SJLD-2** films (500x)

The SM-SFM microscopy experiments (Tomoko Gray, Prof. René Overney, Department of Chemical Engineering, University of Washington),[38] in addition to exploring the surface morphology (Section 4.5.3), also attempted to investigate the thermal properties of **SJLD-2** by monitoring changes in the shear forces of an AFM tip in contact mode with an amorphous film. These experiments identified morphological changes at 52 °C on first heating of a sample, and at around 80 °C on second heating of the sample. Repetition on multiple samples confirmed these properties. The first change likely corresponds to the initial reorganization of the isotropic material into the

LC phase, which becomes evident at around 65 °C in VTM as a color change. The second transition may correspond to the DSC transition at 72 °C, although the DSC was performed on as-prepared material, not LC films. The nature of this transition is unknown, although one possibility is a LC to LC transition, perhaps due to a change in the molecular orientation axis.

All the thermal experiments utilized failed to identify the T_g of **SJLD-2**. These experiments shared a commonality that they started at room temperature. This, combined with some of the properties of the material, suggests the T_g may be below room temperature. EO characterization experiments (Section 4.5.5) were actually able to verify this hypothesis, and have estimated the T_g at 8-15 °C. The details of this experiment are presented in the following section.

4.5.5 Electro-Optic Characterization. The use of an *in-situ* pole and probe simple reflection apparatus developed by Dr. Philip Sullivan in the Dalton Research Group (Section 3.5.2),[27,41,42] proved critical in the EO characterization of **SJLD-2**. This apparatus allowed for evaluation of the EO activity of the material, via an applied AC voltage of (half-maximum) amplitude V_m at frequency ω (in our case 1 kHz), while simultaneously applying a DC poling voltage (V_{DC}) (Equation 4.2) to induce noncentrosymmetric order.

$$V(t) = V_{DC} + V_m \sin \omega t \qquad (4.2)$$

The linear EO coefficient (r_{33}) is directly proportional to the ratio of the (half-maximum) amplitudes of the modulated signal (I_m, at frequency ω), which is measured with a lock-in amplifier, and the unmodulated signal (I_c) as a function of the phase angle

(Ψ_{sp}). The numerous improvements made to the apparatus by Benjamin Olbricht in the Dalton Research Group also proved helpful in the real-time poling and data analysis.

Samples were prepared for EO characterization by spin casting on patterned indium tin oxide (ITO) coated glass slides, which served as bottom electrodes and substrate. Samples were cured at either room temperature or at 85 °C in a vacuum oven, depending of whether the amorphous or LC phase was under study. Patterned gold top electrodes were then sputtered onto the samples, which also served as a reflection surface for the probe beam. Film thicknesses were measured via profilometry to allow accurate calculation of the applied electric field from the actual voltage (V_{RMS}) across the sample. Wires were attached using conductive silver paint to allow attachment to the voltage source. For analysis, samples were placed on a temperature-controlled thermoelectric-heated sample stage in an argon-enriched atmosphere. The probe beam (1.3 μm) was transmitted through the substrate and bottom electrode, through the EO sample, bounced off the gold top electrode, transmitted back through the sample and substrate and then collected to measure the intensity of the modulate and unmodulated signals.

Initial experiments were performed on LC phase samples obtained from toluene using the un-optimized procedure. Attempts to use conventional poling procedures by poling with 25-50 V (50-100 V/μm) at temperatures of 50-70 °C, cooling to room temperature, and then removing the field and measuring the r_{33} resulted in low values of 5-10 pm/V. The *in-situ* nature of the experiment allowed us to observe that while the I_m/I_c signal was seen to increase with increasing voltage at a given temperature, it was seen to decrease with increasing temperature at a given voltage, which suggests above-

T_g behavior. Additionally, the samples had large leakage currents (> 100 μA) at these temperatures, which likely contributed to the significant damage these samples sustained. Subsequently, an experiment was performed to measure the EO coefficient (r_{33}) vs. poling field under constant bias conditions at room temperature, 35 °C, and 45 °C (Figure 4.27). The slope of the linear regression best-fit line was seen to decrease with increasing temperatures, a strong indication that the material was above T_g. The magnitude of the measured r_{33} values and slopes are quite large for single-component organic EO materials, particularly at room temperatures with r_{33} values of almost 250 pm/V at around 100 V/μm. It must be acknowledged that there are several factors to consider that may lead to artificial enhancement of these values, however, which will be discussed shortly.

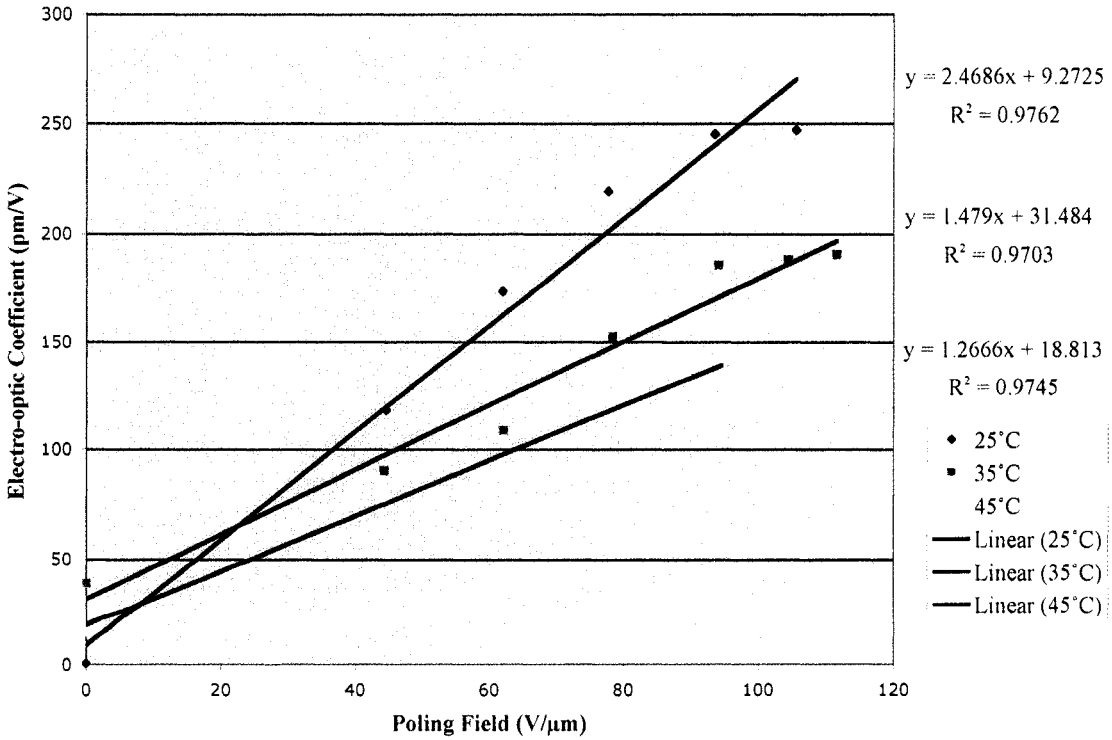

Figure 4.27. Variable temperature constant bias poling data of **SJLD-2** LC films

From the variable temperature constant bias poling data, it was concluded that the material had a T_g below room temperature. Thus, an active cooling system would be required to establish the T_g and perform conventional poling experiments. As the apparatus did not initially allow active cooling of the sample stage, only heating, a new sample stage was required. A new sample stage was designed and fabricated in collaboration with the departmental machine shop (Machine Shop, Department of Chemistry, University of Washington). The new design incorporated a continuous loop within the sample stage to allow circulation of chilled water-ethylene glycol mixture (via a commercial chiller apparatus), in addition to the channels for the embedded thermo-electric heaters. This system allowed the sample to be cooled to temperatures as low as -5 °C.

With the new low-temperature capabilities, experiments were able to identify the T_g of **SJLD-2**. A sample was poled at room temperature with 70 V applied, around 54.7 V_{RMS} actual voltage and 76 μA of current measured, corresponding to a field of about 107 V/μm. The r_{33} measured under constant bias for these conditions was 120 pm/V. As the sample was then cooled to around -2 °C, the current was seen to rise to 167 μA, and some sample damage occurred. The voltage was removed to prevent further sample damage, and the sample continued to cool to the low-temperature limit of the sample stage, around -5 °C. As the sample cooled, the r_{33} was measured, in the absence of the poling field, to be only 43 pm/V. This value is around one-third that measured under constant bias conditions. The large reduction in r_{33} observed could be due to a number of factors, including sample damage. The sample was then slowly heated while monitoring the I_m/I_c signal. The instrument was not configured ideally, so

the data is not ideal, but it initially suggested a transition at around 15 °C. To confirm this, the sample was re-poled at 16 °C with 80 V applied, 59.2 V_{RMS} and 106 μA measured (116 V/μm), and then cooled to -3 °C. The r_{33} was measured at -3 °C, before and after removal of the DC field, to be 143 and 50.0 pm/V, respectively. Again, this is a decrease of almost two-thirds. The instrument was configured for optimal data collection, and the I_m/I_c signal monitored as the sample was heated to room temperature (Figure 4.28). This data shows a clear transition at around 8 °C, at which point the signal drops much more rapidly than before. It should be noted, however, that there is a negative slope even before the transition, indicating some reorganization, and the transition is just 13 °C from the low-temperature limit of the experiment. Thus, this apparatus may simple not be capable of attaining temperatures low enough to freeze a high degree of order in place.

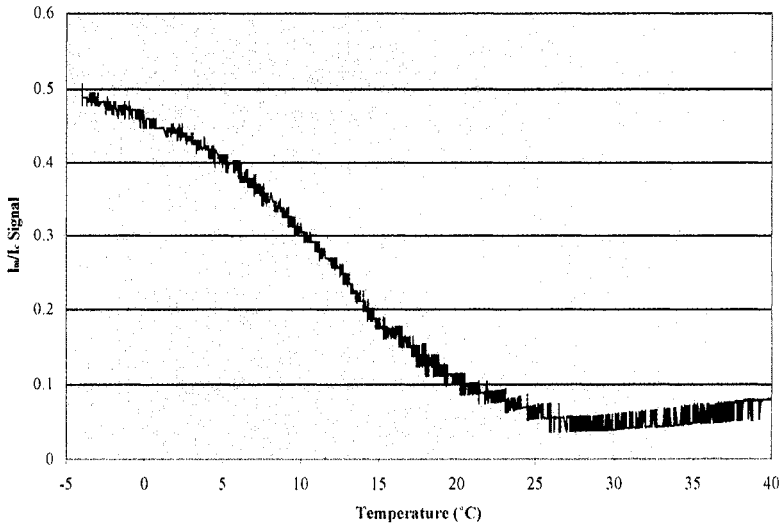

Figure 4.28. Thermally initiated depoling of **SJLD-2** LC films

The low-temperature experiments were plagued by numerous problems. At low-temperatures, the samples consistently exhibited larger currents for a given voltage than were experienced at room temperature and even higher temperatures. As a result,

significantly more sample damage also occurred during low-temperature experiments. This counter-intuitive behavior is likely unrelated to the T_g, and is instead due to condensation. Despite the use of an argon-enriched environment sample chamber, with drying agent to ensure low moisture content argon, condensation was observed on the sample stage during all low-temperature experiments. As such, condensation likely occurred on the samples as well. To ensure an undisrupted beam-path for the probe laser, the sample chamber must have two holes. Although lengthy purge periods of up to 1 hour at high argon flow rates were used, and a continuous flow of around 1 L/min is maintained during the experiment, condensation could not be eliminated. The flow rate during the experiment must be relatively low to avoid disruption of the probe beam. These problems, combined with the relatively poor low-temperature limit of the apparatus (compared to the T_g of the material), prompted the remainder of the poling experiments to focus on room temperature poling.

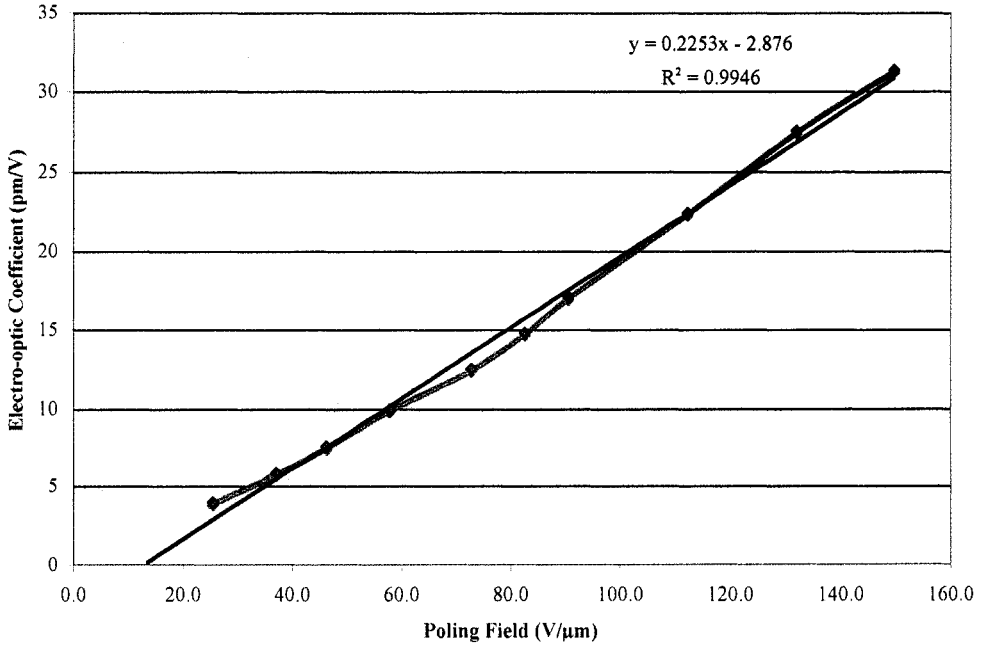

Figure 4.29. Room-temperature poling response of amorphous **SJLD-2** films

Room temperature poling was used to compare the poling response of the amorphous and LC **SJLD-2** films obtained from toluene using the optimized procedure. Samples cured at room temperature and used shortly after preparation to avoid spontaneous SA of the material, were poled at room temperature over a range of voltages, and the r_{33} values were measured under constant bias (Figure 4.29). The poling response of the amorphous material is relatively poor, with a slope of r_{33} vs. poling field of just 0.23, and a maximal r_{33} of 31 pm/V at 150 V/μm. At these high voltages, significant sample damage was seen, and after removal of the poling field, a residual r_{33} of just 1.5 pm/V was observed. In contrast, the poling response of the LC films was much greater, with a slope of 1.91 and a maximal r_{33} of 224 pm/V at 132 V/μm (Figure 4.30). In addition, the LC samples sustained significantly less damage, and a higher residual r_{33} of 21.4 pm/V was observed. Clearly, the response of the LC films is significantly greater than that of the amorphous material.

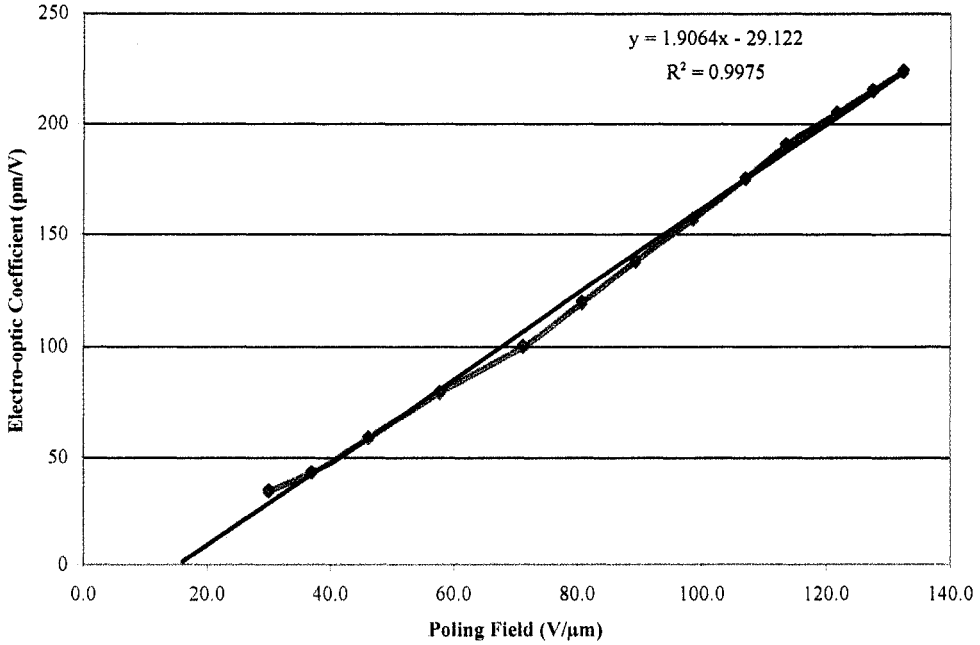

Figure 4.30. Room-temperature poling response of LC **SJLD-2** films

It must be acknowledged that the parameter measured under constant bias is not, in fact, a true r_{33}. As Kippelen and coworkers demonstrated for sub-T_g photorefractive polymers with an EO chromophore component,[43] there are additional contributions to the refractive index change (Δn) from poling-induced birefringence and the Kerr optical effect, as given by Equation 4.3.

$$\Delta n = \frac{2\pi}{n}\left(BE_p^2 + 2CE_pE_T + 3DE_T^2\right) \qquad (4.3)$$

The first term on the right side of the equation describes the poling-induced birefringence effect, where B is related to the polarizability anisotropy ($\Delta\alpha$) and E_p is the poling field. The second term describes the contribution from the linear (Pockels) EO effect, where CE_p is a measure of the EO coefficient (due to the alignment induced by the poling field), and E_T is the total electric field. The final term describes the contribution from the (DC) Kerr optical effect, where D is related to the second hyperpolarizability (γ). Thus, they consider the response factors

$$R(\omega) \propto I_m(\omega)\lambda t / I_c n^3 V_{DC} V_m \quad \text{and} \qquad (4.4)$$

$$R(2\omega) \propto I_m(2\omega)\lambda t / I_c n^3 V_{AC}^2 \qquad (4.5)$$

obtained from a simple reflection measurement (see Section 3.5.2),[27] where I_m is the (half-maximum) intensity of the modulated signal at frequency ω or 2ω, λ is the wavelength of the laser, t is the film thickness, n is the refractive index (at λ) and V_{DC} and V_m are the amplitudes of the respective applied voltages. They then consider the limiting cases where the frequency of the applied AC field is nearly DC ($E_p = E_T$) and where it is too fast for the molecules to reorient ($E_p = E_{DC}$); the low and high frequency limits, respectively. By measuring the frequency dependence of these response factors

from 0.5 Hz to 1 kHz, they demonstrate that the best EO chromophore they studied was effectively at the high-frequency limit at 1 kHz (the frequency used in our measurements), and thus the *dynamic* poling-induced birefringence contribution is small.

The above analysis suggests that for our system any *dynamic* poling-induced birefringence should be small, as our molecules are much larger than the small ones studied by Kippelen *et al.*[43] To conclusively establish this, we would need to explore the r_{33} measured as a function of AC field frequency. Plans are underway to perform these important experiments. Assuming the dynamics effects are minimal, then the effects of poling induced birefringence in the **SJLD-2** films should be no larger than in any high-r_{33} system. For birefringence values of 0.05, demonstrated in high r_{33} systems,[42] the error should only be on the order of -10 %,[44,45] indicating underestimation of the r_{33}. The contribution from the Kerr optical effect in constant DC-biased poling of organic EO based Mach-Zehnder modulators containing AJL8 (an FTC-type chromophore containing the CF_3-TCF acceptor, see Section 2.3) has been estimated at a maximum of 2.05 %,[46] which can be considered negligible.

There are other factors, however, that may also affect the validity of the EO measurements for LC films of **SJLD-2**. As previously mentioned, the absorption tail of the LC films, which extends out to the measurement wavelength of 1.3 μm, can introduce error into the r_{33} measurement.[44,47-49] This is due to dichroism of the poled sample introducing an intensity difference in the s and p waves that is not due to a phase lag Ψ_{sp}, which is assumed to arise from the birefringence due to the different Δn values for the s and the p waves (from the r_{33} and $r_{31} = r_{33}/3$). Accurate analysis of this effect

requires examining the dependence of measurement parameters on the incident angle of the probe beam,[47-49] which is non-trivial. But the magnitude of the effect can be approximated by fitting the curve of I_m signal as a function of Ψ_{sp} to[47]

$$K_0 + K_1 \sin(x + K_2) + K_3 \sin\left(\frac{x}{2} + K_4\right) \qquad (4.6)$$

instead of to Equation 3.18 given in Section 3.5.2. A fit of data for one high-r_{33} sample (around 225 pm/V) based on formula 4.6 gave a K_3 coefficient of only 0.0088, whereas the K_1 coefficient was calculated to be 2.449. A fit of the same data to Equation 3.18 gave an K_1 coefficient of 2.450. This suggests the magnitude of the absorptive effect is small in our case.

Additional error can also be introduced from the electrochromic effect if absorption is an issue,[44] which has the effect of distorting the I_m vs I_{dc} ellipse. If the I_m signal is only evaluated at one or two points on the curve, the distortion of the ellipse can result in large errors. As previously discussed (Section 3.5.2), however, we scan over the whole ellipse and fit the I_m and I_{dc} curves to obtain amplitudes (K_1 coefficients from Equation 3.18) of the sine waves,[41,42] which should effectively eliminate this source of error. A final source of error is introduced through the complex multi-layered nature of the films, and the effects of film thickness and refractive index on the multiple reflections in such a system. A rigorous model has been developed to analyze these effects,[49] but it is beyond the scope of this work. We will simply mention that sub-micrometer thin-films are subject to relatively large (up to 20 %) errors, with a periodic variation between positive and negative contributions, depending on film refractive index and other sample parameters.[49] It is clear there are many factors affecting the

measurement of r_{33}, but most are relatively small in magnitude, and there are both positive and negative contributions. Taken altogether, we feel confident that the relative magnitude of the measured values remains an accurate description of the potential EO activity of the discotic chromophores, although the exact values are not considered accurate.

4.5.6 Conclusions. **SJLD-2** proved to have significantly improved properties with respect to **SJLD-1**. The solubility was improved, which allowed the formation of highly amorphous thin films. It appears **SJLD-1** was indeed close to exhibiting LC properties, as the slight changes in **SJLD-2** resulted in the formation of LC films on curing at elevated temperatures. To our knowledge, this is the first instance of LC behavior in a system with such a strong electron acceptor as the TCF acceptor. Generally, strong acceptors tend to quench the meosgenic properties of molecules,[50] likely due to the introduction of large dipole moments and the resulting strong dipole-dipole interactions. These dipole-dipole interactions are generally much stronger than the other, relatively weak forces present in LCs, and thus they tend to disrupt the delicate balance required to obtain LC behavior. Although **SJLD-2** was seen to crystallize in thin films under certain conditions, attempts to grow single-crystals have so far been unsuccessful. We will continue to pursue these experiments.

Unfortunately, the slight changes in **SJLD-2** also resulted in a substantially lower T_g than that of **SJLD-1**, of around 8 °C. This low T_g results in rapid reorientation of molecules at room temperature and prevents traditional EO characterization. The use of an *in-situ* pole and probe simple reflection apparatus allowed for evaluation of EO activity under constant bias conditions, in addition to measurement of the T_g itself. The

LC films gave r_{33} values up to around 225-250 pm/V under constant bias fields of 120-130 V/μm. We acknowledge that the parameters measured are not true r_{33} values due to the nature of the constant bias measurement, and may be subject to error introduced from a variety of factors including absorption effects, AC Kerr optical effects, electrochromic effects, and film thickness effects. These effects can introduce both positive and negative errors, and thus we feel the measured values still accurately indicate the enormous potential of these materials although the exact values are not considered accurate. The considerably lower r_{33} values (up to around 50 pm/V) obtained through low-temperature "conventional" poling procedures are likely hampered by condensation-induced conductivity and incomplete restriction of molecular reorientation at only 11-13 °C below T_g.

Although **SJLD-2** will likely never be useful for EO applications due to its sub-room temperature T_g, it may find application in terahertz (THz) frequency emission and detection applications.[51-53] Potential THz applications include medical imaging, and spectroscopy and detection (for security purposes) of chemical and biological compounds. Organic EO materials have numerous advantages for these application, including large r_{33} values that correspond to efficient THz emission and detection,[51] and gap-free emission from polymeric and dendrimeric systems.[52] In particular, active beam steering applications where interdigitated electrodes can vary the r_{33} of a sub-T_g material in a continuous manner would be an excellent application for **SJLD-2**.[53] Plans are underway to explore these applications in collaboration with Prof. L Michael Hayden (Department of Physics, University of Maryland).

4.6 SJLD-3

The third discotic chromophore system studied was **SJLD-3** (Figure 4.31), which was designed to be significantly more polar and rigid than **SJLD-1**. The dendron consists of two succinic acid di-ester chains attached to the standard phenyl core structure. Previous work by Sullivan and coworkers in the Dalton Group suggested that the succcinic diester linkage was highly rigid.[41,42] The polar nature of these linkages was also expected to increase the solubility of **SJLD-3** with respect to **SJLD-1**, and explore the effect of different intermolecular interactions. This system was calculated to possess an aspect ratio (A) of 1.48 (MM2 geometry optimization, Chem 3D, Cambridge Software; fully extended conformation) and loading and number densities of 20.9 wt. % and 2.56 x 10^{20} molecules/cc, respectively. Unfortunately, consistently low yields (19-56 %) in the coupling of dendron **4.22** to **4.13** to form **SJLD-3** resulted in a very restricted mass budget for this system, which limited characterization efforts.

4.6.1 Molecular Properties. **SJLD-3** exhibited considerably enhanced solubility, with respect to **SJLD-1** and **SJLD-2**, in a variety of polar organic solvents. Unsurprisingly, it did not exhibit solubility in non-polar solvents such as hexanes. UV-vis absorption spectroscopy in a dilute chloroform solution (Figure 4.32) identified a λ_{max} of 733 nm with an ε of 63600 L/mol*cm.

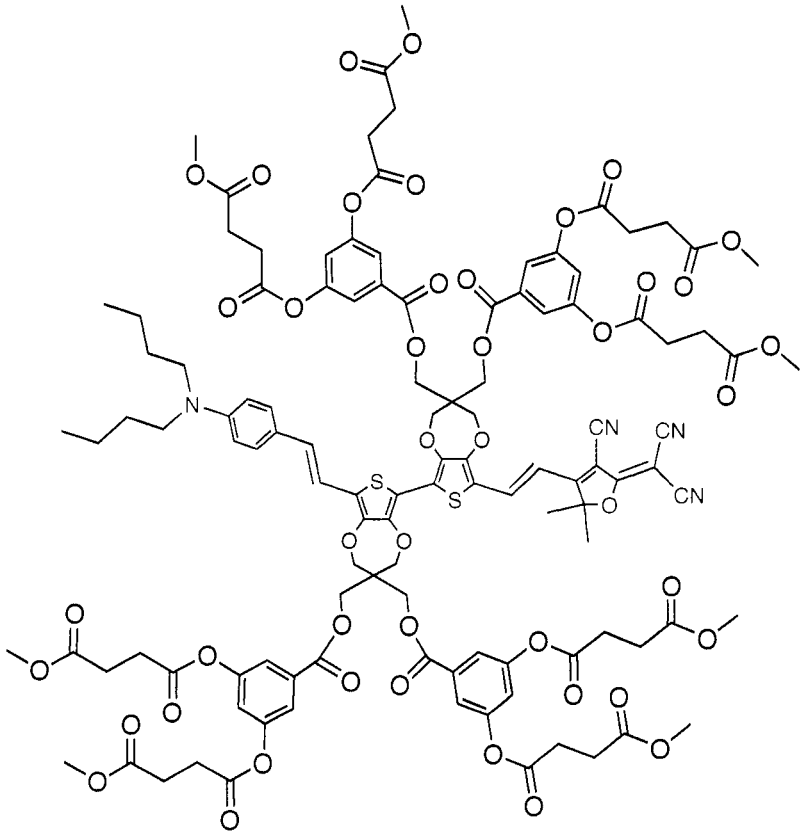

Figure 4.31. Structure of **SJLD-3** with active chromophore highlighted

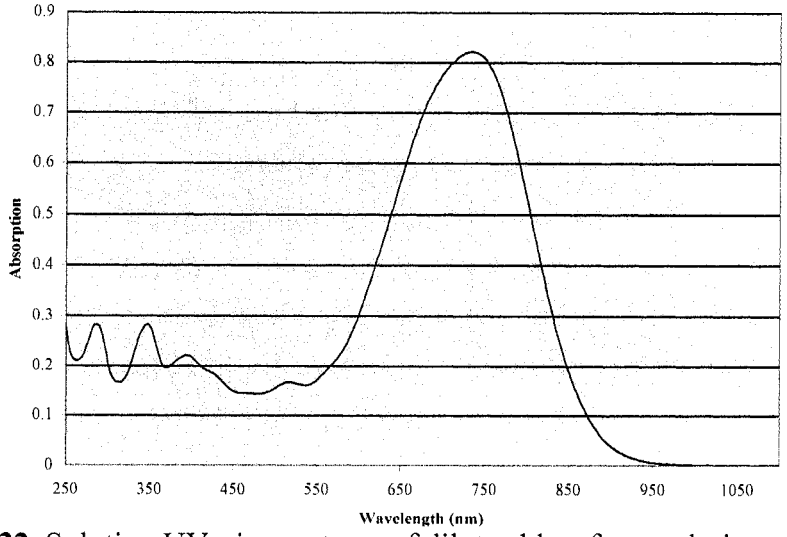

Figure 4.32. Solution UV-vis spectrum of dilute chloroform solution of **SJLD-3**

4.6.2 Film Properties and Morphology. Presumably due to the enhanced surface polar character of **SJLD-3**, it exhibited sufficient solubility for spin casting in a variety of solvents. Drop-cast tests suggested most of these could afford optical quality films,

including toluene, 1,4-dioxane, cyclopentanone (CP), 1,2-dichloroethane (DCE), and 1,1,2-trichloroethane (TCE). Interestingly, after curing these drop-cast films at room temperature in a vacuum oven for over 24 hours, they exhibited a range of λ_{max} values from 689 nm (CP) - 719 nm (dioxane) (Figure 4.33). This does not follow the trend of polarity (as measured by dielectric constant) of the solvents, as dioxane (2.2) and CP (2.3) have nearly the same dielectric constant, while DCE (10.7) and TCE (7.5) are much higher; regardless, all the solvent should be removed after the curing step. We tentatively assign this behavior to slightly different conformations, of the diester chains, for example, leading to slightly different polarity environments in the films. This is supported by the peak shapes in the different spectra (Figure 4.33), with many exhibiting shoulders or otherwise very broad absorption peaks, which further suggests there is a range of environments within each film. These variations in conformation and film morphology might be expected to affect the poling behavior of the films.

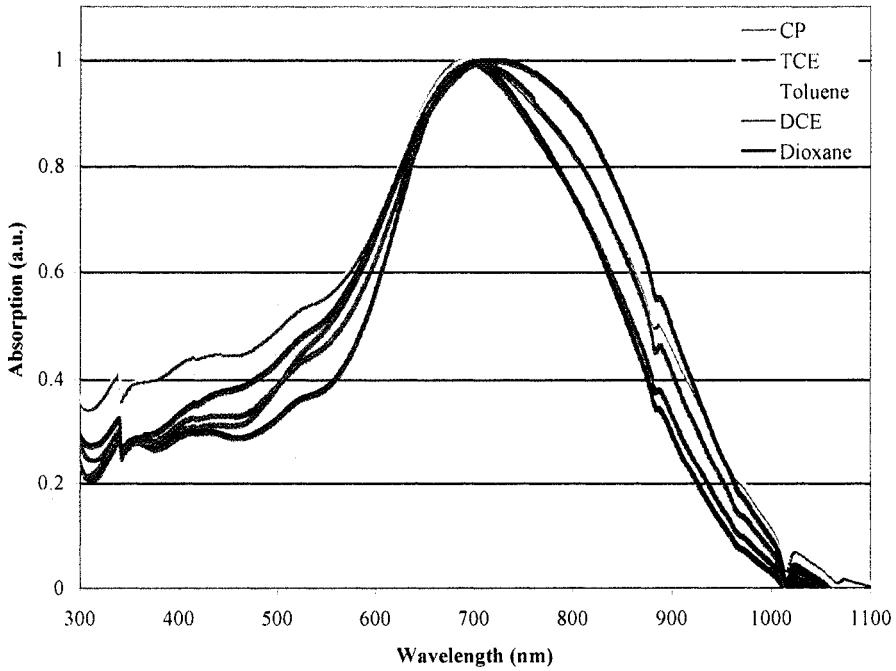

Figure 4.33. Normalized UV-vis spectra of cured **SJLD-3** test films

Initially, CP and dioxane were chosen to explore the spin-casting properties, as these represent the far extremes of behavior in the test films. **SJLD-3** was proved highly soluble in these solvents, with solutions as high as 10.4 wt. % (dioxane) and 11.8 wt. % (CP) exhibiting no particulates. After mixing overnight, these solutions were filtered (0.2 μm) and spun onto patterned ITO/glass substrates using the optimized organic glass conditions (5 seconds at 500 RPM with an acceleration of 5, followed by 30 seconds at 850 RPM with an acceleration of 10) used for **SJLD-2**. These films were treated to an initial soft-bake at 100 °C, and cured in a vacuum oven at 80 °C overnight, at which point they appeared slightly hazy in appearance and green in color. The film thicknesses were measure by profilometry to be 0.73-0.96 μm for the CP films, and 1.4-1.7 for the DO films. Unfortunately, all of these films proved to contain a large number of crystallites, which resulted in electrical shorts after deposition of the top gold electrode. We believe the crystallization occurred due to curing well above the T_g (see Section 4.6.3), which allowed efficient reorganization and packing of the molecules.

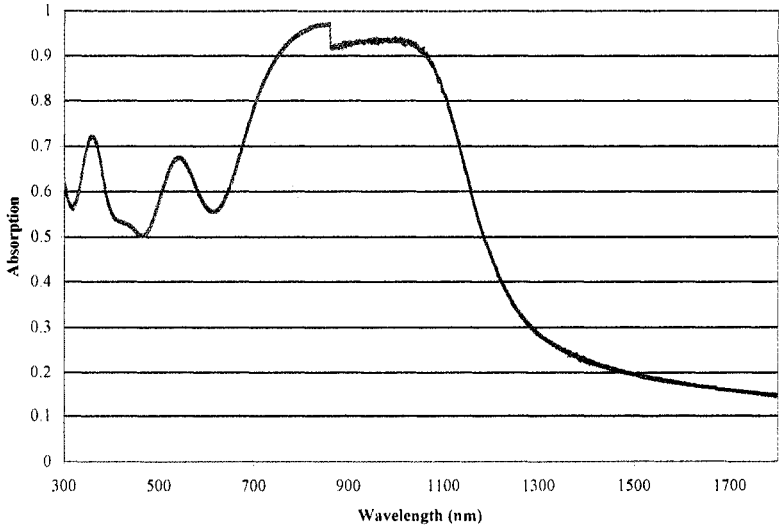

Figure 4.34. UV-vis spectrum of **SJLD-3** film from TCE, cured at 70 °C

We subsequently explored TCE as a spin casting solvent. Surprisingly, **SJLD-3** proved significantly less soluble in TCE than CP and dioxane, with a solubility limit of around 7 wt. %. A solution was mixed overnight and filtered (0.2 μm), before spinning films on patterned ITO/glass substrates using the organic glass spin program. These films were subjected to a very brief soft-bake at 80 °C, followed by curing in a vacuum oven at 70 °C overnight. These films appeared purple in color (Figure 4.34), as for the LC films of **SJLD-2**, and of optical quality (shiny). The large discontinuity at around 850 nm is due to an instrumental error, and the high baseline is due to the excessive optical density of the film. Although this is suggestive of LC morphology, as for the red-shifted **SJLD-2** films, the limited quantity of material available prevented the conclusive characterization of these films with XRD.

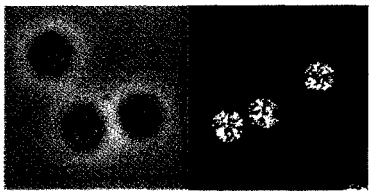

Figure 4.35. Optical microscopy images of **SJLD-3** crystals under normal (left) and crossed polarizer (right) illumination (100x)

Films spun from TCE under similar conditions, but cured without a soft-bake and at room temperature in a vacuum oven remained green in color. Subsequent attempts to cure these films at elevated temperatures resulted only in widespread growth of crystalline platelets in the films. This suggests that the removal of the solvent during the curing process plays a part in assisting the assembly of the molecules into the LC phase (red-shifted films). The morphology of these polycrystalline films was investigated using POM and XRD. Pictures of distinct crystals of **SJLD-3** in an amorphous background film under both normal and crossed polarizer illumination are

shown in Figure 4.35. In Figure 4.36 we present the XRD spectrum from one of the partially crystallized films. Although it appears superficially similar to the XRD spectrum of the LC films of **SJLD-2** and **SJLD-4** (Sections 4.5.3 and 4.7.2, respectively), there are significant differences. The peaks are extremely sharp, indicating a high degree of order. Additionally, the relative intensity of the second peak is greater than that of the primary peak, whereas in LCs, the primary peak always has the greatest intensity. These features, combined with the birefringence seen from the polycrystalline films, but not the LC films, under POM allow the two morphologies to be readily distinguished.

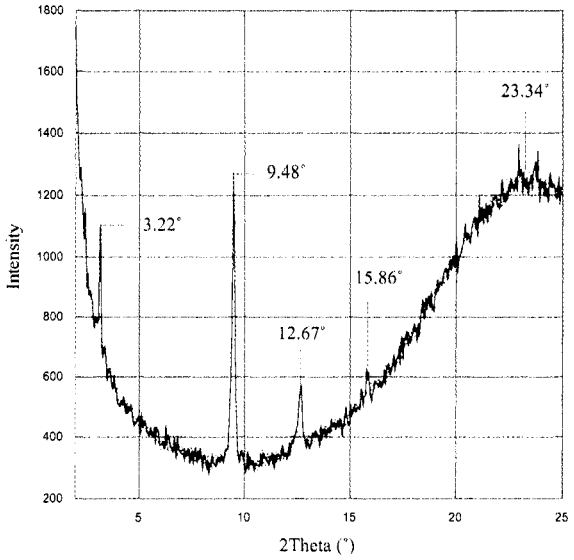

Figure 4.36. XRD spectrum of **SJLD-3** polycrystalline and amorphous film

Although **SJLD-3** exhibits crystalline behavior in thin films, our initial attempts to grow single-crystals for synchrotron XRD analysis have been unsuccessful. Due to the limited quantities of material available, we have been unable to explore crystallization conditions in detail. Further experiments along these lines await the synthesis of more material.

4.6.3 Thermal Properties. The thermal properties of **SJLD-3** were initially investigated using DSC. DSC of the as-prepared bulk material appeared to identify no transitions until decomposition around 260 °C. Further analysis of this data, after EO poling and depoling experiments suggested a T_g in the range of 50-60 °C, suggested the presence of multiple transitions, including a glass transition at 54 °C, hidden in the steep slope and noise of the baseline (Figure 4.37). Subsequent SM-SFM experiments, in collaboration with Tomoko Gray (Prof. René Overney, Department of Chemical Engineering, University of Washington), confirmed a T_g of 54 +/- 1 °C.

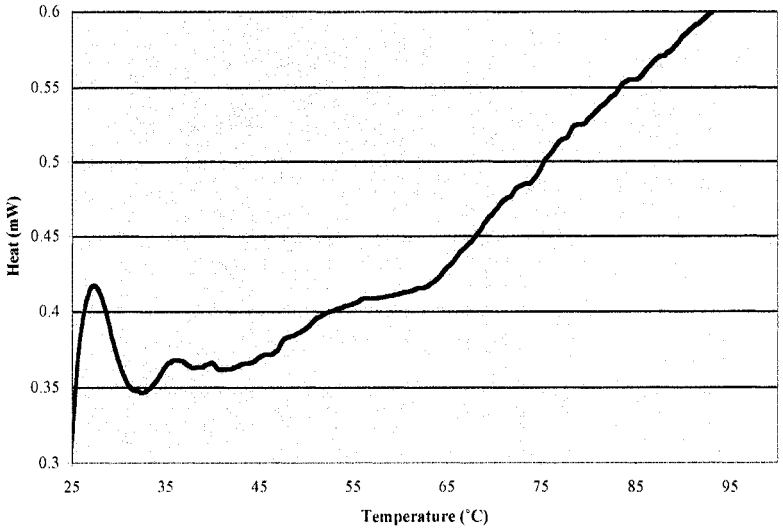

Figure 4.37. Expanded view of DSC of bulk **SJLD-3**

The thermal properties of **SJLD-3** were investigated in more detail with VTM of cured amorphous films spin cast from TCE, with and without crystallites. On slowly heating a purely amorphous film from room temperature, there was no indication of any changes in the film at low temperatures. Around 90 °C, the film appeared to show signs of melting, as indicated by the slow formation of new pinholes in the film. On heating to 100 °C, the pinholes appeared to slowly grow in size. On heating to 120 °C the pinholes grew at a visible rate, and it became clear that the material was repelling from

the glass. Further heating lead to faster repelling from the surface, and by 154 °C the material formed a dense region of distinct beads packed together. On cooling at 20 °C/min, the material remained in a densely packed region as apparently amorphous material with no signs of crystallization or birefringence of any kind.

In contrast, amorphous films that were treated to an annealing step at 80 °C (after the initial cure at room temperature) and contained crystal as a result, were heated from room temperature at 20 °C/min and did not show any signs of change at 90 °C, even after holding for several minutes. Similarly, no changes were seen on holding at 100 °C. The material, crystals and amorphous, clearly began to melt at around 130 °C, albeit slowly. Heating to 140 °C increased the rate of melting and resulted in fully melted, but surface-wetted green material. On cooling at 20 °C/min there was no sign of crystallization, birefringence, or color change, and the material remained an apparently smooth green amorphous film. This indicates the complex thermal behavior of this system, which is likely also connected to the complex film morphologies. The only hypothesis we have for this behavior is different conformations of dendrons, arising from different previous thermal treatments, results in different intermolecular interactions and thus subsequent thermal behavior.

4.6.4 Electro-Optic Characterization. The complex thermal and morphological behavior of **SJLD-3**, combined with the limited mass budget, severely hampered the EO characterization of this material. We initially investigated the optical quality red-shifted films obtained by curing films cast from TCE at 70 °C. These films appeared to show enhanced I_m signals and increased current flow at 60 °C, so our early experiments attempted to pole that temperature, with poor results. Depoling experiments of these

initial, poorly poled, samples suggested relaxation actually began at around 55 °C. These experiments lead to a re-evaluation of the DSC data, which eventually lead to a concrete assignment of 54 °C for the T_g. The final sample of this red-shifted material was poled at 55°C, and yielded a r_{33} value under constant bias conditions of around 100 pm/V at the relatively low poling field of 30 V/μm, before catastrophic sample damage occurred. As previously mentioned for **SJLD-2** (Section 4.5.5), constant bias conditions are far from ideal for obtaining accurate r_{33} values. Considerably more work is required to optimize sample treatment and poling conditions before any concrete analysis of the poling behavior of these red-shifted films can be made.

Subsequent experiments explored the behavior of the purely amorphous (green) material obtained by curing TCE-cast films at room temperature. Conventional poling of samples at both 50 °C (r_{33} of 11 pm/V) and 55 °C (r_{33} of 29 pm/V), established the latter as a superior poling temperature. The values obtained however are not particularly good, considering the relatively large voltages (around 85 V/ μm) required. Based upon the measured T_g, it is probable that poling at 53 °C might be preferable, but the limited accuracy of the temperature controller does not allow for such fine control. Again, considerably more work is required to optimize the sample treatment and poling procedures for these amorphous films, but the initial results do not appear promising.

4.6.5 Conclusions. Clearly, **SJLD-3** shows complex behavior in the morphology of its thin films, with amorphous, (presumably) LC, and polycrystalline phases all evident. We believe that different solvents result in subtly different molecular conformations within the films, as evidenced by the different λ_{max}, spectral broadening, and shoulder peaks in the spectra for films spun under various conditions. Additionally, curing films

at the standard 80-85 °C apparently results in crystallization, while in the case of TCE, curing at a slightly lower 70 °C results in apparent self-assembly into a LC phase.

The thermal properties of these films also seem to depend strongly on the deposition conditions, and the previous thermal treatment of the material. This behavior is presumably also related to the molecular conformation of the material. Surprisingly, based on the previous work with the succinic acid based diester moiety that suggested a highly rigid molecular conformation in that system,[41,42] the T_g of the material is rather low. Although preliminary characterization of the polycrystalline morphology, via XRD, shows similarity to the LC films of **SJLD-2**, there are distinct differences as well. Further characterization is required to study the morphology of the various phases, including single-crystals if possible, as a function of the variables outlined above.

These complex morphological and thermal behaviors all have significant consequences for the poling response of the films, which has significantly complicated characterization of **SJLD-3**. Although initial experiments suggest that the red-shifted films, which are likely LC as for the **SJLD-2** films, show enhanced poling behavior with respect to the amorphous films, neither material is optimized. Again, the limited amount of material available has significantly restricted characterization efforts. It seems clear, however, that **SJLD-3** is not behaving in manner like the original Monte Carlo simulations. This is likely because the aspect ratio is not truly 1.5, as the dendron chains can reorganize and pack in different ways. Indeed, the reorganization of the dendrons appears critical to the present behavior.

4.7 SJLD-4

The fourth discotic chromophore studied was **SJLD-4** (Figure 4.38), which incorporates the commercially available, Fréchet-type dibenyloxybenzoic acid dendron. This dendron has been used previously in EO research,[54] and has been shown to induce excellent solubility and film-forming properties in dendronized chromophore organic glasses. The primary intermolecular interactions arising from the dendrons are expected to be π-π stacking and edge-to-face type interactions between the phenyl rings and other aromatic rings in the molecules. Calculations suggest such a system should exhibit an aspect ratio A of 1.48 (MM2 geometry optimization, Chem 3D, Cambridge Software; fully extended conformation) and loading and number densities of 22.8 wt. % and 2.82 x 10^{20} molecules/cc, respectively.

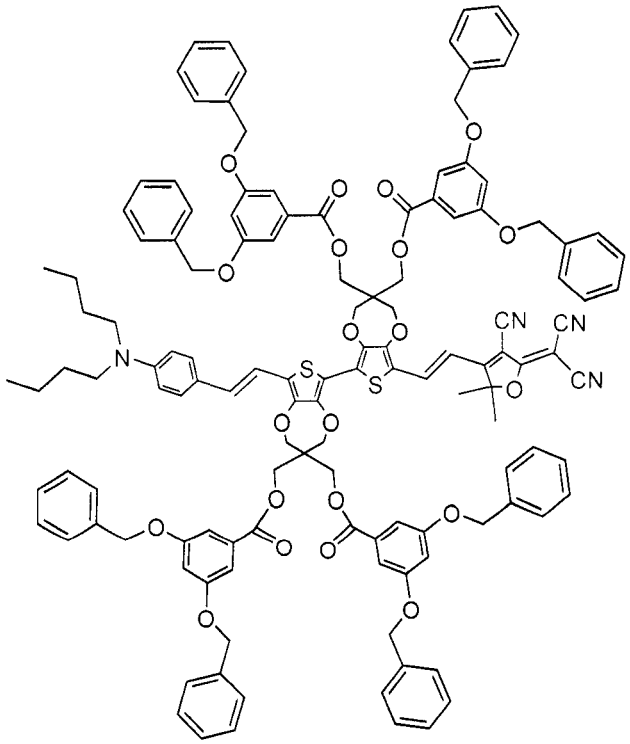

Figure 4.38. Structure of **SJLD-4** with active chromophore highlighted

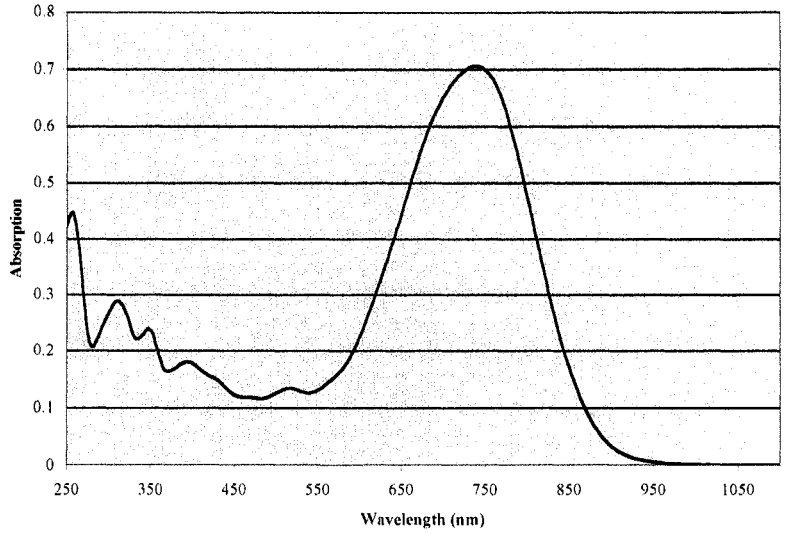

Figure 4.39. Solution UV-vis spectrum of dilute chloroform solution of **SJLD-4**

4.7.1 Molecular Properties. As anticipated, **SJLD-4** exhibited excellent solubility in a wide variety of organic solvents, from toluene to TCE. As expected, it displayed no solubility in hexanes. UV-vis absorption spectroscopy in a dilute chloroform solution (Figure 4.39) identified a λ_{max} of 738 nm with an ε of 68300 L/mol*cm.

4.7.2 Film Properties and Morphology. Due to the excellent solubility of **SJLD-4**, a variety of solvents were identified as having potential for depositing films. Drop-cast tests indicated that the best film quality was obtained from TCE. The solubility limit was determined to be around 12 wt. %, suggesting very thick films could be obtained if so desired. Films were generally cast from filtered (0.2 μm) 9-10 wt. % solutions, spin-cast using the organic glass spin program (5 seconds at 500 RPM with an acceleration of 5, followed by 30 seconds at 850 RPM with an acceleration of 10), resulting in thicknesses of 1.3-1.8 μm. These films were treated to an initial soft-bake at around 85 °C, and then cured in a vacuum oven overnight at either room temperature or 85 °C. Films cured at room temperature remained green, suggesting an amorphous

morphology, while films cured at elevated temperatures exhibited a red-shifted absorption (Figure 4.40) in a manner similar to the films of **SJLD-2**.

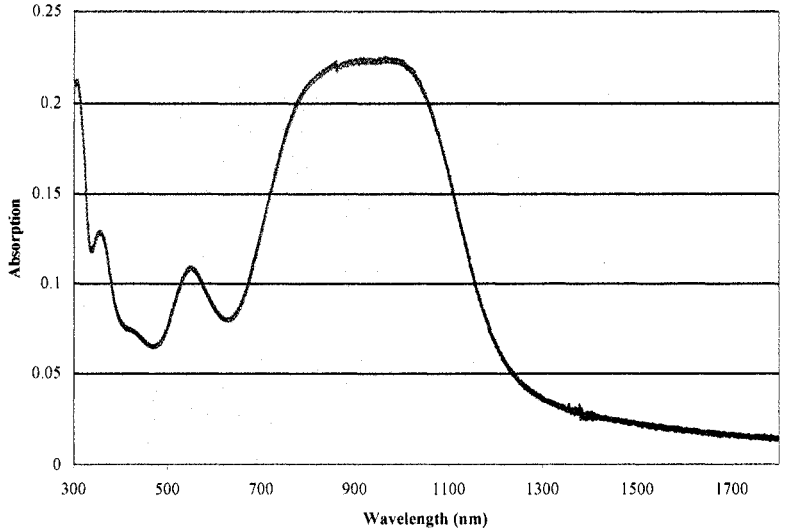

Figure 4.40. UV-vis-NIR spectrum of **SJLD-4** film cured at 85 °C

The morphology of the red-shifted films was examined using thin-film small-angle XRD. These films exhibited four orders of diffraction in the small-angle region (Figure 4.41), in addition to the broad amorphous peak at 24°, indicating a high degree of order in the films. Note, however, that the peaks are broad, and have a similar ratio of intensities as in the **SJLD-2** LC films (Section 4.5.3), but not as in the **SJLD-3** crystallized films (Section 4.6.2). The primary peak the most intense, and the third order diffraction peak significantly more intense than the second and fourth order peaks (which were not evident in **SJLD-2**). Taken together with the peak spacing ratio of 1:2:3:4, this allowed a conclusive assignment to one of two semectic LC phases: SmA or SmC.

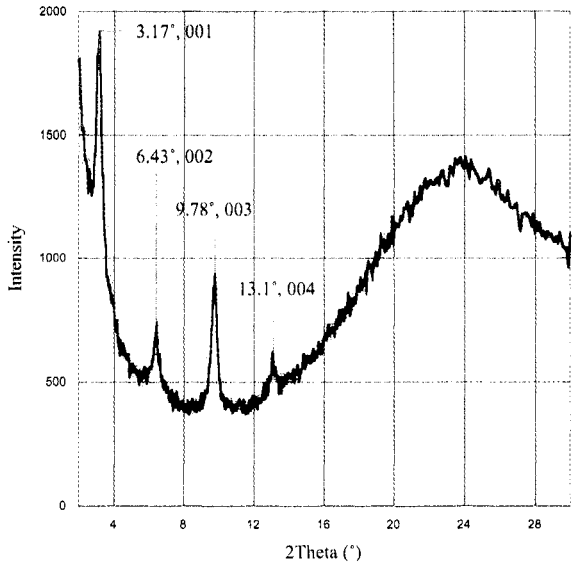

Figure 4.41. XRD spectra of red-shifted **SJLD-4** films with *hkl* assignments

As mentioned previously (Section 4.5.3), both SmA and SmC have a 1-D lamellar structure. The only difference between the two phases is the orientation of the molecules within the lamellae; normal to the lamellae or tilted at an angle with respect to the normal, respectively.[37] Based upon the identification of a semectic phase, we have assigned *hkl* values to the diffraction peaks, and calculated an interlayer (d) spacing of 27.8 Å. This value is nearly identical to the calculated chromophore length (MM2 geometry optimization, Chem 3D, Cambridge Software; fully extended conformation) of 27.4 Å, which initially suggested to us a SmA phase.

The lack of any visible texture in the POM of these LC films, referred to as a homeotropic or pseudoisotropic texture,[37,40] suggests a relatively defect-free film with the lamellae oriented uniformly parallel to the substrate, although other explanations exist (see Section 4.5.4). Thus, if the molecules were all aligned normal to the lamellae as in SmA, one might expect a large birefringence from the sample at the appropriate wavelengths. As the red-shift in the main charge transfer band shifts it primarily

outside of the visible wavelengths of light, this birefringence might not be evident visually. We therefore examined the refractive index of the amorphous and LC films of **SJLD-4** in the near IR (NIR) using a commercial prism-coupling instrument (Metricon Corporation, Model 2010 Prism Coupler) at the telecommunications frequencies of 1300 and 1550 nm. The results are presented in Table 4.3. The larger refractive index, at identical wavelengths and polarizations, of the LC films with respect to the amorphous films, could be due to the presumably higher density of the LC films, or due to the red-shifted absorption of the LC films. Within experimental error, however, the amorphous and LC films have identical small values of birefringence at 1300 nm. Although a purely isotropic film should have no birefringence, the amorphous film likely exhibits some birefringence due to spin-casting induced anisotropy. The TM value for the LC film at 1550 nm is likely erroneous, as the value should not be larger than the TM value at 1300 nm.

Table 4.3. Refractive index of amorphous and LC films of **SJLD-4**

	LC Film		Amorphous Film	
	1300 nm	1550 nm	1300 nm	1550 nm
TE	1.802	1.801	1.742	NA[a]
TM	1.784	1.796	1.723	NA[a]
Birefringence	0.018	0.004	0.019	NA[a]

[a]this film supported only one mode at 1550 nm, precluding data at this wavelength

From the refractive index data, it is clear that there is only relatively weak birefringence in the LC films in the NIR. This suggests that the phase is not SmA. Additionally, as previously mentioned (Section 4.5.3), the d spacing in SmA is generally slightly smaller than the calculated molecular length, due to imperfect orientational order, rather than the slightly larger value calculated. This suggests that the LC phase is likely SmC, where the d spacing is related to the chromophore width

and the average angle with respect to the surface normal (θ) by Equation 4.1. From this, we calculate $\theta \sim 43.3^{\circ}$, although this value is only approximate as it is based upon a fully extended conformation that likely does not exist within the films. A smaller width would result in a larger angle. This is reasonably comparable to the value of 47.6° obtained for the **SJLD-2** LC films (Section 4.5.3), although the same caveats apply.

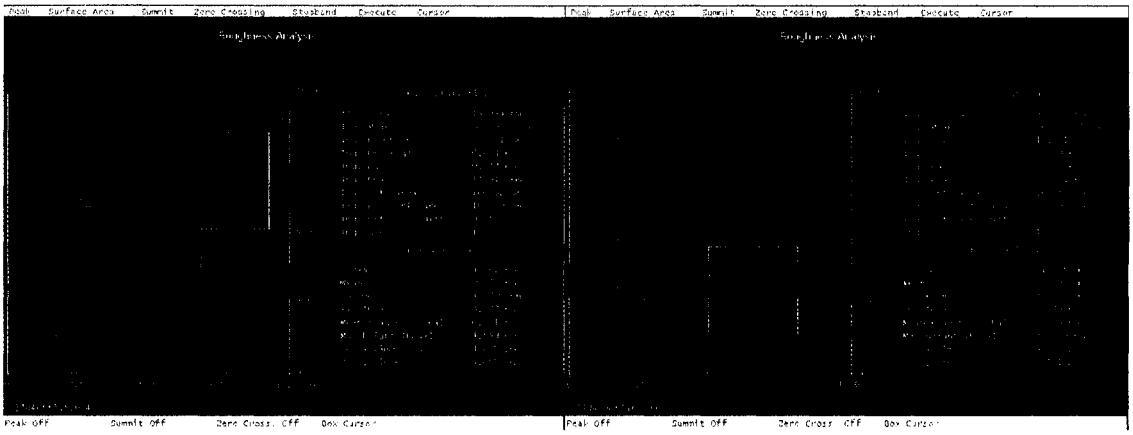

Figure 4.42. AFM images of amorphous (left) and LC films (right) of **SJLD-4**

The morphology of both the amorphous and LC films was also examined by AFM in the Nanotechnology User Facility (NUF, Center for Nanotechnology, University of Washington). Although these investigations were not very conclusive, they do show a relatively smooth surface morphology in the amorphous films (Figure 4.42, left) and a slightly increased roughness (although still relatively smooth) in the LC films (Figure 4.42, right). The nature of the depressions and rises in the amorphous film is unclear. SM-SFM (Tomoko Gray, Prof. René Overney, Department of Chemical Engineering, University of Washington) also confirmed a relatively smooth morphology of the LC films, with a RMS surface roughness of 1.7 nm.

4.7.3 Thermal Properties. The thermal properties of **SJLD-4** were initially investigated with DSC. DSC of the as-prepared bulk material (Figure 4.43, left) identified a T_g of

145 °C and suggested the presence of multiple additional transitions at lower temperatures, and possibly one at a higher temperature. The T_d of the material was also estimated as approximately 265 °C. In contrast, when a cured LC film was scraped into a DSC pan and heated to 250 °C and then slowly cooled (Figure 4.43, right) the low temperature transitions from the bulk were not present or muted, but a distinct transition at 110 °C (heating and cooling) was identified in addition to the T_g. This indicates the complex thermal behavior and sensitivity to previous treatment of this material.

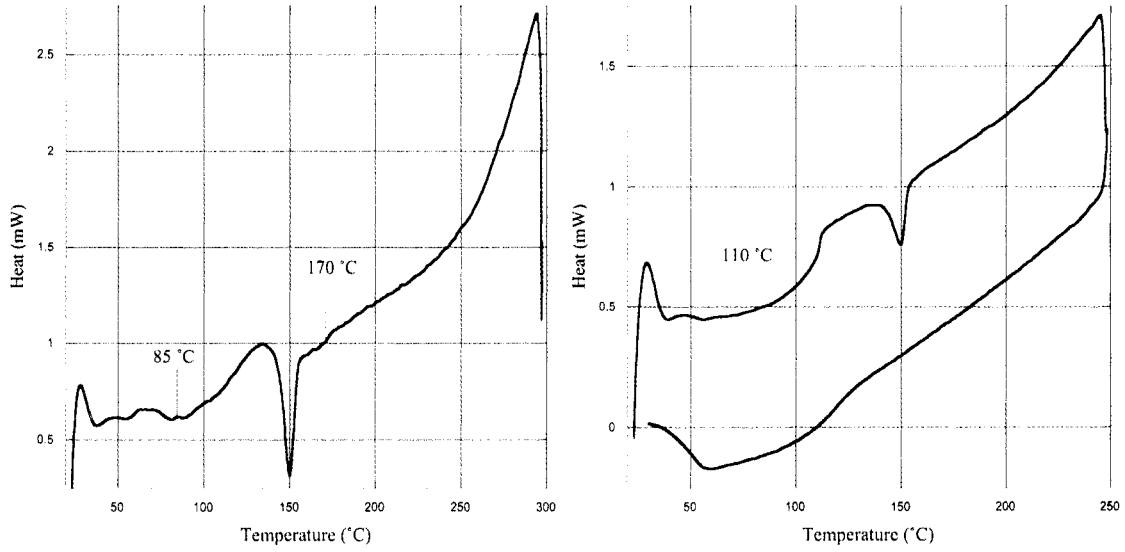

Figure 4.43. DSC traces for bulk (left) and LC film (right) **SJLD-4**

The thermal properties of **SJLD-4** were investigated in more detail with VTM of both amorphous and LC films. On initially heating a cured amorphous film from room temperature, there was no sign of any changes in the film until around 165 °C. At this temperature, graininess developed in the film that grew more pronounced on further heating. By around 205 °C, bright spots under crossed polarizer illumination indicated birefringence, which suggested the grains were tiny crystallites. These were seen to start to disappear by around 208 °C, and by 210 °C the material was clearly melted. On

slow cooling, the material began to crystallize at around 200 °C in the form of needles. By 150 °C, the entire film had crystallized in a network of crystals, shown in Figure 4.44 under normal and crossed polarizer illumination at 100x magnification, ranging from around 10 x 50 μm, to 10 x 150 μm in size. The dichroism of these crystals under polarized illumination indicates that the transition dipole moment of the chromophore (molecular long axis) is perpendicular to the long axis of the crystals. It is also interesting to note that the crystals appear green, as indicated in Figure 4.44, which suggests there may be a different molecular conformation than in the LC films or in the crystals of **SJLD-1**. We have been unsuccessful in our attempts to grow single-crystals of **SJLD-4** from solution so far. We will continue to pursue this goal, as a XRD crystal structure of this different polymorph could provide useful information.

Figure 4.44. Optical microscopy images of **SJLD-4** crystals under normal (left) and crossed polarizer (right) illumination (100x)

In contrast, VTM of cured LC films showed markedly different behavior. The initially purple films shown no obvious changes until around 125 °C, when the purple color began to slowly bleach form the film, resulting in a light beige or gray color by around 135 °C. On further heating the film began to revert to a green color, which was fully developed by around 145 °C, the T_g of the material. Around 150 °C, grains were seen to develop that exhibited some birefringence under POM, however these disappeared again by around 158 °C. The film showed distinct signs of dewetting by

185 °C, suggesting melting considerably lower than the amorphous film. On rapid cooling at 20 °C/min the films were not seen to crystallize or revert to a purple color, and on reaching room temperature the films appeared shiny, green, and amorphous in nature.

Although the thermal behavior is very complex, there is some congruity between the DSC and VTM data. In the amorphous film, the apparent formation of crystallites by VTM appeared to begin around 165 °C, which is near the possible high-temperature transition in the DSC trace. There was no visible sign by VTM, however, of any of the lower temperature transitions, and no sign of melting in the DSC. In the LC film, the purple color appeared to begin bleaching out by VTM at around 125 °C, which is somewhat close to both the transition at 110 °C and the T_g. On cooling, however, there is evidence of the transition at 110 °C by DSC, but there was no sign of recovery of the purple color by VTM. The complete reversion to a green film color by VTM occurred at the exact T_g identified by DSC. The brief formation of crystallites seen by VTM from 150-158 °C, and the apparent melting behavior below 185 °C are not substantiated by DSC.

The thermal behavior of the LC films of **SJLD-4** was also investigated by SM-SFM in collaboration with Tomoko Gray (Prof. René Overney, Department of Chemical Engineering, University of Washington). The films exhibited changes in morphology at 113 °C, 133 °C, and 158 °C, as evidenced by changes in the shear forces exerted on the AFM tip in contact with the film. The transition at 113 °C is likely associated with the transition seen at 110 °C in the DSC, and with the bleaching seen at 125 °C in the VTM experiments. The transition at 133 °C was not observed in any of

the other characterization methods, however. After 158 °C, the film starts to dewet from the surface, suggesting it is melted. This correlates reasonably well with the VTM observations of melting in the LC films at significantly lower temperatures than in the amorphous films. Additionally, the sample underwent a gradual change in morphology over time, as evidenced by a change in the baseline signal over the temperature range studied. Multiple repetitions of this procedure on fresh samples suggest these results are accurate. Taken altogether, **SJLD-4** has very complex thermal behavior, with possible evidence of multiple crystal polymorphs, and clearly different behavior in the LC and amorphous films likely associated with different molecular conformations.

4.7.4 Electro-Optic Characterization. Based upon the significantly enhanced EO activities of the LC films of **SJLD-2** and **SJLD-3** with respect to their amorphous counterparts, we have focused on the characterization of the LC films of **SJLD-4**, particularly due to their attractive features vis-à-vis the other LC films (e.g. high T_g). Our initial attempt to use the *in situ* pole and probe simple reflection apparatus (Section 3.5.2)[41,42] to pole a LC sample resulted in catastrophic sample damage at low temperature (120 °C), voltage (30 V/μm), and current (5-25 μA) values (Figure 4.45). Inspection of this curve suggests poling at around 120 °C might prove optimal. Interestingly, inspection of the sample showed the only damage was at the focal spot of the laser on the sample, where the entire film was ablated (not just the electrode as is generally the case). This suggested to us that absorption at 1.3 μm might be responsible for this behavior.

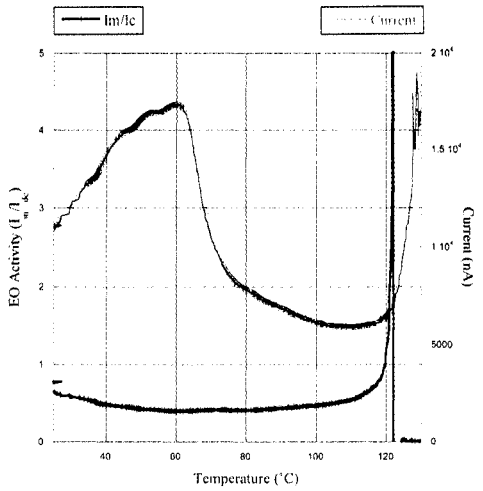

Figure 4.45. *In situ* poling of initial **SJLD-4** sample

A second attempt to pole a LC film using the *in situ* apparatus again resulted in significant damage. For this sample, holding at 123 °C with around 20 V/μm produced no significant increase in EO activity or current, but further heating to 126 °C resulted in a sudden spike in the EO resulting in a loss of all activity, as in the initial sample, followed by a gradual current rise. Inspection of the sample again showed ablation of the film at the focal spot of the laser, which suggests the spike in I_m/I_c signal is due to a spurious optical effect and does not indicate a true rise in EO activity. In this case, however, the sample was not shorted, and after cooling to room temperature and refocusing the laser on an undamaged area, we measured an r_{33} of about 25 pm/V. This relatively low value is not particularly encouraging, although a relatively low field was applied.

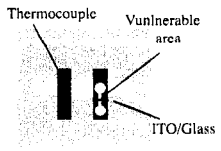

Figure 4.46. Schematic of sample poling stage configuration

Subsequently, we attempted to block the laser before poling samples. Although this eliminated the benefits of using the *in situ* instrument, it was hoped it might prevent ablation of the films. The initial sample poled in this manner, with around 50 V/μm, exhibited an extremely large initial current of 160 μA, whereas previous samples exhibited initial currents of around 13 μA, despite possessing a relatively large resistance of around 20 MΩ. Although this value rapidly decreased, at 123˚C the current spiked from 8 μA to 80 μA. Inspection of the sample this time showed significant damage to the narrow bridge (on the ITO half of the substrate) between the poling electrode and the electrical connection point on the etched half of the substrate (Figure 4.46). The position damaged is in direct contact with the sample mounting stage, which also contains the thermoelectric heaters, and thus is likely subjected to significantly higher temperatures than the poling electrode and thermocouple. Although this has never been an issue for other EO materials, the complex and sensitive thermal behavior of the discotic chromophores makes this configuration problematic.

Although attempts were made to pole samples by placing them in full contact with the sample stage to ensure more uniform heating, these were hampered by complications from the relative position of the thermocouple and sample with respect to the heating elements. In all poling configurations, samples continued to exhibit large leakage currents and sudden spikes in current, rather than gradual increases that could be reacted to. Although another sample was measured to exhibit an r_{33} of 29 pm/V after poling with 50 V/μm at a temperature of around 120 ˚C, most samples were shorted during poling around these temperatures. Attempts to pole at higher temperatures result

in phase transitions in the film, as evidenced by buckling in the electrode structure and color changes in the films, and without fail were unsuccessful. One attempt to pole lower temperatures, around 95 °C with 50 V/μm, using the standard sample stage configuration with the laser blocked, resulted in a lower r_{33} after poling (1.7 pm/V) than was measured before poling (3.1 pm/V). The existence of an initial r_{33} before poling is a common feature of many LC discotic chromophore samples, and is discussed in more detail in Section 4.9.

4.7.5 Conclusions. **SJLD-4** exhibits significantly enhanced solubility and film-forming properties, with respect to the previous systems studied. These are highly desirable attributes for organic EO materials. The excellent optical quality films produced can be cured to produce either amorphous or LC morphologies, and careful heating and cooling can control the formation of needle-like polycrystalline films as well. The facile control over the bulk film morphology is a significant improvement over the complex morphological behavior of **SJLD-3**. The LC films of **SJLD-4** are highly ordered, as evidenced by the four orders of diffraction in the XRD spectrum. The XRD and refractive index data obtained from these films proved critical in the analysis of the SmC phase and interpretation of the properties of the LC films of all the discotic chromophores. Characterization of the crystalline needles of **SJLD-4** represents an exciting area for future work. Although our initial attempts to grow single-crystals from solution have been unsuccessful, we will continue to explore these avenues. Additionally, XRD from the polycrystalline sample could also provide useful information.

Although **SJLD-4** exhibits a considerably enhanced T_g, with respect to the previous systems studied, the complex thermal behavior of this material is a significant disadvantage. The amorphous and LC films display distinctly different behaviors, and different methods of characterization identify different transition temperatures in the material properties. Although some of these have been tentatively correlated with molecular behaviors such as the clearing (T_{SmC-I}) transition at 110 °C disrupting the close noncentrosymmetric aggregates, others remain unidentified.

The EO characterization of **SJLD-4** was significantly hampered by complex thermal behavior, large leakage currents, and an apparently rigid LC lattice structure. The material appears to exhibit large leakage currents at a variety of temperatures and voltages. An initial attempt was made to characterize the bulk conductivity of the LC films through a bottom-contact thin-film transistor device in collaboration with Alejandro L. Briseno (Prof. Younan Xia, Prof. Samson Jenekhe, Department of Chemistry, University of Washington). Although this was unsuccessful, likely due to energy-level mismatch, other methods for measuring the conductivity are being explored. The thermal behavior of the LC films is dominated by the apparent clearing transition at 110 °C (or around 126 °C in the *in situ* apparatus). This transition, or other related transitions, appears to result in large, sudden current increases that often result in catastrophic sample damage. Even slightly below this transition, however, the lattice appears to be highly rigid and resists attempts to introduce extensive noncentrosymmetric order.

The rigid nature of the LC lattice suggests that if considerable macroscopically aligned noncentrosymmetric order could be obtained in the LC films, it would likely be

highly stable at all temperatures below this clearing temperature. Based upon the data for the LC films, we have developed a hypothetical structure for the molecular configuration in the LC films. The details of this proposed structure are presented in Section 4.9. Based upon this structure, we believe it may be possible to introduce asymmetry into the lattice during the initial curing process. Alternatively, we may be able to induce crystallization in a noncentrosymmetric fashion. These concepts are explained in more detail in Section 4.9.

4.8 SJLD-5

The fifth and final discotic chromophore studied was **SJLD-5** (Figure 4.47), which incorporates the fluorinated version of the Frechét-type dendron. Similarly to the non-fluorinated version, this dendron has also been used previously in EO applications,[55] where it was found to introduce excellent film-forming properties. The electron deficiency induced in the phenyl ring by the pentafluoro substitution has been shown to result in strong π-π interactions with other, more electron rich aromatic systems (such as monosubstituted phenyl rings).[55] This strong π-π interaction may result in enhanced thermal properties for **SJLD-5**. Additionally, the phase separation of perfluoro regions of a material from the non-fluorous regions, as in block-copolymers for example,[56] presents an intriguing additional possibility for introducing order into the system. Finally, fluorine substitution for hydrogen has also been shown to be beneficial in reducing optical loss at the telecommunications frequencies introduced by C-H stretching overtones.[57] Calculations suggest such a system should exhibit an aspect

ratio (A) of 1.46 (MM2 geometry optimization, Chem 3D, Cambridge Software; fully extended conformation) and loading and number densities of 17.0 wt. % and 2.11 x 10^{20} molecules/cc, respectively.

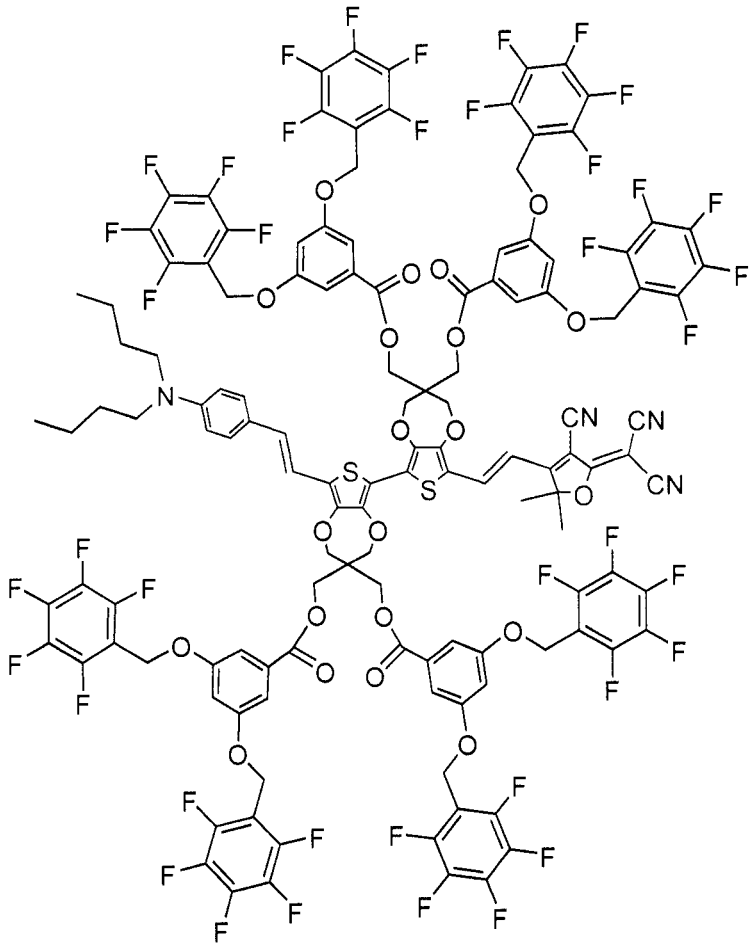

Figure 4.47. Structure of **SJLD-5** with active chromophore highlighted

4.8.1 Molecular Properties. Surprisingly, **SJLD-5** did not exhibit the excellent solubility of **SJLD-4**, although it was considerably more soluble than **SJLD-1** or **SJLD-2**, and displayed moderate solubility in a range of organic solvents. As expected, it displayed no solubility in hexanes. UV-vis absorption spectroscopy in a dilute chloroform solution (Figure 4.48) identified a λ_{max} of 733 nm with an ε of 66100 L/mol*cm.

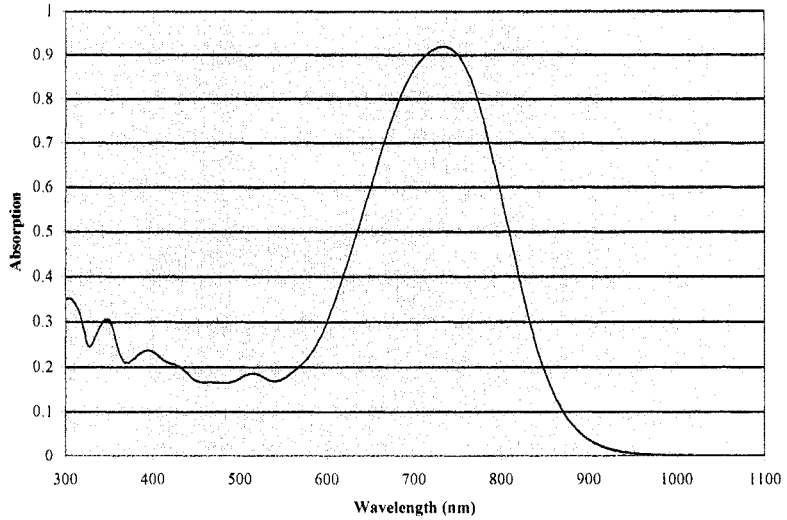

Figure 4.48. Solution UV-vis spectrum of dilute chloroform solution of **SJLD-5**

We also examined the molecular hyperpolarizability (β) of **SJLD-5** and **OLD-5** via hyper-Rayleigh scattering (HRS, Section 2.4.3) in collaboration with Dr. Kim Firestone in the Dalton Research Group (Department of Chemistry, University of Washington). The intensity of the second-harmonic (2ω) generated light produced from dilute chloroform solutions of **SJLD-5** and **OLD-5** excited with a femtosecond pulsed laser at 1907 nm was related to the 2ω signal intensity from EZ-FTC, which was in turn related to the β_{HRS} of chloroform. The results for **SJLD-5** and **OLD-5**, along with those of the previous OLD chromophores, are presented in Table 4.4 as β_{rel}, values relative to the β_{HRS} of chloroform, assuming a β_{rel} for EZ-FTC of 2781.[13,26] The β values for **OLD-5** and **SJLD-5** are just within experimental error of each other, but are considerably higher than the results for the previous OLD chromophores, except for the resonance-enhanced **OLD-4**. Although unexpected, this suggests all of the discotic chromophores likely exhibit β values even larger than the previous OLD chromophores, which were already significantly larger than benchmark chromophores such as EZ-FTC and CLD-5 (Table 4.1).

Table 4.4. Hyperpolarizabilities of **SJLD-5**, **OLD-5**, and other OLD chromophores[13,26]

Chromophore	λ_{max} **(nm)**[a]	β_{rel}**(1907 nm)**[b]
OLD-1	750	4584 +/- 181
OLD-2	746	4859 +/- 523
OLD-3	674	3823 +/- 398
OLD-4	825	14790 +/- 970[c]
OLD-5	754	5766 +/- 392
SJLD-5	733	6396 +/- 330

[a]in $CHCl_3$ [b]HRS data is measured relative to chloroform [c]Resonance enhanced

4.8.2 Film Properties and Morphology. **SJLD-5** proved to have sufficient solubility for spin-casting films in a variety of solvents. Drop-cast tests indicated that the best film quality was obtained from 1,4-dioxane, with only slightly lower qualities obtained from TCE. The solubility limit was determined to be around 9 wt. % in these solvents. Films cast from filtered (0.2 μm) 8.4-8.6 wt. % solutions of dioxane, spin-cast using the standard organic glass conditions, resulting in excellent optical quality films with thicknesses of 0.77-1.05 μm. Films cast from TCE solutions under similar conditions yielded similar results. In all cases, these films were treated to an initial soft-bake at 85 °C, and then cured in a vacuum oven overnight at elevated temperatures. Surprisingly, these films always remained green in color after curing, with a λ_{max} of 690 nm, and a slight shoulder at around 820 nm (Figure 4.49), even for very high curing temperatures up to 150 °C.

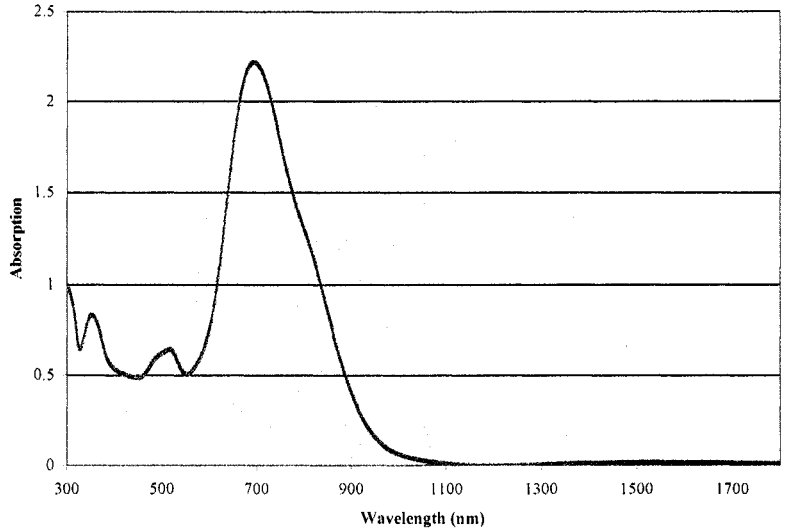

Figure 4.49. UV-vis spectrum of cured amorphous films of **SJLD-5**

Although we initially assumed the green films obtained from dioxane possessed a purely amorphous morphology, the presence of a shoulder suggested the possibility of some order within the films. Therefore, we examined the morphology of these films using small-angle XRD. Repeated scans over the entire angular range of the instrument identified only the broad amorphous peak at around 24°, confirming out initial hypothesis of purely amorphous morphology. SM-SFM (Tomoko Gray, Prof. René Overney, Department of Chemical Engineering, University of Washington) indicates the films are extremely smooth, with an RMS surface roughness of 0.48 nm. The absence of a LC morphology in films of **SJLD-5** was somewhat surprising, considering all of the other discotic chromophores that formed high-quality films (**SJLD-2-4**) exhibited such behavior under the correct conditions. We tentatively attribute this behavior to the theorized strong π-π interactions between the pentafluorophenyl dendrons and other aromatic moieties in the molecules, which might prevent facile reorganization of the molecules on curing.

The dielectric constant (ε) of EO films is an important characteristic that is gaining attention for its affect on molecular properties, intermolecular interactions, and device properties (Chapter 6). We have performed an initial estimate of the ε (at a single frequency) of amorphous films of **SJLD-5** from the capacitance and geometry of an EO sample. We obtained a value of 3.82 +/- 0.25 (at 1 kHz). This number should be considered very preliminary, however, as it is from a single sample rather than a statistical average of many samples. This value is significantly higher than the statistically averaged value obtained for pure APC films (3.08 +/- 0.17, 1 kHz, Section 6.3.3), which is expected based on the enhanced polar content. The ε of **SJLD-5** is considerably lower than the statistically averaged value obtained for a multichromophore dendrimer (PSLD33, 4.80 +/- 0.27, 1 kHz, Section 6.4.3), but this is readily explained by the significantly higher chromophore content in the dendrimer (40 %) as compared to **SJLD-5** (17 %). A rigorous analysis of the dielectric properties of all of the discotic films, particular examining the differences between the LC and amorphous films, would be desirable. Plans are underway to perform these experiments.

4.8.3 Thermal Properties. The thermal properties of **SJLD-5** were initially investigated using DSC. A preliminary DSC of as-prepared bulk material identified a distinct melting transition at 204 °C, and suggested a T_d of around 270 °C. A second sample was initially heated to 220 °C and allowed to slowly cool to room temperature. On second heating, the sample yielded the trace shown in Figure 4.50, which suggests a glass transition temperature of 191 °C, followed almost immediately by the melting transition. This suggests that the pentafluorophenyl dendrons due indeed exhibit strong

π-π interactions with other aromatic moieties in the material, and this leads to a very rigid material.

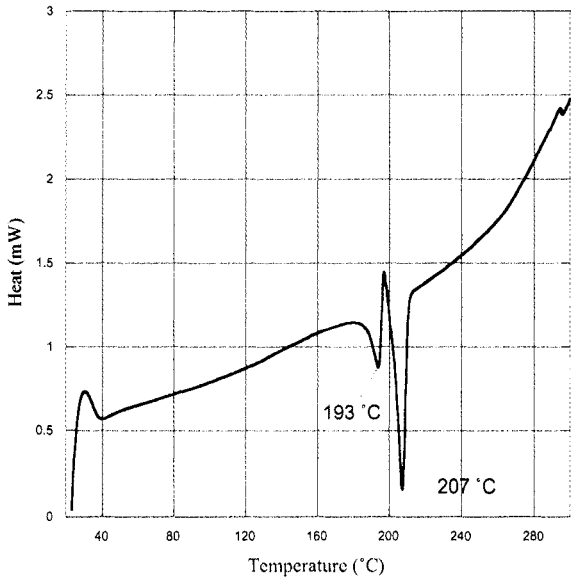

Figure 4.50. Second heating DSC trace of **SJLD-5** bulk material

The thermal properties were investigated in more detail by VTM of the cured amorphous films obtained from TCE. On heating from room temperature, there were no visible changes until around 190 °C, at which point small grains were seen to develop in the film. On further heating, these grains were seen to grow in size, until around 200 °C, when they were visible as bright spots under crossed polarizer illumination, suggesting birefringent crystallites. These crystallites were not seen to begin to melt until 209 °C, and in some cases 210 °C. This suggests the formation of crystallites above the T_g, followed by melting as indicated form the DSC trace, although there is a slight discrepancy in T_m, likely due to calibration issues. On cooling at 10 °C/min, the material began to crystallize in the form of needles at 205 °C. By around 175 °C the entire film had crystallized in a network of crystals, shown in Figure 4.51 under normal and crossed polarizer illumination at 100x magnification. Similarly to

SJLD-4 (Section 4.7.3), the crystals ranged in size from around 10 x 50 μm, to 10 x 150 μm and the dichroism suggested that the molecular long axis was oriented perpendicular to the crystal long axis. The crystals also appear green, as indicated in Figure 4.51 (left), which suggests that the crystals of **SJLD-4** and **SJLD-5** may exhibit significantly different molecular conformations than in the LC films or in the crystals of **SJLD-1**. We have been unsuccessful in our attempts to grow single-crystals of **SJLD-5** from solution so far. We will continue to pursue this goal, as a XRD crystal structure of this different polymorph could provide useful information.

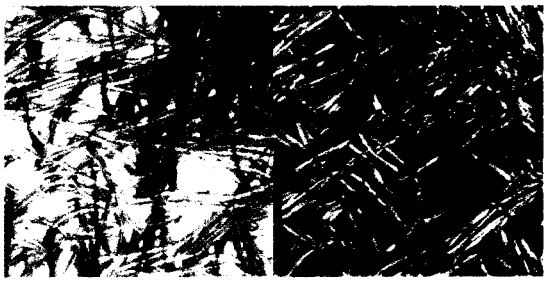

Figure 4.51. Optical microscopy images of **SJLD-5** crystals under normal (left) and crossed polarizer (right) illumination (100x)

Unfortunately, the SM-SFM instrument (Tomoko Gray, Prof. René Overney, Department of Chemical Engineering, University of Washington) is restricted to a maximum temperature of 180 °C, and thus cannot verify the transitions seen in the DSC and VTM experiments. Interestingly, it does identify a transition, indicated by a change in shear force on the AFM tip in contact with the film surface, at 125 °C. Although this transition is not evident by either of the other thermal characterization methods, repetition of the measurement ensures this is not an artifact. The nature of this transition remains unknown.

4.8.4 Electro-Optic Characterization. As for the EO characterization of **SJLD-4** (Section 4.7.4), the poling of **SJLD-5** was significantly hampered by large leakage

currents, confusing thermal behavior, an apparently rigid lattice structure, and issues with the *in situ* poling apparatus sample stage design. Our initial attempt to pole **SJLD-5** using the *in situ* simple reflection apparatus with 20 V/μm applied showed significant current increases at 170 °C (40 μA) and 190 °C (90 μA), but no increase in EO activity was evident at any temperature. After cooling to room temperature and realigning the laser, no r_{33} value could be measured. A subsequent attempt with 50 V/μm applied showed an increase in the EO activity slightly below 100 °C, which peaked shortly after 100 °C and then steadily decreased thereafter (Figure 4.52). The current, however, did not increase until around 130 °C, by which time the EO activity was nearly zero. This is distinctly non-standard poling behavior, which is characterized by an increase in the EO signal, followed immediately by an increase in current. After cooling, the sample gave no measurable r_{33} value, and inspection identified damage to the vulnerable bridge area of the electrode, identified in Figure 4.46. Repetition of this poling program with another sample showed a similar behavior.

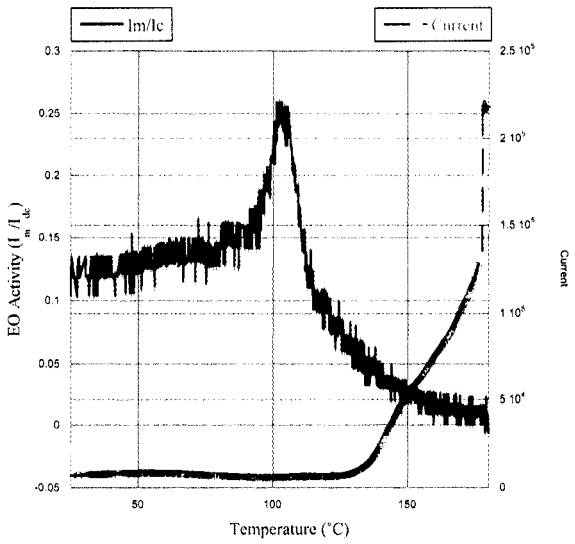

Figure 4.52. *In situ* poling of **SJLD-5** sample

Based upon the repeated sample damage on the vulnerable gold bridge area, likely due to contact with the sample stage exposing the material to significantly higher temperatures, we explored the use of ex-situ poling using an apparatus in Dr. Antao Chen's laboratory (Applied Physics Laboratory, University of Washington). In this instrument, the entire sample was placed in full contact with the temperature controlled heating stage. Our initial experiments with this apparatus showed increases in current at around 120 °C. Subsequent attempts to pole around 160 °C (32 V/μm) and 120 °C (50 V/ μm) resulted in low r_{33} values of 2.0 and 3.4 pm/V, respectively. Although this suggests that lower poling temperatures are better, the higher voltage in the second sample makes conclusions difficult. Another study using the *in situ* apparatus, but with the sample and thermocouple reconfigured to be in full contact with the sample stage, attempted to pole with 50 V/μm at 120 °C, 140 °C, and 160 °C, resulting in r_{33} values of 2.0, 0.4, and 0.3 pm/V, respectively. Based upon these results, we attempted to pole another sample at 125 °C, immediately after the current started to rise, but this resulted in no measurable r_{33} value.

4.8.5 Conclusions. The HRS results for **SJLD-5** and **OLD-5** indicate the excellent microscopic nonlinear activity of all the discotic chromophores. In terms of macrosopic behavior, **SJLD-5** exhibits significantly stronger intermolecular interactions, with respect to the previous discotic chromophores, as evidenced by the lack of LC film behavior and the high transition (T_g and T_m) temperatures. This is likely due to strong π-π interactions between the electron deficient pentafluorophenyl dendrons and electron rich aromatic moieties in the chromophores. Although such high transition temperatures are attractive features for organic EO materials due to the implied thermal

and temporal stability of EO activity, in this case they are associated with a very rigid, non-plastic material lattice, as evidenced by the proximity of the T_g and T_m transitions. This resulted in very low poling-induced EO activities, due to the high leakage currents and poor molecular mobility associated with such a rigid lattice.

The poling behavior suggests a possible method for enhancing the thermal properties of **SJLD-5** by doping the material with a plasticizer. In particular, EO chromophores have been shown to act as plasticizers on their polymer hosts, and the relatively new class of binary organic EO glasses has been shown to exhibit extremely large EO activities.[42,55] Thus, doping EO chromophores into **SJLD-5** presents an attractive opportunity to simultaneously enhance the thermal properties and the EO activity. In particular, binary organic glasses composed of equal parts **SJLD-4** and **SJLD-5** may possess attractive properties, as this is analogous to previous systems studied.[55] Additionally, similar doping studies in the other discotic chromophores are also attractive avenues for future research, particularly in those systems that exhibit LC behavior. The effect of EO chromophore dopants on the intermolecular interactions that give rise to the LC behaviors would be intriguing.

4.9 Discotic Chromophore Conclusions

The discotic chromophores as a group exhibit a number of highly desirable properties for organic EO materials. All of the chromophores possess very large molecular hyperpolarizabilities (β values), as indicated by the similar solution absorption properties and the HRS results for **SJLD-5** and **OLD-5**. Additionally, all of

the molecules decompose at or above 250 °C, indicating excellent thermal stability. A number of the systems exhibit good solubility in a wide range of solvents, from toluene to TCE, and **SJLD-1** and **SJLD-2** can dissolve in nonpolar solvents such as hexanes. Most of the chromophores also possess excellent film-forming properties, allowing the casting of optical quality films without the need for a polymer host. These films exhibit amorphous, liquid crystalline, and polycrystalline morphologies that can often be specifically addressed by varying deposition, curing, and annealing conditions. This achievement of LC order in materials incorporating strong electron acceptors (such as TCF), and that exhibit strong dipole-dipole interactions, is, to our knowledge, unprecedented. Normally, the introduction of strong acceptors such as TCF has been seen to quench LC behavior in otherwise mesogenic systems.[50]

Except for **SJLD-3**, whose characterization was hampered by the small quantities of material available, each of the individual systems has demonstrated desirable EO properties. **SJLD-1** afforded a synchrotron XRD crystal structure that, while overall centrosymmetric, exhibits a unique noncentrosymmetric aggreagate structure that has promising implications for the other discotic chromophores. **SJLD-2** has shown extremely large EO activity in LC films, as indicated by approximate r_{33} values obtained under constant bias measurements of up to 250 pm/V at 130 V/μm. **SJLD-4** and **SJLD-5** both possess large glass transition and melting temperatures, which shows promise for high thermal and temporal stabilities of EO activity.

Unfortunately, no one system has demonstrated all of these desirable properties. In many cases, the properties seem mutually exclusive, such as high EO activity in low T_g materials, and vice versa. Additionally, the numerous complexities in the behavior

of these materials are a significant impediment to reliable and reproducible applications in EO devices. In particular, the complex thermal behavior demonstrated by all of the systems, coupled with the large leakage currents, makes reliable poling extremely difficult. Based upon the poling studies so far, it is clear that these materials require carefully designed and controlled thermal environments beyond that required for other EO materials. It should be emphasized that these undesirable properties are not to due impurities, as all of the materials have been analyzed by elemental analysis and, except for **SJLD-1**, which was likely contaminated by the presence of excess dendron material, have been shown to be highly pure (see Section 4.10). These behaviors are instead attributed to complex intermolecular interactions.

Clearly, considerably more work is necessary to completely characterize these complex interactions, and their effects on the properties of these intriguing materials. One attractive method to explore these interactions is through further crystal structures. All of the discotic chromophores have shown evidence of crystalline morphologies, and some suggest the existence of multiple polymorphs. In particular, the needle-like crystals of **SJLD-1** originally obtained from dichloromethane and methanol are distinctly different from the prisms obtained from *n*-hexane and ethanol, and would not suffer from the incorporation of *n*-hexane that complicated analysis of the latter polymorph (Section 4.4.4). This needle-like polymorph is similar to the crystals of **SJLD-4** and **SJLD-5** seen in the VTM experiments (Sections 4.7.3 and 4.8.3, and Figures 4.44 and 4.51, respectively). **SJLD-3** exhibits plate-like crystals in the films (Section 4.6.2, Figure 4.35) that appear similar to the crystals of **SJLD-1** originally seen

in films (Figure 4.11), which are likely different from the solution grown crystals. The morphology of the **SJLD-2** crystallites has not yet been determined.

One potential method to tune these intermolecular interactions is through the introduction of EO chromophore dopants into the discotic host materials. The resultant binary organic glasses, which are a recently discovered class of EO materials with extraordinary EO activites, might exhibit enhanced properties. In particular, EO chromophores have been shown to act as plasticizers on their polymer hosts, which might enhance the molecular mobility of the rigid high-T_g systems, and might enhance the thermal properties of the low-T_g systems. In particular, binary organic glasses composed of equal parts **SJLD-4** and **SJLD-5** may possess attractive properties, as this is analogous to previous systems studied.[54] Additionally, the effect of EO chromophore dopants on the intermolecular interactions that give rise to the LC behaviors would be particularly intriguing. It is possible the dopants would disrupt the LC behavior entirely, or they may be incorporated into the LC lattice.

Although the nature of the intermolecular interactions vary to some extent from system to system, it appears that the noncentrosymmetric aggregate structure found in the crystal structure of **SJLD-1** (Figure 4.12) is likely a key interaction affecting the properties of all systems. From this interaction, it is clear that the molecules are not behaving as originally intended. We sought to prevent close side-on-side approach of the chromophores by extensive functionalization around the bridge structures. With the possible exception of **SJLD-5**, where the strong π-π interactions between the pentafluorophenyl dendrons and other aromatic rings may prevent such close approach, all the other molecules likely exhibit this close side-on-side aggregate structure, as

evidenced by the large red-shift and broadening of absorption features in the cured films and in the crystal powder of **SJLD-1**. Although the noncentrosymmetric nature of this aggregate is intriguing, and potentially could lead to large-scale acentric order, it clearly demonstrates that the chromophores do not possess effective width to charge-transfer axis length aspect ratios approaching 1.5. Thus, the predictions of the Monte Carlo simulations that inspired this project are not applicable to these materials. We instead focus on the noncentrosymmetric aggregate structure and its implications for the LC films.

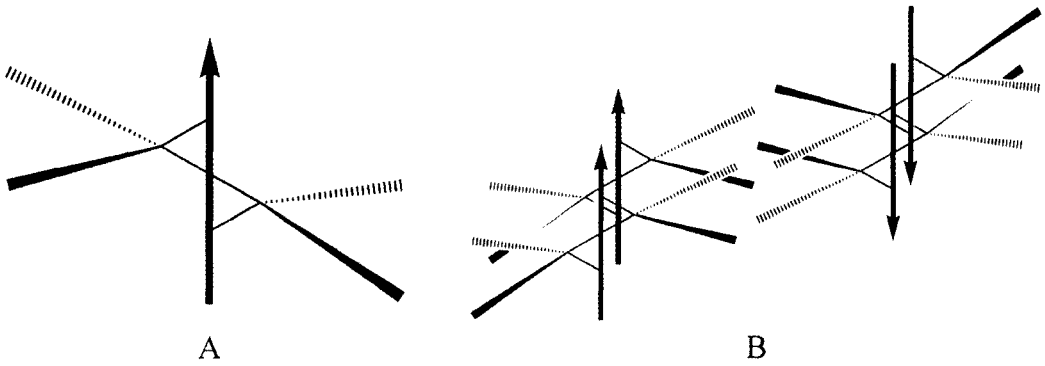

Figure 4.53. Schematic of A) Discotic chromophore and B) **SJLD-1** crystal structure

If we consider the structure of an individual discotic chromophore as represented by the structure shown in Figure 4.53A, then the unit cell of the **SJLD-1** crystal structure (Section 4.4.4, Figure 4.12) can be represented by the structure shown in Figure 4.53B. Again, the noncentrosymmetric aggregate is clearly the dominant intermolecular interaction in the crystal, and presumably gives rise to the large red-shift in absorption seen in the spectrum of the crystal powder (Figure 4.18). Due to the similar nature of the absorption properties of the LC films, we believe a similar aggregate structure is present in the LC films.

We have assigned a SmC phase to the LC films based on a variety of data, including small-angle XRD, refractive index measurements, and calculated chromophore geometries. The layered structure of the SmC phase should exhibit a relatively uniform molecular tilt angle and interlayer spacing, but possess significant variations of molecular spacing and dipole orientation within the layers. The lamellae or planes are likely similar in nature to the layers seen along the crystallographic c axis (Figure 4.16) in the crystal structure of **SJLD-1.** Based upon the data mentioned above for **SJLD-2** and **SJLD-4**, we have calculated average molecular tilt angles of 47.6° and 43.3°, respectively, although these values are likely slightly underestimated due to overestimation of the effective chromophore width from the molecular mechanics calculations (MM2 geometry optimization, Chem 3D, Cambridge Software). With this underestimation in mind, these values match well with the measured birefringence for films of **SJLD-4** (Table 4.3).

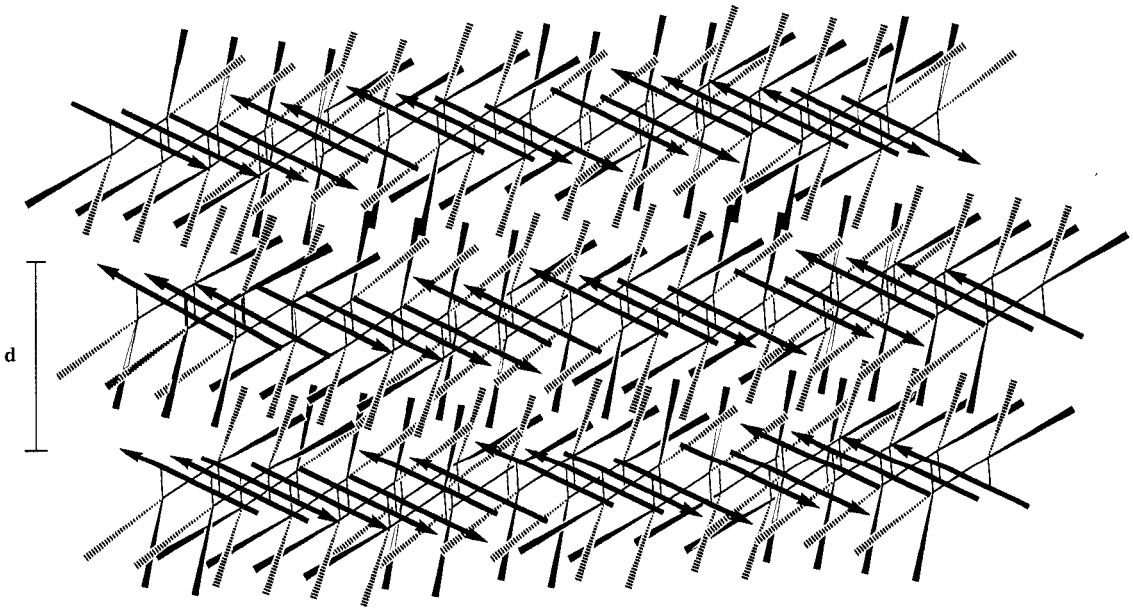

Figure 4.54. Schematic of proposed structure for discotic LC films

Based upon all of the data for the LC films and the **SJLD-1** crystal structure, we have developed a hypothetical structure for the LC films, which is shown schematically in Figure 4.54, in only the x and z dimensions for clarity. The proposed structure includes, however, extended chromophore aggregates in both the x and y dimensions within the lamellae of the LC structure. Variations in the size, dipole orientation, and intermolecular distance within and between these aggregates could give rise to the characteristic disorder expected within the lamellae. These variations might also explain the broad nature of the absorption in the LC films, with aggregates of different size and strength of intermolecular interactions giving rise to absorptions at different wavelengths. In this model, the crystal of **SJLD-1** is simply an extension of this structure to a higher degree of order associated with defined aggregate size and orientation. The extremely broad nature of the spectrum obtained from the crystal powder is likely due to random disruption of this ordered structure caused by the shearing forces used to create the powder from the crystals.

One piece of data that may support this proposed structure is the fact that many, but not all, of the discotic LC EO samples from all three LC-morphology systems (**SJLD-2-4**) showed a distinct non-zero r_{33} before initial poling. These initial r_{33} values ranged from so low they are likely instrumental error (< 0.5 pm/V), to as high as 9 pm/V in one sample of **SJLD-4**. There were significant variations within each system, and even between the three samples obtained from the same initial plate (1"x1" substrate upon which films are spin-cast). The proposed film structure provides a possible explanation for this behavior. While the dipole orientation of aggregates within individual layers and multi-layered regions of the SmC lattice may have net

noncentrosymmetry, the average orientation over the whole lattice structure should be net centrosymmetric. It is feasible, however, for small variations in the net distribution of aggregate orientation or chromophore densities to result in slight net noncentrosymmetric orientation, which would give rise to a non-zero r_{33}. This is analogous to the conditions giving rise to HRS in solution (Section 2.4.3), except that surface effects and kinetic trapping of non-equilibrium behavior might be expected to increase the magnitude of these effects. This could explain the readily observed levels of EO activity measured in the LC films (1-9 pm/V), as opposed to the extremely low signals present in the solution-based HRS experiment (requiring femtosecond pulsed lasers and cryogenically cooled CCD cameras).

There are other possible explanations for this initial non-zero r_{33} behavior, however. In the case of **SJLD-2**, the dynamic induced birefringence from the (relatively small) AC voltage could be a potential source, with variations due to differences in film quality restricting the mobility of the molecules. Although measurements as a function of AC frequency would be required to conclusively explore this, previous work by Kippelen suggest the **SJLD-2** molecules should be unable to respond at all to the 1 kHz frequency signal used in our measurements.[43] Regardless, this explanation cannot apply to the other discotic LC systems, with T_g values above room temperature.

As previously mentioned (Section 4.5.5), the absorption tail of the LC films extends out to 1.3 μm, which may introduce error into the measurement of the r_{33} due to dichroism introducing an intensity difference not arising from the electric-field induced phase lag. It is possible that this initial non-zero r_{33} is due to that effect, and that the

magnitude of the error introduced is on the order of 2-9 pm/V (this could be positive or negative due to the measurement method). If so, this is clearly a relatively small contribution to the large r_{33} values exhibited by **SJLD-2**. The absorption induced error theory does not explain, however, why the initial r_{33} value varies between samples from the same system and even the same initial film. All of the films from a given system exhibit relatively similar absorption properties, and the variations in absorption properties within a single films should be extremely small. Additionally, it does not explain why some LC samples from each system exhibited no initial r_{33}. Another potential explanation that is related to absorption effects is the introduction of an electrochromic effect from the AC field. The variation in initial r_{33} could be explained by this hypothesis if variations in film conductivity/resistance or dielectric constant result in varying effective fields within the films. Although we have not attempted to correlate these properties with the measured initial r_{33} values, this is a likely area for future exploration.

Based partially upon the proposed molecular structure of the LC films, there exists an intriguing possibility of an alternative to traditional poling for introducing noncentrosymmetry in the discotic chromophores. The SmC LC lattice exhibits a high degree of orientational order, although in a centrosymmetric fashion due to the equivalency of the two dipole orientations in the absence of a field. As the LC films are also associated, through the **SJLD-1** crystal structure, with noncentrosymmetric aggregates potentially over an extended area, there is reason to suspect an acentric LC or crystalline lattice would be feasible. As all of the discotic chromophores that display LC behavior, except for **SJLD-2**, self-assemble into the LC phase only on initial curing

after spin casting, this represents a key opportunity for introducing asymmetry into the LC lattice. Alternatively, crystallization on cooling from the melt represents another potential opportunity to introduce asymmetry in an ordered lattice structure. Using traditional contact poling methods, neither of these opportunities is accessible. While corona poling might be feasible for the former, it is not for the latter, and corona poling can introduce charges into the films and is often not very effective.

We have recently obtained some commercial LC test cells (LC3-5.0, Instec Research Instrumentation Technology), which consist of ITO sandwich structures with well-defined electrode spacing (5.0 +/- 0.2 μm) and alignment promotion layers. Heating the cell above the melting temperature for the system under study should allow the material to be drawn into the cell by capillary action. If a (small) voltage is applied to the cell, then the resulting field may allow (partial) alignment of the molecules in this melt, provided the current is not too large. The cell could then be cooled, either rapidly to prevent crystallization, or slowly to encourage it. In the case of **SJLD-2**, the cell could be cooled rapidly to the $T_{I\text{-}SmC}$, and thereafter slowly to encourage formation of a stable LC lattice. Although this will likely not allow the high-T_g materials to form LC phases, it will allow us to explore the feasibility of this concept.

If the initial experiments prove promising, the results would likely be directly applicable to the recently developed slotted ring-resonators and slotted Mach-Zehnder modulators (Section 1.4). These devices could either be heated to the melting point and the material applied directly in a manner similar to the LC test cells, or the material could be spin-cast on directly. In the latter case, a special vacuum oven that allows for electrical connections could then be utilized to cure the high T_g films at elevated

temperatures while applying a voltage. The nanoscale nature of the gap in such rings (50-100 nm) would likely enhance the possibility of achieving a high degree of noncentrosymmetric LC or crystalline order. Particularly in the high-T_g materials, such as **SJLD-4**, the alignment stability is expected to be excellent at temperatures below the clearing (T_{SmC-I}) or melting (T_m) temperatures due to the rigid nature of the lattice structure.

In conclusion, the discotic chromophores display a complex, confusing, and intriguing set of properties. Significantly more work is necessary to further understand these materials, but they show a number of promising behaviors that suggest possible avenues to obtain very large EO activity through extension of an ordered nanostructure to a macroscopically oriented material.

4.10 Experimental

General: All commercially available starting materials were purchased from Sigma-Aldrich, ACROS, or TCI and used without further purification unless otherwise stated. HPLC grade tetrahydrofuran (THF), diethyl ether, methylene chloride, and toluene were purchased from Fisher chemical and purified by passing through alumina in a Seca Solvent Systems (GlassContour Systems) solvent purification system. Alkyl lithium reagents were purchased from ACROS and titrated using 4-biphenylmethanol according to the literature method.[58] All reactions were performed under a nitrogen or argon atmosphere unless otherwise stated. Flash chromatography was performed manually using fine mesh silica.

Instrumentation: ^{1}H and ^{13}C NMR spectra were obtained on a Bruker AV300 or AV301 system at 300Mhz and referenced to residual solvent. Mass spectrum data was obtained from positive ion ESI or MALDI at the Medicinal Chemistry Mass Spectrometry facilities at the University of Washington. Elemental analyses were performed at Prevalere Life Science Inc. (Whitesboro, New York). UV-visible spectroscopy was performed on a Shimadzu UV 1601 Spectrophotometer and UV-visible-near IR spectroscopy was performed on a Perkin-Elmer Lambda 9 Spectrophotometer.

Differental scanning calorimetry (unless otherwise specified) was performed on the bulk material under nitrogen with a scan rate of 10 °C/min using a Shimadzu DSC-60 thermal analyzer. Variable temperature microscopy was performed using a Mettler FP900 Thermo System microscope hot stage in an Olympus binocular microscope at the stated magnification under normal or crossed-polarizer illumination. Thin-film small-angle X-ray diffraction (XRD) was performed on a Rigaku rotating anode high brilliance (RU-200BH) X-ray diffractometer in the angular range from 2°-30° (2θ) in the laboratories of Prof. Kannan Krishnan (Department of Materials Science and Engineering, University of Washington). The unsuccessful single-crystal XRD was performed in the XRD facilities in the Department of Chemistry (University of Washington, and in the Medicinal Chemistry Department (University of Washington), in collaboration with Jason Benedict (Prof. Bart Kahr, Department of Chemistry). The successful single-crystal XRD was performed at LS-CAT at Sector 21 of the Advanced Photon Source at Argonne National Laboratory in collaboration with Dr. Zdzislaw Wawrzak.

Atomic force microscopy was performed on a Digital Multimode AFM in the Nanotechnology User Facility (Center for Nanotechnology, University of Washington). The shear-modulated scanning force microscopy experiments were performed on a custom built AFM apparatus,[38] in collaboration with Tomoko Gray (Prof. René Overney, Department of Chemical Engineering, University of Washington). Refractive index measurements were performed on a Model 2010 Prism Coupler from Metricon Corporation. Poling and macroscopic EO characterization was performed on a custom-built *in situ* pole and probe simple reflection apparatus at a measurement wavelength of 1.3 μm.[41,42] Hyper-Rayleigh scattering was performed in dilute chloroform solutions on a custom-built femtosecond pulsed laser system with a cryogenically cooled CCD detector at a measurement wavelength of 1907 nm in collaboration with Dr. Kim Firestone (Dalton Group, Department of Chemistry, University of Washington).[26]

2-[3-Cyano-4-(2-{5-[2-(4-diethylaminophenyl)vinyl]-[bi(ProDOT(CH_2OH)$_2$)-yl]}-vinyl)-5,5-dimethyl-5H-furan-2-ylidene]-malononitrile (tetra-ol, 4.13). In an oven-dried flask, **OLD-5** (0.891 g, 0.672 mmol) was dissolved in 60 mL of dry THF and cooled to 0 °C in an ice-water bath. Tetrabutylammonium fluoride (TBAF, 5.375 mL, 1 M in THF) was slowly added to the solution. The ice bath was then removed and the reaction was allowed to stir for 2.5 hours while monitoring by TLC. If necessary, an additional 2.688 mL TBAF was added, and the reaction allowed to stir for an additional 1 hour to ensure complete reaction. The reaction was then quenched with 50 mL of deionized water, concentrated under reduced pressured, and the product was isolated via filtration. The crude material was purified via filtration from hot methanol to yield

relatively pure product (0.501 g, 85.8%), which was used without further purification. ^{1}H NMR (acetone-d_6): δ 8.08(d, J = 15.7 Hz, 1H), 7.41(d, 8.9 Hz, 2H), 7.05(d, 16.2 Hz, 1H), 6.91(d, 16.4 Hz, 1H), 6.75(d, 15.9 Hz, 1H), 6.70(d, 8.9 Hz, 2H), 4.36-4.02(m, 8H), 3.79(m, 8H), 3.38(m, 4H), 1.82(s, 6H), 1.60(m, 4H), 1.40(m, 4H), 0.96(t, 6H).

General procedure for synthesis of the discotic chromophores. An oven-dried flask was charged with dicyclohexylcarbodiimide (DCC, 0.185 g, 0.898 mmol) and the appropriate dendron carboxylic acid (0.690 mmol), which were mechanically mixed and dried under reduced pressure. These were then dissolved in 5 mL dry dichloromethane under argon and allowed to react for 15 min. Dimethylaminopyridine (DMAP, 0.013 g, 0.104 mmol) was then added and the mixture allowed to react for an additional 10 min. To this was added dropwise a solution of the tetra-ol (**4.13**, 0.100 g, 0.115 mmol) in 2 mL dichloromethane and 0.25 mL DMF. The reactants were stirred at room temperature for 72 hours. The reaction mixture was then diluted with 50 mL dichloromethane and extracted 2 x 50 mL deionized water. The organic fraction was dried over Na_2SO_4 and the solvent was removed under reduced pressure. This crude material was initially purified by filtration from hot methanol, and then further purified via column chromatography.

SJLD-1. 50.0 mg (0.0575 mmol) **4.13**, 175 mg (0.345 mmol) **4.16**, 94.0 mg (0.456 mmol) DCC, 9.0 mg (0.074 mmol) DMAP. Column chromatography in 98:2 dichloromethane : acetone afforded 98.0 mg (60.5%) pure product. ^{1}H NMR ($CDCl_3$): δ 7.77(d, 15.6 Hz, 1H), 7.32(d, 8.8 Hz, 2H), 7.24(s, 8H), 6.96(d, 16.0 Hz, 1H), 6.86(d, 15.9 Hz, 1H), 6.58(d, 8.2 Hz, 2H), 6.46(d, 15.8 Hz, 1H), 4.72-4.41(m, 16H), 3.89(m,

24H), 3.29(m, 4H), 1.76-1.33(m, 122H), 0.92(m, 78H). MALDI MS 2823.79 (M^+). Elem. Anal.: Calc.: C 72.30, H 9.28 %, N 1.98 %. Found: C 74.14, H 9.83 % N 1.69 %.

SJLD-2. 100 mg (0.115 mmol) **4.13**, 224 mg (0.695 mmol) **4.19**, 188 mg (0.913 mmol) DCC, 20.0 mg (0.160 mmol) DMAP. Column chromatography in 99:1 dichloromethane : acetone afforded 205 mg (85.4%) pure product. ^{1}H NMR ($CDCl_3$): δ 7.75(d, 15.3 Hz, 1H), 7.35(d, 8.9 Hz, 2H), 7.12(m, 8H), 6.98(d, 16.1 Hz, 1H), 6.87(d, 16.2 Hz, 1H), 6.65(m, 4H), 6.58(d, 9.0 Hz, 2H), 6.47(d, 15.6 Hz, 1H), 4.65-4.40(m, 16H), 3.95(t, 5.9 Hz, 16H), 3.29(t, 7.1 Hz, 4H), 1.75-1.32(m, 78H), 0.98-0.90(m, 30H). MALDI MS 2085.96 (M^+). Elem. Anal.: Calc.: C 70.22, H 7.92 %, N 2.68 %. Found: C 70.22, H 7.86 % N 2.79 %.

SJLD-3. 40.0 mg (0.0460 mmol) **4.13**, 110 mg (0.288 mmol) **4.22**, 95.0 mg (0.461 mmol) DCC, 9.0 mg (0.074 mmol) DMAP. Column chromatography in 93:7 dichloromethane : acetone afforded 60.1 mg (56.1%) pure product. ^{1}H NMR ($CDCl_3$): δ 7.80-7.65(m, 9H), 7.35(d, 9.1 Hz, 2H), 7.26-7.21(m, 4H), 6.98(d, 16.2 Hz, 1H), 6.87(d, 16.3 Hz, 1H), 6.59(d, 8.4 Hz, 2H), 6.51(d, 15.7 Hz, 1H), 4.67-4.38(m, 16H), 3.71(s, 24H), 3.29(t, 7.1 Hz, 4H), 2.88(m, 16H), 2.73(m, 16H), 1.75(s, 6H), 1.56(m, 4H), 1.40-1.25(m, 4H), 0.96(t, 7.2 Hz, 6H). MALDI MS 2325.35 (M^+). Elem. Anal.: Calc.: C 58.86, H 5.03 %, N 2.41 %. Found: C 58.72, H 4.70 % N 2.41 %.

SJLD-4. 100 mg (0.115 mmol) **4.13**, 238 mg (0.712 mmol) **4.23**, 434 mg (2.10 mmol) DCC, 35.0 mg (0.280 mmol) DMAP. Column chromatography in 98:2 dichloromethane : acetone afforded 221 mg (90.0%) pure product. ^{1}H NMR ($CDCl_3$): δ 7.71(d, 15.7 Hz, 1H), 7.43-7.28(m, 42H), 7.24(t, 2.2 Hz, 8H), 6.97(d, 16.1 Hz, 1H),

6.89-6.79(m, 5H), 6.56(d, 8.9 Hz, 2H), 6.43(d, 15.7 Hz, 1H), 5.03(s, 16H), 4.62-4.29(m, 16H), 3.28(t, 7.1 Hz, 4H), 1.67(s, 6H), 1.55(m, 4H), 1.40-1.25(m, 4H), 0.96(t, 7.2 Hz, 6H). MALDI MS 2133.70 (M^+). Elem. Anal.: Calc.: C 73.15, H 5.48 %, N 2.62 %. Found: C 72.87, H 4.94 % N 2.04 %.

SJLD-5. 100 mg (0.115 mmol) **4.13**, 385 mg (0.696 mmol) **4.25**, 188 mg (0.913 mmol) DCC, 25.0 mg (0.200 mmol) DMAP. Column chromatography in 99:1 dichloromethane : acetone afforded 280 mg (85.4%) pure product. ^{1}H NMR ($CDCl_3$): δ 7.69(d, 15.7 Hz, 1H), 7.31(t, 2.5 Hz, 8H), 7.19(d, 9.3 Hz, 2H), 6.87(d, 16.1 Hz, 1H), 6.80-6.71(m, 5H), 6.54-6.48(m, 3H), 5.13(s, 16H), 4.65-4.45(m, 16H), 3.29(t, 8.5 Hz, 4H), 1.76(s, 6H), 1.61(m, 4H), 1.38-1.31(m, 4H), 0.97(t, 7.3 Hz, 6H). MALDI MS 2853.19 (M^+). Elem. Anal.: Calc.: C 54.71, H 2.68 %, N 1.96 %. Found: C 54.52, H 2.10 % N 1.39 %.

Methyl 3,5-Bis-hexyloxy-benzoate (4.18). A mixture of methyl 3,5-dihydroxybenzoate (**4.17**, 2.500 g, 14.87 mmol), 1-bromohexane (20.8 mL, 149 mmol), K_2CO_3 (20.5 g, 149 mmol), and 5 drops of Aliquat 336 phase-transfer catalyst were brought to reflux with vigorous stirring. The reactants were stirred at reflux for 24 hours. The cooled solution was then filtered and washed 2 x 50 mL deionized water. The organic layer was dried with Na_2SO_4 and the solvent was removed under reduced pressure. The resulting crude product was purified by silica column chromatography using 9:1 hexanes : ethyl acetate to afford 3.797 g (75.9%) of pure product. ^{1}H NMR ($CDCl_3$): δ 7.15 ppm(d, 2.3 Hz, 2H), 6.63(t, 2.3 Hz, 1H), 3.96(t, 6.5 Hz, 4H), 3.87(s, 3H), 1.74(m, 4H), 1.45-1.30(m, 12H), 0.90(t, 7.1 Hz, 6H). ^{13}C NMR ($CDCl_3$): δ 166.91 ppm, 160.11, 131.76, 107.56, 106.51, 68.25, 52.08, 31.51, 29.11, 25.65, 22.55,

13.97. ES+ HR-MS 337.2378 (M+H). Elem. Anal.: Calc.: C 71.39, H 9.59 %. Found: C 71.73, H 9.81 %

3,5-Bis-hexyloxy-benzoic acid (4.19). The methyl ester (**4.18**, 2.499 g, 7.427 mmol) and sodium hydroxide (2.395 g, 59.86 mmol) were dissolved in a mixture of 45 mL methanol, 15 mL THF, and 15 mL deionized water with stirring. Three drops of Aliquat 336 phase-transfer catalyst were added the mixture was heated to 60 °C for 18 hours. The cooled solution was concentrated under reduced pressure, neutralized with 6 M hydrochloric acid (~ 6 mL), and extracted 3 x 25 mL ethyl acetate. The combined organic extracts were dried over Na2SO4 and the solvent was removed under reduced pressure. The resulting crude product was purified by column chromatography using 8:2 hexanes : ethyl acetate to afford 2.246 g (93.8 %) of pure product. ^{1}H NMR (Acetone-d_6): δ 7.16 ppm(d, 1.8 Hz, 2H), 6.70(s, 1H), 4.01(t, 6.4 Hz, 4H), 1.77(m, 4H), 1.55-1.25(m, 12H), 0.90(t, 6.5 Hz, 6H). ^{13}C NMR (Acetone-d_6): δ 207.21 ppm, 162.21, 134.24, 109.53, 107.66, 69.85, 33.30, 30.90, 27.41, 24.27, 15.31. ES+ HR-MS 345.2042 (M+Na). Elem. Anal.: Calc.: C 70.77, H 9.38 %. Found: C 70.74, H 9.25 N 0.10 %

3,5-Bis-(methyl succinate)-benzoic acid 2,2,2-trichloro-ethyl ester (4.21). An oven-dried flask was charged with DCC (8.030 g, 38.92 mmol) and mono-methyl succinate (3.962 g, 29.99 mmol), which were mechanically mixed and dried under reduced pressure. These were then dissolved in 100 mL dry dichloromethane under argon and allowed to react for 15 min. DMAP (0.552 g, 4.518 mmol) was then added and the mixture allowed to react for an additional 10 min. To this was added dropwise 10 mL of a 1 M solution of 3,5-dihydroxy-benzoic acid 2,2,2-trichloroethyl ester (**4.20**) in

dichloromethane. The reactants were stirred at room temperature for 72 hours. The reaction mixture was filtered through a glass frit, washing with excess deionized water and dichloromethane, and then extracted 2 x 50 mL dichloromethane. The combined organic extracts were dried over Na_2SO_4 and the solvent was removed under reduced pressure. The crude material was purified via column chromatography in 6:4 ethyl acetate : hexanes, after loading the material in 7:3 ethyl acetate : hexanes, to afford 4.617 g (89.9%) pure product. ^{1}H NMR ($CDCl_3$): δ 7.72 ppm(d, 2.2 Hz, 2H), 7.22(t, 2.2 Hz, 1H), 4.95(2, 2H), 3.71(s, 6H), 2.89(m, 4H), 2.74(m, 4H). ^{13}C NMR ($CDCl_3$): δ 172.26 ppm, 170.22, 163.15, 150.97, 130.69, 121.05, 120.58, 94.64, 74.59, 51.97, 29.17, 28.70. ES+ HR-MS 534.9960 (M+Na). Elem. Anal.: Calc.: C 44.42, H 3.73 %. Found: C 44.56, H 3.59 %

3,5-Bis-(methyl succinate)-benzoic acid (4.22). The 2,2,2-trichloroethyl ester (**4.21**, 1.347 g, 2.622 mmol) was dissolved in a mixture of 5 mL THF and 5 mL glacial acetic acid, to which zinc dust (1.198 g, 18.32 mmol) was added with stirring. The reaction was monitored by TLC, which indicated complete reaction after 3 hours. The mixture was then filtered, washing with ethyl acetate and deionized water, and brought to pH ~ 8 with sodium bicarbonate. This was extracted 3 x 50 mL ethyl acetate, and the water layer was then acidified to pH ~ 6 with 6 M hydrochloric acid. The acidic solution was then extracted 3 x 75 mL ethyl acetate, and these organic extracts were dried over Na_2SO_4 and the solvent removed under reduced pressure. The crude material was purified via column chromatography in 6:4 ethyl acetate : hexanes, after loading the material in pure ethyl acetate, to afford 0.789 g (79.1 %) of pure product. ^{1}H NMR (Acetone-d_6): δ 7.68 ppm(d, 2.2 Hz, 2H), 7.22(t, 2.2 Hz, 1H), 3.67(s, 6H), 2.96(m, 4H),

2.75(m, 4H). ES+ HR-MS 405.0798 (M+Na). Elem. Anal.: Calc.: C 53.41, H 4.75 %. Found: C 53.28, H 4.70 %

Notes to Chapter 4

(1) Dalton, L. R.; Harper, A. W.; Robinson, B. H. The role of london forces in defining noncentrosymmetric order of high dipole moment-high hyperpolarizability chromophores in electrically poled polymeric thin films. *Proc. Natl. Acad. Sci. U. S. A.* **1997**, *94*, 4842-4847.

(2) Robinson, B. H.; Dalton, L. R. Monte carlo statistical mechanical simulations of the competition of intermolecular electrostatic and poling-field interactions in defining macroscopic electro-optic activity for organic chromophore/polymer materials. *J. Phys. Chem. A* **2000**, *104*, 4785-4795.

(3) Robinson, B. H.; Dalton, L. R.; Harper, A. W.; Ren, A.; Wang, F.; Zhang, C.; Todorova, G.; Lee, M.; Aniszfeld, R.; Garner, S.; Chen, A.; Steier, W. H.; Houbrecht, S.; Persoons, A.; Ledoux, I.; Zyss, J.; Jen, A. K. Y. The molecular and supramolecular engineering of polymeric electro-optic materials. *Chem. Phys.* **1999**, *245*, 35-50.

(4) Shi, Y.; Zhang, C.; Zhang, H.; Bechtel, J. H.; Dalton, L. R.; Robinson, B. H.; Steier, W. H. Low (sub-1-volt) halfwave voltage polymeric electro-optic modulators achieved by controlling chromophore shape. *Science* **2000**, *288*, 119-122.

(5) Nielsen, R. D.; Rommel, H. L.; Robinson, B. H. Simulation of the loading parameter in organic nonlinear optical materials. *J. Phys. Chem. B* **2004**, *108*, 8659-8667.

(6) Nielsen, R., Harrison, H., Robinson, B. personal communication

(7) Chandrasekhar, S.; Sadashiva, B. K.; Suresh, K. A. Liquid crystals of disc-like molecules. *Pramana* **1977**, *9*, 471-480.

(8) Kouwer, P. H. J.; Jager, W. F.; Mijs, W. J.; Picken, S. J. Specific interactions in discotic liquid crystals. *J. Mater. Chem.* **2003**, *13*, 458-469.

(9) Bushby, R. J.; Lozman, O. R. Discotic liquid crystals 25 years on. *Curr. Opin. Colloid Interface Sci.* **2002**, *7*, 343-354.

(10) Ma, H.; Jen, A. K. Y.; Dalton, L. R. Polymer-based optical waveguides: Materials, processing, and devices. *Adv. Mater.* **2002**, *14*, 1339-1365.

(11) Zhang, C.; Dalton, L. R.; Oh, M.-C.; Zhang, H.; Steier, W. H. Low vp electrooptic modulators from cld-1: Chromophore design and synthesis, material processing, and characterization. *Chem. Mater.* **2001**, *13*, 3043-3050.

(12) Sorai, M.; Saito, K. Alkyl chains acting as entropy reservoir in liquid crystalline materials. *Chem. Rec.* **2003**, *3*, 29-39.

(13) Clot, O.; Firestone, K. A.; Hammond, S.; Sinness, J.; Carlson, B.; Phelan, G.; Bale, D.; Lao, D. B.; Robinson, B. H.; Reid, P. J.; Dalton, L. R.; Universty of Washington, 2007.

(14) Kumar, A.; Welsh, D. M.; Morvant, M. C.; Piroux, F.; Abboud, K. A.; Reynolds, J. R. Conducting poly(3,4-alkylenedioxythiophene) derivatives as fast electrochromics with high-contrast ratios. *Chem. Mater.* **1998**, *10*, 896-902.

(15) Schwendeman, I.; Hwang, J.; Welsh, D. M.; Tanner, D. B.; Reynolds, J. R. Combined visible and infrared electrochromism using dual polymer devices. *Adv. Mater.* **2001**, *13*, 634-637.

(16) Donat-Bouillud, A.; Levesque, I.; Tao, Y.; D'Iorio, M.; Beaupre, S.; Blondin, P.; Ranger, M.; Bouchard, J.; Leclerc, M. Light-emitting diodes from fluorene-based pi-conjugated polymers. *Chem. Mater.* **2000**, *12*, 1931-1936.

(17) Welsh, D. M.; Kloeppner, L. J.; Madrigal, L.; Pinto, M. R.; Thompson, B. C.; Schanze, K. S.; Abboud, K. A.; Powell, D.; Reynolds, J. R. Regiosymmetric dibutyl-substituted poly(3,4-propylenedioxythiophene)s as highly electron-rich electroactive and luminescent polymers. *Macromolecules* **2002**, *35*, 6517-6525.

(18) Dimitrakopoulos, C. D.; Malenfant, P. R. L. Organic thin film transistors for large area electronics. *Adv. Mater.* **2002**, *14*, 99-117.

(19) Groenendaal, L.; Jonas, F.; Freitag, D.; Pielartzik, H.; Reynolds, J. R. Poly(3,4-ethylenedioxythiophene) and its derivatives: Past, present, and future. *Adv. Mater.* **2000**, *12*, 481-494.

(20) Roncali, J.; Blanchard, P.; Frere, P. 3,4-ethylenedioxythiophene (edot) as a versatile building block for advanced functional p-conjugated systems. *J. Mater. Chem.* **2005**, *15*, 1589-1610.

(21) Raimundo, J.-M.; Blanchard, P.; Frere, P.; Mercier, N.; Ledoux-Rak, I.; Hierle, R.; Roncali, J. Push-pull chromophores based on 2,2'-bi(3,4-ethylenedioxythiophene) (bedot) [pi]-conjugating spacer. *Tetrahedron Lett.* **2001**, *42*, 1507-1510.

(22) Raimundo, J. M.; Blanchard, P.; Gallego-Planas, N.; Mercier, N.; Ledoux-Rak, I.; Hierle, R.; Roncali, J. Design and synthesis of push-pull chromophores for second-order nonlinear optics derived from rigidified thiophene-based pi-conjugating spacers. *J. Org. Chem.* **2002**, *67*, 205-218.

(23) Delgado, M. C. R.; Hernåndez, V.; Casado, J.; Navarrete, J.; Raimundo, J.-M.; Blanchard, P.; Roncali, J. Vibrational and quantum-chemical study of push-pull

chromophores for second-order nonlinear optics from rigidified thiophene-based pi-conjugating spacers. *Chem. Eur. J.* **2003**, *9*, 3670-3682.

(24) Van Bolhuis, F.; Wynberg, H.; Havinga, E. E.; Meijer, E. W.; Staring, E. G. J. The x-ray structure and mndo calculations of [alpha]-terthienyl: A model for polythiophenes. *Synth. Met.* **1989**, *30*, 381-389.

(25) Krishnamoorthy, K.; Ambade, A. V.; Kanungo, M.; Contractor, A. Q.; Kumar, A. Rational design of an electrochromic polymer with high contrast in the visible region: Dibenzyl substituted poly(3,4-propylenedioxythiophene). *J. Mater. Chem.* **2001**, *11*, 2909-2911.

(26) Firestone, K. A., University, 2005.

(27) Teng, C. C.; Man, H. T. Simple reflection technique for measuring the electro-optic coefficient of poled polymers. *Appl. Phys. Lett.* **1990**, *56*, 1734-1736.

(28) Sinness, J., University of Washington, 2006.

(29) Sinness, J.; Clot, O.; Hammond, S. R.; Bhatambrekar, N.; Rommel, H. L.; Robinson, B.; Jen, A. K. Y.; Dalton, L. Synthesis of dendridic nlo chromophores for the improvement of order in electro-optics. *Mater. Res. Soc. Symp. Proc.* **2005**, *846*, 121-126.

(30) Reeves, B. D.; Grenier, C. R. G.; Argun, A. A.; Cirpan, A.; McCarley, T. D.; Reynolds, J. R. Spray coatable electrochromic dioxythiophene polymers with high coloration efficiencies. *Macromolecules* **2004**, *37*, 7559-7569.

(31) Reeves, B. D.; Thompson, B. C.; Abboud, K. A.; Smart, B. E.; Reynolds, J. R. Dual cathodically and anodically coloring electrochromic polymer based on a spiro bipropylenedioxythiophene [(poly(spirobiprodot)]. *Adv. Mater.* **2002**, *14*, 717-719.

(32) Bhatambrekar, N.; Hammond, S.; Sinness, J.; Clot, O.; Rommel, H.; Chen, A.; Robinson, B.; Jen, A. K. Y.; Dalton, L. Highly ordered pseudo-discotic chromophore systems for electro-optic materials and devices. *Mater. Res. Soc. Symp. Proc.* **2005**, *846*, 115-120.

(33) Hammond, S. R.; Sinness, J.; Clot, O.; Dalton, L. R. Characterization of a series of molecularly engineered discotic electro-optic chromophores. *Polym. Prepr. (Am. Chem. Soc., Div. Polym. Chem.)* **2006**, *47*, 985-986.

(34) Lee, J. W.; Wang, C. S.; Song, H. H.; Price, G. E. Void formation in coagulated rigid-rod polymer thin films. *Polymer* **1995**, *36*, 955-958.

(35) Rezzonico, D.; Jazbinsek, M.; Bosshard, C.; Günter, P.; Bale, D.; Liao, Y.; Dalton, L. R.; Reid, P. J. Photostability of pi-conjugated chromophores by

resonant and nonresonant light excitations for long-life polymeric telecommunication devices. *in preparation* **2007**.

(36) Demus, D.; Goodby, J.; Gray, G. W.; Spiess, H.-W.; Vill, V. *Handbook of liquid crystals*; Wiley-VCH: New York, 1998; Vol. 1.

(37) Demus, D.; Goodby, J.; Gray, G. W.; Spiess, H.-W.; Vill, V. *Handbook of liquid crystals*; Wiley-VCH: New York, 1998; Vol. 2A.

(38) Gray, T.; Overney, R. M.; Haller, M.; Luo, J.; Jen, A. K. Y. Low temperature relaxations and effects on poling efficiencies of dendronized nonlinear optical side-chain polymers. *Appl. Phys. Lett.* **2005**, *86*, 211908-211903.

(39) Soref, R. The past, present, and future of silicon photonics. *IEEE J. Sel. Top. Quantum Electron.* **2006**, *12*, 1678-1687.

(40) Demus, D.; Richter, L. *Textures of liquid crystals*; Verlag Chemie: New York, 1978.

(41) Sullivan, P. A.; Akelaitis, A. J. P.; Lee, S. K.; McGrew, G.; Lee, S. K.; Choi, D. H.; Dalton, L. R. Novel dendritic chromophores for electro-optics: Influence of binding mode and attachment flexibility on electro-optic behavior. *Chem. Mater.* **2006**, *18*, 344-351.

(42) Sullivan, P. A., University of Washington, 2006.

(43) Sandalphon; Kippelen, B.; Meerholz, K.; Peyghambarian, N. Ellipsometric measurements of poling birefringence, the pockels effect, and the kerr effect in high-performance photorefractive polymer composites. *Appl. Opt.* **1996**, *35*, 2346-2354.

(44) Clays, K.; Schildkraut, J. S. Dispersion of the complex electrooptic coefficient and electrochromic effects in poled polymer films. *J. Opt. Soc. Am. B: Opt. Phys.* **1992**, *9*, 2274-2282.

(45) Schildkraut, J. S. Determination of the electrooptic coefficient of a poled polymer film. *Appl. Opt.* **1990**, *29*, 2839-2841.

(46) Bhatambrekar, N. P.; Dalton, L.; Luo, J.; Jen, A. K. Y.; Chen, A. Third-order nonlinearity contribution to electro-optic activity in polymer materials in a constant bias field. *Appl. Phys. Lett.* **2006**, *88*, 041115/041111-041115/041113.

(47) Han, S. H.; Wu, J. W. Single-beam polarization interferometry measurement of the linear electro-optic effect in poled polymer films with a reflection configuration. *J. Opt. Soc. Am. B: Opt. Phys.* **1997**, *14*, 1131-1137.

(48) Park, D. H.; Kang, J. W.; Luo, J. D.; Kim, T. D.; Jen, A. K. Y.; Lee, C. H.; Herman, W. N. Nonlinear ellipsometric analysis of poled organic glasses having very large electro-optic coefficients. *Proc. SPIE* **2005**, *5935*, 59350O/59351-59350O/59312.

(49) Park, D. H.; Lee, C. H.; Herman, W. N. Analysis of multiple relfection effects in reflective measurements of electro-optic coefficients of poled polymers in multilayer structures. *Opt. Express* **2006**, *14*, 8866-8884.

(50) Lemaitre, N.; Attias, A. J.; Ledoux, I.; Zyss, J. New second-order nlo chromophores based on 3,3'-bipyridine: Tuning of liquid crystal and nlo properties. *Chem. Mater.* **2001**, *13*, 1420-1427.

(51) Sinyukov, A. M.; Leahy, M. R.; Hayden, L. M.; Haller, M.; Luo, J.; Jen, A. K. Y.; Dalton, L. R. Resonance enhanced thz generation in electro-optic polymers near the absorption maximum. *Appl. Phys. Lett.* **2004**, *85*, 5827-5829.

(52) Zheng, X.; McLaughlin, C. V.; Cunningham, P.; Hayden, L. M. Terahertz science and applications based on poled electro-optic polymers. *Proc. SPIE* **2007**, *6472*, 64720F.

(53) Hayden, L. M.; Sauter, G. F.; (Unisys Corporation, USA). Application: US US, 1991; pp No pp given.

(54) Kim, T.-D.; Luo, J.; Ka, J.-W.; Hau, S.; Tian, Y.; Shi, Z.; Tucker, N. M.; Jang, S.-H.; Kang, J.-W.; Jen, A. K. Y. Ultralarge and thermally stable electro-optic activities from diels-alder crosslinkable polymers containing binary chromophore systems. *Adv. Mater.* **2006**, *18*, 3038-3042.

(55) Kim, T.-D.; Kang, J.-W.; Luo, J.; Jang, S.-H.; Ka, J.-W.; Tucker, N.; Benedict, J. B.; Dalton, L. R.; Gray, T.; Overney, R. M.; Park, D. H.; Herman, W. N.; Jen, A. K. Y. Ultralarge and thermally stable electro-optic activities from supramolecular self-assembled molecular glasses. *J. Am. Chem. Soc.* **2007**, *129*, 488-489.

(56) Tan, H.; Guo, M.; Du, R.; Xie, X.; Li, J.; Zhong, Y.; Fu, Q. The effect of fluorinated side chain attached on hard segment on the phase separation and surface topography of polyurethanes. *Polymer* **2004**, *45*, 1647-1657.

(57) Eldada, L.; Shacklette, L. W. Advances in polymer integrated optics. *IEEE J. Sel. Top. Quantum Electron.* **2000**, *6*, 54-68.

(58) Furniss, B. S.; Hannaford, A. J.; G., S. P. W.; Tatchell, A. R. *Vogel's textbook of practical organic chemistry*; Addison Wesley Longman: Singapore, 1989.

Chapter 5: Molecular Engineering of Chromophore Dipole Moments

5.1 Introduction

Experimental results, equilibrium statistical mechanics calculations, and Monte Carlo statistical mechanics simulations from Dalton, Robinson, and coworkers indicates that the electric-field induced macromolecular acentric order of organic electro-optic (EO) materials depends significantly on the dipole moment (μ) of the constituent chromophores (Section 3.3.5).[1-4] Beyond the expected dipole-poling field interaction, the dipole-dipole, dipole-induced dipole, and induced dipole-induced dipole interactions, collectively known as the London forces (Section 3.3.5), also play a critical role in the overall order of the system when the dipole moments are large, such as in high β chromophores. In particular, for μ in excess of ~ 7 Debye (D),[4] the centrosymmetric London forces tend to dominate over the noncentrosymmetric dipole-poling field interaction at high loading densities (Figure 3.4), thus limiting the useable chromophore loading densities and the r_{33} values obtainable.

The μ of modern EO chromophores are significantly higher than 7 D, although their exact values are not known. The μ of most EO chromophores are not experimentally measured; rather they are calculated using density functional theory (DFT, Section 2.2.2) with questionable accuracy as the calculations often return values in excess of 20 D.[5] The μ of the benchmark chromophore, FTC, has been experimentally measured as 13 D,[6] from the dielectric constant of dilute solutions.[7]

Most state-of-the-art EO chromophores have stronger donors and acceptors and more efficient bridges than FTC (Section 2.3), and thus likely have larger dipole moments.

The μ of a dipolar EO chromophore (in both the ground and excited states) is intimately connected to its β value, as indicated by the two-level model (TLM, Section 2.2.4), Equation 2.6.[8] In general, reducing the μ of a dipolar EO chromophore will also reduce the β value. Although multiple donor and acceptor chromophores, including through-space charge transfer chromophores and octupolar chromophores, can exhibit reduced μ values without sacrificing β,[9] poling of such chromophores can be difficult to impossible, and the structure-property relationships are not as well understood as in dipole chromophores. Thus, it is not straightforward to reduce the μ of a chromophore via alteration of the charge-transfer backbone without also reducing the β value. It is, however, theoretically possible to reduce the *effective* μ of a chromophore by altering the periphery of the molecule to shield the charges.

The covalent attachment of a conventional neutral ground state (NGS) dipolar chromophore with a zwitterionic (ZI) dipolar chromophore provides an excellent opportunity to tune the effective μ of a chromophore. ZI chromophores generally exhibit very large ground-state dipole moments and modest *negative* β values (Section 2.2.5),[10-12] while modern NGS chromophores exhibit large dipole moments and large *positive* β values.[3] If covalently linked, yet retaining flexibility through careful molecular design, the ZI and NGS chromophores would likely self-assemble pairwise in a centrosymmetric nanostructured manner (Figure 5.1) due to the strong dipole-dipole interactions expected from such close association of large dipole moments. The dipole

moments would therefore theoretically add destructively, and the β components would theoretically add constructively due to the opposite sign and orientation. This could produce a nanostructured macromolecular system with an enhanced effective β and reduced effective dipole moment.

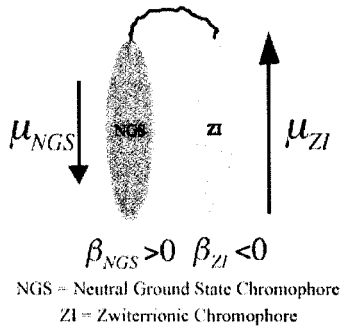

Figure 5.1. Conceptual ZI and NGS interaction

The dielectric properties of organic EO materials are becoming an increasingly important consideration. In particular, the development of binary organic glasses with extremely large r_{33} values has brought the question of dielectric effects to the forefront, as optimization of these attractive materials will require detailed understanding of these effects. Binary organic glasses have large chromophore loading densities, and thus significantly higher dielectric constants than conventional guest-host amorphous polycarbonate (APC) films. Just as the polarity of a chromophore's nanoscale environment can affect the energy of the optical absorption, as in solvatochromism (Section 2.4.1), so too can the polarity of the medium, as measured by dielectric constant, affect the nonlinear activity of the chromophore. An initial success in this area utilized the experimental dielectric constant to achieve enhanced understanding of and agreement between theoretical and experimental microscopic and macroscopic nonlinear properties in a multi-chromophore dendrimer system (Section 6.4.3).

In the case of binary chromophore glasses, however, the bulk dielectric constant and the Onsager and Lorenz field factors (Section 3.2.1) may not adequately approximate the nanoscale environment of the heterogeneous mixture of chromophores. In particular the Onsager field factor terms assume spherical molecules, uniform cavities and polarizabilities, and linear dielectrics of high symmetry.[13] Clearly these approximations will likely break down on the nanoscale in these systems. The molecular consequences of close approach of dissimilar chromophores is thus of significant interest. The NGS-ZI chromophore pairs provide an attractive opportunity to explore the consequences of such interactions through a detailed analysis of the microscopic properties of such pairs, in addition to their other attractive properties.

5.2 Previous Work

Previous work in the Dalton Research Group (Department of Chemistry, University of Washington), performed by Dr. Yi Liao, Dr. Sanchali Battacharjee and coworkers, has investigated the concept of NGS-ZI chromophore pairs.[14] They synthesized a covalently attached, NGS-ZI antiparallel aligned bichromophore (**5.1**), along with the separate NGS (**5.2**) and ZI (**5.3**) control chromophores (Figure 5.2). Through 1D and 2D (ROSEY) ^{1}H NMR techniques, they provide evidence in support of an antiparallel chromophore alignment, which was predicted by molecular dynamics calculations that also predict partial effective dipole cancellation in such a geometry. Comparison of the absorption spectra for **5.1-5.3** shows that the total extinction coefficient of the main charge-transfer bands for **5.1** is slightly less than the sum of **5.2**

and **5.3**, and that the peaks are slightly broader. This suggests some interaction between the two chromophores that prevents a purely additive contribution, although the nature of the interaction is unclear. Furthermore, the β values of **5.1-5.3** were examined by HRS (Section 2.4.3) and the results are presented in Table 5.1. For a completely uncorrelated system, $\beta_{1,HRS}/\beta_{2,HRS} = 1.01$, while for a perfectly additive correlation $\beta_{1,HRS}/\beta_{2,HRS} = 1.16$, and for a perfectly subtractive correlation $\beta_{1,HRS}/\beta_{2,HRS} = 0.84$. The experimental HRS data thus also suggests a slightly less than purely additive correlation in the bichromophore.

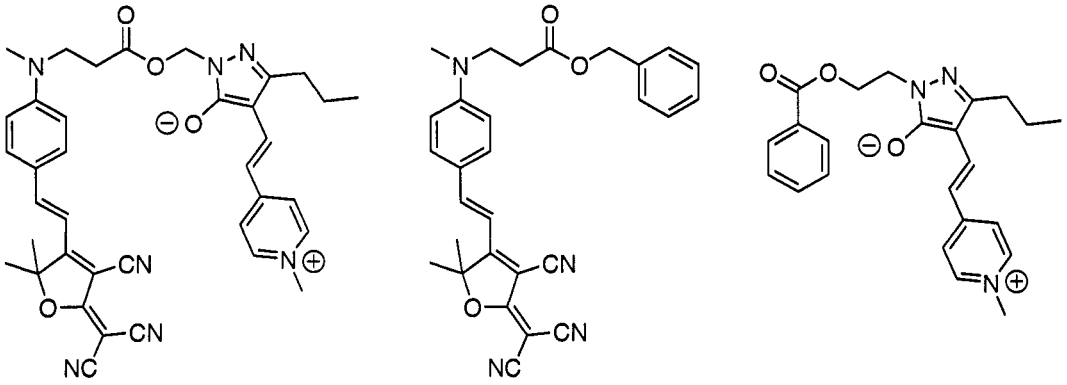

5.1 **5.2** **5.3**

Figure 5.2. Previous bichromophore (**5.1**) and NGS (**5.2**) and ZI (**5.3**) reference chromophores

Although the experimental evidence suggests a nearly additive contribution, with a slight interaction that causes deviation from linear behavior, the systems explored in this work are not ideal for these comparisons. The NGS and ZI chromophores have nearly the same λ_{max}, which complicates the analysis of the UV-vis spectra. If the absorptions were sufficiently separated, the effects on the two different units in the bichromophore could be analyzed separately. Additionally, the ZI chromophore has such a small β value that the HRS results for **5.1** and **5.2** are nearly within experimental error of each other. While they are sufficiently different to allow

confidence that the general trend is accurate, it does not allow any analysis of the fine details of the interactions between the chromophore units. Thus, while this study proved the concept of molecular engineering of β and μ with NGS-ZI bichromophores and demonstrated the existence of a more complex intramolecular interaction, further work is necessary to refine the concept and explore the detailed intramolecular interactions.

Table 5.1 Experimental HRS[a] results for bichromophore and control chromophores

Compound	$\beta_{HRS}/\beta_{CHCl3,HRS}$	$\beta_{HRS}/\beta_{5.1,HRS}$	$\beta_{HRS}/\beta_{5.2,HRS}$	$\beta_{HRS}/\beta_{5.3,HRS}$
5.1	2273 +/- 74	1	1.113	6.951
5.2	2043 +/- 91	0.899	1	6.248
5.3	327 +/- 31	0.144	0.160	1

[a]All data taken at 880 nm excitation wavelength[14]

5.3 Target Structures

Mindful of the successes and limitations of the previous work on bichromophores, we set out to synthesis the NGS-ZI bichromophore **5.4**, based on an analog of the well-characterized benchmark chromophore FTC (Section 2.3.3), and the reference NGS (**5.5**) and merocyanine ZI (**5.6**) chromophores (Figure 5.3). While the optical and nonlinear optical properties of **5.5** and **5.6** will need to be measured for careful comparison to those of **5.4**, the literature properties of related compounds can give guidance in the expected behaviors.

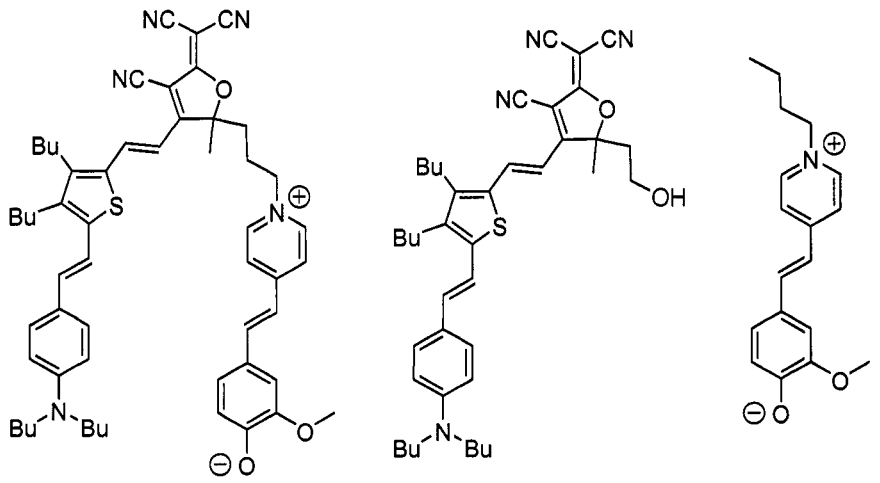

5.4 **5.5** **5.6**

Figure 5.3. Target bichromophore (**5.4**) and NGS (**5.5**) and ZI (**5.6**) reference chromophores

FTC (Section 2.3.3) is one of the most well-characterized organic EO NGS chromophores to date,[2,15] and serves as a fundamental benchmark chromophore. The exact optical and nonlinear optical (NLO) properties of the chromophore depend not only on the charge-transfer backbone, but also on the peripheral functionalization of the molecule (Figure 5.4).[2,15,16] The wavelength of the maximum charge-transfer absorption (λ_{max}) of dilute chloroform solutions of FTC derivatives ranges from 630-700 nm. There is also considerable variation in the β_{HRS} values, although this is likely due in part to variations in instrumental conditions, including excitation wavelength (due to dispersion), and the value of $\beta_{CHCl3,HRS}$ chosen (e.g. 0.16 x 10^{-30} esu or -0.49 x 10^{-30} esu)[16] to convert from relative units to esu. Minimizing these factors by comparing just the relative values for EZ-FTC and NBLP from Dr. Kim Firestone's Ph.D. Dissertation,[16] gives $\beta_{HRS}/\beta_{CHCl3,HRS}$ values of 9834 +/- 637 and 10769 +/- 663, respectively, both at 880 nm excitation. Extinction coefficients for FTC derivatives, at the λ_{max}, range from around 61000-65000 L/mol*cm.

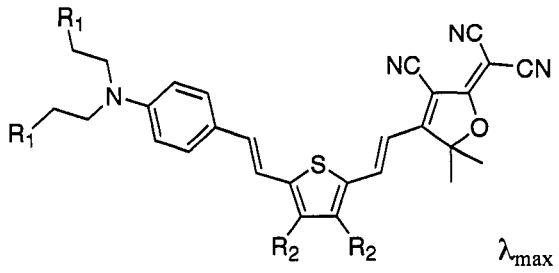

R_1 = OAc, R_2 = Butyl	FTC	650 nm
R_1 = OAc, R_2 = H	FTC-2H	630 nm
R_1,R_2 = H	EZ-FTC	676 nm
R_1 = H, R_2 = Butyl	NBLP	700 nm

Figure 5.4. Nomenclature and λ_{max} of chloroform solutions of FTC derivatives

In contrast, a close analog of **5.6** (with a longer octadecyl chain in place of the butyl group) has been shown to have a λ_{max} of 635 nm, with an extinction coefficient of 69100 L/mol*cm in dilute chloroform solutions. Although this is very close to the λ_{max} of some of the FTC derivatives, it is expected that the NGS derivative chosen will be sufficiently red-shifted to allow for reasonable spectral resolution. The merocyanine dye also exhibited no fluorescence, which is important for accurate HRS studies.[10] Interestingly, the study also explored the optical properties of the oxygen-protonated (hydroxystilbazolium salt) form, which had a λ_{max} of 411 nm and extinction coefficient of 15,500 L/mol*cm, and fluoresced at 512 nm.[10] The pK_a of the hydroxystilbazolium salt was determined to be 9.08. Although the pK_a of the ZI chromophore is likely too high for practical use, and may prove to be too high for the planned experiments, we feel it is a reasonable starting-place for these studies. Should the ZI be too easily protonated, the structure-property relationships of merocyanine acidities are well understood and should allow facile tuning of such properties,[12] which can also allow tuning of the λ_{max}. The synthetic methodology for the bichromophore (Section 5.5) will

allow coupling the NGS and ZI chromophores as a final step, allowing relatively rapid changes to the NGS-ZI bichromophore structure.

The optical and NLO properties of related merocyanine ZI chromophores, including one with a N-methyl group and lacking the 3-methoxy substituent,[11] have also been explored in dilute aqueous solutions. This is a considerably more polar environment than chloroform, and so the significantly blue-shifted absorption (negative solvatochromism, characteristic of ZI chromophores; see Section 2.4.1), λ_{max} = 444 nm, is expected. Again, the more polar environment is also expected to affect the NLO properties of the chromophore, although the details of this effect are not well understood, particularly for a ZI chromophore. HRS at 1064 nm, with *p*-nitroaniline (pNA) as a reference, yields a β_{HRS} of 550 +/- 130 x 10^{-30} esu. Direct comparison of this value with the values for FTC derivatives is complicated by the different reference procedure (pNA vs. chloroform), different wavelength (1064 nm vs. 880 nm), and the different solvent (chloroform vs. alkaline water). If we neglect the effect of solution and wavelength, we can divide the experimental β_{HRS} value by the β_{HRS} value used for the pNA reference (34 x 10^{-30} esu), multiply by the $\beta_{HRS}/\beta_{CHCl3,HRS}$ value for pNA (79 +/- 7 x 10^{-30} esu at 1000 nm) from Dr. Firestone's dissertation,[16] and obtain a $\beta_{HRS}/\beta_{CHCl3,HRS}$ of 1280. Dividing the average $\beta_{HRS}/\beta_{CHCl3,HRS}$ of the two FTC derivatives (EZ-FTC and NBLP) above by this value, we have a relative $\beta_{NGS,HRS}/\beta_{ZI,HRS}$ of about 8.0, as compared to 6.2 in the previous bichromophore work. This suggests that the current study may suffer from the same difficulties as the previous work, with the β enhancement of the bichromophore being swamped by instrumental error. It should be noted, however that in the above merocyanine HRS

study, addition of 3,5-diemthoxy substituents gave nearly a 2-fold enhancement in the experimental β_{HRS}, which would decrease the relative β factor to about 4.0 (although it might increase the spectral overlap).

In conclusion, although the present study may suffer from some of the same difficulties as the previous study, the NGS and ZI units are considerably better studied. Thus, any changes in the properties of the bichromophore should be easier to interpret. Additionally, the structure-property relationships of the merocyanine ZI dyes are well understood, and any changes to the structure to improve the spectral resolution, acid-base properties, or the relative β values should be straightforward. Finally, the synthetic methodology (Section 5.5) will allow coupling of the NGS and ZI units as the final step, limiting the extra synthetic effort required to change ZI groups in the bichromophore to the relatively simple synthesis of the ZI backbone.

5.4 Theoretical Treatment

The properties of bichromophore **5.4** and the NGS and ZI reference chromophores, **5.5** and **5.6** respectively, have been explored using densitry functional theory (DFT, Section 2.2.2) calculations with the generalized gradient approximation (GGA) performed by Dr. Bruce Eichinger (Department of Chemistry, University of Washington). Geometries were optimized with DMol using PBE/dnp with *medium* convergence. The lowest-energy optimized geometry conformation of **5.4** (sans butyl chains on the FTC NGS chromophore unit) shows both chromophore backbones as planar and the molecular charge-transfer axes highly aligned in the desired

nanostructured orientation (Figure 5.5), which supports the dipole-pairing argument. It must be considered, however, that these calculations were performed in a gas phase environment, where Van der Waals forces would likely also lead to an aligned or overlapped geometry. Additionally, conformations with only a few kcal/mol higher energies exist with significantly twisted geometries, approximating more of a V-type geometry.

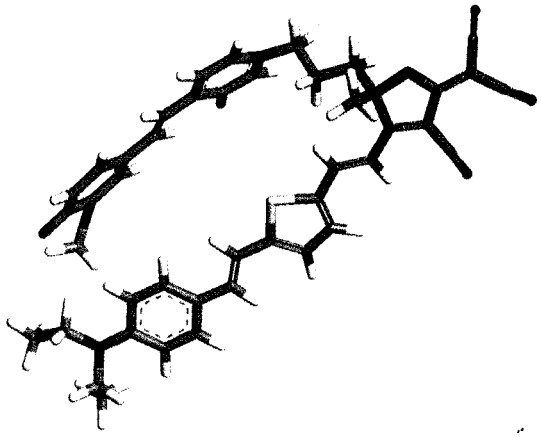

Figure 5.5. DFT optimized geometry of bichromophore **5.4**

Electrostatic moments were calculated with Gaussian03 using B3LYP/3-21g* and default parameters. The calculated dipole moments (μ), hyperpolarizabilities (β_{zzz} and β_{HRS}), and absorption maxima (λ_{max}) for bichromophore **5.4**, EZ-FTC, and the ZI reference chromophore **5.6** are presented in Table 5.2. The first thing to note is that EZ-FTC has a much higher calculated dipole than the measured value (23.4 D vs. 13 D for FTC),[17] and that **5.6** has a much lower calculated dipole than EZ-FTC (14.8 D vs. 23.4 D). The latter is likely due to the relatively non-polar environment in these calculations (essentially gas-phase), and is expected to be reversed in polar environments. The former demonstrates the questionable absolute accuracy of quantum mechanical calculations, which are generally excellent in reproducing trends, however, for complex

systems such as these. The calculated dipole moment for **5.4** is 12.9 D (in the direction of FTC's dipole), which is significantly larger than a simple vector sum of the two component dipoles (8.6 D). This suggests that the polar ZI chromophore unit enhances the μ of the NGS unit more than the NGS unit enhances the μ of the ZI unit, although again the gas-phase nature of these calculations makes it difficult to extrapolate such properties to actual experimental conditions.

Table 5.2. Calculated bichromophore and reference chromophore properties

Compound	μ (D)	β_{zzz} (10^{-30} esu)	β_{HRS} (10^{-30} esu)	λ_{max} (nm)
5.4	12.9	273	148	857
EZ-FTC	23.4	374	170	604
5.6	14.8	-15.6	6.4	546

The calculated hyperpolarizabilities (β_{zzz} and β_{HRS}) for **5.4**, EZ-FTC, and **5.6** (Table 5.2) do not show the results expected from the previous NGS-ZI bichromophore work. In fact, the β_{zzz} and β_{HRS} for **5.4** is significantly less even than a completely subtractive interaction (358 x 10^{-30} esu and 164 x 10^{-30} esu, respectively) between the NGS and ZI units. Also, it is interesting to note that the calculated $\beta_{NGS,zzz}/\beta_{ZI,zzz}$ is 24 and $\beta_{NGS,HRS}/\beta_{ZI,HRS}$ is 26, both of which are much larger than the 4-8 factor estimated from experimental HRS results above. The reason for the significantly reduced calculated β_{zzz} of **5.4** can be seen from the calculated molecular orbitals (Figure 5.6). The energies for the orbitals (which should not be considered accurate in an absolute sense) line up in such a way that the highest occupied molecular orbital (HOMO) resides almost entirely on the ZI chromophore unit, and the lowest unoccupied molecular orbital (LUMO) resides almost entirely on the NGS chromophore unit. This means that the orbital overlap, which is related to the transition dipole moment (μ_{eg}), is

extremely small. In terms of the two-level model (TLM, Equation 2.6, Section 2.2.4), this means the β should be significantly reduced. The small energy of this HOMO-LUMO transition gives rise to a long-wavelength transition, calculated to be 857 nm (in the pseudo gas-phase environment), although the intensity of this transition should be small because the oscillator strength/extinction coefficient is also related to μ_{eg}. Thus, the calculations suggest the UV-vis spectrum should look nearly like the sum of the NGS and ZI spectrum, with the addition of a weak transition in the long-wavelength region.

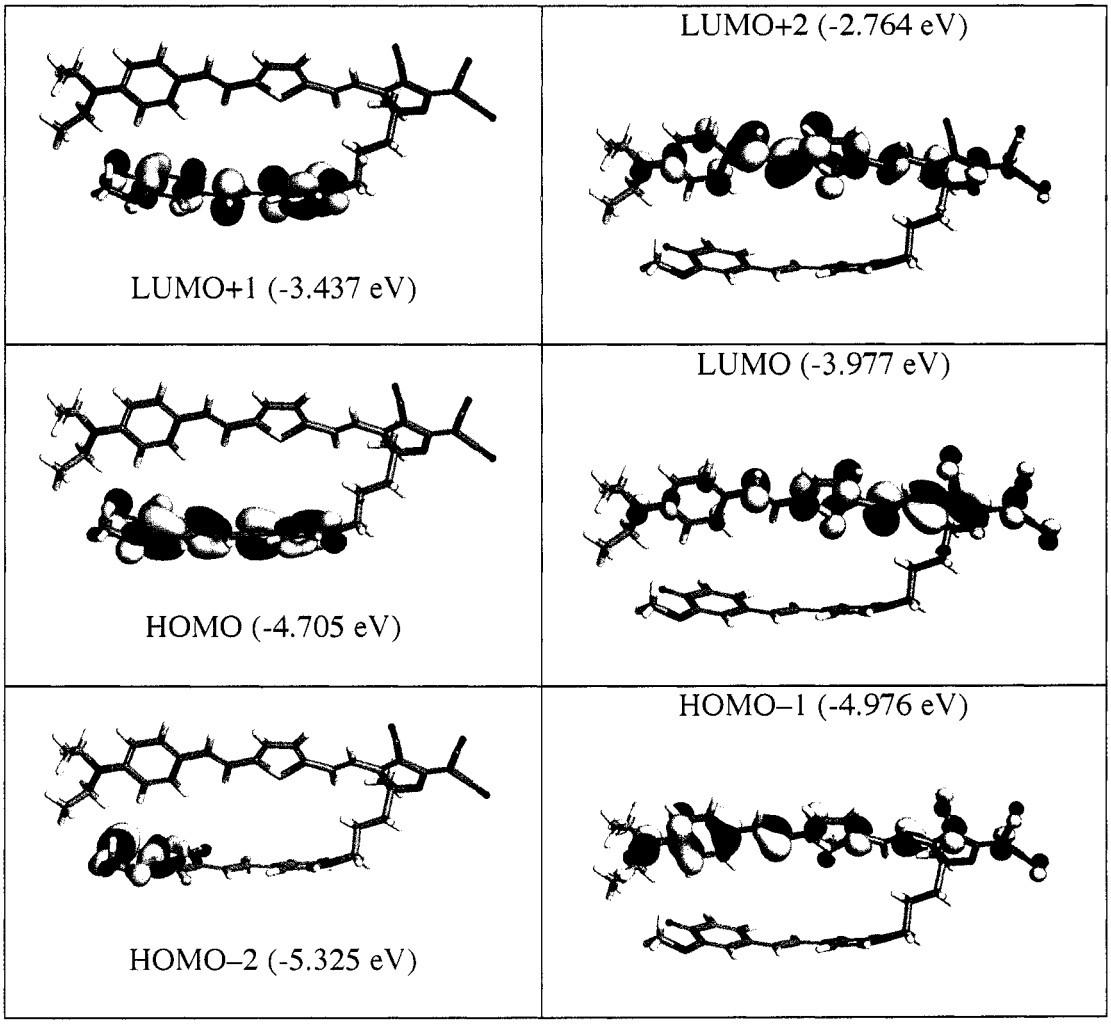

Figure 5.6. Calculated molecular orbitals of bichromophore **5.4**

This picture can only be considered accurate if there is a strong interaction between the two chromophore units, such that they behave as a single entity. For this to be the case, the chromophores would likely need to be in very close contact, such as around 3.5 Å, which corresponds to strong π-π stacking interaction. In contrast, if there is considerable separation between the two chromophore units, then they will likely act more nearly independently. Considering the HOMO-2 to HOMO transition, and the HOMO-1 to LUMO transition, the ZI and NGS charge-transfer transitions, respectively, still appear to be intact. A detailed comparison with the HOMO-LUMO transition for the NGS and ZI reference chromophores might provide additional information, but the actual properties will ultimately depend on the molecular geometry adopted in solution (and in the solid-state).

5.5 Synthesis

The synthesis of bichromophore **5.4** started with the NGS chromophore unit and reference chromophore (**5.5**). The key portion of the NGS unit is the functionalizable acceptor, a hydroxyl functionalized version of the tricyanofuran-based (TCF) acceptor (HO-TCF) derived from MOM-TCF (Figure 2.6a, Section 2.3.2), which allows attachment of the ZI and NGS units in the appropriate anti-parallel dipole moment geometry. Synthesis of this acceptor, which relied mostly on the literature method developed by Dr. Sen Liu (Prof. Alex Jen, Department of Materials Science and Engineering, University of Washington),[18,19] is presented in Scheme 5.1. The commercially available 3-acetyl-1-propanol (**5.7**) was protected with chloromethyl

methyl ether in moderate yields. The hydroxyl-protected ketone (**5.8**) was then treated with the lithiated enol ether of ethyl vinyl ether to afford the enol ether (**5.9**), which was hydrolyzed without purification to the α-hydroxy ketone (**5.10**) in low overall yield. As the use of microwave reactors has been demonstrated to be advantageous for the synthesis of other TCF-based acceptors,[19] here the synthesis deviated from the thermally activated ring-closure method developed by Dr. Liu. An optimized procedure for the methoxymethyl (MOM) protected TCF ring closure using a Focused Microwave Reactor (Discover Model, CEM Corporation) was developed. The optimized conditions, 40 watts for 20 minutes, afforded slightly increased yields (by ~ 8 %) over the traditional thermally activated method, in around 1/100 the reaction time. Additionally, the use of concentrated hydrochloric acid diluted to 1 M in methanol afforded considerably enhanced yields (by ~ 17 %) in the deprotection of **5.11** to yield the HO-TCF acceptor (**5.12**), with respect to previous methods.

Scheme 5.1 Modified literature synthesis of MOM-TCF acceptor

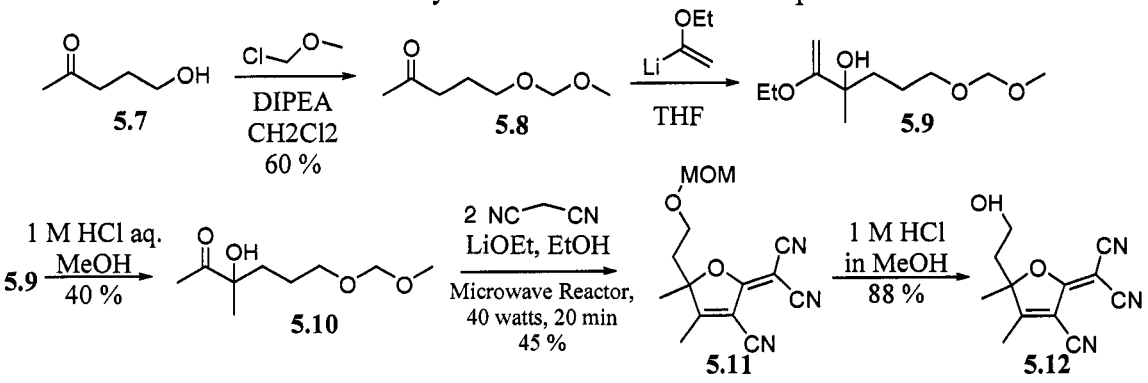

The synthesis of the NGS chromophore (Scheme 5.2) used primarily conventional NGS chromophore synthetic techniques. Diethyl N,N-dibutylaminobenzylphosphonate (**5.13**) and 3,4-dibutylthiophenecarboxaldehyde (**5.14**) were coupled under Horner-Wadsworth-Emmons conditions in relatively low yield,

likely due to steric hindrance from the butyl groups on the thiophene. The bridge (**5.15**) was then formylated using *n*-butyllithium (*n*-BuLi) and N,N-dimethylformamide (DMF) in good yield. In initial test reactions, the Knoevenagel condensation of the acceptor **5.12** and the aldehyde **5.16** afforded low yields with numerous byproducts under the two most common conditions: catalytic triethylamine (TEA) in chloroform (10 %), and catalytic ammonium acetate (NH_4OAc) in ethanol (33 %). Normally the Knoevenagel condensation of TCF acceptors with donor-bridge-aldehydes affords very high yields (> 90%) of NGS EO chromophores. It was subsequently determined that exclusion of the base catalyst allowed the condensation to proceed in high yield (79 %), affording the NGS reference chromophore (**5.5**) and the bulk of the NGS half of the bichromophore. This indicates the highly activated nature of the reactive methyl on HO-TCF, and suggests there exists an unfavorable reaction between the base catalysts and the hydroxyl moiety.

Scheme 5.2 Synthesis of NGS chromophore unit

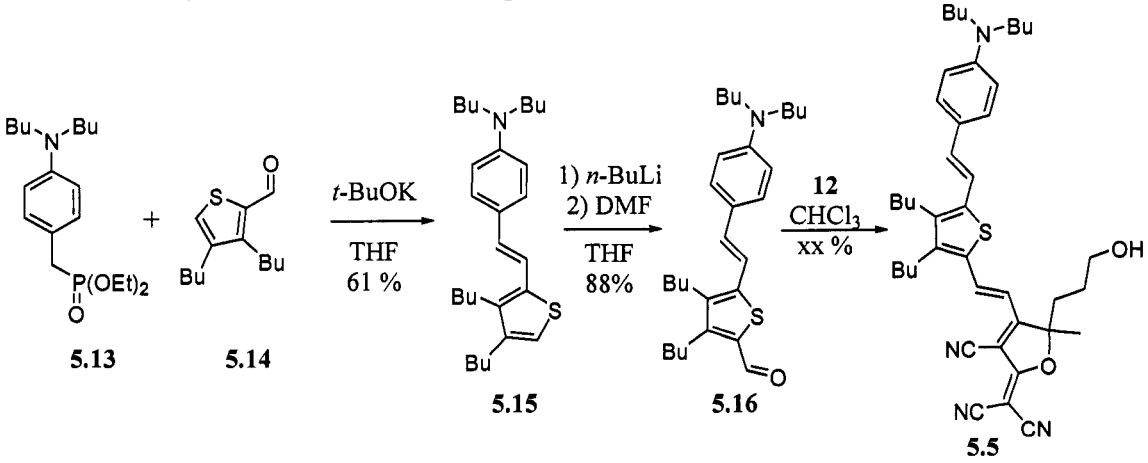

The ZI backbone (**5.26**) was synthesized in one step from 4-picoline (**5.21**) and vanillin (**5.23**) using a novel, although low-yielding (around 50 %), reaction (Scheme 5.3b). Typically ZI chromophores of this type are synthesized from a quaternized

picolinium salt (**5.17**, Scheme 5.3a), which reacts rapidly with the aldehyde (**5.18**) in a Knoevenagel condensation.[20] To enable coupling of the two chromophore elements last, however, a modified procedure was found,[21] which likely involves acetylation of the picoline (**5.21**, Scheme 5.3b). This *N*-acetylpicolinium (**5.22**) presumably then reacts in a Knoevenagel fashion, with subsequent hydrolysis of the *N*-acetyl group (**5.24**) to yield the desired product (**5.26**). It is suspected that incomplete hydrolysis of this *N*-acetylated intermediate contributed to the low yield, although all attempts to optimize the procedure based on this hypothesis failed to increase the yield. The reaction conditions also lead to undesirable partial acetylation of the phenol to yield a mixture of **5.25** and **5.26** (Scheme 5.3b), which required an additional deprotection step (1 M HCl in MeOH, H_20) to regenerate the desired product (**5.26**). Although the ZI reference chromophore (**5.6**) can be synthesized from the ZI backbone (**5.26**) with 1-bromobutane and mild base, it is considerably easier and higher yielding to use the conventional route with N-butylpicolinium iodide and vanillin. This material was provided by Dr. Jessica Sinness (Dalton Group, Department of Chemistry, University of Washington).

To allow coupling of the NGS unit to the ZI backbone, the hydroxyl group must be converted to a good leaving group. Initially, this was planned to be a simple bromide. In test reactions, however, both EZ-FTC and the TCF acceptor proved unstable to a variety of bromination conditions, including hydrobromic acid, phosphorous tribromide, and carbon tetrabromide/triphenylphosphine. Test reactions indicated EZ-FTC and TCF are both stable to tosylation conditions, however, and the toluenesulfonate moiety is an excellent leaving group.[22] Repeated reaction of NGS

chromophore **5.5** with *p*-toluenesulfonylchloride (Tosyl-Cl) and pyridine in dry methylene chloride (CH_2Cl_2) overnight afforded only the chloride (**5.27**), in low yields (Scheme 5.4). Test couplings of this chloride with the ZI backbone (**5.26**) did not produce the desired bichromophore however. Test reactions of **5.26** with 1-chlorobutane also failed to produce the ZI reference chromophore (**5.6**), suggesting that chlorine is too poor a leaving group for the coupling reaction. A procedure was found to prepare *p*-toluenesulfonylbromide (Tosyl-Br),[23] and reaction of this with **5.5** under tosylation conditions overnight afforded a mixture of the bromide (**5.28**) the tosylate (**5.29**) in poor yield. Subsequent reactions indicated that reaction for one hour affords the tosylate in good yield (Scheme 5.4), contaminated with only a very small percentage of the bromide.

Scheme 5.3. Synthesis of ZI backbone

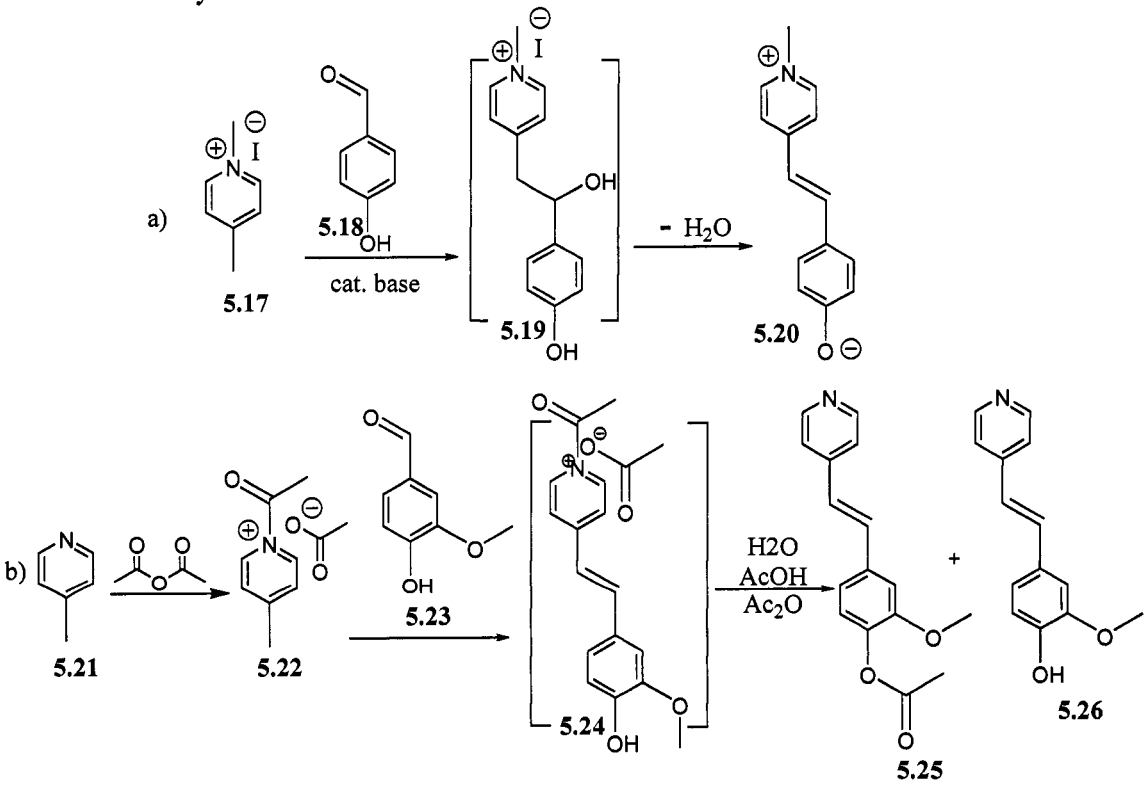

Scheme 5.4. Tosylation of NGS chromophore

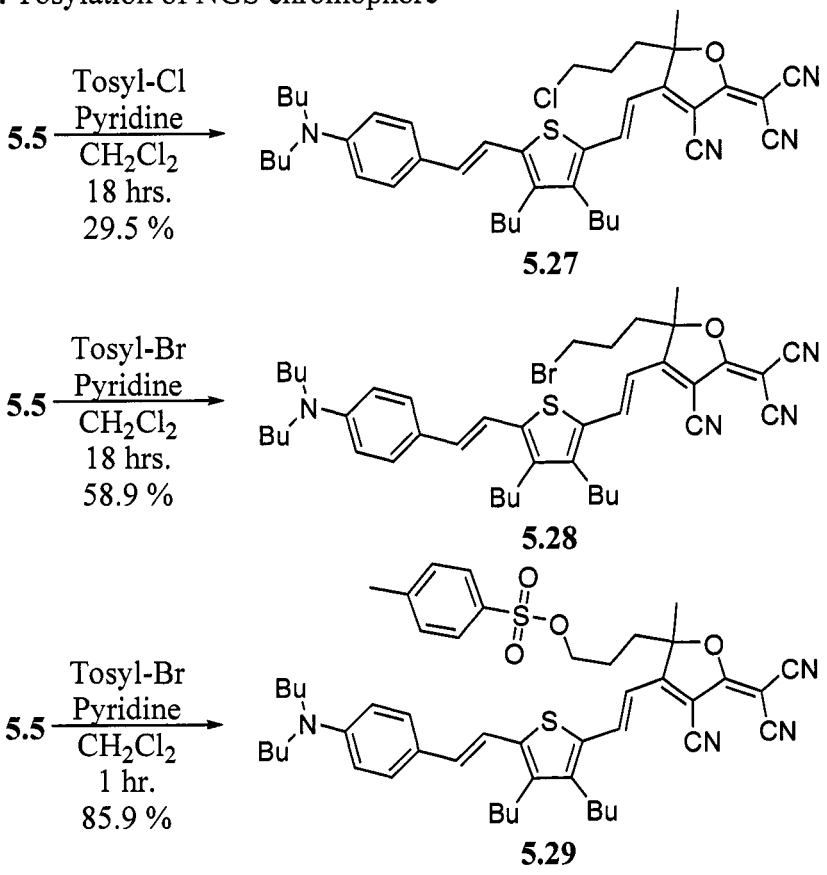

The SN_2 coupling of the tosylate (**5.29**), or bromide (**5.28**), with the ZI backbone (**5.26**) proceeds in apparently high yields to produce a green chromophoric compound (Scheme 5.5). Matrix-assisted laser desorption mass spectrometry (MALDI-MS) of the crude material confirms production of the desired product (primary peak: 888.33), either as the salt (**5.30**, M^+), or the bichromophore (**5.4**, M^++H). Most chromophores appear in MALDI-MS as the M^+ peak, however MS cannot be used to distinguish conclusively between the two forms. Unfortunately, we have been unsuccessful so far in our attempts to obtain analytically pure samples of the material, which are required for accurate EO characterization. In thin-layer chromatography (TLC) experiments on

silica, the polar material moves from the baseline only in highly polar solvent systems such as 75 %/25 % acetonitrile/ethyl acetate or 90 %/10 % methanol/ethyl acetate. Attempts to perform column chromatography in both these systems were largely unsuccessful, as the material appears to remain adsorbed to the silica gel. Attempts to use reverse phase silica TLC (silica particles coated in octadecyl hydrocarbon chains) proved unsuccessful, likely due to the nonpolar surface character imparted by the numerous butyl chains). Selective dissolution and precipitation experiments have been only partially successful. Some of the impurities have been removed by dissolving the material in a polar solvent, such as methanol, ethanol, or ethyl acetate (partially soluble), and then precipitating the material in hexanes or diethyl ether. There remains a fluorescent impurity, however, that appears to exhibit similar polarity as the desired product. Attempts to precipitate ethanol solutions of the product in water, in which it is insoluble (again likely due to the non-polar surface character), were also unsuccessful in removing the impurity.

Scheme 5.5. Synthesis of bichromophore

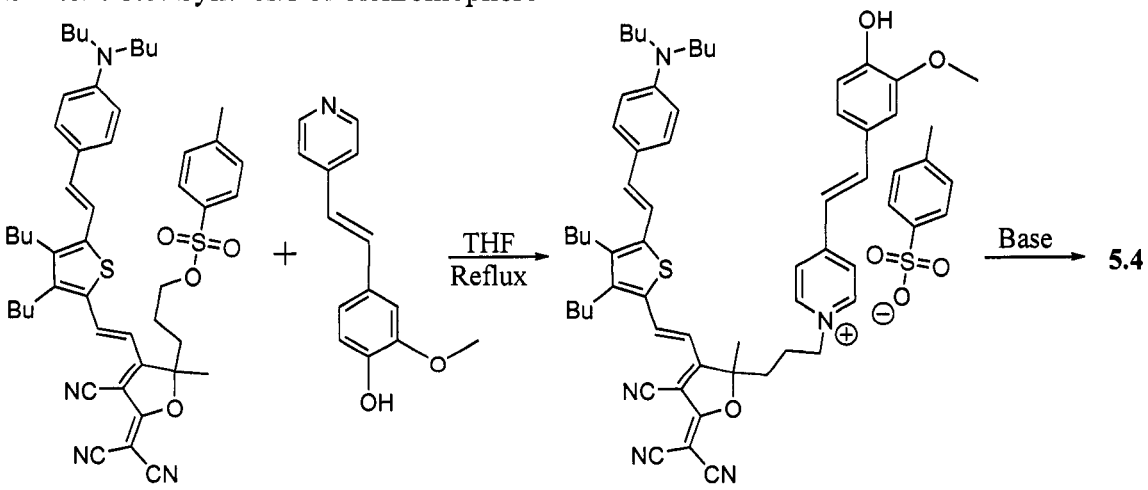

5.29 **5.26** **5.30**

A UV-vis absorption spectrum of a dilute chloroform solution of the partially-purified material is presented in Figure 5.7. The λ_{max} for the NGS chromophore is 744 nm, while the λ_{max} for the ZI chromophore is 416 nm. This suggests that the ZI chromophore is actually in the hydroxystilbazolium salt form, and thus that the material is actually the salt (**5.30**). This may partially explain the purification issues due to reduced solubility from the enhanced polarity of the salt. It is possible, however, that the material simply became protonated in the chloroform solution, which can be acidic. This warrants further study with the use of basic stabilizers (such as TEA). The λ_{max} of the NGS unit suggests it is in a highly polar environment, as expected, because the absorption has red-shifted nearly 50 nm from the expected value. The lack of a peak in the long-wavelength region (around 857 nm) is not conclusive at this time, because of the protonated form of the hydroxystilbazolium dye.

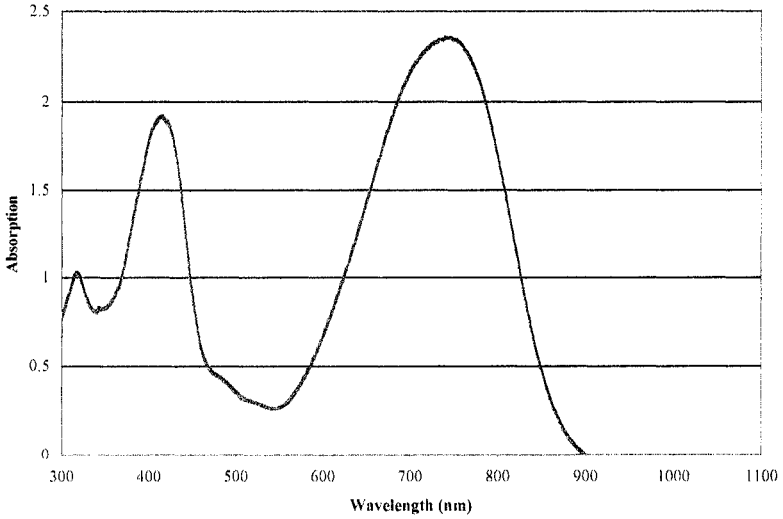

Figure 5.7. UV-vis spectrum of dilute chloroform solution of impure bichromophore **5.4**

We have also examined the UV-vis absorption spectra of dilute chloroform solutions of **5.5** and **5.6**, which are presented together in Figure 5.8. The HO-FTC reference chromophore, **5.5**, exhibits a relatively broad peak with a λ_{max} of 718 nm. The ZI reference chromophore, **5.6**, exhibits a peak at 416 nm, and a bimodal peak at 599 and 640 nm. We have no explanation currently for the surprising bimodal nature of the second peak. The multiple peaks indicate that **5.6** is partially in the protonated form in the chloroform solution, which suggests that basic stabilizers (such as TEA) will likely be required for accurate analysis of these systems. Although the position of the peak for the ZI form of **5.6** is relatively close to the peak for **5.5**, which results in an unfortunate amount of spectral overlap, there is more spectral separation than in the previous work. The lack of any sign of a shoulder in the main peak of the bichromophore (Figure 5.7) suggests that all of the ZI chromophore is actually in the hydroxystilbazolium salt form, as opposed to the mixture present in the solution of **5.6**. Taken together, this suggests development of a new ZI chromophore, with a lower pK_a and more spectral resolution, for use in the bichromophore and as a reference chromophore and ZI half of the bichromophore might prove beneficial in the purification and data analysis of these systems.

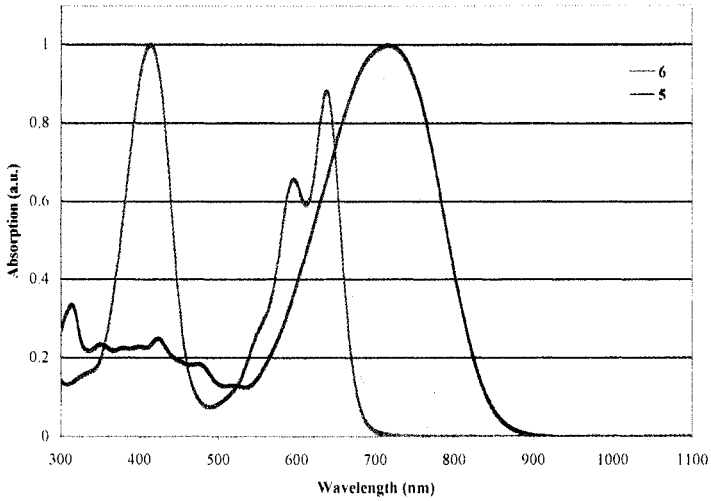

Figure 5.8. Normalized UV-vis spectra of dilute chloroform solutions of reference chromophores **5.5** and **5.6**

5.6 Future Work

Clearly purification of bichromophore **5.4** and conclusive establishment of its protonation state remains the primary work of this project. After this is complete, complete characterization of the optical and NLO properties of **5.4**, **5.5**, and **5.6** can commence. Of primary importance, UV-visible absorption spectroscopy of **5.4** will be performed to establish the presence of absence of a peak in the long-wavelength region that might indicate a ZI-HOMO to NGS-LUMO transition in this material. Investigation of the UV-vis spectra of all three compounds in a variety of solvents will allow analysis of their solvatochromic properties. This can give insight into the degree of independence of the two chromophore units by comparing the solvatochromic shifts of the reference dyes to the bichromophore. Establishment of the acid-base properties of **5.4** and **5.6** will be critical to these analyses.

The molecular geometry in solution is critical for the properties of bichromophore **5.4**. It is conceivable that the antiparallel geometry might be preferred in some solvents, but not in others. Thus, 1D (^{1}H, ^{13}C) and 2D (COSEY, NOESY, ROSEY) NMR spectroscopy will be preformed in a variety of solvents to provide insight into the structure. If **5.4** shows any tendency to form crystals, we will also attempt to grow single crystals and obtain a X-ray diffraction crystal structure, which would provide a wealth of structural information (although in the solid-state, not in solution).

Once we have established the solution-state geometry of **5.4**, we will investigate the effects of that geometry on the molecular properties. We are currently building a dipole measurement apparatus based on the liquid cell capacitance method,[7] which will allow us to conclusively demonstrate the effective reduction in μ, if any, of **5.4** relative to the reference chromophores. Additionally, if any variations in the geometry as a function of solvent are identified, this will allow us to explore the effect of those changes on μ in more detail. The hyperpolarizability (β_{HRS}) of the three chromophores will also be determined via HRS to explore whether the previously observed trend is supported, and the NGS-ZI bichromophore concept is general. Current efforts in the Dalton Group to extend HRS to multiple solvents may also allow us to explore the effect of changes in geometry of **5.4** in different solvents on the NLO properties.

Finally, while the immediate results of this project are not expected to be device-relevant materials, we will also explore the properties of bichromophore **5.4** in guest-host thin films. While it is expected that amorphous polycarbonate (APC) is too non-polar an environment for **5.4**, we will explore more polar polymer hosts. The poling

behavior of this material is likely unpredictable. The geometry may change radically with temperature or application of an electric field. To extend any benefits from the reduced μ (if any) in the bichromophore, a new bichromophore that is covalently functionalized at both ends will likely be required.

Based upon the above data we plan to obtain, conclusions may be made about the nature of the inter-chromophore interactions, especially with regard to the hypotheses initially outlined. These conclusions should provide fundamental insight into chromophore behavior as a function of environment, particularly with respect to the field factor terms in the expression for $\chi^{(2)}$ and the interactions between two dissimilar chromophores, with consequences for binary organic glasses and other systems well beyond this project. If the initial results are favorable in terms of μ reduction and β enhancement, then future iterations of NGS-ZI bichromophores could aim to produce a system that is covalently functionalized on both ends. Such a system could be applicable to solid-state systems, rather than the present system, which is likely only applicable to fundamental solution studies.

In a covalently fixed NGS-ZI bichromophore system, work could then be performed to tune the donor and acceptor groups on the two chromophores. One goal of such work would be to produce a bichromophore with a net dipole moment (in an appropriate environment) ideal for poling, around 7 D.[4] In theory, such a system should allow attainment of enhanced r_{33} values of electrically poled thin-films, with respect to the appropriate reference NGS chromophore, due to reduced intermolecular dipole-dipole interactions and the enhanced spherical shape. Additionally, there are self-assembly techniques that don't rely on poling to orient organic EO chromophores

(Section 3.2.2), including Langmuir-Blodgett films and sequentially synthesized noncentrosymmetric films.[24-27] These systems have traditionally been characterized by excellent nanoscale noncentrosymmetric order, but poor mid- and long-range (mesoscopic) order,[24-27] likely due to dipole-dipole interactions and defects disrupting the order over long distances. If the dipole moment of a bichromophore could be made sufficiently low without sacrificing the β value, then the dipole-dipole forces might be sufficiently weak as to not disrupt the long-range self-assembled order. This could provide access to highly nanostructured materials with extremely large order parameters, and if sufficient β was preserved, then very large r_{33} values might be attainable.

5.7 Experimental

All commercially available starting materials were purchased from Sigma-Aldrich, ACROS, or TCI and used without further purification unless otherwise stated. HPLC grade tetrahydrofuran (THF), diethyl ether, methylene chloride, and toluene were purchased from Fisher chemical and purified by passing through alumina in a Seca Solvent Systems (GlassContour Systems) solvent purification system. Alkyl lithium reagents were purchased from ACROS and titrated using 4-biphenylmethanol according to the literature method.[22] Diethyl N,N-dibutylaminobenzylphosphonate,[28] 3,4-dibutylthiophenecarboxaldehyde,[29] and *para*-toluenesulfonyl bromide were prepared according to literature procedures.[23] All reactions were performed under a nitrogen or

argon atmosphere unless otherwise stated. Flash chromatography was performed manually using fine mesh silica.

Instrumentation: ^{1}H and ^{13}C NMR spectra were obtained on a Bruker AV300 or AV301 system at 300Mhz and referenced to residual solvent. Mass spectrum data was obtained from positive ion ESI or MALDI at the Medicinal Chemistry Mass Spectrometry facilities at the University of Washington. Elemental analyses were performed at Prevalere Life Science Inc. (Whitesboro, New York). UV-visible spectroscopy was performed on a Shimadzu UV 1601 Spectrophotometer and UV-visible-near IR spectroscopy was performed on a Perkin-Elmer Lambda 9 Spectrophotometer.

5-Methoxymethoxy-pentan-2-one (5.8). To a solution of 25 mL diisopropylethylamine (DIPEA, 143 mmol) in 200 mL methylene chloride was added 13.2 mL (130 mmol) 5-hydroxy-penta-2-one (**5.7**) at 0 °C under N_2 with stirring, and the mixture allowed to react for 30 min. To this was added 12.3 mL of chloromethyl methyl ether (162.5 mmol) and the mixture allowed to react at 0 °C for an additional 1 hr, and then slowly warmed to room temperature overnight. The solution was concentrated under reduced pressure, 100 mL brine was added, and the mixture extracted 3 x 140 mL diethyl ether. The combined organic extracts were dried over sodium sulfate and then concentrated under reduced pressure. The crude material was purified by vacuum distillation (~2 torr, ~60 °C) to yield 11.325 g (60%) pale straw oil. ^{1}H NMR ($CDCl_3$): δ 4.57 s, 2H), 3.50 (t, 6.3 Hz, 2H), 3.33 (s, 3H), 2.52 (t, 7.2 Hz, 2H), 2.13 (s, 3H), 1.85 (quint., 6.3 Hz, 2H).

2-Ethoxy-6-methoxymethoxy-3-methyl-hex-1-en-3-ol (5.9). To a solution of 17.6 mL (184 mmol) ethyl vinyl ether in 100 mL dry THF at –78 °C was added 125 mL 0.80 M *tert*-butyllithium (titrated, 100 mmol) dropwise with stirring under N_2. After the addition was complete the reaction was allowed to react at –78 °C for 15 min, then it was warmed to 0 °C for 1 hr, and finally cooled back to –78 °C. To the reaction was added a solution of 8.985 g (61.5 mmol) **5.8** in 10 mL dry THF cooled to –78 °C. The reaction was allowed to proceed at –78 °C for 1 hr, followed by 1.5 hr at 0 °C, and then allowed to warm to room temperature (~20 min). The reaction was then immediately quenched with 70 mL aqueous ammonium chloride solution, and the mixture extracted 3 x 80 mL ether. The combined organic extracts were dried over sodium sulfate and then concentrated under reduced pressure to yield 13.37 g (near quantitative). The crude material was used in the subsequent reaction without further purification. ^{1}H NMR ($CDCl_3$): δ4.60 s, 2H), 4.20 (d, 2.4 Hz, 1H), 3.94 (d, 2.1 Hz, 1H), 3.72 (q, 7.2 Hz, 2H), 3.55 (m, 2H), 3.34 (s, 3H), 1.84 (m, 2H), 1.60 (m, 2H), 1.32 (s, 3H), 1.28 (t, 6.9 Hz, 3H).

3-Hydroxy-6-methoxymethoxy-3-methyl-hexan-2-one (5.10). To a solution of 13.37 g (61.25 mmol) crude **5.9** in 50 mL methanol at 0 °C was added 100 mL 1 M HCl dropwise. After the addition was complete the reaction was allowed to react at 0 °C for 3 hours, and then quenched with aqueous saturated sodium bicarbonate solution to bring the pH to ~ 7. The solution was then concentrated under reduced pressure and the residue extracted 3 x 100 mL methylene chloride. The combined organic extracts were dried over sodium sulfate and then concentrated under reduced pressure. The crude material was purified by flash chromatography in 50:50 hexanes:ethyl acetate to yield

5.292 g (40%, two steps) of a pale straw oil. ^{1}H NMR ($CDCl_3$): δ4.60 s, 2H), 4.20 (d, 2.4 Hz, 1H), 3.94 (d, 2.1 Hz, 1H), 3.72 (q, 7.2 Hz, 2H), 3.55 (m, 2H), 3.34 (s, 3H), 1.84 (m, 2H), 1.60 (m, 2H), 1.32 (s, 3H), 1.28 (t, 6.9 Hz, 3H).

2-[3-Cyano-5-(2-methoxymethoxy-ethyl)-4,5-dimethyl-5*H*-furan-2-ylidene]-malononitrile (5.11). A mixture of 1.00 g dry **5.10** (5.27 mmol, stored over magnesium sulfate) and 1.354 g (20.50 mmol) malononitrile was dissolved in 4 mL absolute ethanol. To this was added 0.80 mL 1 M lithium ethoxide in ethanol, and the solution heated in a focused microwave reactor at 40 watts for 40 minutes. The viscous solution was concentrated under reduced pressure and the crude product purified by flash chromatography in 30:70 hexanes:ethyl acetate to yield 0.689 g (45%) red oil. ^{1}H NMR ($CDCl_3$): δ4.60 (s, 2H), 3.54 (m, 2H), 3.35 (s, 3H), 2.34 (s, 3H), 2.21-1.90 (m, 2H), 1.62 (s, 3H), 1.58-1.25 (m, 2H).

2-[3-Cyano-5-(3-hydroxy-propyl)-4,5-dimethyl-5*H*-furan-2-ylidene]-malononitrile (5.12). Dissolved 3.069 g (10.68 mmol) **5.11** in 120 mL of HCl diluted to 1 M in methanol, and allowed to stir overnight under N_2. The solution was concentrated under reduced pressure, neutralized with ~ 20 mL 6 M NaOH, and extracted 3 x 100 mL ethyl acetate. The combined organic extracts were dried over sodium sulfate and then concentrated under reduced pressure. The crude material was purified by flash chromatography in 25:75 hexanes:acetone to yield 2.257 g (88%) of a green oil that crystallized slowly in the freezer. ^{1}H NMR ($CDCl_3$): δ 3.52 (brd. s, 2H), 2.66 (brd. s, 1H), 2.30 (s, 3H), 2.10-1.65 (m, 2H), 1.55 (s, 3H), 1.45-1.17 (m, 2H).

Dibutyl-{4-[2-(3,4-dibutyl-thiophen-2-yl)-vinyl]-phenyl}-amine (5.15). To a 0 °C dry THF solution (60 mL) of **13** (10.762 g, 30.277 mmol) and **5.14** (5.659 g, 25.223

mmol) was added dropwise with stirring under N_2 301.0 mL (31.0 mmol) of a 1M THF solution of potassium *t*-butoxide. The resulting mixture was allowed to stir overnight, warming to room temperature, and was then quenched with deionized water. This was extracted 3 x 60 mL diethyl ether, and the combined organic extracts were dried over sodium sulfate and then concentrated under reduced pressure. The crude material was purified by flash chromatography in a gradient from hexanes to 95:5 hexanes:ethyl acetate to yield 6.594 g (61%) of a yellow oil. ^{1}H NMR ($CDCl_3$): δ 7.32 (d, 2H), 7.01 (d, 1H), 6.79 (d, 1H), 6.68 (s, 1H), 6.61 (d, 2H), 3.28 (t, 4H) 2.61 (t, 2H), 2.49 (t, 2H), 1.66-1.26 (m, 16H), 0.96 (t, 12H).

3,4-Dibutyl-5-[2-(4-dibutylamino-phenyl)-vinyl]-thiophene-2-carbaldehyde (5.16). To a dry THF solution (100 mL) of **5.15** (6.594 g, 15.49 mmol) at –78 °C was added dropwise with stirring under N_2 12.1 mL (19.36 mmol) 1.6 M *n*-butyl lithium in THF. After the addition was complete, the reaction was allowed to react for 10 min, then it was warmed to 0 °C for 10 min, and then it was cooled back to –78 °C. The reaction was stirred for an additional 1 hr at –78 °C, and then 4.8 mL (39.27 mmol) anhydrous dimethyl formamide (DMF) was added dropwise, and the solution was allowed to warm to room temperature overnight, and then the reaction was slowly quenched with deionized water (~100 mL). This was extracted 3 x 80 mL with ether, and the combined organic extracts were dried over sodium sulfate and then concentrated under reduced pressure. The crude material was purified by flash chromatography in a gradient from 95:5 hexanes:ethyl acetate to 80:20 hexanes:ethyl acetate to yield 6.185 g (88%) of a red solid. ^{1}H NMR ($CDCl_3$): δ 9.95 (s, 1H), 7.36 (d, 2H), 7.04 (apparent t,

2H), 6.34 (d, 2H), 3.30 (t, 4H) 2.85 (t, 2H), 2.61 (t, 2H), 1.66-1.26 (m, 16H), 0.96 (t, 12H).

2-[3-Cyano-4-(2-{3,4-dibutyl-5-[2-(4-dibutylamino-phenyl)-vinyl]-thiophen-2-yl}-vinyl)-5-(3-hydroxypropyl)-5-methyl-5*H*-furan-2-ylidene]-malononitrile (5.5, HO-FTC). A mixture of **5.16** (1.262 g, 2.781 mmol) and **5.12** (0.752 g, 3.091 mmol) was dissolved in 10 mL of a 3:1 ethanol:THF solution and refluxed for 72 hr. After cooling, the mixture was dilute to 50 mL with ethyl acetate and extracted 3 x 50 mL brine. The organic fraction was dried over sodium sulfate and the solvent removed under reduced pressure. The crude material was purified by flash chromatography in 95:5 dichloromethane:ethyl acetate, ramping to 9:1, to yield 1.492 g (79%) of metallic copper/blue solid. ^{1}H NMR ($CDCl_3$): δ 8.18 (d, 15.2 Hz, 1H), 7.39 (d, 8.9 Hz, 2H), 7.10 (d, 15.7 Hz, 1H) 7.00 (d, 15.7 Hz, 1H), 6.64 (d, 9.0 Hz, 2H), 6.39 (d, 15.2 Hz, 1H), 3.66 (m, 2H), 3.33 (t, 7.6 Hz, 4H), 2.71-2.60 (m, 4H), 2.27-1.99 (m, 2H), 1.69 (s, 3H), 1.63-1.26 (m, 18H), 0.97 (t, 12H).

Acetic acid 2-methoxy-4-(2-pyridin-4-yl-vinyl)-phenyl ester (5.25). A mixture of vanillin (**5.23**, 8.258 g, 54.3 mmol), 4-picoline (**5.21**, 4.80 mL, 49.3 mmol), and acetic anhydride (50 mL) was refluxed for 22 hours. The resulting mixture was concentrated under reduced pressure, and then poured over an ice-water mixture (100 g) and brought to pH 1 with 6 N HCl. This was then extracted 5 x 100 mL methylene chloride, using brine to dissapate any emulsions. The aqueous portion was then brought to pH ~ 7 with 6 N NaOH, and extracted 5 x 100 mL methylene chloride. The combined organic extracts were dried over sodium sulfate, and then concentrated under reduced pressure. The crude oil was purified via column chromatography to yield 4.65 g (~35%) of a light

yellow solid, determined by NMR to be a mixture of the phenol and the corresponding acetate. ^{1}H NMR ($CDCl_3$): δ 8.58 (d, acetate), 8.55 (d, phenol), 7.36 (d, acetate), 7.33 (d, phenol), 7.24 (s, acetate) 7.21 (s, phenol), 7.29-6.83 (m, mixture of phenol and acetate), 3.97 (s, phenol), 3.90 (s, acetate), 2.33 (s, acetate).

2-Methoxy-4-(2-pyridin-4-yl-vinyl)-phenol (5.26). To a 500 mL flask was added a mixture of **5.25** and **5.26** (1.45 g), followed by 200 mL 1 M HCl. The initial suspension became clear on heating. The solution was refluxed over night. The reaction was then cooled, brought to pH ~ 9 with 6 M NaOH, and then extracted 3 x 100 mL ethyl acetate. The solvent was removed under reduced pressure to yield 1.050 g (~ 85%) of light yellow solid, determined to be pure phenol. ^{1}H NMR ($CDCl_3$): δ 8.56 (dd, 6.1 Hz, 2H), 7.34 (dd, 6.1 Hz, 2H), 7.2 (s, 1H), 7.07 (m, 2H), 6.94 (d, 8.7 Hz, 1H), 6.86 (d, 16.3 Hz, 1H), 3.97 (s, 3H).

Toluene-4-sulfonic acid 3-[4-cyano-3-(2-{3,4-dibutyl-5-[2-(4-dibutylamino-phenyl-vinyl]-thiophen-2-yl}-vinyl)-5-dicyanomethylene-2-methyl-2,5-dihydro-furan-2-yl]-propyl ester (5.29, Tosylate). A mixture of **5.5** (0.414 g, 0.609 mmol), 4-toluenesulfonyl bromide (0.710 g, 3.02 mmol), and pyridine (0.25 mL, 3.09 mmol) were dissolved in 10 mL dry dichloromethane with stirring. The reaction was followed by TLC in 99:1 dicholormethane:ethyl acetate, after running in pure hexanes to remove the pyridine. After the reaction was complete (100 min.), the mixture was diluted to 50 mL with dichloromethane and washed 2 x 60 mL dilute HCl (pH ~3) and 1 x 60 mL brine. The organic fraction was dried over sodium sulfate and the solvent removed under reduced pressure. The crude material was purified via column chromatography in 99:1 dicholormethane:ethyl acetate to yield 0.436 g (85.9%). ^{1}H NMR (Acetone-d_6):

δ 8.33 (d, 15.2 Hz, 1H), 7.77 (d, 8.3 Hz, 2H), 7.51 (d, 8.9 Hz, 2H), 7.45 (d, 8.5 Hz, 2H), 7.28 (d, 15.6 Hz, 1H), 7.16 (d, 16.0 Hz, 1H), 6.73 (d, 8.9 Hz, 2H), 6.63 (d, 15.3 Hz, 1H), 4.13 (t, 6.3 Hz, 2H), 3.41 (t, 7.7 Hz, 4H), 2.84-2.75 (m, 4H), 2.44 (s, 3H), 2.24 (m, 2H), 1.81 (s, 3H), 1.64-1.36 (m, 18H), 0.96 (m, 12H). ES+ MS 833.41 (M+H).

Tosylate Salt (5.30) and/or Bichromophore (5.4). A mixture of 0.367 g (0.440 mmol) tosylate (**5.29**) and 0.500 g (2.202 mmol) phenol (**5.26**) was dissolved in 10 mL dry THF and refluxed for 72 hr. After cooling, the mixture was dissolved in 25 mL ethyl acetate and extracted 3 x 25 mL deionized water. The organic fraction was dried over sodium sulfate and the solvent removed under reduced pressure to afford 0.797 g (187%) dark green solid. The crude material was partially purified by precipitation of concentrated methanol solutions in hexanes or ether. ^{1}H NMR (Acetone-d_6): δ 8.99 (d, 6.3 Hz, 2H), 8.32 (d, 15.2 Hz, 1H), 8.02 (d, 6.2 Hz, 2H), 7.80-7.76 (m, 3H), 7.41 (d, 8.8 Hz, 2H), 7.32 (s, 1H), 7.20 (d, 16.4 Hz, 1H), 7.12 (m, 5H), 6.92 (d, 8.2 Hz, 1H), 6.70 (d, 9.0 Hz, 2H), 6.63 (d, 15.3 Hz, 1H), 4.74 (m, 2H), 3.80 (s, 3H), 3.40 (t, 7.6 Hz, 4H), 2.60 (m, 2H), 2.29 (m, 4H) 1.79 (s, 3H), 1.64-1.21 (m, 18H), 0.97 (m, 12H). MALDI-MS 888.33 (M^+ or M+H for **5.30** or **5.4**, respectively).

Notes to Chapter 5

(1) Dalton, L. R.; Harper, A. W.; Robinson, B. H. The role of london forces in defining noncentrosymmetric order of high dipole moment-high hyperpolarizability chromophores in electrically poled polymeric thin films. *Proc. Natl. Acad. Sci. U. S. A.* **1997**, *94*, 4842-4847.

(2) Robinson, B. H.; Dalton, L. R.; Harper, A. W.; Ren, A.; Wang, F.; Zhang, C.; Todorova, G.; Lee, M.; Aniszfeld, R.; Garner, S.; Chen, A.; Steier, W. H.; Houbrecht, S.; Persoons, A.; Ledoux, I.; Zyss, J.; Jen, A. K. Y. The molecular and supramolecular engineering of polymeric electro-optic materials. *Chem. Phys.* **1999**, *245*, 35-50.

(3) Shi, Y.; Zhang, C.; Zhang, H.; Bechtel, J. H.; Dalton, L. R.; Robinson, B. H.; Steier, W. H. Low (sub-1-volt) halfwave voltage polymeric electro-optic modulators achieved by controlling chromophore shape. *Science* **2000**, *288*, 119-122.

(4) Robinson, B. H.; Dalton, L. R. Monte carlo statistical mechanical simulations of the competition of intermolecular electrostatic and poling-field interactions in defining macroscopic electro-optic activity for organic chromophore/polymer materials. *J. Phys. Chem. A* **2000**, *104*, 4785-4795.

(5) Eichinger, B., Department of Chemistry, University of Washington, unpublished results

(6) Wang, F., University of Southern California.

(7) Breitung, E. M.; Vaughan, W. E.; McMahon, R. J. Measurement of solute dipole moments in dilute solution: A simple three-terminal cell. *Rev. Sci. Instrum.* **2000**, *71*, 224-227.

(8) Oudar, J. L.; Chemla, D. S. Hyperpolarizabilities of the nitroanilines and their relations to the excited state dipole moment. *J. Chem. Phys.* **1977**, *66*, 2664-2668.

(9) Blanchard-Desce, M.; Baudin, J.-B.; Jullien, L.; Lorne, R.; Ruel, O.; Brasselet, S.; Zyss, J. Towards highly efficient nonlinear optical chromophores: Molecular engineering of octupolar molecules. *Opt. Mater.* **1999**, *12*, 333-338.

(10) Lehmann, F.; Mohr, G. J.; Grummt, U. W. Synthesis and structure-property relationships of amphiphilic acidochromic hydroxystilbazolium dyes. *Sens. Actuators, B* **1997**, *39*, 229-234.

(11) Wyss, C. J.; Smith, G. J.; Woolhouse, A. D.; Kay, A. J.; Wadsworth, W. J.; McKinnie, I. T.; Haskell, T. G. The first-order hyperpolarizabilities of some charge transfer conjugated molecules with high transmission in the far red. *Opt. Mater.* **2001**, *16*, 341-347.

(12) Martins, C. T.; Lima, M. S.; Seoud, O. A. E. A novel, convenient, quinoline-based merocyanine dye: Probing solvation in pure and mixed solvents and in the interfacial region of an anionic micelle. *J. Phys. Org. Chem.* **2005**, *18*, 1072-1085.

(13) Onsager, L. Electric moments of molecules in liquids. *J. Am. Chem. Soc.* **1936**, *58*, 1486-1493.

(14) Liao, Y.; Bhattacharjee, S.; Firestone, K. A.; Eichinger, B. E.; Paranji, R.; Anderson, C. A.; Robinson, B. H.; Reid, P. J.; Dalton, L. R. Antiparallel-aligned neutral-ground-state and zwitterionic chromophores as a nonlinear optical material. *J. Am. Chem. Soc.* **2006**, *128*, 6847-6853.

(15) Zhang, C.; Wang, C.; Dalton, L. R.; Zhang, H.; Steier, W. H. Progress toward device-quality second-order nonlinear optical materials. 4. A trilink high mb nlo chromophore in thermoset polyurethane: A \"Guest-host\" Approach to larger electrooptic coefficients. *Macromolecules* **2001**, *34*, 253-261.

(16) Firestone, K. A., University, 2005.

(17) Soref, R. The past, present, and future of silicon photonics. *IEEE J. Sel. Top. Quantum Electron.* **2006**, *12*, 1678-1687.

(18) Huang, D.; Chen, B.; (USA). Application: US
US, 2004; pp 23 pp , Cont -in-part of U S Ser No 395,610.

(19) Liu, S.; Haller, M. A.; Ma, H.; Dalton, L. R.; Jang, S.-H.; Jen, A. K. Y. Focused microwave-assisted synthesis of 2,5-dihydrofuran derivatives as electron acceptors for highly efficient nonlinear optical chromophores. *Adv. Mater.* **2003**, *15*, 603-607.

(20) Kay, A. J.; Woolhouse, A. D.; Gainsford, G. J.; Haskell, T. G.; Barnes, T. H.; McKinnie, I. T.; Wyss, C. P. A simple, novel method for the preparation of polymer-tetherable, zwitterionic merocyanine nlo-chromophores. *J. Mater. Chem.* **2001**, *11*, 996-1002.

(21) Shaw, B. D.; Wagstaff, E. A. Reaction between 2-picoline and aromatic aldehydes. *J. Chem. Soc.* **1933**, 77-79.

(22) Furniss, B. S.; Hannaford, A. J.; G., S. P. W.; Tatchell, A. R. *Vogel's textbook of practical organic chemistry*; Addison Wesley Longman: Singapore, 1989.

(23) Poshkus, A. C.; Herweh, J. E.; Magnotta, F. A. The synthesis of aromatic sulfonyl bromides from sulfonylhydrazides. *J. Org. Chem.* **1963**, *28*, 2766-2769.

(24) Ashwell, G. J. Langmuir-blodgett films: Molecular engineering of non-centrosymmetric structures for second-order nonlinear optical applications. *J. Mater. Chem.* **1999**, *9*, 1991-2003.

(25) van der Boom, M. E.; Richter, A. G.; Malinsky, J. E.; Lee, P. A.; Armstrong, N. R.; Dutta, P.; Marks, T. J. Single reactor route to polar superlattices. Layer-by-layer self-assembly of large-response molecular electrooptic materials by protection-deprotection. *Chem. Mater.* **2001**, *13*, 15-17.

(26) Marks, T. J.; Ho, S. T.; Liu, Z.; Zhu, P.; Sun, D.-G.; Ma, J.; Xiao, Y.; Kang, H. Electro-optic waveguide modulators by the integration of self-assembled superlattices with polymeric and semiconductor materials. *Proc. SPIE* **2003**, *4991*, 133-143.

(27) Facchetti, A.; Abbotto, A.; Beverina, L.; van der Boom, M. E.; Dutta, P.; Evmenenko, G.; Pagani, G. A.; Marks, T. J. Layer-by-layer self-assembled pyrrole-based donor-acceptor chromophores as electro-optic materials. *Chem. Mater.* **2003**, *15*, 1064-1072.

(28) Marder, S.; Perry, J.; Zhou, W.; Kuebler, S. M.; Cammack, J. K.; (USA). Application: WO
WO, 2002; pp 181 pp.

(29) Spangler, C. W.; He, M. Preparation and oxidative doping studies of dithienyl polyenes stabilized by alkyl group substitution. *J. Chem. Soc., Perkin Trans. 1* **1995**, 715-720.

Chapter 6: Dielectric Constants of Electro-Optic Films

6.1 Introduction

Until very recently, the exact dielectric constant (ε) of organic EO films was not considered very important. The relatively low dielectric of organic materials (~ 3) as compared to inorganic materials (~28) has been considered as an advantage, however. It ensures a good velocity match between the traveling optical and electrical signals in a device, allowing for long device interaction lengths. The recent development of binary organic glasses,[1-3] consisting of EO chromophores doped into EO active organic hosts, has brought questions relating to the dielectric constant to the fore. Such systems have considerably higher chromophore content than traditional guest-host systems, which should increase the dielectric constant of the medium. As a result of the high r_{33} values exhibited by these materials, the effect of dielectric constant on both the β value of chromophores, and on the dipole-dipole and dipole-electrical field interactions in the material have come under consideration.

There is some preliminary evidence that an increased dielectric constant can enhance the molecular properties of EO chromophores. The effect that the polarity of the nanoscale environment has on the energy of the optical absorption of a chromophore has long been known, and is referred to as solvatochromism (Section 2.4.1). More recently, the effect of the polarity of the medium on the nonlinear activity of the chromophore has been investigated. Density functional theory (DFT, Section 2.2.2) calculations (among others) performed by Dr. Bruce Eichinger (Department of

Chemistry, University of Washington) that incorporate theoretical reaction fields to approximate dielectric properties suggest that medium polarity can significantly enhance the effective nonlinear properties of EO chromophores (Table 6.1).[4]

Table 6.1. YLD156 reaction field study: variation of electrostatics with solvent parameters

E[a]	Radius (Å)[a]	Density (1/Å^3)[a]	μ (D)[b]	β_{HRS} (10^{-30} esu)[b]	β_{zzz} (10^{-30} esu)[b]
1.0	0.0	0.0	23.1	164	338
2.0	3.0	0.006	27.01	321	669
3.0	3.0	0.006	28.81	426	890
4.0	3.0	0.006	29.87	499	1043
4.0	4.0	0.006	29.85	495	1035
5.0	3.0	0.006	30.56	552	1155
8.0	3.0	0.006	31.70	650	1362
16.0	3.0	0.006	32.76	755	1581

[a]Input solvent parameters [b]Properties calculated with B3LYP/3-21g* PCM

Data on the μβ of a bithiophene-based chromophore, CC172, from electric field induced second harmonic generation (EFISH, Section 2.4.2) experiments in a variety of solvents by Olivier Ostinelli and coworkers in the laboratories of Prof. Peter Günter (ETH, Zürich, Switzerland) supports the importance of solvent polarity on μβ (Table 6.2).[5] The data show a large variation in the experimental values, with over 100 % change across the full solvent range. EFISH is far from ideal for these experiments, however, because the data obtained is actually a combination of μ, β, and γ (Section 2.4.2). Thus, it is difficult to make conclusions about the effect of the polarity on β specifically.

Table 6.2. Variation of experimental μβ of CC172 as a function of solvent[5]

Solvent	μβ (esu)
Dichloromethane	20700
Chloroform	16270
Tetrahydrofuran	12920
Dioxane	10530
Carbon tetrachloride	9720
Toluene	8610

Preliminary work by Denise Bale and coworkers in the Dalton Group (Department of Chemistry, University of Washington) has explored the effect of solvent polarity on β as measured by HRS (Section 2.4.3), which is more suited to such investigations because the data is related directly to β.[6] For EZ-FTC, the β_{HRS} in toluene (ε = 2.38) relative to the β_{HRS} in chloroform (ε = 4.81), measured at 1.9 μm, was only 0.45 +/- 0.03. This supports the strong effect of polarity on β. However, the relative β_{HRS} in 1,1,2-trichloroethane (TCE, ε = 7.24) was only 0.893 +/- 0.003, which is not consistent with the predicted trend. It has been suggested that chloroform may exhibit anomalous properties due to the potential for strong hydrogen bonding or other electrostatic interactions with the chromophores. It should be emphasized that this work is only preliminary, and a more in-depth study is currently underway.

In addition to the dielectric effects on molecular properties, the dielectric properties of a medium can also affect the intermolecular interactions that are critical to achieving acentric order in the poling process (Section 3.3). There are two separate interactions, the dipole-poling field interaction and the dipole-dipole interactions, that the dielectric can screen. Any reduction in the dipole-dipole interactions is beneficial for enhancing the poling-induced order, so a high dielectric constant would be favorable from that perspective. While a high dielectric constant would also reduce the dipole-poling field interaction, this reduction is already effectively accounted for by the V_{RMS} measured in the poling experiment. The V_{RMS} returned depends on both the dielectric reduction of field and the leakage current of the material, but one can effectively just

increase the applied field to account for the reduced effective field. Thus, an increased ε should conceivably have a net positive effect on the poling-induced order.

Until now, the dielectric properties of EO films have been considered isotropic. This is clearly only the case, however, in an un-poled sample (assuming a truly isotropic film is produced from spin-casting, which is approximately true). A poled sample with (partially) aligned dipoles should produce an anisotropic ε. The dielectric constant of an anisotropic material is only a second-rank tensor, however, as the dielectric properties are insensitive to the distinction between centrosymmetric and noncentrosymmetric dipole orientations. Additonally, in the case of a uniaxially oriented sample, as produced by poling, there are only two independent elements. There are two consequences of this dielectric anisotropy; the first is that the previously mentioned microscopic and macroscopic dielectric effects will depend on the order of the sample. The second consequence is that the dielectric anisotropy can theoretically provide information about the $\langle\cos^2\theta\rangle$ poling-induced order in a sample. Although the insensitivity of dielectric properties to dipole direction precludes obtaining information on the $\langle\cos^3\theta\rangle$ order parameter that is critical in EO materials, the $\langle\cos^2\theta\rangle$ order parameter is also of significant interest.

6.2 Theoretical Guidance

The dielectric constant (ε), also known as the relative permittivity, is defined as

$$\varepsilon = \frac{\varepsilon_a}{\varepsilon_0} \tag{6.1}$$

where ε_a is the (absolute) permittivity of the material, and ε_0 is the permittivity of a vacuum as defined by Maxwell's equations. The permittivity is in turn defined as

$$\mathbf{D} = \varepsilon_a \mathbf{E} \tag{6.2}$$

where **D** is the electric displacement field, which describes the effect of the electric field (**E**) on the distribution of charges in the material. The permittivity thus describes the material's response to an applied electric field, and relates to the amount of electrical energy stored within the material, relative to that of a vacuum. The permittivity thus relates to the polarizability of the material, and in the case of a linear dielectric (non-conducting, non-magnetic), the dielectric constant can be related to the linear susceptibility ($\chi^{(1)}$) by Equation 6.3 (in SI units, in CGS units the relationship is given by Equation 1.6).

$$\varepsilon = 1 + \chi^{(1)} \tag{6.3}$$

In general, the permittivity (absolute or relative) is a complex quantity that depends on the frequency (ω) of the applied electric field. The real (ε') and imaginary (ε'') parts can be separated such that

$$\varepsilon(\omega) = \varepsilon'(\omega) + i\varepsilon''(\omega) = \frac{E_0}{D_0}(\cos\delta + i\sin\delta) \tag{6.4}$$

where *i* is the square root of -1, and d is the phase lag between **D** and **E**. The imaginary part describes the rate of energy loss to the medium (as heat) due to frequency mis-match between the applied field and the response of the medium. The frequency dispersion of the permittivity is generally very complex due to the different dispersion properties of the various contributions to the permittivity, including (from low to high

frequency): molecular (dipole) rotations, molecular vibrations, ionic polarizations, and electronic excitations.

The various dispersive properties of the different contributions to the dielectric constant make accurate analysis of the dielectric anisotropy ($\Delta\varepsilon$) of anisotropic materials extremely challenging. In the context of uniaxial orientation, the $\Delta\varepsilon$ is defined by

$$\Delta\varepsilon = \varepsilon_{\parallel} - \varepsilon_{\perp} \tag{6.5}$$

where $\varepsilon_{\parallel} = \varepsilon_{zz}$ and

$$\varepsilon_{\perp} = \frac{1}{2}(\varepsilon_{xx} + \varepsilon_{zz})^{7} \tag{6.6}$$

A variety of assumptions must be made in order to relate the $\Delta\varepsilon$ to dipolar orientation, which limits the quantitative accuracy of the relationship. In the context of polar nematic liquid crystals (LC), however, Maier and Meier have derived a relationship (Equation 6.7) between $\Delta\varepsilon$ and the angle (ψ) between the dipole moment (μ) and the molecular long axis, which is presumed to be aligned with the LC director (z axis).[7,8]

$$\Delta\varepsilon \propto \left[\Delta\alpha + \frac{\mu^2 F}{2k_B T}\left(3\cos^2\varphi - 1\right)\right] \tag{6.7}$$

The relationship also depends on the polarizability anisotropy ($\Delta\alpha$), the field factors (F) and the thermal energy, as described by the Boltzmann constant (k_B)-temperature product. Although this could likely be altered to apply it to non-LC systems with dipolar order of $\langle\cos^2\theta\rangle$, it is beyond the scope of this work. Regardless, the dependence on $\Delta\alpha$ and the non-quantitative nature of the relationship limits the usefulness in experimental determination of $\langle\cos^2\theta\rangle$ dipolar order from $\Delta\varepsilon$. As a result,

we can only state with confidence that $\Delta\varepsilon$, and thus both $\varepsilon_{\parallel}$ and $\varepsilon_{\perp}$, will depend on the degree of orientation of the dipolar chromophores, as is indeed the case (see Section 6.4.2).

6.3 Experimental Method

The dielectric constant of a material (ε_m) can be readily determined from the capacitance ratios of a capacitor filled with the material and the capacitor filled with vacuum (or air, which has nearly the same ε)

$$\varepsilon_m = \frac{C_m}{C_0} \tag{6.8}$$

where C_m is the capacitance in the presence of the material, and C_0 the capacitance in vacuum (or air). Alternatively, ε_m may be determined from the capacitance of a capacitor of known dimensions

$$\varepsilon_m = \frac{C_m t}{A\varepsilon_0} \tag{6.9}$$

where t is the distance between the electrodes (the thickness of the material), and A is the area of the electrodes. This latter method is more applicable to the experimental determination of ε_m of organic EO materials.

6.3.1 Experimental Details. The experimental method makes use of the conventional organic EO thin-film sample format to evaluate the dielectric constant of the EO materials under relevant conditions.[3] The samples are deposited on indium tin oxide

(ITO) coated glass substrates that are chemically etched to create a substrate that is roughly half electrode and half bare glass. Organic EO chromophore-containing polymer or dendrimer solutions are then spin-cast on these substrates to produce films on the order of 1 μm thick, with the exact thickness measured by via profilometry. After curing, a patterned top gold electrode is deposited by sputter coating through a pattern mask of known dimensions. In the present work, this pattern consists of a dumbbell-shape; two circles connected by a thin rod, where one of the circles is entirely on the ITO half of the substrate, and the other circle is entirely on the glass half of the substrate. Electrical connections are made by using silver paint to glue wires to the to the top gold electrode via the electrode circle on the glass half of the substrate, and to the ITO bottom electrode by removing a portion of the film. The capacitance across the sample is then measured at the frequency of choice, and the ε_m of the material is calculated using Equation 6.9 and the measured sample geometry.

For our experiments, the ITO substrates were initially determined to exhibit sheet resistances of around 50 Ω, which should introduce minimal capacitance to the measurement. The film thicknesses were measured on a Sloan Dektak 3030 Profilometer. The area of the active electrode area was initially estimated to be 1.137 x 10^{-5} m^2 assuming half of the total area of the dumbbell mask. The wire leads were determined to introduce resistances on the order of 1-5 Ω, which should produce a negligible contribution to the capacitance. Finally, the capacitance (C) was measured on a BK Precision Model 885 Synthesized In-Circuit LCR/ESR Meter. We chose a measurement frequency of 1 kHz, as this is the frequency of the AC electric field applied in the *in situ* pole and probe simple reflection apparatus for the measurement of

EO activity (Section 3.5.2).[3,9] For these experiments, we exclusively measured the parallel capacitance, although comparisons with the series capacitance on multiple samples showed differences of only 5-10 picofarads (pF).

6.3.2 Experimental Error. Although conceptually very simple, this measurement technique is subject to numerous sources of error. For these experiments, we have chosen to ignore to effects of fringing fields,[10] as the magnitude of these effects are reported to be small.[11] This source of error, however, could easily be accounted for in future experiments if the magnitude was seen to be significant. The LCR meter used has a 0.5 % base accuracy, with also introduces error of up to +/- 0.05 in ε_m. In the future, a higher-precision instrument will allow better accuracy to be obtained. The measurement of film thickness introduces another source of error; with an accuracy of +/- 0.01 μm, it can introduce errors of up to +/- 0.05 in the calculated ε_m. Additionally, each sample must be measured individually to eliminate additional error from variations in sample thickness across the substrate.

A major source of error was determined to be the value estimated for the active electrode area. Even with the best of measurements, uncertainty in the measurements contributes error of roughly +/- 0.05 ε, leading to a minimum overall error of roughly +/- 0.15. Although initially this area was estimated as half of the mask area, which was determined from simple measurements of the electrode dimensions, this is an overestimation of the actual area. The effects of this overestimation are demonstrated in Section 6.3.3 in the validation experiments on pure amorphous polycarbonate (APC) films. Careful measurements of the interior dimensions of the mask with digital calipers indicated not only that previous values were overestimating the area, but also

that each of the masks used possess slightly different areas. Additionally, the positioning of the mask on the sample, with respect to the interface between the ITO and bare glass regions, results in slightly different dimensions for every sample. Thus, for maximum accuracy every individual sample would be associated the dimensions of the mask used and the position of the mask on the sample to provide the exact area of the active electrode. We have performed such a careful analysis in determining the ε_m of PSLD33, a state-of-the-art multichromophore dendrimer (Section 6.4.3). Although this was not performed for most of the samples, including the APC films used to validate the method, we can use the average sample area from the PSLD33 measurements (9.84×10^{-6} m^2) to obtain more accurate ε_m values.

A final source of error that must be considered is due to the anisotropic nature of poled EO films. A large number of the samples used in these studies were obtained from other researchers in the Dalton Group (Dr. Philip Sullivan and Benjamin Olbricht, Department of Chemistry, University of Washington), after they had been previously poled and their EO activity measured. As previously mentioned, the dielectric properties are expected to depend on the degree of orientation of the dipoles. For the geometries of our samples, we are measuring $\varepsilon_{\parallel} = \varepsilon_{zz}$ and the poling is expected to increase the alignment of dipoles along the z axis (poling axis). Thus, poling should increase the measured capacitance and the calculated ε_m value, as we demonstrate in Section 6.4.2. Although this effect can serve as a qualitative evaluation of the poling-induced orientational ($<\cos^2\theta>$) order, if samples are measured before and after poling, it can simply introduce error if samples with unknown degrees of orientational order are measured only after poling.

6.3.3 Validation of Experimental Method. For our initial studies, we chose to explore the dielectric properties of the pure polymer host used in our guest-host EO films. This polymer, poly[bisphenol A carbonate-*co*-4,4'-(3,3,5-trimethylcyclohexylidene)diphenol carbonate] (hereafter, APC) has been previously measured to have a bulk isotropic dielectric constant (ε) of 2.90 at 1 MHz.[12] We cast films from filtered (0.2 μm) 14.95 wt. % cyclopentanone (CP) solutions with the following spin program: 5 s at 600 RPM with an acceleration parameter of 7, followed by 30 s at 1000 RPM with an acceleration of 10. The films were initially soft-baked on a hot plate at 85 °C, and then cured overnight in vacuum oven at 85 °C. For these initial experiments, we measured only one thickness (t) per initial film (3 samples), which contributes to the sample error. The properties of these samples along with the calculated ε_m values are presented in Table 6.3. For these samples the measured values presumably corresponds to the isotropic ε. The dissipation constant (D) is a ratio of the real and imaginary parts of the dielectric constant, and thus is a measure of the energy lost to the medium. Anomalously large values indicated invalid samples.

Table 6.3. APC film measured and calculated properties

Sample	t (μm)	C (pF)	D	ε	
1.1	1.414	194.7	0.035	2.73	
1.2	1.414	204.3	0.009	2.87	
1.3	1.414	197.1	0.009	2.77	
2.1	1.413	180.7	0.019	2.54	
2.2	1.413	186.1	0.015	2.61	
2.3	1.413	178.2	0.014	2.50	
			Average	2.67	@ 1 KHz
			SD	0.14	
			Lit Value	2.90	@ 1 MHz

The initial value returned based on a single estimated electrode area was 2.67 +/- 0.14 (at 1 kHz), which is slightly lower than the literature value of 2.90 (at 1 MHz).

The discrepancy between these measurement frequencies is expected to be negligible in this frequency range. As previously mentioned, from our work to obtain a highly accurate measurement of PSLD33 (Section 6.4.3), we identified the initial estimate of electrode area as inaccurate. Although the actual area for each sample depends on the dimensions of the particular mask used, we can obtain a more accurate estimate with the existing data. By using the average electrode area (9.84×10^{-6} m^2) for all of the samples of PSLD33 (Section 6.4.3), we can obtain a value of 3.08 +/- 0.17, which is slightly closer to the literature value. As previously mentioned, the thickness should be measured individually for each sample. From the data in Table 6.3, it is clear that the capacitance, and thus the calculated ε_m, is highest in the middle sample of a given plate, and is reduced for the other two samples. This suggests that the films are thinner in the middle, and thicker on the edges, which is exactly what we have seen in the films of PSLD33 (Section 6.4.3). Therefore, we conclude even greater agreement with the literature value could be obtained if the thicknesses of each film had been measured. Based upon these results, we take our measurement technique to be valid. This work emphasizes, however, the importance of accurate measurements of all parameters and the susceptibility of these values to error from a variety of factors.

6.4 Results

Our initial experiments on actual EO samples examined individual films of three different EO systems (obtained from Dr. Philip Sullivan, Dalton Group, Department of Chemistry, University of Washington) with varying chromophore concentration as a

test of the theory that increased chromophore content should result in increased ε. The lowest chromophore content system (I) consisted of a guest-host mixture of 25 % YLD156,[3,9] a FTC-type (Section 2.3.3) chromophore, in the above tested blend of APC. The next highest chromophore content system (II) consisted of a pure multichromophore dendrimer, PSLD41,[3,9] with a roughly 41 % active loading density of an FTC-type chromophore. The highest chromophore content system (III) consisted of the PSLD41 dendrimer doped with an additional 20 wt. % of YLD124,[3,9] a CLD-type (Section 2.3.3) chromophore, which is an example of the new class of binary organic glasses that exhibit extremely large r_{33} values up to 300 pm/V (see Section 3.4.3). These samples represent a good cross-section of organic EO materials of current interest. The structures of these EO materials, along with those of the PSLD33 multichromophore dendrimer,[3,9] and a disperse red 1 side-chain functionalized polymethylmethacrylate (DR1-PMMA)[13] system used in future studies, are presented in Figure 6.1.

The results for our initial film studies are presented in Table 6.4, with calculated $\varepsilon_{\|}$ values (at 1kHz) based on both the original electrode area estimate, and the value obtained form the PSD33 studies (Section 6.4.3) presented. Although the data appears to support the initial hypothesis, the increase in ε does not appear to be linear with chromophore loading in these samples. It should be noted, however, that these results are from individual samples, as opposed to statistically averaged sample sets. Additionally, these samples were obtained from other researchers, and thus exact values for the thicknesses and electrode area could not be obtained. Thus, the experimental error may be significantly in excess of the minimum +/- 0.15 value estimated previously

(Section 6.3.2); we estimate a value of +/- 0.30 per sample. Even more importantly, these samples had been previously poled; indicating that the values measured are actually $\varepsilon_{\parallel} = \varepsilon_{zz}$, which suggests they may be considerably enhanced from the poling-induced order. Although this is not an error, per se, it does affect the measured value in an unpredictable way. Additionally, differences in the degree of poling induced order may contribute to the variation between the different samples.

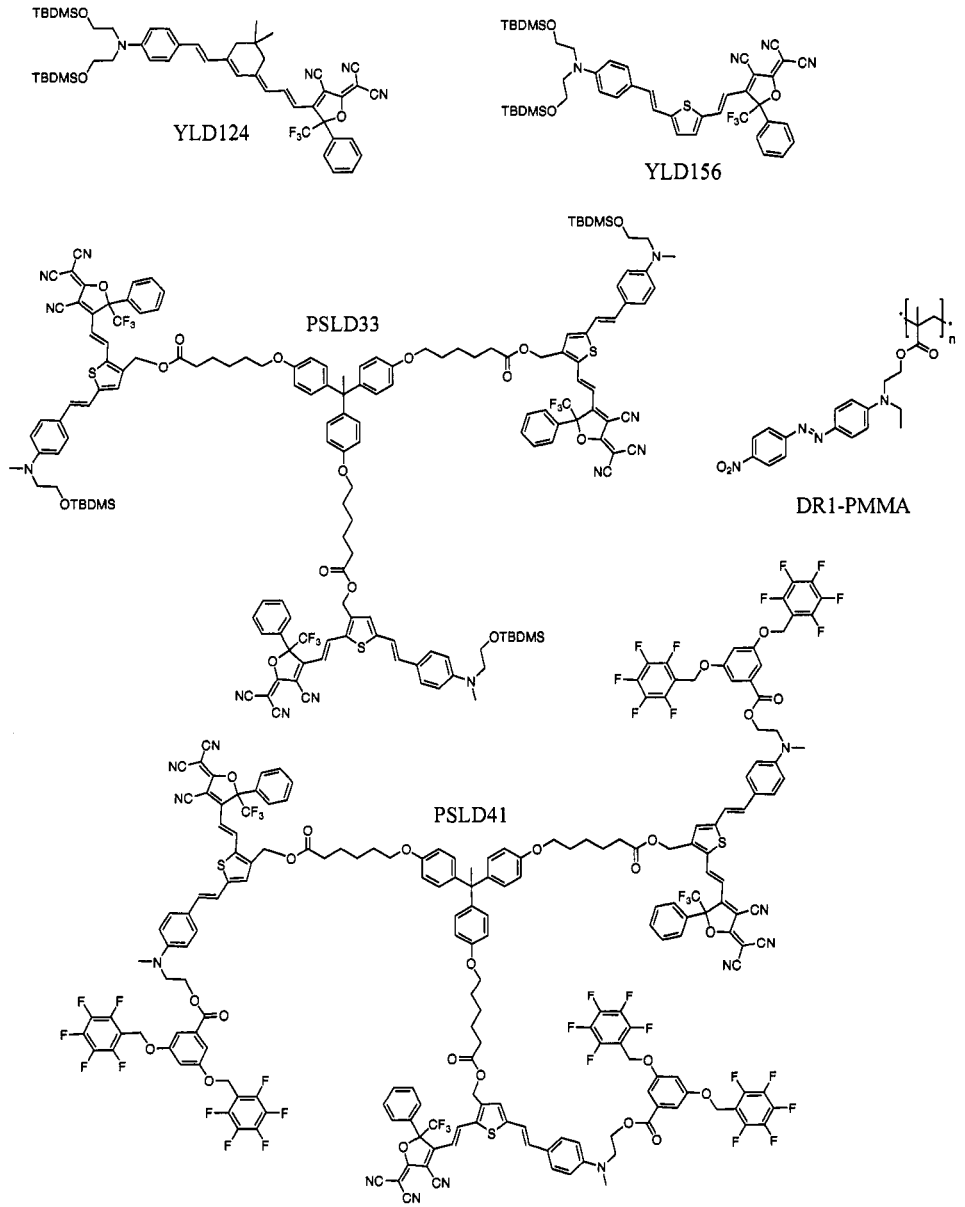

Figure 6.1. Structures of EO materials used in the dielectric studies

Table 6.4. Initial dielectric data for representative EO materials

Sample	t (μm)	C (pF)	D	$\varepsilon_{\|}$ (A=11.3 mm^2)[a]	$\varepsilon_{\|}$ (A=9.85 mm^2)[a]
I	1.95	180	0.002	3.49	4.02
II	0.77	566	0.007	4.33	5.00
III	0.973	497	0.004	4.80	5.54

[a]Measured at 1 kHz

6.4.1 Loading Density Studies. Based upon the encouraging results from our initial studies, we performed a much larger study to explore the dielectric properties of three different hosts, the APC blend previously studied, the PSLD41 multichromophore dendrimer, and the DR1-PMMA material, as a function of loading density of two EO chromophores, YLD156 and YLD124. All of the samples were obtained from other researchers (Dr. Philip Sullivan and Benjamin Olbricht, Dalton Group, Department of Chemistry, University of Washington), and so the same considerations with regard to sources of error apply as in our initial studies. Although the data was analyzed using both values for electrode area, the data is presented and discussed based solely on the average electrode area (9.85×10^{-6} m^2, or 9.85 mm^2) obtained from the accurate PSLD33 measurements (Section 6.4.3). Whenever possible, multiple samples were measured and statistical averages taken, although in most cases the number of samples is rather low. Again, we estimate an experimental error of +/- 0.30 for each sample. Although statistical averaging could reduce error for the systems with sufficient samples, we simply take this error as valid for all the samples studied. Additionally, significant variations are seen in some cases (YLD156 15% DR1-PMMA, and YLD124 15% and 35% PSLD41) between samples with the same composition, and it should be emphasized that the degree of poling-induced order of each sample is an unknown factor affecting the values measured. It would be desirable to correlate these results

with the r_{33} values measured from the samples, unfortunately that data is not available at this time. The data for the entire sample set is presented in Table 6.5.

Table 6.5. Dielectric properties as a function of host and chromophore guest loading

Material/Sample	t (μm)	C (pF)	D	$\varepsilon_{\|}$ [a]	Average
YLD156 15% APC					
1.2	2.36	125.2	0.002	3.39	
1.3	2.36	126.5	0.002	3.42	
2.2	2.24	123.2	0.002	3.16	3.33
YLD156 25% APC					
1.1	2.26	154.8	0.002	4.01	
2.1	1.95	175.3	0.002	3.92	3.97
YLD156 35% APC					
1.1	1.77	178.1	0.002	3.61	
2.3	1.6	200.7	0.078	3.68	3.65
YLD156 15% DR1-PMMA					
1.3	1.12	254.5	0.025	3.27	
2.1	1.6	278.9	0.025	5.12	4.19
YLD156 25% DR1-PMMA					
2.1	1.07	310.8	0.022	3.81	
2.2	1.07	323	0.022	3.96	3.89
YLD156 35% DR1-PMMA					
1.1	0.988	1.269	0.003	0.01	X[b]
1.2	0.988	351.8	0.021	3.99	
1.3	0.988	345.4	0.021	3.91	3.95
YLD124 25% APC					
2.1	1.6	193.8	0.001	3.56	
2.2	1.6	193.5	0.004	3.55	3.55
YLD124 26% DR1-PMMA					
2.1	1.4	227.7	0.022	3.66	
2.2	1.4	228.1	0.023	3.66	
3.3	1.2	283.5	0.023	3.90	
6.1	1.3	291.9	0.023	4.35	3.89
8.3	1.3	318.3	217.4	4.74	X[b]
YLD124 15% PSLD41					
3.1	0.95	402.9	0.004	4.39	
3.2	0.95	386.1	0.004	4.21	
4.1	1.05	428	0.013	5.15	4.58
YLD124 25% PSLD41					
2.1	1.6	289.5	0.005	5.31	5.31
YLD124 35% PSLD41					
1.2	1.46	371.9	0.01	6.23	
2.2	1.54	324.6	0.015	5.73	5.98

[a]Measured at 1 kHz [b]These samples were determined to be bad due to anomalous values of C or D, and were excluded from the averaged values.

The average $\varepsilon_{||}$ values (at 1 kHz) from Table 6.5 are graphed in Figure 6.2 as a function of loading density in order to facilitate analysis. It is apparent that the PSLD41 host samples all have significantly higher $\varepsilon_{||}$ values than the other hosts. Additionally, the average $\varepsilon_{||}$ values for this host system indicate a linear ($R^2 = 0.9994$) trend, which allows estimation of a $\varepsilon_{||}$ value of 3.54 for the neat host material. This value is significantly lower than the value obtained in our initial studies (5.00), however. This could be simply due to excessive experimental error, particularly from the initial single-sample, or it arise from different degrees of poling-induced order in the pure and doped samples. Alternatively, it may suggest that complex interactions influence the dielectric properties of these binary organic glass systems.

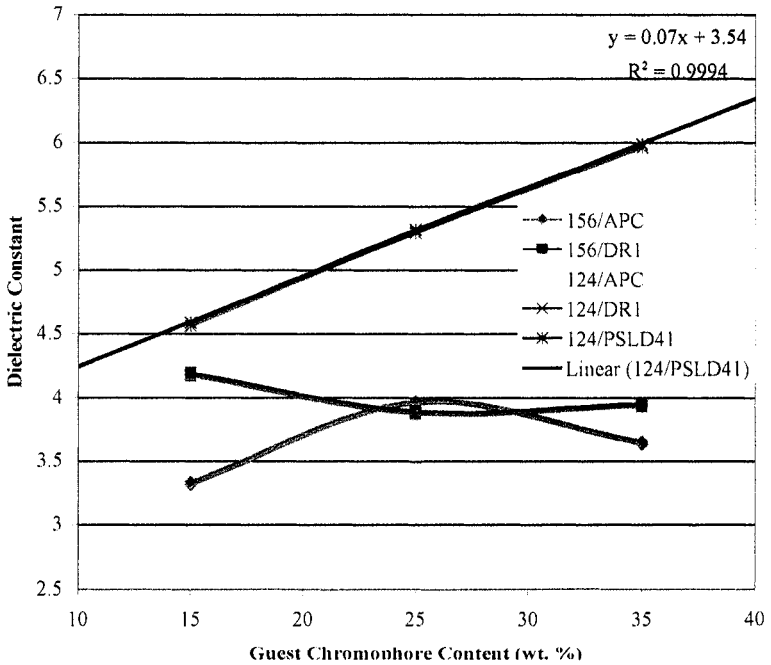

Figure 6.2. Average dielectric constant at 1 kHz as a function of host and chromophore loading

In contrast to the linear behavior of the PSLD41 host, the other systems where samples over the entire range studied were available (YLD 156 in APC and DR1-

PMMA) exhibited distinctly nonlinear behavior. In fact, the trends in these materials appear superficially similar to the trends in r_{33} values of poled guest-host systems as a function of chromophore number density; that is r_{33} values initially increase with loading density as predicted by the simple linear Langevin model (Section 3.3.3), but then decrease at higher loading densities. This behavior was described by Dalton and Robinson as arising from decreased $\langle\cos^3\theta\rangle$ order due to increased centrosymmetric dipole-dipole interactions at higher chromophore densities (see Section 3.3.5 and 3.3.6, Figures 3.4 and 3.5).[14,15]

Based upon the discussion of anisotropy in Section 6.2, and the relationship suggested by Equation 6.7, the present data suggests that the YLD156/DR1-PMMA blend achieves a maximum orientational ($\langle\cos^2\theta\rangle$) order at low loading densities. We arise at this conclusion based on the fact that the addition of more chromophore does not significantly enhance the measured $\varepsilon_{\parallel}$, as would be expected if the orientiational order was kept constant (or increased) with the addition of further chromophore content. In the case of the YLD156/APC blend, the data suggests that the system achieves maximum orientational order at around 25 wt. %, as additional chromophore actually significantly decreases the measured $\varepsilon_{\parallel}$. Again, these results apply only to $\langle\cos^2\theta\rangle$ order parameters, not $\langle\cos^3\theta\rangle$, and thus conclusions cannot be made about the r_{33} values of these samples.

The position of the maximum in $\varepsilon_{\parallel}$ as a function of chromophore loading for the YLD156/APC blend (25 wt. %) is in good agreement with the maximum in r_{33} as a function of chromophore loading.[3,9] Additionally, a reduction in $\langle\cos^2\theta\rangle$ order necessitates a reduction in $\langle\cos^3\theta\rangle$ order (although the converse is not true). Taken

altogether, this suggests that dipole-dipole interactions not only reduced $\langle\cos^3\theta\rangle$ order, due to the centrosymmetric nature of the interaction, but also reduce $\langle\cos^2\theta\rangle$ order. This may be due to the strong dipole-dipole interactions creating intense anisotropic field factors. These field factors may alter the orientation of the effective field felt by the chromophores within the films, resulting in reduced macroscopic alignment with the applied E field vector. These field factors also affect the macroscopic EO activity (see Section 3.3.1, Equation 3.2). This analysis suggests that the standard Onsager and Lorentz field factors commonly used (see Section 3.3.1, Equations 3.3 and 3.4) may not be applicable in any system where a significant degree of centrosymmetric aggregation of chromophores exists.

An alternative possible explanation for this effect is that centrosymmetric dipole-dipole pairs may simply stop contributing a significant amount to the dielectric properties of the medium. These dipole pairs may not respond to the applied field at all, and thus the contribution from the dipole polarization effect may become negligible. Although this might change the details of the orientational order argument above, the net effect on the properties of the medium is still the same.

6.4.2 Poling Response of Dielectric Constant. We chose to explore the effects of sample poling-induced anisotropy on the measured $\varepsilon_{\|}$ value (at 1 kHz) in more detail by examining the dielectric constant of samples before and after poling. Towards this end, we obtained two unpoled samples of 15 wt. % YLD124 in PSLD41 (Dr. Philip Sullivan, Dalton Group, Department of Chemistry, University of Washington), which is known to exhibit very large r_{33} values.[3] We measured the capacitance of these samples before and after poling with 75-100 V/μm (E_p), and we measured the r_{33} values with the simple

reflection technique at 1.31 μm (Section 3.5.2).[3,9] We also examined the same properties for samples of 18 wt. % OLD-1 in APC (Dr. Olivier Clot, Dalton Group, Department of Chemistry, University of Washington; see Section 4.1).[16] For all samples, we used the average electrode area obtained from our studies of PSLD33. We again estimate an error in $\varepsilon_{\parallel}$ of +/- 0.30 for each sample. The data is presented in Table 6.6.

Table 6.6. Poling response of dielectric properties

Material Sample	t (μm)	Before Poling		E_p (V/μm)	r_{33} (pm/V)	After Poling		$\Delta\varepsilon_{\parallel}$ [a]
		C (pF)	$\varepsilon_{\parallel}$ [a]			C (pF)	$\varepsilon_{\parallel}$ [a]	
15% YLD124/PSLD41								
4.2	0.973	424.7	4.74	75	161	470.7	5.25	0.51
4.3	0.973	434.1	4.84	100	~200[b]	465.2[b]	5.19[b]	0.35[b]
18% OLD-1/APC								
1.1	1.37	193	3.03	50	15.2	185.8	2.92	-0.11
1.3	1.37	194.7	3.06	75	18.5	186	2.92	-0.14
2.1	1.27	239.9	3.49	100	2.5	228.8	3.33	-0.16
3.1	1.24	245.8	3.49	100	6.07	237.8	3.38	-0.11
3.2	1.24	237.3	3.37	100	3.65	231.8	3.30	-0.08

[a]Measured at 1 kHz [b]This sample sustained some damage to the electrode during poling, which hindered the r_{33} measurement and likely resulted in reduced C and $\varepsilon_{\parallel}$ values.

Based upon the data in Table 6.6, it is clear that samples with large r_{33} values exhibit a significant enhancement in the measured $\varepsilon_{\parallel}$ value, while samples with low r_{33} values show a negligible increase or even a reduction in the measured $\varepsilon_{\parallel}$ value. Unfortunately, the electrode damage to sample 4.3 of the binary organic glass, combined with the measurement error, makes any correlation between the change in $\varepsilon_{\parallel}$ value and the r_{33} value impossible. In the case of the OLD-1 samples, which display very low r_{33} values, and thus very low $\langle\cos^3\theta\rangle$ order, the data is particularly confusing. We limit our discussion to observing that the samples have low r_{33} values and negative $\Delta\varepsilon_{\parallel}$ values after poling, which suggests poor order and likely extensive dipole-dipole

aggregation. Considerably more work is needed on large sample sets with well-defined poling behavior to be able to make any conclusions about the relationship between $\Delta\varepsilon_{ll}$ and r_{33}.

6.4.3 Dielectric Constant of PSLD33. Our final study to date is a rigorous determination of the isotropic dielectric constant (ε, at 1 kHz) of the multichromophore dendrimer, PSLD33 (Figure 6.1),[3,9] which has an active chromophore loading density of 60 wt. %. As discussed previously, ε can have significant effects on the molecular properties and intermolecular interactions, and thus the macroscopic properties, of EO materials. An accurate analysis of these effects was the motivation for this study. The samples were spin-cast from filtered (0.2 μm) 9.5 wt. % solutions of pure PSLD33 dendrimer in 1,1,2-trichloroethane on the patterned ITO/glass substrates prepared using the following spin program: 5s at 500 RPM with an acceleration parameter of 6, followed by 30 s at 850 RPM with an acceleration of 10. These films were initially soft-baked on a hot plate at 85 °C, and then cured overnight in a vacuum oven at 85 °C.

Based upon our previous studies, we identified the major source of error as inaccurate determination of the sample geometries. We therefore independently measured the interior dimensions of each electrode mask using digital calipers. The diameters of the main electrode area varied from 3.24 to 3.47 mm, while the widths of the narrow bridge varied from 0.65 to 0.72 mm. We then identified which mask was used for each sample during the top electrode gold sputtering process. The length of the bridge that overlapped with the bottom ITO electrode was also measured for each sample. We then measured the film thickness via profilometery for each sample. Thus, each sample had completely independently measured geometries, which should enhance

the overall accuracy of the calculated ε values. We estimate the error in ε of each sample at +/- 0.20. The average electrode area was found to be 9.85 $x10^{-6}$ m^2 (9.85 mm^2), which is considerably less than the previously used electrode area of 11.37 x 10^{-6} m^2 (11.37 mm^2).

Table 6.7. Dielectric constant of PSLD33 at 1 kHz

Sample	Area (mm^2)	t (μm)	C (pF)	D	ε[a]
1.1	9.674	1.350	321.6	0.016	5.07
1.2	10.074	1.095	386.9	0.019	4.75
1.3	9.760	1.241	341.3	0.019	4.90
2.1	9.295	1.253	307.4	0.014	4.68
2.2	9.673	1.088	341.1	0.013	4.33
2.3	9.520	1.297	304.0	0.021	4.68
3.2	10.128	1.153	342.7	0.020	4.41
4.1	9.602	1.233	357.5	0.018	5.19
4.2	10.074	1.030	417.9	0.019	4.83
4.3	9.865	1.206	357.6	0.018	4.94
5.3	10.596	1.213	389.1	0.014	5.03
Average	9.85			Average	4.80
Variation of one sample				SD	0.27
4.2	10.074	1.030	418.5	0.018	4.83
4.2	10.074	1.030	410.3	0.02	4.74
4.2	10.074	1.030	414	0.019	4.78
4.2	10.074	1.030	422.3	0.02	4.88
4.2	10.074	1.030	424.4	0.019	4.90
		Average	417.9	0.0192	4.83
		SD	5.808	0.001	0.067

[a]Measured at 1 kHz

After attaching the wires for electrical connection to the LCR meter, the resistance of each sample was checked to ensure good electrical properties. Multiple samples exhibited low resistance values, and these were eliminated from the calculation. All of the remaining samples had resistances at or above the limit of detection (40 MΩ). The samples were then connected to the LCR meter and the C and D values measured. The results are presented in Table 6.7. Despite our efforts, the

samples still yielded ε values with a surprising degree of variation. The large sample size allowed a good statistical average to be taken, resulting in a value of 4.80 +/- 0.27. As another test of the accuracy of our capacitance measurement, we measured the C and D of a single sample, 4.2, several times over a period of several hours.

The ε value determined for PSLD33 has been used to investigate the dielectric effects upon the EO properties in this system. PSLD33 has been extremely well studied by a variety of methods,[3,9] and has been shown to exhibit a poling response r_{33}/E_p of 1.42 +/- 0.04 nm^2/V. This system has also been extensively explored by theoretical methods, including DFT calculations and pseudo-atomistic Monte Carlo statistical mechanics simulations by Dr Bruce Eichinger, Dr. Harrison Rommel, and Prof. Bruce Eichinger (Department of Chemistry, University of Washington).[3] The DFT calculations provide values of the molecular linear and nonlinear properties of the molecules, including the dipole moment (μ), polarizability (α), and the hyperpolarizability (β), all in a vacuum phase environment. Use of the measured ε value allowed these values to be corrected following the methods of Onsager.[17] Although the μ value calculated for chromophores in the vacuum phase (20-30 Debye) are considerably larger than the values measured in solution (~ 13 Debye),[18] this has now been adequately explained by an increase in dipole from the dielectric environment and reaction field, that is then shielded by the dielectric properties of the medium. Taking the dielectric affect on β into account has also resulted in excellent agreement between the calculated and experimental values.[3] The dielectric properties of the medium also shield the chromophores from the applied poling field (E_p), and from the interactions with other chromophore dipole moments. Incorporating these corrections

into the Monte Carlo simulations allows accurate calculation of $\langle\cos^3\theta\rangle$ order parameters as a function of E_p. From these and other properties calculated from first principles, the r_{33}/E_p can then be calculated, using Equation 3.1. The calculated value is 1.4 nm^2/V, which is in excellent agreement with the experimental value. A more detailed analysis of these calculations will be presented elsewhere.[19]

6.5 Conclusions and Future Work

In conclusion, our studies of the dielectric properties of organic EO materials have resulted in a number of significant results. We have demonstrated that the dielectric constant of organic EO films can be readily determined from simple measurements under EO sample relevant conditions. We have also identified the most important contributions to error, and have attempted to reduce these whenever possible. Of particular interest, our experimental result for PSLD33 has finally allowed for excellent agreement to be obtained between experimental EO properties and those calculated using first principles methods. Finally, we have identified a clear correlation between poling induced anisotropy and the calculated $\varepsilon_{\parallel}$ value, which is likely associated with the $\langle\cos^2\theta\rangle$ order of the system. This correlation may provide significant insight into the poling-induced order and the parasitic effects of centrosymmetric dipole-dipole pairs.

Considerably more work is needed to fully characterize the relationship between the poling-induced anisotropy, the dielectric properties, and the r_{33} of EO materials. Towards this end, we propose a comprehensive systematic study of the dielectric

properties of organic EO materials as a function of host identity, EO chromophore identity and loading density, and poling response. Potential hosts to be examined include the APC blend studied here, the DR1-PMMA side-chain polymer, PSLD33 or PSLD41, and discotic chromophores (Chapter 4) such as **SJLD-5**. The best candidates for EO guest chromophores to study would be YLD124 and YLD156, as these are well characterized chromophores with excellent EO properties.[3,9] The loading densities studied should, at a minimum cover the 15-35 % range studied here, and a range of 5-35 % would likely provide even more useful information. In such a study, a large sample would be required to ensure sufficient statistical averaging, and every sample would have all of its properties measured independently, before and after poling, to minimize error. The data provided from such a study would be enormously helpful in analyzing the dependence of dielectric properties on poling-induced anisotropy. Although even more information would be provided if $\varepsilon_{\perp}$ could be measured as well, this is not feasible for our sample configuration, and no simple method of adapting the sample to allow simultaneous measurement of both components exists. An additional variable that might warrant study is the frequency dispersion of the dielectric properties. Although we chose 1 kHz because of its applicability to the EO measurement technique, further information could likely be gained by exploring the response at very low frequencies, in addition to relatively high frequencies.

6.6 Experimental

The APC polymer blend, poly[bisphenol A carbonate-*co*-4,4'-(3,3,5-trimethylcyclohexylidene)diphenol carbonate, was purchased from Sigma-Aldrich and fractionated using THF/methanol, with the medium-low molecular weight fraction being used. The DR1-PMMA side-chain functionalized polymer was purchase from Sigma-Aldrich and used without further purification. The PSLD-33 dendrimer was obtained from Dr. Philip Sullivan in the Dalton Group (Department of Chemistry, University of Washington)[3,9] and verified to be pure before use. All other organic EO materials used in these studies were obtained as already-prepared thin films from Dr. Philip Sullivan, Dr. Olivier Clot, and Benjamin Olbricht in the Dalton Group (Department of Chemistry, University of Washington).

Samples were spin-cast on a Laurell WS-400A-6NPP/LITE spin coater with the specified spin program. Commercial ITO coated glass slides were half-etched using a chemically resistant tape in 36 N hydrochloric acid, washed with the water, and then sonicated in *i*-propanol and acetone respectively for 5 min. each. The slides were additionally cleaned immediately before depositing the chromophore solution with isopropanol and acetone at 5000 RPM. Top gold electrodes were deposited through a mask in a Denton Desk II Sputtering system. The dimensions of the masks were measured using digital calipers. Sample thicknesses were measured on a Sloan Dektak 3030 Profilometer. Capacitance and dissipation measurements were performed with a BK Precision Model 885 Synthesized In-Circuit LCR/ESR Meter. EO characterization was performed on an *in situ* simple reflection apparatus at 1300 nm.[3,9]

Notes to Chapter 6

(1) Kim, T.-D.; Kang, J.-W.; Luo, J.; Jang, S.-H.; Ka, J.-W.; Tucker, N.; Benedict, J. B.; Dalton, L. R.; Gray, T.; Overney, R. M.; Park, D. H.; Herman, W. N.; Jen, A. K. Y. Ultralarge and thermally stable electro-optic activities from supramolecular self-assembled molecular glasses. *J. Am. Chem. Soc.* **2007**, *129*, 488-489.

(2) Kim, T.-D.; Luo, J.; Ka, J.-W.; Hau, S.; Tian, Y.; Shi, Z.; Tucker, N. M.; Jang, S.-H.; Kang, J.-W.; Jen, A. K. Y. Ultralarge and thermally stable electro-optic activities from diels-alder crosslinkable polymers containing binary chromophore systems. *Adv. Mater.* **2006**, *18*, 3038-3042.

(3) Sullivan, P. A., University of Washington, 2006.

(4) Eichinger, B., Department of Chemistry, University of Washington, unpublished results

(5) Ostinelli, O., ETH, 2000.

(6) Bale, D., Department of Chemistry, University of Washington, unpublished results

(7) Maier, W.; Meier, G. A simple theory of the dielectric characteristics of homogeneous oriented crystalline-liquid phases of the nematic type. *Z. Naturforsch.* **1961**, *16a*, 262-267.

(8) Maier, W.; Meier, G. The principal dielectric constants of homogeneously oriented liquid-crystal phase of p,p'-azoxyanisole. *Z. Naturforsch.* **1961**, *16a*, 470-477.

(9) Sullivan, P. A.; Akelaitis, A. J. P.; Lee, S. K.; McGrew, G.; Lee, S. K.; Choi, D. H.; Dalton, L. R. Novel dendritic chromophores for electro-optics: Influence of binding mode and attachment flexibility on electro-optic behavior. *Chem. Mater.* **2006**, *18*, 344-351.

(10) see ASTM D1531

(11) Chen, A., Applied Physics Laboratory, University of Washington, personal communication

(12) Dielectric constant and material obtained from Sigma-Aldrich

(13) Purchased from Sigma-Aldrich

(14) Dalton, L. R.; Harper, A. W.; Robinson, B. H. The role of london forces in defining noncentrosymmetric order of high dipole moment-high hyperpolarizability chromophores in electrically poled polymeric thin films. *Proc. Natl. Acad. Sci. U. S. A.* **1997**, *94*, 4842-4847.

(15) Robinson, B. H.; Dalton, L. R. Monte carlo statistical mechanical simulations of the competition of intermolecular electrostatic and poling-field interactions in defining macroscopic electro-optic activity for organic chromophore/polymer materials. *J. Phys. Chem. A* **2000**, *104*, 4785-4795.

(16) Clot, O.; Firestone, K. A.; Hammond, S.; Sinness, J.; Carlson, B.; Phelan, G.; Bale, D.; Lao, D. B.; Robinson, B. H.; Reid, P. J.; Dalton, L. R.; Universty of Washington, 2007.

(17) Onsager, L. Electric moments of molecules in liquids. *J. Am. Chem. Soc.* **1936**, *58*, 1486-1493.

(18) Wang, F., University of Southern California.

(19) Sullivan, P. A.; Rommel, H. L.; Eichinger, B. E.; Robinson, B. H.; Hammond, S.; Bale, D.; University of Washington, 2007.

Bibliography

(1) Abbott, D. J.; Colonna, S.; Stirling, C. J. M. Elimination and addition reactions. Part xxvi. Asymmetric induction in additions of nucleophiles and electrophiles to a,b-unsaturated sulfoxides. *J. Chem. Soc., Perkin Trans. 1* **1976**, 492-498.

(2) Alain, V.; Fort, A.; Barzoukas, M.; Chen, C.-T.; Blanchard-Desce, M.; Marder, S. R.; Perry, J. W. The linear and non-linear optical properties of some conjugated ferrocene compounds with potent heterocyclic acceptors. *Inorg. Chim. Acta* **1996**, *242*, 43-49.

(3) Albota, M.; Beljonne, D.; Bredas, J. L.; Ehrlich, J. E.; Fu, J. Y.; Heikal, A. A.; Hess, S. E.; Kogej, T.; Levin, M. D.; Marder, S. R.; McCord-Maughon, D.; Perry, J. W.; Rockel, H.; Rumi, M.; Subramaniam, G.; Webb, W. W.; Wu, X. L.; Xu, C. Design of organic molecules with large two-photon absorption cross sections. *Science* **1998**, *281*, 1653-1656.

(4) Annoni, E.; Pizzotti, M.; Ugo, R.; Quici, S.; Morotti, T.; Bruschi, M.; Mussini, P. Synthesis, electronic characterisation and significant second-order non-linear optical responses of meso-tetraphenylporphyrins and their zn(ii) complexes carrying a push or pull group in the beta pyrrolic position. *Eur. J. Inorg. Chem.* **2005**, *2005*, 3857-3874.

(5) Aoki, K.; Kondo, J.; Kondo, A.; Mori, T.; Mizuno, Y.; Shimodaira, S.; Imaeda, M.; Kozuka, Y.; Mitomi, O.; Minakata, M. High-performance optical modulator with a wide center electrode and thin x-cut linbo3 substrate. *IEEE Photonic Tech. Lett.* **2004**, *16*, 2610-2612.

(6) Argaman, N.; Makov, G. Density functional theory: An introduction. *Am. J. Phys.* **2000**, *68*, 69-79.

(7) Ashwell, G. J. Langmuir-blodgett films: Molecular engineering of non-centrosymmetric structures for second-order nonlinear optical applications. *J. Mater. Chem.* **1999**, *9*, 1991-2003.

(8) Baehr-Jones, T.; Hochberg, M.; Wang, G.; Lawson, R.; Liao, Y.; Sullivan, P. A.; Dalton, L.; Jen, A. K. Y.; Scherer, A. Optical modulation and detection in slotted silicon waveguides. *Opt. Express* **2005**, *13*, 5216-5226.

(9) Bai, Y.; Song, N.; Gao, J. P.; Sun, X.; Wang, X.; Yu, G.; Wang, Z. Y. A new approach to highly electrooptically active materials using cross-linkable, hyperbranced chromophore-containing oligomers as a macromolecular dopant. *J. Am. Chem. Soc.* **2005**, *127*, 2060-2061.

(10) Bailey, R. T.; Cruickshank, F. R.; Pavlides, P.; Pugh, D.; Sherwood, J. N. Organic materials for nonlinear optics: Interrelationships between molecular properties, crystal structure, and optical properties. *J. Phys. D: Appl. Phys.* **1991**, *24*, 135-145.

(11) Bartholomew, G. P.; Ledoux, I.; Mukamel, S.; Bazan, G. C.; Zyss, J. Three-dimensional nonlinear optical chromophores based on through-space delocalization. *J. Am. Chem. Soc.* **2002**, *124*, 13480-13485.

(12) Bergman, J. G.; McFee, J. H.; Crane, G. R. Pyroelectricity and optical second harmonic generation in poly(vinylidene fluoride) films. *Appl. Phys. Lett.* **1971**, *18*, 203-205.

(13) Bethea, C. G. Experimental technique of d.C. Induced shg [second harmonic generation] in liquids. Measurement of the nonlinearity of diiodomethane. *Appl. Opt.* **1975**, *14*, 1447-1451.

(14) Bhatambrekar, N.; Hammond, S.; Sinness, J.; Clot, O.; Rommel, H.; Chen, A.; Robinson, B.; Jen, A. K. Y.; Dalton, L. Highly ordered pseudo-discotic chromophore systems for electro-optic materials and devices. *Mater. Res. Soc. Symp. Proc.* **2005**, *846*, 115-120.

(15) Bhatambrekar, N. P.; Dalton, L.; Luo, J.; Jen, A. K. Y.; Chen, A. Third-order nonlinearity contribution to electro-optic activity in polymer materials in a constant bias field. *Appl. Phys. Lett.* **2006**, *88*, 041115/041111-041115/041113.

(16) Blanchard-Desce, M.; Baudin, J.-B.; Jullien, L.; Lorne, R.; Ruel, O.; Brasselet, S.; Zyss, J. Towards highly efficient nonlinear optical chromophores: Molecular engineering of octupolar molecules. *Opt. Mater.* **1999**, *12*, 333-338.

(17) Boldt, P.; Eisenträger, T.; Glania, C.; Göldenitz, J.; Krämer, P.; Matschiner, R.; Rase, J.; Schwesinger, R.; Wichern, J.; Wortmann, R. Guanidyl and phosphoraniminyl substituents: New electron donors in second-order nonlinear optical chromophores. *Adv. Mater.* **1996**, *8*, 672-675.

(18) Bortnik, B.; Hung, Y.-C.; Tazawa, H.; Seo, B.-J.; Luo, J.; Jen, A. K. Y.; Steier, W. H.; Fetterman, H. R. Electrooptic polymer ring resonator modulation up to 165 ghz. *IEEE J. Sel. Top. Quantum Electron.* **2007**, *13*, 104-110.

(19) Bosshard, C.; Knopfle, G.; Pretre, P.; Gunter, P. Second-order polarizabilities of nitropyridine derivatives determined with electric-field-induced second-harmonic generation and a solvatochromic method: A comparative study. *J. Appl. Phys.* **1992**, *71*, 1594-1605.

(20) Bourhill, G.; Bredas, J.-L.; Cheng, L.-T.; Marder, S. R.; Meyers, F.; Perry, J.

W.; Tiemann, B. G. Experimental demonstration of the dependence of the first hyperpolarizability of donor-acceptor-substituted polyenes on the ground-state polarization and bond length alternation. *J. Am. Chem. Soc.* **1994**, *116*, 2619-2620.

(21) Breitung, E. M.; Vaughan, W. E.; McMahon, R. J. Measurement of solute dipole moments in dilute solution: A simple three-terminal cell. *Rev. Sci. Instrum.* **2000**, *71*, 224-227.

(22) Brooker, L. G. S.; Sprague, R. H.; Smyth, C. P.; Lewis, G. L. Color and constitution. I. Halochromism of anhydronium bases related to the cyanine dyes. *J. Am. Chem. Soc.* **1940**, *62*, 1116-1125.

(23) Burke, K.; Werschnik, J.; Gross, E. K. U. Time-dependent density functional theory: Past, present, and future. *J. Chem. Phys.* **2005**, *123*, 062206-062209.

(24) Bushby, R. J.; Lozman, O. R. Discotic liquid crystals 25 years on. *Curr. Opin. Colloid Interface Sci.* **2002**, *7*, 343-354.

(25) Cai, C.; Bosch, M. M.; Tao, Y.; Muller, B.; Gan, Z.; Kundig, A.; Bosshard, C.; Liakatas, I.; Jager, M.; Gunter, P. Self-assembly in ultrahigh vacuum: Growth of organic thin films with a stable in-plane directional order. *J. Am. Chem. Soc.* **1998**, *120*, 8563-8564.

(26) Chalupczak, W.; Fiorini, C.; Charra, F.; Nunzi, J.-M.; Raimond, P. Efficient all-optical poling of an azo-dye copolymer using a low power laser. *Opt. Commun.* **1996**, *126*, 103-107.

(27) Chandrasekhar, S.; Sadashiva, B. K.; Suresh, K. A. Liquid crystals of disc-like molecules. *Pramana* **1977**, *9*, 471-480.

(28) Chemla, D. S.; Zyss, J. *Nonlinear optical properties of organic molecules and crystals*; Academic: New York, 1987; Vol. 1.

(29) Chen, A.; Dalton, L.; Sherwood, T.; Jen, A. K.; Rabiei, P.; Steier, W.; Huang, Y.; Paloczi, G. T.; Poon, J. K. S.; Scherer, A.; Yariv, A. All-organic and organic-silicon photonic ring micro-resonators. *Proc. SPIE* **2005**, *5708*, 187-197.

(30) Chen, D.; Fetterman, H. R.; Chen, A.; Steier, W. H.; Dalton, L. R.; Wang, W.; Shi, Y. Demonstration of 110 ghz electro-optic polymer modulators. *Appl. Phys. Lett.* **1997**, *70*, 3335-3337.

(31) Cheng, Y. J.; Luo, J.; Hau, S.; Bale, D. H.; Kim, T. D.; Shi, Z.; Lao, D. B.; Tucker, N. M.; Tian, Y.; Dalton, L. R.; Reid, P. J.; Jen, A. K. Y. Large electro-

optic activity and enhanced thermal stability from diarylaminophenyl-containing high-beta nonlinear optical chromophores. *Chem. Mater.* **2007**, *19*, 1154-1163.

(32) Chollet, P. A.; Gadret, G.; Kajzar, F.; Raimond, P. Electro-optic coefficient determination in stratified organized molecular thin films: Application to poled polymers. *Thin Solid Films* **1994**, *242*, 132-138.

(33) Clare, A. G. Photonics: A light introduction. *Am. Ceram. Soc. Bull.* **2003**, *82*, 17-22.

(34) Clays, K.; Persoons, A. Hyper-rayleigh scattering in solution. *Phys. Rev. Lett.* **1991**, *66*, 2980.

(35) Clays, K.; Persoons, A. Hyper-rayleigh scattering in solution. *Rev. Sci. Instrum.* **1992**, *63*, 3285-3289.

(36) Clays, K.; Schildkraut, J. S. Dispersion of the complex electrooptic coefficient and electrochromic effects in poled polymer films. *J. Opt. Soc. Am. B: Opt. Phys.* **1992**, *9*, 2274-2282.

(37) Clot, O.; Firestone, K. A.; Hammond, S.; Sinness, J.; Carlson, B.; Phelan, G.; Bale, D.; Lao, D. B.; Robinson, B. H.; Reid, P. J.; Dalton, L. R.; Universty of Washington, 2007.

(38) Coe Benjamin, J.; Harris James, A.; Brunschwig Bruce, S.; Asselberghs, I.; Clays, K.; Garin, J.; Orduna, J. Three-dimensional nonlinear optical chromophores based on metal-to-ligand charge-transfer from ruthenium(ii) or iron(ii) centers. *J. Am. Chem. Soc.* **2005**, *127*, 13399-13410.

(39) Dalton, L.; Scherer, A.; Chen, A.; Jen, A.; Reid, P.; Robinson, B.; Eichinger, B.; Hochberg, M.; Baehr-Jones, T.; Pyajt, A.; Takayesu, J.; Sullivan, P.; Akelaitis, A.; Lawson, R.; Bale, D.; Haller, M.; Luo, J.; Liu, S.; Liao, Y.; Firestone, K.; Bhattacharjee, S.; Sinness, J.; Hammond, S.; Sgro, A.; Buker, N.; Snoeberger, R.; Lingwood, M.; Steier, W. Organic electro-optic glasses for wdm applications. *Proc. SPIE* **2005**, *6014*, 60140P/60141-60140P/60115.

(40) Dalton, L. D. Nonlinear optical polymeric materials: From chromophore design to commercial applications. In *Polymers for photonics applications i*; Springer Berlin: Heidelberg, 2002; Vol. 158; pp 1-86.

(41) Dalton, L. R.; Harper, A. W.; Ghosn, R.; Steier, W. H.; Ziari, M.; Fetterman, H.; Shi, Y.; Mustacich, R. V.; Jen, A. K. Y.; Shea, K. J. Synthesis and processing of improved organic second-order nonlinear optical materials for applications in photonics. *Chem. Mater.* **1995**, *7*, 1060-1081.

(42) Dalton, L. R.; Harper, A. W.; Robinson, B. H. The role of london forces in defining noncentrosymmetric order of high dipole moment-high hyperpolarizability chromophores in electrically poled polymeric thin films. *Proc. Natl. Acad. Sci. U. S. A.* **1997**, *94*, 4842-4847.

(43) Dao, P. T.; Williams, D. J. Constant current corona charging as a technique for poling organic nonlinear optical thin films and the effect of ambient gas. *J. Appl. Phys.* **1993**, *73*, 2043-2050.

(44) Delgado, M. C. R.; Hernåndez, V.; Casado, J.; Navarrete, J.; Raimundo, J.-M.; Blanchard, P.; Roncali, J. Vibrational and quantum-chemical study of push-pull chromophores for second-order nonlinear optics from rigidified thiophene-based pi-conjugating spacers. *Chem. Eur. J.* **2003**, *9*, 3670-3682.

(45) Demus, D.; Goodby, J.; Gray, G. W.; Spiess, H.-W.; Vill, V. *Handbook of liquid crystals*; Wiley-VCH: New York, 1998; Vol. 1.

(46) Demus, D.; Goodby, J.; Gray, G. W.; Spiess, H.-W.; Vill, V. *Handbook of liquid crystals*; Wiley-VCH: New York, 1998; Vol. 2A.

(47) Demus, D.; Richter, L. *Textures of liquid crystals*; Verlag Chemie: New York, 1978.

(48) DeRosa, M. E.; He, M.; Cites, J. S.; Garner, S. M.; Tang, Y. R. Photostability of high beta electro-optic chromophores at 1550 nm. *J. Phys. Chem. A* **2004**, *108*, 8725-8730.

(49) Diaz, J. L.; Dobarro, A.; Villacampa, B.; Velasco, D. Structure and optical properties of 2,3,7,9-polysubstituted carbazole derivatives. Experimental and theoretical studies. *Chem. Mater.* **2001**, *13*, 2528-2536.

(50) Diaz, J. L.; Villacampa, B.; Lopez-Calahorra, F.; Velasco, D. Experimental and theoretical study of a new class of acceptor group in chromophores for nonlinear optics: 2-substituted 4-methylene-4-h-oxazol-5-ones. *Chem. Mater.* **2002**, *14*, 2240-2251.

(51) Dimitrakopoulos, C. D.; Malenfant, P. R. L. Organic thin film transistors for large area electronics. *Adv. Mater.* **2002**, *14*, 99-117.

(52) Donat-Bouillud, A.; Levesque, I.; Tao, Y.; D'Iorio, M.; Beaupre, S.; Blondin, P.; Ranger, M.; Bouchard, J.; Leclerc, M. Light-emitting diodes from fluorene-based pi-conjugated polymers. *Chem. Mater.* **2000**, *12*, 1931-1936.

(53) Donval, A.; Toussaere, E.; Brasselet, S.; Zyss, J. Comparative assessment of

electrical, photoassisted and all optical in-plane poling of polymer based electrooptic modulators. *Opt. Mater.* **1999**, *12*, 215-219.

(54) Drobizhev, M.; Karotki, A.; Dzenis, Y.; Rebane, A.; Suo, Z.; Spangler, C. W. Strong cooperative enhancement of two-photon absorption in dendrimers. *J. Phys. Chem. B* **2003**, *107*, 7540-7543.

(55) Dubois, A.; Canva, M.; Brun, A.; Chaput, F.; Boilot, J.-P. Photostability of dye molecules trapped in solid matrixes. *Appl. Opt.* **1996**, *35*, 3193-3199.

(56) Eldada, L.; Shacklette, L. W. Advances in polymer integrated optics. *IEEE J. Sel. Top. Quantum Electron.* **2000**, *6*, 54-68.

(57) Facchetti, A.; Abbotto, A.; Beverina, L.; van der Boom, M. E.; Dutta, P.; Evmenenko, G.; Marks, T. J.; Pagani, G. A. Azinium-p-bridge-pyrrole nlo-phores: Influence of heterocycle acceptors on chromophoric and self-assembled thin-film properties. *Chem. Mater.* **2002**, *14*, 4996-5005.

(58) Facchetti, A.; Abbotto, A.; Beverina, L.; van der Boom, M. E.; Dutta, P.; Evmenenko, G.; Pagani, G. A.; Marks, T. J. Layer-by-layer self-assembled pyrrole-based donor-acceptor chromophores as electro-optic materials. *Chem. Mater.* **2003**, *15*, 1064-1072.

(59) Facchetti, A.; Annoni, E.; Beverina, L.; Morone, M.; Zhu, P.; Marks, T. J.; Pagani, G. A. Very large electro-optic responses in h-bonded heteroaromatic films grown by physical vapor deposition. *Nat. Mater.* **2004**, *3*, 910-917.

(60) Fazludeen, R.; Barai, S.; Pattnaik, P. K.; Srinivas, T.; Selvarajan, A. A novel technique to measure the propagation loss of integrated optical waveguides. *IEEE Photonic Tech. Lett.* **2005**, *17*, 360-362.

(61) Finn, R. S.; Ward, J. F. Measurements of hyperpolarizabilities for some halogenated methanes. *J. Chem. Phys.* **1974**, *60*, 454-458.

(62) Firestone, K. A., University, 2005.

(63) Furniss, B. S.; Hannaford, A. J.; G., S. P. W.; Tatchell, A. R. *Vogel's textbook of practical organic chemistry*; Addison Wesley Longman: Singapore, 1989.

(64) Galvan-Gonzalez, A.; Belfield, K. D.; Stegeman, G. I.; Canva, M.; Chan, K. P.; Park, K.; Sukhomlinova, L.; Twieg, R. J. Photostability enhancement of an azobenzene photonic polymer. *Appl. Phys. Lett.* **2000**, *77*, 2083-2085.

(65) Galvan-Gonzalez, A.; Belfield, K. D.; Stegeman, G. I.; Canva, M.; Marder, S. R.; Staub, K.; Levina, G.; Twieg, R. J. Photodegradation of selected p-

conjugated electrooptic chromophores. *J. Appl. Phys.* **2003**, *94*, 756-763.

(66) Galvan-Gonzalez, A.; Canva, M.; Stegeman, G. I.; Twieg, R.; Kowalczyk, T. C.; Lackritz, H. S. Effect of temperature and atmospheric environment on the photodegradation of disperse red 1-type polymers. *Opt. Lett.* **1999**, *24*, 1741-1743.

(67) Galvan-Gonzalez, A.; Stegeman, G. I.; Jen, A. K. Y.; Wu, X.; Canva, M.; Kowalczyk, A. C.; Zhang, X. Q.; Lackritz, H. S.; Marder, S.; Thayumanavan, S.; Levina, G. Photostability of electro-optic polymers possessing chromophores with efficient amino donors and cyano-containing acceptors. *J. Opt. Soc. Am. B: Opt. Phys.* **2001**, *18*, 1846-1853.

(68) Gan, H.; Zhang, H.; DeRose, C. T.; Norwood, R. A.; Fallahi, M.; Luo, J.; Jen, A. K. Y.; Liu, B.; Ho, S.-T.; Peyghambarian, N. Hybrid fabry-perot etalon using an electro-optic polymer for optical modulation. *Appl. Phys. Lett.* **2006**, *89*, 141113/141111-141113/141113.

(69) Goldoni, F.; Langeveld-Voss, B. M. W.; Meijer, E. W. Convenient synthesis of 3,4-bis(alkylthio) thiophenes. *Synth. Commun.* **1998**, *28*, 2237 - 2244.

(70) Gonzalez, M.; Segura, J. L.; Seoane, C.; Martin, N.; Garin, J.; Orduna, J.; Alcala, R.; Villacampa, B.; Hernandez, V.; LopezNavarrete, J. T. Tetrathiafulvalene derivatives as nlo-phores: Synthesis, electrochemistry, raman spectroscopy, theoretical calculations, and nlo properties of novel ttf-derived donor-pi-acceptor dyads. *J. Org. Chem.* **2001**, *66*, 8872-8882.

(71) Gray, T.; Overney, R. M.; Haller, M.; Luo, J.; Jen, A. K. Y. Low temperature relaxations and effects on poling efficiencies of dendronized nonlinear optical side-chain polymers. *Appl. Phys. Lett.* **2005**, *86*, 211908-211903.

(72) Groenendaal, L.; Jonas, F.; Freitag, D.; Pielartzik, H.; Reynolds, J. R. Poly(3,4-ethylenedioxythiophene) and its derivatives: Past, present, and future. *Adv. Mater.* **2000**, *12*, 481-494.

(73) Grover, R.; Van, V.; Ibrahim, T. A.; Absil, P. P.; Calhoun, L. C.; Johnson, F. G.; Hryniewicz, J. V.; Ho, P. T. Parallel-cascaded semiconductor microring resonators for high-order and wide-fsr filters. *J. Lightwave Technol.* **2002**, *20*, 900-905.

(74) Haller, M.; Luo, J.; Li, H.; Kim, T.-D.; Liao, Y.; Robinson, B. H.; Dalton, L. R.; Jen, A. K.-Y. A novel lattice-hardening process to achieve highly efficient and thermally stable nonlinear optical polymers. *Macromolecules* **2004**, *37*, 688-690.

(75) Hammond, S. R.; Sinness, J.; Clot, O.; Dalton, L. R. Characterization of a series

of molecularly engineered discotic electro-optic chromophores. *Polym. Prepr. (Am. Chem. Soc., Div. Polym. Chem.)* **2006**, *47*, 985-986.

(76) Han, S. H.; Wu, J. W. Single-beam polarization interferometry measurement of the linear electro-optic effect in poled polymer films with a reflection configuration. *J. Opt. Soc. Am. B: Opt. Phys.* **1997**, *14*, 1131-1137.

(77) Hayden, L. M.; Sauter, G. F.; (Unisys Corporation, USA). Application: US US, 1991; pp No pp given.

(78) Hehre, W. J.; Radom, L.; Schleyer, P. R.; Pople, J. A. *Ab initio molecular orbital theory*; Wiley Interscience: New York, 1986.

(79) Hochberg, M.; Baehr-Jones, T.; Wang, G.; Shearn, M.; Harvard, K.; Luo, J.; Chen, B.; Shi, Z.; Lawson, R.; Sullivan, P.; Jen, A. K. Y.; Dalton, L.; Scherer, A. Terahertz all-optical modulation in a silicon-polymer hybrid system. *Nat. Mater.* **2006**, *5*, 703-709.

(80) Hohenberg, P.; Kohn, W. Inhomogeneous electron gas. *Phys. Rev.* **1964**, *136*, B864.

(81) Hsu, C.-C.; Liu, S.; Wang, C. C.; Wang, C. H. Dispersion of the first hyperpolarizability of a strongly charge-transfer chromophore investigated by tunable wavelength hyper-rayleigh scattering. *J. Chem. Phys.* **2001**, *114*, 7103-7108.

(82) Huang, D.; Chen, B.; (USA). Application: US US, 2004; pp 23 pp , Cont -in-part of U S Ser No 395,610.

(83) Huang, D.; Zhang, C.; Dalton, L. R.; Weber, W. P. Synthesis and characterization of main-chain nlo oligomers and polymer that contain 4-dialkylamino-4'(alkylsulfonyl)azobenzene chromophores. *J. Polym. Sci., Part A: Polym. Chem.* **2000**, *38*, 546-559.

(84) Huang, Y.; Paloczi, G. T.; Yariv, A.; Zhang, C.; Dalton, L. R. Fabrication and replication of polymer integrated optical devices using electron-beam lithography and soft lithography. *J. Phys. Chem. B* **2004**, *108*, 8606-8613.

(85) Janowska, I.; Zakrzewski, J.; Nakatani, K.; Delaire, J. A.; Palusiak, M.; Walak, M.; Scholl, H. Ferrocenyl d-[pi]-a chromophores containing 3-dicyanomethylidene-1-indanone and 1,3-bis(dicyanomethylidene)indane acceptor groups. *J. Organomet. Chem.* **2003**, *675*, 35-41.

(86) Jiang, Y.; Cao, Z.; Shen, Q.; Dou, X.; Chen, Y.; Ozaki, Y. Improved attenuated-total-reflection technique for measuring the electro-optic coefficients of

nonlinear optical polymers. *J. Opt. Soc. Am. B: Opt. Phys.* **2000**, *17*, 805-808.

(87) Kang, S. H.; Luo, J.; Ma, H.; Barto, R. R.; Frank, C. W.; Dalton, L. R.; Jen, A. K.-Y. A hyperbranched aromatic fluoropolyester for photonic applications. *Macromolecules* **2003**, *36*, 4355-4359.

(88) Katti, K. V.; Raghuraman, K.; Pillarsetty, N.; Karra, S. R.; Gulotty, R. J.; Chartier, M. A.; Langhoff, C. A. First examples of azaphosphanes as efficient electron donors in the chemical architecture of thermally stable new nonlinear optical materials. *Chem. Mater.* **2002**, *14*, 2436-2438.

(89) Kay, A. J.; Woolhouse, A. D.; Gainsford, G. J.; Haskell, T. G.; Barnes, T. H.; McKinnie, I. T.; Wyss, C. P. A simple, novel method for the preparation of polymer-tetherable, zwitterionic merocyanine nlo-chromophores. *J. Mater. Chem.* **2001**, *11*, 996-1002.

(90) Kerr, J. *Philos. Mag.* **1875**, *50*, 337.

(91) Kim, M.-s.; Ju, J. J.; Park, S. K.; Do, J. Y.; Lee, M.-H. Evaluation of nonlinear optical polymers for second-harmonic generation: Toward the balance of absorption and nonlinearity against intrinsic trade-off. *Chem. Phys. Lett.* **2006**, *417*, 277-281.

(92) Kim, T.-D.; Kang, J.-W.; Luo, J.; Jang, S.-H.; Ka, J.-W.; Tucker, N.; Benedict, J. B.; Dalton, L. R.; Gray, T.; Overney, R. M.; Park, D. H.; Herman, W. N.; Jen, A. K. Y. Ultralarge and thermally stable electro-optic activities from supramolecular self-assembled molecular glasses. *J. Am. Chem. Soc.* **2007**, *129*, 488-489.

(93) Kim, T.-D.; Luo, J.; Ka, J.-W.; Hau, S.; Tian, Y.; Shi, Z.; Tucker, N. M.; Jang, S.-H.; Kang, J.-W.; Jen, A. K. Y. Ultralarge and thermally stable electro-optic activities from diels-alder crosslinkable polymers containing binary chromophore systems. *Adv. Mater.* **2006**, *18*, 3038-3042.

(94) Koch, A. T. H.; Fridrikh, S. V.; Warner, M.; Schwarzwalder, C. E.; Moratti, S. C.; Friend, R. H. Second order nonlinear optical response of nematic liquid crystalline main chain polymers. *Synth. Met.* **1999**, *101*, 244-245.

(95) Kouwer, P. H. J.; Jager, W. F.; Mijs, W. J.; Picken, S. J. Specific interactions in discotic liquid crystals. *J. Mater. Chem.* **2003**, *13*, 458-469.

(96) Krishnamoorthy, K.; Ambade, A. V.; Kanungo, M.; Contractor, A. Q.; Kumar, A. Rational design of an electrochromic polymer with high contrast in the visible region: Dibenzyl substituted poly(3,4-propylenedioxythiophene). *J.*

Mater. Chem. **2001**, *11*, 2909-2911.

(97) Kumar, A.; Welsh, D. M.; Morvant, M. C.; Piroux, F.; Abboud, K. A.; Reynolds, J. R. Conducting poly(3,4-alkylenedioxythiophene) derivatives as fast electrochromics with high-contrast ratios. *Chem. Mater.* **1998**, *10*, 896-902.

(98) Kurtz, S. K.; Perry, T. T. Powder technique for the evaluation of nonlinear optical materials. *J. Appl. Phys.* **1968**, *39*, 3798-3813.

(99) Kwon, O. P.; Ruiz, B.; Choubey, A.; Mutter, L.; Schneider, A.; Jazbinsek, M.; Gramlich, V.; Guenter, P. Organic nonlinear optical crystals based on configurationally locked polyene for melt growth. *Chem. Mater.* **2006**, *18*, 4049-4054.

(100) Kwon, S.-J.; Kwon, O. P.; Jazbinsek, M.; Gramlich, V.; Gunter, P. Nonlinear optical co-crystal of analogous polyene chromophores with tailored physical properties. *Chem. Commun.* **2006**, 3729-3731.

(101) Lee, J. W.; Wang, C. S.; Song, H. H.; Price, G. E. Void formation in coagulated rigid-rod polymer thin films. *Polymer* **1995**, *36*, 955-958.

(102) Lee, R. W. Linear electro-optic (pockels) effect in hexamethylenetetramine: Influence of crystal strain. *J. Opt. Soc. Am.* **1969**, *59*, 1574-1580.

(103) Lee, S.-H.; Balasubramanian, S.; Kim, D. Y.; Viswanathan, N. K.; Bian, S.; Kumar, J.; Tripathy, S. K. Azo polymer multilayer films by electrostatic self-assembly and layer-by-layer post azo functionalization. *Macromolecules* **2000**, *33*, 6534-6540.

(104) Lehmann, F.; Mohr, G. J.; Grummt, U. W. Synthesis and structure-property relationships of amphiphilic acidochromic hydroxystilbazolium dyes. *Sens. Actuators, B* **1997**, *39*, 229-234.

(105) Lemaitre, N.; Attias, A. J.; Ledoux, I.; Zyss, J. New second-order nlo chromophores based on 3,3'-bipyridine: Tuning of liquid crystal and nlo properties. *Chem. Mater.* **2001**, *13*, 1420-1427.

(106) Levine, B. F. Conjugated electron contributions to the second order hyperpolarizability of substituted benzene molecules. *J. Chem. Phys.* **1975**, *63*, 115-117.

(107) Levine, B. F. Donor--acceptor charge transfer contributions to the second order hyperpolarizability. *Chem. Phys. Lett.* **1976**, *37*, 516-520.

(108) Levine, B. F.; Bethea, C. G. Molecular hyperpolarizabilities determined from

conjugated and nonconjugated organic liquids. *Appl. Phys. Lett.* **1974**, *24*, 445-447.

(109) Levine, B. F.; Bethea, C. G.; Thurmond, C. D.; Lynch, R. T.; Bernstein, J. L. An organic crystal with an exceptionally large optical second-harmonic coefficient: 2-methyl-4-nitroaniline. *J. Appl. Phys.* **1979**, *50*, 2523-2527.

(110) Liang, Z.; Yang, Z.; Sun, S.-S.; Wu, B.; Dalton, L. R.; Garner, S. M.; Kalluri, S.; Chen, A.; Steier, W. H. Processible and thermally stable heterocyclic polymers for second-order nonlinear optical studies. *Chem. Mater.* **1996**, *8*, 2681-2685.

(111) Liao, Y.; Anderson, C. A.; Sullivan, P. A.; Akelaitis, A. J. P.; Robinson, B. H.; Dalton, L. R. Electro-optical properties of polymers containing alternating nonlinear optical chromophores and bulky spacers. *Chem. Mater.* **2006**, *18*, 1062-1067.

(112) Liao, Y.; Bhattacharjee, S.; Firestone, K. A.; Eichinger, B. E.; Paranji, R.; Anderson, C. A.; Robinson, B. H.; Reid, P. J.; Dalton, L. R. Antiparallel-aligned neutral-ground-state and zwitterionic chromophores as a nonlinear optical material. *J. Am. Chem. Soc.* **2006**, *128*, 6847-6853.

(113) Liao, Y.; Eichinger, B. E.; Firestone, K. A.; Haller, M.; Luo, J.; Kaminsky, W.; Benedict, J. B.; Reid, P. J.; Jen, A. K. Y.; Dalton, L. R.; Robinson, B. H. Systematic study of the structure-property relationship of a series of ferrocenyl nonlinear optical chromophores. *J. Am. Chem. Soc.* **2005**, *127*, 2758-2766.

(114) Lin, W.; Lin, W.; Wong, G. K.; Marks, T. J. Supramolecular approaches to second-order nonlinear optical materials. Self-assembly and microstructural characterization of intrinsically acentric [(aminophenyl)azo]pyridinium superlattices. *J. Am. Chem. Soc.* **1996**, *118*, 8034-8042.

(115) Lindsay, G. A.; Roberts, M. J.; Chafin, A. P.; Hollins, R. A.; Merwin, L. H.; Stenger-Smith, J. D.; Yee, R. Y.; Zarras, P.; Wynne, K. J. Ordered films by alternating polyelectrolyte deposition of cationic side chain and anionic main chain chromophoric polymers. *Chem. Mater.* **1999**, *11*, 924-929.

(116) Lipscomb, G. F.; Garito, A. F.; Narang, R. S. A large linear electrooptic effect in a polar organic crystal 2-methyl-4-nitroaniline. *Appl. Phys. Lett.* **1981**, *38*, 663-665.

(117) Liu, S.; Haller, M. A.; Ma, H.; Dalton, L. R.; Jang, S.-H.; Jen, A. K. Y. Focused microwave-assisted synthesis of 2,5-dihydrofuran derivatives as electron acceptors for highly efficient nonlinear optical chromophores. *Adv. Mater.* **2003**, *15*, 603-607.

(118) Lu, J.; Yin, J. Synthesis and characterization of photocrosslinkable, side-chain, second-order nonlinear optical poly(ester imide)s with great film-forming ability and long-term dipole orientation stability. *J. Polym. Sci., Part A: Polym. Chem.* **2002**, *41*, 303-312.

(119) Luo, J.; Cheng, Y.-J.; Kim, T.-D.; Hau, S.; Jang, S.-H.; Shi, Z.; Zhou, X.-H.; Jen, A. K. Y. Facile synthesis of highly efficient phenyltetraene-based nonlinear optical chromophores for electrooptics. *Org. Lett.* **2006**, *8*, 1387-1390.

(120) Luo, J.; Haller, M.; Li, H.; Kim, T.-D.; Jen, A. K.-Y. Highly efficient and thermally stable electro-optic polymer from a smartly controlled crosslinking process. *Adv. Mater.* **2003**, *15*, 1635-1638.

(121) Luo, J.; Liu, S.; Haller, M.; Liu, L.; Ma, H.; Jen, A. K.-Y. Design, synthesis, and properties of highly efficient side-chain dendronized nonlinear optical polymers for electro-optics. *Adv. Mater.* **2002**, *14*, 1763-1768.

(122) Ma, H.; Chen, B.; Sassa, T.; Dalton, L. R.; Jen, A. K.-Y. Highly efficient and thermally stable nonlinear optical dendrimer for electrooptics. *J. Am. Chem. Soc.* **2001**, *123*, 986-987.

(123) Ma, H.; Jen, A. K. Y.; Dalton, L. R. Polymer-based optical waveguides: Materials, processing, and devices. *Adv. Mater.* **2002**, *14*, 1339-1365.

(124) Ma, H.; Liu, S.; Luo, J.; Suresh, S.; Liu, L.; Kang, S. H.; Haller, M.; Sassa, T.; Dalton, L. R.; Jen, A. K.-Y. Highly efficient and thermally stable electro-optical dendrimers for photonics. *Adv. Funct. Mater.* **2002**, *12*, 565-574.

(125) Maier, W.; Meier, G. A simple theory of the dielectric characteristics of homogeneous oriented crystalline-liquid phases of the nematic type. *Z. Naturforsch.* **1961**, *16a*, 262-267.

(126) Maier, W.; Meier, G. The principal dielectric constants of homogeneously oriented liquid-crystal phase of p,p'-azoxyanisole. *Z. Naturforsch.* **1961**, *16a*, 470-477.

(127) Maiman, T. H. Stimulated optical radiation in ruby. *Nature* **1960**, *187*, 493-494.

(128) Mao, S. S. H.; Ra, Y.; Guo, L.; Zhang, C.; Dalton, L. R.; Chen, A.; Garner, S. M.; Steier, W. H. Progress toward device-quality second-order nonlinear optical materials. 1. Influence of composition and processing conditions on nonlinearity, temporal stability, and optical loss. *Chem. Mater.* **1998**, *10*, 146-155.

(129) Marder, S.; Perry, J.; Zhou, W.; Kuebler, S. M.; Cammack, J. K.; (USA).

Application: WO, WO, 2002; pp 181 pp.

(130) Marder, S. R.; Cheng, L. T.; Tiemann, B. G.; Friedli, A. C.; Blanchard-Desce, M.; Perry, J. W.; Skindhoej, J. Large first hyperpolarizabilities in push-pull polyenes by tuning of the bond length alternation and aromaticity. *Science* **1994**, *263*, 511-514.

(131) Marder, S. R.; Perry, J. W.; Bourhill, G.; Gorman, C. B.; Tiemann, B. G.; Mansour, K. Relation between bond-length alternation and second electronic hyperpolarizability of conjugated organic molecules. *Science* **1993**, *261*, 186-189.

(132) Marks, T. J.; Ho, S. T.; Liu, Z.; Zhu, P.; Sun, D.-G.; Ma, J.; Xiao, Y.; Kang, H. Electro-optic waveguide modulators by the integration of self-assembled superlattices with polymeric and semiconductor materials. *Proc. SPIE* **2003**, *4991*, 133-143.

(133) Martins, C. T.; Lima, M. S.; Seoud, O. A. E. A novel, convenient, quinoline-based merocyanine dye: Probing solvation in pure and mixed solvents and in the interfacial region of an anionic micelle. *J. Phys. Org. Chem.* **2005**, *18*, 1072-1085.

(134) McQuaid, R. W. The pockels effect of hexamethylenetetramine, in letters to the editor. *Appl. Opt.* **1963**, *2*, 319-323.

(135) Melikian, G.; Rouessac, F. P.; Alexandre, C. Synthesis of substituted dicyanomethylendihydrofurans. *Synth. Commun.* **1995**, *25*, 3045-3051.

(136) Meyers, F.; Marder, S. R.; Pierce, B. M.; Bredas, J. L. Electric field modulated nonlinear optical properties of donor-acceptor polyenes: Sum-over-states investigation of the relationship between molecular polarizabilities (.Alpha., .Beta., and .Gamma.) and bond length alternation. *J. Am. Chem. Soc.* **1994**, *116*, 10703-10714.

(137) Michalak, R. J.; Kuo, Y.-H.; Nash, F. D.; Szep, A.; Caffey, J. R.; Payson, P. M.; Haas, F.; McKeon, B. F.; Cook, P. R.; Brost, G. A.; Luo, J.; Jen, A. K. Y.; Dalton, L. R.; Steier, W. H. High-speed ajl8/apc polymer modulator. *IEEE Photonic Tech. Lett.* **2006**, *18*, 1207-1209.

(138) Michelotti, F.; Toussaere, E.; Levenson, R.; Liang, J.; Zyss, J. Real-time pole and probe assessment of orientational processes in electro-optic polymers. *Appl. Phys. Lett.* **1995**, *67*, 2765-2767.

(139) Moore, A. J.; Chesney, A.; Bryce, M. R.; Batsanov, A. S.; Kelly, J. F.; Howard, J. A. K.; Perepichka, I. F.; Perepichka, D. F.; Meshulam, G.; Berkovic, G.;

Kotler, Z.; Mazor, R.; Khodorkovsky, V. Synthesis, structures and nonlinear optical properties of novel d-p-a chromophores: Intramolecular charge transfer from 1,3-dithiole or ferrocene moieties to polynitrofluorene or dicyanomethylene moieties through conjugated linkers. *Eur. J. Org. Chem.* **2001**, *2001*, 2671-2687.

(140) Morrell, J. A.; Albrecht, A. C.; Levin, K. H.; Tang, C. L. The electrooptic coefficients of urea. *J. Chem. Phys.* **1979**, *71*, 5063-5068.

(141) Nahata, A.; Auston, D. H.; Wu, C.; Yardley, J. T. Generation of terahertz radiation from a poled polymer. *Appl. Phys. Lett.* **1995**, *67*, 1358-1360.

(142) Ner, M. S.; Sharp, C.; Gibson, D. R. Environmental performance of lithium niobate (linbo3) based guided wave optical devices. *Proc. SPIE* **1990**, *1180*, 183-194.

(143) Nguyen, T. T.; Salle, M.; Delaunay, J.; Riou, A.; Richomme, P.; Raimundo, J. M.; Gorgues, A.; Ledoux, I.; Dhenaut, C.; Zyss, J.; Orduna, J.; Garin, J. Functionalized polyolefinic nonlinear optic chromophores incorporating the 1,3-dithiol-2-ylidene moiety as the electron-donating part. *J. Mater. Chem.* **1998**, *8*, 1185-1192.

(144) Nielsen, R. D.; Rommel, H. L.; Robinson, B. H. Simulation of the loading parameter in organic nonlinear optical materials. *J. Phys. Chem. B* **2004**, *108*, 8659-8667.

(145) Okamura, Y.; Yoshinaka, S.; Yamamoto, S. Measuring mode propagation losses of integrated optical waveguides: A simple method. *Appl. Opt.* **1983**, *22*, 3892-3894.

(146) Onsager, L. Electric moments of molecules in liquids. *J. Am. Chem. Soc.* **1936**, *58*, 1486-1493.

(147) Ostinelli, O., ETH, 2000.

(148) Otomo, A.; Jager, M.; Stegeman, G. I.; Flipse, M. C.; Diemeer, M. Key trade-offs for second harmonic generation in poled polymers. *Appl. Phys. Lett.* **1996**, *69*, 1991-1993.

(149) Oudar, J. L.; Chemla, D. S. Theory of second-order optical susceptibilities of benzene substitutes. *Opt. Commun.* **1975**, *13*, 164-168.

(150) Oudar, J. L.; Chemla, D. S. Hyperpolarizabilities of the nitroanilines and their relations to the excited state dipole moment. *J. Chem. Phys.* **1977**, *66*, 2664-2668.

(151) Paley, M. S.; Harris, J. M.; Looser, H.; Baumert, J. C.; Bjorklund, G. C.; Jundt, D.; Twieg, R. J. A solvatochromic method for determining second-order polarizabilities of organic molecules. *J. Org. Chem.* **1989**, *54*, 3774-3778.

(152) Pan, F.; Wong, M. S.; Bosshard, C.; Guenter, P. Crystal growth and characterization of the organic salt 4-n,n-dimethylamino-4'-n'-methyl-stilbazolium tosylate (dast). *Adv. Mater.* **1996**, *8*, 592-595.

(153) Pan, F.; Wong, M. S.; Gramlich, V.; Bosshard, C.; Guenter, P. A novel and perfectly aligned highly electro-optic organic cocrystal of a merocyanine dye and 2,4-dihydroxybenzaldehyde. *J. Am. Chem. Soc.* **1996**, *118*, 6315-6316.

(154) Pan, Q.; Fang, C.; Zhang, Z.; Qin, Z.; Li, F.; Gu, Q.; Wu, X.; Yu, J. Synthesis and characterization of nonlinear optical chromophores containing [alpha]-cyan with thermal stability. *Opt. Mater.* **2003**, *22*, 45-49.

(155) Park, D. H.; Kang, J. W.; Luo, J. D.; Kim, T. D.; Jen, A. K. Y.; Lee, C. H.; Herman, W. N. Nonlinear ellipsometric analysis of poled organic glasses having very large electro-optic coefficients. *Proc. SPIE* **2005**, *5935*, 59350O/59351-59350O/59312.

(156) Park, D. H.; Lee, C. H.; Herman, W. N. Analysis of multiple relfection effects in reflective measurements of electro-optic coefficients of poled polymers in multilayer structures. *Opt. Express* **2006**, *14*, 8866-8884.

(157) Pauley, M. A.; Wang, C. H. Hyper-rayleigh scattering measurements of nonlinear optical chromophores at 1907 nm. *Chem. Phys. Lett.* **1997**, *280*, 544-550.

(158) Pereverzev, Y. V.; Prezhdo, O. V.; Dalton, L. R. Structural origin of the enhanced electro-optic response of dendrimer systems. *Chem. Phys. Lett.* **2003**, *373*, 207-212.

(159) Piekara, A. A theory of electric polarization, electro-optical kerr effect and electric saturation in liquids and solutions. *Proc. R. Soc. London A* **1939**, *172*, 360-383.

(160) Pockels, F. *Lehrbuch der kristalloptic*; B. G. Teubner: Leipzig, 1906.

(161) Poshkus, A. C.; Herweh, J. E.; Magnotta, F. A. The synthesis of aromatic sulfonyl bromides from sulfonylhydrazides. *J. Org. Chem.* **1963**, *28*, 2766-2769.

(162) Prasad, P. N. W., D. J. *Introduction to nonlinear optical effects in molecules and polymers*; John Wiley and Sons: New York, 1991.

(163) Rabiei, P.; Steier, W. H.; Cheng, Z.; Dalton, L. R. Polymer micro-ring filters and modulators. *J. Lightwave Technol.* **2002**, *20*, 1968-1975.

(164) Raimundo, J.-M.; Blanchard, P.; Frere, P.; Mercier, N.; Ledoux-Rak, I.; Hierle, R.; Roncali, J. Push-pull chromophores based on 2,2'-bi(3,4-ethylenedioxythiophene) (bedot) [pi]-conjugating spacer. *Tetrahedron Lett.* **2001**, *42*, 1507-1510.

(165) Raimundo, J. M.; Blanchard, P.; Gallego-Planas, N.; Mercier, N.; Ledoux-Rak, I.; Hierle, R.; Roncali, J. Design and synthesis of push-pull chromophores for second-order nonlinear optics derived from rigidified thiophene-based pi-conjugating spacers. *J. Org. Chem.* **2002**, *67*, 205-218.

(166) Ramos-Ortiz, G.; Cha, M.; Kippelen, B.; Walker Gregory, A.; Barlow, S.; Marder Seth, R. Direct imaging through scattering media by use of efficient third-harmonic generation in organic materials. *Opt. Lett.* **2004**, *29*, 2515-2517.

(167) Rashid, A. N.; Erny, C.; Gunter, P. Hydrogen-bond-directed orientation in nonlinear optical thin films. *Adv. Mater.* **2003**, *15*, 2024-2027.

(168) Reeves, B. D.; Grenier, C. R. G.; Argun, A. A.; Cirpan, A.; McCarley, T. D.; Reynolds, J. R. Spray coatable electrochromic dioxythiophene polymers with high coloration efficiencies. *Macromolecules* **2004**, *37*, 7559-7569.

(169) Reeves, B. D.; Thompson, B. C.; Abboud, K. A.; Smart, B. E.; Reynolds, J. R. Dual cathodically and anodically coloring electrochromic polymer based on a spiro bipropylenedioxythiophene [(poly(spirobiprodot)]. *Adv. Mater.* **2002**, *14*, 717-719.

(170) Rezzonico, D.; Jazbinsek, M.; Bosshard, C.; Günter, P.; Bale, D.; Liao, Y.; Dalton, L. R.; Reid, P. J. Photostability of pi-conjugated chromophores by resonant and nonresonant light excitations for long-life polymeric telecommunication devices. *in preparation* **2007**.

(171) Robinson, B. H.; Dalton, L. R. Monte carlo statistical mechanical simulations of the competition of intermolecular electrostatic and poling-field interactions in defining macroscopic electro-optic activity for organic chromophore/polymer materials. *J. Phys. Chem. A* **2000**, *104*, 4785-4795.

(172) Robinson, B. H.; Dalton, L. R.; Harper, A. W.; Ren, A.; Wang, F.; Zhang, C.; Todorova, G.; Lee, M.; Aniszfeld, R.; Garner, S.; Chen, A.; Steier, W. H.; Houbrecht, S.; Persoons, A.; Ledoux, I.; Zyss, J.; Jen, A. K. Y. The molecular and supramolecular engineering of polymeric electro-optic materials. *Chem. Phys.* **1999**, *245*, 35-50.

(173) Roncali, J.; Blanchard, P.; Frere, P. 3,4-ethylenedioxythiophene (edot) as a versatile building block for advanced functional p-conjugated systems. *J. Mater. Chem.* **2005**, *15*, 1589-1610.

(174) Sandalphon; Kippelen, B.; Meerholz, K.; Peyghambarian, N. Ellipsometric measurements of poling birefringence, the pockels effect, and the kerr effect in high-performance photorefractive polymer composites. *Appl. Opt.* **1996**, *35*, 2346-2354.

(175) Sandhya, K. Y.; Pillai, C. K. S.; Sato, M.; Tsutsumi, N. Nonlinear optical properties and liquid-crystalline behavior of new polyesters with dipole moments aligned transverse to the backbone. *Macromol. Chem. Phys.* **2002**, *203*, 1126-1134.

(176) Schildkraut, J. S. Determination of the electrooptic coefficient of a poled polymer film. *Appl. Opt.* **1990**, *29*, 2839-2841.

(177) Schwendeman, I.; Hwang, J.; Welsh, D. M.; Tanner, D. B.; Reynolds, J. R. Combined visible and infrared electrochromism using dual polymer devices. *Adv. Mater.* **2001**, *13*, 634-637.

(178) Shaw, B. D.; Wagstaff, E. A. Reaction between 2-picoline and aromatic aldehydes. *J. Chem. Soc.* **1933**, 77-79.

(179) Shi, Y.; Zhang, C.; Zhang, H.; Bechtel, J. H.; Dalton, L. R.; Robinson, B. H.; Steier, W. H. Low (sub-1-volt) halfwave voltage polymeric electro-optic modulators achieved by controlling chromophore shape. *Science* **2000**, *288*, 119-122.

(180) Shockley, W.; Pearson, G. L. Modulation of conductance of thin films of semiconductors by surface charges. *Phys. Rev.* **1948**, *74*, 232-233.

(181) Sinness, J., University of Washington, 2006.

(182) Sinness, J.; Clot, O.; Hammond, S. R.; Bhatambrekar, N.; Rommel, H. L.; Robinson, B.; Jen, A. K. Y.; Dalton, L. Synthesis of dendridic nlo chromophores for the improvement of order in electro-optics. *Mater. Res. Soc. Symp. Proc.* **2005**, *846*, 121-126.

(183) Sinyukov, A. M.; Leahy, M. R.; Hayden, L. M.; Haller, M.; Luo, J.; Jen, A. K. Y.; Dalton, L. R. Resonance enhanced thz generation in electro-optic polymers near the absorption maximum. *Appl. Phys. Lett.* **2004**, *85*, 5827-5829.

(184) Sorai, M.; Saito, K. Alkyl chains acting as entropy reservoir in liquid crystalline

materials. *Chem. Rec.* **2003**, *3*, 29-39.

(185) Soref, R. The past, present, and future of silicon photonics. *IEEE J. Sel. Top. Quantum Electron.* **2006**, *12*, 1678-1687.

(186) Spangler, C. W.; He, M. Preparation and oxidative doping studies of dithienyl polyenes stabilized by alkyl group substitution. *J. Chem. Soc., Perkin Trans. 1* **1995**, 715-720.

(187) Spraul, B. K.; Suresh, S.; Sassa, T.; Angeles Herranz, M.; Echegoyen, L.; Wada, T.; Perahia, D.; Smith, D. W. Thermally stable triaryl amino chromophores with high molecular hyperpolarizabilities. *Tetrahedron Lett.* **2004**, *45*, 3253-3256.

(188) Staub, K.; Levina, G. A.; Barlow, S.; Kowalczyk, T. C.; Lackritz, H. S.; Barzoukas, M.; Fort, A.; Marder, S. R. Synthesis and stability studies of conformationally locked 4-(diarylamino)aryl- and 4-(dialkylamino)phenyl-substituted second-order nonlinear optical polyene chromophores. *J. Mater. Chem.* **2003**, *13*, 825-833.

(189) Stenger-Smith, J. D.; Zarras, P.; Hollins, R. A.; Chafin, A. P.; Merwin, L. H.; Yee, R.; Lindsay, G. A.; Herman, W. N.; Gratz, R. F.; Nickel, E. G. Main-chain syndioregic nonlinear optical polymers. Ii. Extended pi conjugated and improved thermal properties. *J. Polym. Sci., Part A: Polym. Chem.* **2000**, *38*.

(190) Sullivan, P. A., University of Washington, 2006.

(191) Sullivan, P. A.; Akelaitis, A. J. P.; Lee, S. K.; McGrew, G.; Lee, S. K.; Choi, D. H.; Dalton, L. R. Novel dendritic chromophores for electro-optics: Influence of binding mode and attachment flexibility on electro-optic behavior. *Chem. Mater.* **2006**, *18*, 344-351.

(192) Sullivan, P. A.; Rommel, H. L.; Eichinger, B. E.; Robinson, B. H.; Hammond, S.; Bale, D.; University of Washington, 2007.

(193) Sun, H.; Pyajt, A.; Luo, J.; Shi, Z.; Hau, S.; Jen, A.; Dalton, L.; Chen, A. Broadband electric field sensor with electro-optic polymer micro-ring resonator on side-polished optical fiber. *Proc. SPIE* **2006**, *6117*, 611713/611711-611713/611712.

(194) Sun, S.-S.; Zhang, C.; Dalton, L. R.; Garner, S. M.; Chen, A.; Steier, W. H. 1,3-bis(dicyanomethylidene)indane-based second-order nlo materials. *Chem. Mater.* **1996**, *8*, 2539-2541.

(195) Sundberg, K. R. A group--dipole interaction model of the molecular polarizability and the molecular first and second hyperpolarizabilities. *J. Chem.*

Phys. **1977**, *66*, 114-118.

(196) Suresh, S.; Zengin, H.; Spraul, B. K.; Sassa, T.; Wada, T.; Smith, J. D. W. Synthesis and hyperpolarizabilities of high temperature triarylamine-polyene chromophores. *Tetrahedron Lett.* **2005**, *46*, 3913-3916.

(197) Tan, H.; Guo, M.; Du, R.; Xie, X.; Li, J.; Zhong, Y.; Fu, Q. The effect of fluorinated side chain attached on hard segment on the phase separation and surface topography of polyurethanes. *Polymer* **2004**, *45*, 1647-1657.

(198) Teng, C. C. Precision measurements of the optical attenuation profile along the propagation path in thin-film waveguides. *Appl. Opt.* **1993**, *32*, 1051-1054.

(199) Teng, C. C.; Man, H. T. Simple reflection technique for measuring the electro-optic coefficient of poled polymers. *Appl. Phys. Lett.* **1990**, *56*, 1734-1736.

(200) Terhune, R. W.; Maker, P. D.; Savage, C. M. Measurements of nonlinear light scattering. *Phys. Rev. Lett.* **1965**, *14*, 681.

(201) Turner, E. H. High-frequency electrooptic coefficients of lithium niobate. *Appl. Phys. Lett.* **1966**, *8*, 303-304.

(202) Van Bolhuis, F.; Wynberg, H.; Havinga, E. E.; Meijer, E. W.; Staring, E. G. J. The x-ray structure and mndo calculations of [alpha]-terthienyl: A model for polythiophenes. *Synth. Met.* **1989**, *30*, 381-389.

(203) van der Boom, M. E.; Richter, A. G.; Malinsky, J. E.; Lee, P. A.; Armstrong, N. R.; Dutta, P.; Marks, T. J. Single reactor route to polar superlattices. Layer-by-layer self-assembly of large-response molecular electrooptic materials by protection-deprotection. *Chem. Mater.* **2001**, *13*, 15-17.

(204) Villemin, D.; Liao, L. Rapid and efficient synthesis of 2-[3-cyano-4-(2-arylidene)-5,5-dimethyl-5h-furan-2-ylidene]-malononitrile under focused microwave irradiation. *Synth. Commun.* **2001**, *31*, 1771-1780.

(205) Wang, C. H. Effects of dephasing and vibronic structure on the first hyperpolarizability of strongly charge-transfer molecules. *J. Chem. Phys.* **2000**, *112*, 1917-1924.

(206) Wang, F., University of Southern California.

(207) Ward, J. F. Calculation of nonlinear optical susceptibilities using diagrammatic perturbation theory. *Rev. Mod. Phys.* **1965**, *37*, 1.

(208) Welsh, D. M.; Kloeppner, L. J.; Madrigal, L.; Pinto, M. R.; Thompson, B. C.;

Schanze, K. S.; Abboud, K. A.; Powell, D.; Reynolds, J. R. Regiosymmetric dibutyl-substituted poly(3,4-propylenedioxythiophene)s as highly electron-rich electroactive and luminescent polymers. *Macromolecules* **2002**, *35*, 6517-6525.

(209) Whittall, I. R.; Cifuentes, M. P.; Humphrey, M. G.; Luther-Davies, B.; Samoc, M.; Houbrechts, S.; Persoons, A.; Heath, G. A.; Bogsanyi, D. Organometallic complexes for nonlinear optics. 11. Molecular quadratic and cubic hyperpolarizabilities of systematically varied (cyclopentadienyl)(triphenylphosphine)nickel sigma-arylacetylides. *Organometallics* **1997**, *16*, 2631-2637.

(210) Wong, S.; Ma, H.; Jen, A. K.-Y.; Barto, R.; Frank, C. W. Highly fluorinated trifluorovinyl aryl ether monomers and perfluorocyclobutane aromatic ether polymers for optical waveguide applications. *Macromolecules* **2003**, *36*, 8001-8007.

(211) Wyss, C. J.; Smith, G. J.; Woolhouse, A. D.; Kay, A. J.; Wadsworth, W. J.; McKinnie, I. T.; Haskell, T. G. The first-order hyperpolarizabilities of some charge transfer conjugated molecules with high transmission in the far red. *Opt. Mater.* **2001**, *16*, 341-347.

(212) Xu, G.; Si, J.; Liu, X.; Yang, Q. G.; Ye, P.; Li, Z.; Shen, Y. Comparison of the temperature dependence of optical poling between guest-host and side-chain polymer films. *J. Appl. Phys.* **1999**, *85*, 681-685.

(213) Yitzchaik, S.; Di Bella, S.; Lundquist, P. M.; Wong, G. K.; Marks, T. J. Anomalous second-order nonlinear optical response of in-plane poled glassy polymers. Spectroscopic and theoretical support for the importance of charged chromophore aggregates. *J. Am. Chem. Soc.* **1997**, *119*, 2995-3002.

(214) Yitzchaik, S.; Marks, T. J. Chromophoric self-assembled superlattices. *Acc. Chem. Res.* **1996**, *29*, 197-202.

(215) Zhang, C.; Dalton, L. R.; Oh, M.-C.; Zhang, H.; Steier, W. H. Low vp electrooptic modulators from cld-1: Chromophore design and synthesis, material processing, and characterization. *Chem. Mater.* **2001**, *13*, 3043-3050.

(216) Zhang, C.; Wang, C.; Dalton, L. R.; Zhang, H.; Steier, W. H. Progress toward device-quality second-order nonlinear optical materials. 4. A trilink high mb nlo chromophore in thermoset polyurethane: A \"Guest-host\" Approach to larger electrooptic coefficients. *Macromolecules* **2001**, *34*, 253-261.

(217) Zhang, S.; Zhou, G.; Yang, Z.; Qin, A.; Wang, P.; Ye, C. Design and synthesis of low dipole moment chromophores: 2,6-disubstitute cycloheptimidazoles. *Synth. Met.* **2003**, *137*, 1545-1546.

(218) Zhang, Y.; Wada, T.; Sasabe, H. A new hyperbranched polymer with polar chromophores for nonlinear optics. *Polymer* **1997**, *38*, 2893-2897.

(219) Zheng, Q.; Yao, Z.; Cheng, J.; Shen, Y.; Lu, Z. Synthesis and nonlinear optical properties of p-(dimethylamino)benzylidene dyes containing different acceptors. *Chem. Lett.* **2000**, 1426-1427.

(220) Zheng, X.; McLaughlin, C. V.; Cunningham, P.; Hayden, L. M. Terahertz science and applications based on poled electro-optic polymers. *Proc. SPIE* **2007**, *6472*, 64720F.

(221) Zheng, X.; McLaughlin, C. V.; Leahy-Hoppa, M. R.; Sinyukov, A. M.; Hayden, L. M. Modeling a broadband terahertz system based on an electro-optic polymer emitter-sensor pair. *J. Opt. Soc. Am. B: Opt. Phys.* **2006**, *23*, 1338-1347.

(222) Zhu, P.; Kang, H.; Facchetti, A.; Evmenenko, G.; Dutta, P.; Marks, T. J. Vapor phase self-assembly of electrooptic thin films via triple hydrogen bonds. *J. Am. Chem. Soc.* **2003**, *125*, 11496-11497.

(223) Zhu, P.; van der Boom, M. E.; Kang, H.; Evmenenko, G.; Dutta, P.; Marks, T. J. Realization of expeditious layer-by-layer siloxane-based self-assembly as an efficient route to structurally regular acentric superlattices with large electro-optic responses. *Chem. Mater.* **2002**, *14*, 4982-4989.

(224) Zook, J. D.; Chen, D.; Otto, G. N. Temperature dependence and model of the electrooptic effect in lithium niobate. *Appl. Phys. Lett.* **1967**, *11*, 159-161.

Appendix 1: SJLD-1 Crystal Structure Details

```
TITL X3C   - SHELXL
CELL 0.71000  23.6100  28.0500  32.0000  67.835  70.115  68.953
ZERR 1        0.0100   0.0100   0.0100   0.003   0.003   0.003
LATT  1
SFAC C  2.31000 20.84392  1.02000 10.20751  1.58860  0.56870  0.86500 =
     51.65125  0.21560  0.00330  0.00160  11.500  0.68000 12.01000
SFAC H  0.49300 10.51091  0.32291 26.12573  0.14019  3.14236  0.04081 =
     57.79977  0.00304  0.00000  0.00000   0.624  0.35000  1.00800
SFAC N 12.21261  0.00570  3.13220  9.89331  2.01250 28.99754  1.16630 =
      0.58260 -11.52901  0.00610  0.00330  19.600  0.68000 14.01000
SFAC O  3.04850 13.27711  2.28680  5.70111  1.54630  0.32390  0.86700 =
     32.90894  0.25080  0.01060  0.00600  32.500  0.68000 16.00000
SFAC S  6.90531  1.46790  5.20341 22.21512  1.43790  0.25360  1.58630 =
     56.17207  0.86690  0.12460  0.12340  532.000  1.04000 32.07000
UNIT  434   0  16 104   8
L.S. 5
ACTA
BOND $H
FVAR   1.00000
S1   5  0.06288  0.72300  0.34042  11.00000   0.1093
S2   5  0.13091  0.85210  0.22289  11.00000   0.0956
O1   4  0.15535  0.76077  0.14827  11.00000   0.1009
O2   4  0.19956  0.60770  0.23540  11.00000   0.1168
O3   4  0.23629  0.52121  0.24136  11.00000   0.1597
O4   4  0.38968  0.46173  0.34759  11.00000   0.2359
O5   4  0.36685  0.54681  0.37562  11.00000   0.2704
O6   4  0.28563  0.63597  0.34804  11.00000   0.2325
O7   4  0.04440  0.65004  0.18025  11.00000   0.1334
O8   4 -0.01012  0.70127  0.12839  11.00000   0.1496
O9   4 -0.07816  0.51870  0.29512  11.00000   0.2066
O10  4 -0.19142  0.56096  0.27615  11.00000   0.2218
O11  4 -0.21844  0.64724  0.20686  11.00000   0.2006
O12  4  0.11443  0.70868  0.25101  11.00000   0.1013
O13  4  0.26963  0.99719  0.00918  11.00000   0.1197
O14  4  0.09037  0.86120  0.31471  11.00000   0.1141
O15  4  0.02191  0.94149  0.44324  11.00000   0.1588
O16  4  0.00785  0.87483  0.50260  11.00000   0.2306
O17  4 -0.13902  1.09807  0.48580  11.00000   0.2234
O18  4 -0.18886  1.06769  0.57304  11.00000   0.2424
O19  4 -0.14822  0.96778  0.61684  11.00000   0.3642
O20  4 -0.04338  0.98054  0.37006  11.00000   0.1407
O21  4 -0.04783  1.04725  0.30525  11.00000   0.1980
O22  4 -0.25605  1.01671  0.48022  11.00000   0.1985
```

O23	4	-0.31422	1.11690	0.43755	11.00000	0.2771
O24	4	-0.26989	1.16469	0.34892	11.00000	0.2741
O25	4	0.02840	0.81669	0.41504	11.00000	0.1301
O26	4	-0.00747	0.66712	0.44192	11.00000	0.2004
N1	3	0.26897	0.91059	-0.09169	11.00000	0.1604
N2	3	0.35262	1.03661	-0.10826	11.00000	0.2167
N3	3	0.21678	0.84628	0.01795	11.00000	0.1251
N4	3	-0.13802	0.54858	0.61403	11.00000	0.1692
C1	1	0.08773	0.78139	0.30661	11.00000	0.0979
C2	1	0.11293	0.79205	0.25748	11.00000	0.0953
C3	1	0.14998	0.83317	0.17195	11.00000	0.0929
C4	1	0.14152	0.78356	0.18281	11.00000	0.0929
C5	1	0.18144	0.70381	0.16075	11.00000	0.1065
C6	1	0.13098	0.67184	0.18681	11.00000	0.1030
C7	1	0.16472	0.61357	0.20314	11.00000	0.1221
C8	1	0.23551	0.55813	0.25269	11.00000	0.1363
C9	1	0.26590	0.55718	0.28335	11.00000	0.1314
C10	1	0.31299	0.50786	0.29881	11.00000	0.1595
C11	1	0.34089	0.50815	0.32947	11.00000	0.1746
C12	1	0.39655	0.41916	0.33166	11.00000	0.2355
C13	1	0.33738	0.54801	0.34206	11.00000	0.2099
C14	1	0.40358	0.56636	0.35454	11.00000	0.4698
C15	1	0.29056	0.59984	0.32947	11.00000	0.1826
C16	1	0.22601	0.68301	0.33949	11.00000	0.2587
C17	1	0.22757	0.71636	0.36418	11.00000	0.4065
C18	1	0.25434	0.59946	0.29900	11.00000	0.1488
C19	1	0.09446	0.67880	0.15229	11.00000	0.1259
C20	1	-0.00520	0.66709	0.16600	11.00000	0.1292
C21	1	-0.05283	0.63771	0.19436	11.00000	0.1401
C22	1	-0.03730	0.59285	0.23020	11.00000	0.1530
C23	1	-0.08614	0.56531	0.25736	11.00000	0.1805
C24	1	-0.02095	0.50049	0.30961	11.00000	0.2163
C25	1	-0.02612	0.45012	0.36148	11.00000	0.2367
C26	1	-0.04404	0.41222	0.35456	11.00000	0.2627
C27	1	0.00106	0.39023	0.33268	11.00000	0.4432
C28	1	-0.07416	0.47117	0.39958	11.00000	0.3099
C29	1	-0.09059	0.46390	0.44225	11.00000	0.4069
C30	1	-0.14149	0.58478	0.24779	11.00000	0.1645
C31	1	-0.18090	0.51688	0.25236	11.00000	0.3574
C32	1	-0.25533	0.50571	0.27586	11.00000	0.6770
C33	1	-0.15754	0.62841	0.21418	11.00000	0.1717
C34	1	-0.23821	0.70224	0.17515	11.00000	0.2140
C35	1	-0.30531	0.70680	0.17925	11.00000	0.2779
C36	1	-0.34678	0.70376	0.23138	11.00000	0.3611
C37	1	-0.10880	0.65649	0.18424	11.00000	0.1439

C38	1	0.08303	0.69457	0.22692	11.00000	0.1103
C39	1	0.12453	0.75886	0.22980	11.00000	0.0963
C40	1	0.17397	0.86421	0.12686	11.00000	0.0957
C41	1	0.18985	0.91168	0.11510	11.00000	0.0892
C42	1	0.21633	0.93826	0.06918	11.00000	0.0976
C43	1	0.23821	0.98702	0.05981	11.00000	0.1019
C44	1	0.26474	0.96382	-0.00778	11.00000	0.1141
C45	1	0.28768	0.96696	-0.05474	11.00000	0.1268
C46	1	0.27683	0.93594	-0.07579	11.00000	0.1433
C47	1	0.32083	1.00336	-0.08442	11.00000	0.1813
C48	1	0.23225	0.92700	0.02710	11.00000	0.0980
C49	1	0.22584	0.88164	0.02111	11.00000	0.0999
C50	1	0.18488	1.03531	0.06567	11.00000	0.1172
C51	1	0.28803	0.97451	0.08596	11.00000	0.1262
C52	1	0.07563	0.81297	0.33360	11.00000	0.1018
C53	1	0.10821	0.87693	0.34709	11.00000	0.1397
C54	1	0.04944	0.90445	0.37683	11.00000	0.1289
C55	1	0.07308	0.90784	0.41524	11.00000	0.1561
C56	1	-0.00458	0.92040	0.48450	11.00000	0.1845
C57	1	-0.05186	0.96485	0.50455	11.00000	0.2090
C58	1	-0.06731	1.01686	0.47620	11.00000	0.2004
C59	1	-0.12589	1.05251	0.50897	11.00000	0.2093
C60	1	-0.10797	1.11921	0.43971	11.00000	0.2485
C61	1	-0.14327	1.18434	0.42891	11.00000	0.2605
C62	1	-0.09567	1.21012	0.38274	11.00000	0.3319
C63	1	-0.20092	1.18995	0.42999	11.00000	0.3430
C64	1	-0.14490	1.02652	0.54843	11.00000	0.2019
C65	1	-0.24695	1.07952	0.56944	11.00000	0.2798
C69	1	-0.13393	0.98500	0.57339	11.00000	0.2056
C70	1	-0.12919	0.91162	0.64950	11.00000	0.4263
C71	1	-0.07770	0.93281	0.55671	11.00000	0.2871
C72	1	0.02260	0.95897	0.34602	11.00000	0.1468
C73	1	-0.07370	1.02577	0.34718	11.00000	0.1487
C74	1	-0.13833	1.04720	0.37114	11.00000	0.1516
C75	1	-0.16177	1.01850	0.41434	11.00000	0.1465
C76	1	-0.22564	1.04246	0.43577	11.00000	0.1814
C77	1	-0.22738	0.96530	0.50082	11.00000	0.2046
C78	1	-0.27321	0.93477	0.54738	11.00000	0.3292
C79	1	-0.30159	0.91604	0.53727	11.00000	0.5700
C80	1	-0.25407	1.09145	0.41273	11.00000	0.2026
C81	1	-0.35412	1.10584	0.42519	11.00000	0.2797
C82	1	-0.23005	1.11692	0.36501	11.00000	0.2327
C83	1	-0.23843	1.19280	0.30030	11.00000	0.2808
C84	1	-0.17014	1.09657	0.34614	11.00000	0.1932
C85	1	-0.00033	0.87256	0.39981	11.00000	0.1305

C86	1	0.04875	0.79127	0.38052	11.00000	0.1174
C87	1	0.03662	0.74372	0.38993	11.00000	0.1125
C88	1	0.00781	0.71251	0.43742	11.00000	0.1374
C89	1	-0.03788	0.63490	0.48816	11.00000	0.1202
C90	1	-0.05088	0.58930	0.48954	11.00000	0.1374
C91	1	-0.08108	0.55815	0.53166	11.00000	0.1335
C92	1	-0.10784	0.57914	0.57034	11.00000	0.1370
C93	1	-0.14816	0.49979	0.61630	11.00000	0.1788
C94	1	-0.09487	0.44944	0.62280	11.00000	0.1722
C95	1	-0.07206	0.43766	0.66109	11.00000	0.1630
C96	1	-0.00946	0.39152	0.66246	11.00000	0.1461
C97	1	-0.16857	0.57092	0.65315	11.00000	0.1629
C98	1	-0.23253	0.60918	0.64894	11.00000	0.2001
C99	1	-0.26176	0.63440	0.69139	11.00000	0.2645
C100	1	-0.22367	0.65265	0.70377	11.00000	0.3650
C101	1	-0.09516	0.62466	0.56889	11.00000	0.1520
C102	1	-0.06231	0.65436	0.52611	11.00000	0.1423
S3	5	0.07231	0.99330	0.02890	11.00000	0.0922
S4	5	-0.00207	0.86133	0.13531	11.00000	0.0983
O27	4	-0.02034	0.93524	0.22289	11.00000	0.1107
O28	4	-0.10536	1.10352	0.18779	11.00000	0.1237
O29	4	-0.10136	1.18621	0.17507	11.00000	0.2324
O30	4	-0.29867	1.30716	0.12301	11.00000	0.2596
O31	4	-0.36927	1.23803	0.14114	11.00000	0.2137
O32	4	-0.32821	1.13451	0.18053	11.00000	0.1710
O33	4	0.08366	1.04609	0.18276	11.00000	0.1142
O34	4	0.16969	0.98135	0.20012	11.00000	0.1644
O35	4	0.14195	1.21963	0.12049	11.00000	0.2279
O36	4	0.26996	1.18624	0.11877	11.00000	0.2623
O37	4	0.32962	1.08664	0.15401	11.00000	0.2462
O38	4	0.04059	0.98840	0.12289	11.00000	0.1008
O39	4	0.03233	0.86581	0.03911	11.00000	0.0997
O40	4	0.17632	0.74254	-0.00811	11.00000	0.1174
O41	4	0.14945	0.66886	0.01726	11.00000	0.2392
O42	4	0.30849	0.53571	0.11371	11.00000	0.2369
O43	4	0.38690	0.59578	0.10750	11.00000	0.2563
O44	4	0.35610	0.69837	0.06479	11.00000	0.2208
O45	4	-0.00385	0.80357	-0.01667	11.00000	0.1276
O46	4	-0.07599	0.85611	-0.05757	11.00000	0.1517
O47	4	-0.07180	0.63382	0.07147	11.00000	0.2001
O48	4	-0.19659	0.66364	0.07460	11.00000	0.2454
O49	4	-0.24872	0.76047	0.02285	11.00000	0.2317
O50	4	0.09686	0.91716	-0.05848	11.00000	0.1038
O51	4	0.19945	1.16980	-0.16122	11.00000	0.1245
N5	3	-0.17609	0.64625	0.38994	11.00000	0.1607

N6	3	0.22347	1.11414	-0.29000	11.00000	0.1802
N7	3	0.28012	1.23512	-0.26969	11.00000	0.1803
N8	3	0.16978	1.02496	-0.18726	11.00000	0.1184
C103	1	0.04831	0.93415	0.05693	11.00000	0.0882
C104	1	0.02477	0.91898	0.10700	11.00000	0.0957
C105	1	-0.02346	0.87458	0.18904	11.00000	0.0964
C106	1	-0.01004	0.91882	0.18331	11.00000	0.0998
C107	1	-0.05453	0.99117	0.21872	11.00000	0.1111
C108	1	-0.01091	1.02873	0.18769	11.00000	0.1136
C109	1	-0.04255	1.08453	0.19573	11.00000	0.1235
C110	1	-0.13279	1.15648	0.17589	11.00000	0.1444
C111	1	-0.19388	1.17151	0.17073	11.00000	0.1519
C112	1	-0.21660	1.23352	0.14943	11.00000	0.1875
C113	1	-0.27348	1.24583	0.14230	11.00000	0.1805
C114	1	-0.26202	1.34076	0.11108	11.00000	0.2553
C115	1	-0.30420	1.21803	0.15024	11.00000	0.1593
C116	1	-0.36314	1.24022	0.09679	11.00000	0.2828
C117	1	-0.29245	1.16174	0.17183	11.00000	0.1593
C118	1	-0.31378	1.07956	0.20190	11.00000	0.1737
C119	1	-0.36442	1.05648	0.20879	11.00000	0.1954
C120	1	-0.34762	0.99779	0.22519	11.00000	0.1962
C121	1	-0.40361	0.97247	0.22759	11.00000	0.2432
C122	1	-0.42843	1.09003	0.23910	11.00000	0.2329
C123	1	-0.41558	1.09095	0.27615	11.00000	0.5959
C124	1	-0.22753	1.13963	0.18120	11.00000	0.1450
C125	1	0.05042	1.00522	0.20463	11.00000	0.1139
C126	1	0.14337	1.02838	0.18661	11.00000	0.1352
C127	1	0.17392	1.07370	0.16646	11.00000	0.1329
C128	1	0.14201	1.12495	0.14931	11.00000	0.1413
C129	1	0.17716	1.16404	0.13655	11.00000	0.2063
C130	1	0.08281	1.23514	0.12138	11.00000	0.2005
C131	1	0.03485	1.30102	0.11254	11.00000	0.4731
C133	1	0.23708	1.14729	0.13870	11.00000	0.1861
C134	1	0.28113	1.19687	0.16013	11.00000	0.3550
C135	1	0.26775	1.10054	0.15115	11.00000	0.1848
C136	1	0.36425	1.02831	0.16982	11.00000	0.2447
C137	1	0.43940	1.01898	0.14921	11.00000	0.3047
C139	1	0.23974	1.05647	0.16788	11.00000	0.1761
C140	1	-0.00044	1.03639	0.13685	11.00000	0.1054
C141	1	0.01511	0.94470	0.13818	11.00000	0.0912
C142	1	-0.05057	0.83789	0.23209	11.00000	0.1122
C143	1	-0.06468	0.79432	0.23286	11.00000	0.1148
C144	1	-0.09287	0.75760	0.27423	11.00000	0.1152
C145	1	-0.11738	0.72158	0.26886	11.00000	0.1251
C146	1	-0.14429	0.68585	0.30636	11.00000	0.1346

C147	1	-0.15065	0.68683	0.35059	11.00000	0.1405
C148	1	-0.17919	0.64445	0.43663	11.00000	0.1766
C149	1	-0.22888	0.68391	0.45486	11.00000	0.1912
C150	1	-0.22599	0.67635	0.50583	11.00000	0.2421
C151	1	-0.28088	0.72463	0.51476	11.00000	0.3683
C152	1	-0.23894	0.63374	0.53567	11.00000	0.5553
C153	1	-0.20969	0.61450	0.38433	11.00000	0.1832
C154	1	-0.26907	0.64825	0.37533	11.00000	0.2035
C155	1	-0.30414	0.61510	0.36606	11.00000	0.2784
C156	1	-0.12703	0.71928	0.35907	11.00000	0.1402
C157	1	-0.09681	0.75599	0.32071	11.00000	0.1407
C158	1	0.05750	0.90888	0.02547	11.00000	0.0939
C159	1	0.07447	0.81648	0.02832	11.00000	0.1011
C160	1	0.09052	0.82203	-0.02309	11.00000	0.1063
C161	1	0.12591	0.76730	-0.03105	11.00000	0.1364
C162	1	0.18800	0.69004	0.01699	11.00000	0.1631
C163	1	0.23737	0.66968	0.03871	11.00000	0.1325
C164	1	0.24447	0.61231	0.06753	11.00000	0.1898
C165	1	0.29581	0.59399	0.08976	11.00000	0.1768
C166	1	0.26537	0.51503	0.12037	11.00000	0.2112
C167	1	0.33009	0.61820	0.08703	11.00000	0.1691
C168	1	0.36706	0.60275	0.15591	11.00000	0.2445
C171	1	0.31832	0.67329	0.06436	11.00000	0.1737
C172	1	0.33929	0.74898	0.05382	11.00000	0.2820
C173	1	0.27007	0.69491	0.04036	11.00000	0.1371
C174	1	0.03061	0.84322	-0.04226	11.00000	0.1179
C175	1	-0.05909	0.81545	-0.02686	11.00000	0.1319
C176	1	-0.09370	0.77444	-0.00193	11.00000	0.1377
C177	1	-0.06279	0.72350	0.02502	11.00000	0.1437
C178	1	-0.09822	0.68634	0.04764	11.00000	0.1761
C179	1	-0.00819	0.61822	0.06885	11.00000	0.1866
C180	1	0.02667	0.55356	0.08329	11.00000	0.2680
C181	1	-0.00925	0.54581	0.12805	11.00000	0.2995
C182	1	0.09903	0.53951	0.07912	11.00000	0.3207
C183	1	-0.15455	0.69823	0.04475	11.00000	0.1931
C184	1	-0.18990	0.63560	0.04589	11.00000	0.3837
C185	1	-0.18471	0.74600	0.02335	11.00000	0.1843
C186	1	-0.27492	0.80485	-0.00516	11.00000	0.2257
C187	1	-0.34343	0.80658	0.01185	11.00000	0.2811
C188	1	-0.40034	0.85781	-0.01158	11.00000	0.5338
C189	1	-0.15538	0.78846	-0.00612	11.00000	0.1584
C190	1	0.13103	0.86079	-0.05349	11.00000	0.1206
C191	1	0.08414	0.93388	-0.01959	11.00000	0.0949
C192	1	0.09593	0.98057	-0.02574	11.00000	0.0934
C193	1	0.12166	1.01537	-0.06667	11.00000	0.1001

```
C194  1  0.13228  1.06191 -0.07139  11.00000   0.0987
C195  1  0.15773  1.09679 -0.11233  11.00000   0.1054
C196  1  0.16842  1.14584 -0.11144  11.00000   0.1183
C197  1  0.20196  1.14099 -0.18695  11.00000   0.1347
C198  1  0.22838  1.15691 -0.23547  11.00000   0.1416
C199  1  0.22656  1.13365 -0.26627  11.00000   0.1452
C200  1  0.25543  1.19940 -0.25373  11.00000   0.1569
C201  1  0.17744  1.09600 -0.15933  11.00000   0.1038
C202  1  0.17363  1.05787 -0.17646  11.00000   0.1058
C203  1  0.21401  1.13582 -0.08286  11.00000   0.1318
C204  1  0.10522  1.18733 -0.09979  11.00000   0.1273
O52   4  0.54650  0.41472  0.29348  11.00000   0.5914
C205  1  0.51612  0.40125  0.33330  11.00000   0.2811
C206  1  0.46706  0.37063  0.35977  11.00000   0.2687
C207  1  0.46300  0.32728  0.34660  11.00000   0.3438
C214  1  0.40501  0.29986  0.38661  11.00000   0.3399
C208  1  0.28214  0.45078  0.16223  11.00000   0.1391
C209  1  0.22987  0.43228  0.17767  11.00000   0.1427
C210  1  0.18075  0.44590  0.21994  11.00000   0.6995
C211  1  0.35298  0.42760  0.13495  11.00000   0.1382
C66   1  0.68666  0.13322  0.59757  11.00000   0.3296
C67   1  0.71333  0.16904  0.56438  11.00000   0.3920
C68   1  0.70484  0.08692  0.63218  11.00000   0.5072
C169  1  0.45315  0.57558  0.15648  11.00000   0.4060
C170  1  0.43113  0.58231  0.19216  11.00000   0.3756
C212  1  0.56381  0.27375  0.07965  11.00000   0.3589
C213  1  0.52670  0.23396  0.12345  11.00000   0.2561
C138  1  0.45843  0.04968  0.18033  11.00000   0.5943
C215  1  0.58518  0.69950  0.22080  11.00000   0.3801
C216  1  0.37972  0.34243  0.64217  11.00000   0.3116
C217  1  0.69705  0.28069  0.29472  11.00000   0.1538
C218  1  0.15530  0.10756  0.58725  11.00000   0.2035
HKLF 4 1  1.0000  0.0000  0.0000  0.0000  1.0000  0.0000  0.0000  0.0000  1.0000
END
```

Vita

Scott R. Hammond was born in San Francisco, California, and lived in the San Francisco Bay Area most of his life. He earned a Bachelor of Science degree in Chemistry with High Honors at the University of California, Berkeley in December of 2001. While there, he performed undergraduate research with Prof. Douglas Gin, presenting twice at national American Chemical Society meetings, and culminating in a first-author publication: Synthesis and lyotropic liquid crystalline behavior of a taper-shaped phosphonic acid amphiphile. Hammond, S.; Zhou, W.-J.; Avlyanov, J.; Gin, D. *Liquid Crystals* **2002**, *29(9),* 1151-1159. In 2002, Scott Hammond moved to Seattle, Washington, and began his graduate education at the University of Washington, Seattle with Prof. Larry Dalton. During his education, he presented at both Materials Research Society and American Chemical Society national meetings and co-authored numerous publications. In June of 2007, he earned a Doctor of Philosophy degree in Organic/Materials Chemistry and Nanotechnology.